Chair of Mining Engineering and Mineral Economics

Doctoral Thesis

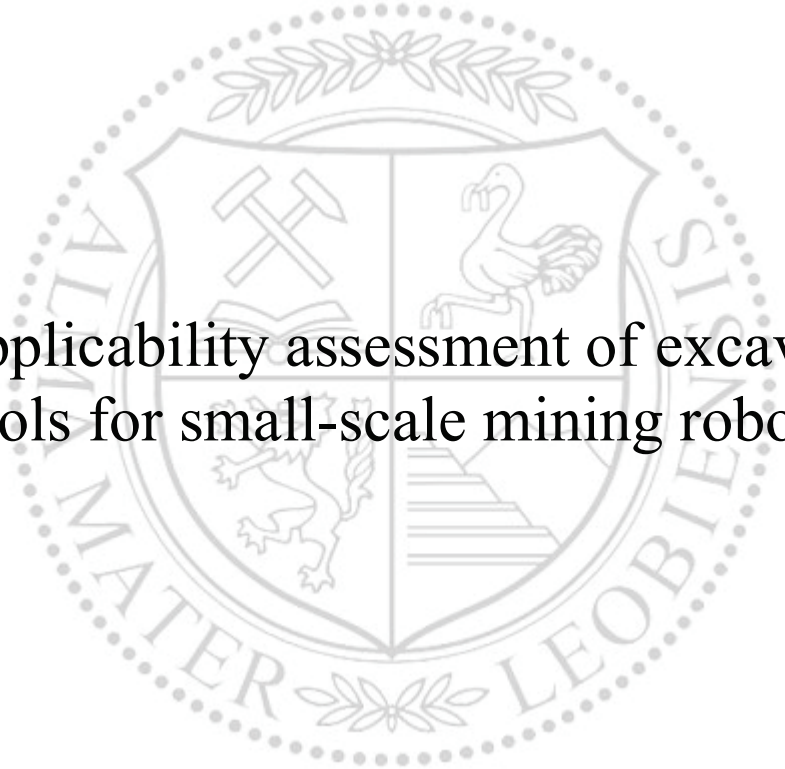

An applicability assessment of excavation tools for small-scale mining robots

Dipl.-Ing. Michael Berner, BSc

September 2023

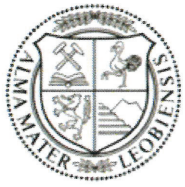

MONTANUNIVERSITÄT LEOBEN
www.unileoben.ac.at

AFFIDAVIT

I declare on oath that I wrote this thesis independently, did not use other than the specified sources and aids, and did not otherwise use any unauthorized aids.

I declare that I have read, understood, and complied with the guidelines of the senate of the Montanuniversität Leoben for "Good Scientific Practice".

Furthermore, I declare that the electronic and printed version of the submitted thesis are identical, both, formally and with regard to content.

Date 13.09.2023

M. Berner

Signature Author
Michael Berner

Bibliographic data

Title:	An applicability assessment of excavation tools for small-scale mining robots
Author:	Michael Berner
Year:	2023
Place:	Leoben, Austria
Type:	Doctoral (PhD) Thesis / Dissertation, University of Leoben
Pages:	291
DOI:	https://doi.org/10.34901/mul.pub.2023.159
Supervisor:	Univ.-Prof. Dipl.-Ing. Dr.mont. Nikolaus August Sifferlinger
Co-Supervisor:	Univ.-Prof. Dipl.-Ing. Dr.mont. Thomas Antretter

Copyright

Acknowledgment

First and foremost, I would like to express my gratitude to my supervisor Univ.-Prof. Dipl.-Ing. Dr.mont. Nikolaus August Sifferlinger, who gave me the opportunity to work in his team, to conduct this thesis and who supported me continuously with his expertise.

I am extremely grateful to Dipl.-Ing. Roman Gerer. This thesis would not have been possible without his effort and dedication for technical topics.

Furthermore, I want to thank my mentor Univ.-Prof. Dipl.-Ing. Dr.mont. Thomas Antretter, who also supported me whenever it was needed.

A debt of gratitude is also owed to the partners of the ROBOMINERS consortium for the great cooperation throughout the last years and the resulting friendships.

I thank all my colleagues at the Chair of Mining Engineering and Mineral Economics, who assisted me with great advice and support, especially while working in the laboratory.

Lena, thank you for supporting me and standing by my side the last years. Without you, I would not be where I am now.

Funding

This work was conducted during the EU-project H2020 - ROBOMINERS. The aim of ROBOMINERS was the development of a bio-inspired and modular robot miner for small and difficult to access deposits. ROBOMINERS received funding from the European Union's Horizon 2020 research and innovation programme under grant agreement No. 820971. The project period was 06/2019 to 11/2023.

ROBOMINERS was executed by the following 14 partners in Europe:

- Montanuniversität Leoben - Chair of Mining Engineering and Mineral Economics - Conveying Technology and Design Methods (Austria).
- Universidad Politécnica de Madrid (Spain).
- Tampere University of Technology (Finland).
- Institut Royal des Sciences Naturelles de Belgique (Belgium).
- Associacao Portuguesa dos Industriais de Marmores e Ramos Afins (Portugal).
- La Palma Research Centre SL (Spain).
- University of Miskolc, Faculty of Earth Science Engineering (Hungary).
- Federation Europeenne des Geologues (Belgium).
- Geoloski Zavod Slovenije (Slovenia).
- Resources Computing International Ltd (United Kingdom).
- Geo-Montan Geologus Ltd (Hungary).
- Tallinn University of Technology (Estonia).

- Polska Academia Nauk Instytut Gospodarki Surowcami Mineralnymi i Energia (Poland).
- K-UTEC AG (Germany).

Publications

Several contents of this thesis were previously published in journal articles in:

- Stein & Kies 167 (2020) [1].
- BHM Berg- und Hüttenmännische Monatshefte 166 (2021) [2, 3].
- BHM Berg- und Hüttenmännische Monatshefte 167 (2022) [4, 5].
- BHM Berg- und Hüttenmännische Monatshefte 168 (2023) [6].

Further content of this thesis was published in conference papers with corresponding presentations at:

- AusIMM Future Mining 2019 - 4th International Future Mining Conference (2019). Sydney, Australia [7].
- ISARC 2020 - The 37th International Symposium on Automation and Robotics in Construction (2020). Kitakyshu, Japan / online [8].
- AusIMM Future Mining 2021 - 5th International Future Mining Conference (2021). Australia / online [9].
- Procemin GEOMET 2022 - 18th International Conference on Mineral Processing and Geometallurgy (2022). Santiago de Chile, Chile / online [10].
- ISCSM 2023 - 15. Internationales Symposium für kontinuierliche Tagebautechnik (2023). Technische Universität Bergakadamie Freiberg, Germany [11].

Some content was also previously submitted in project reports to the European Commission and the research consortium, which will be published collectively after project closing in [12–16]. The individual publications are referenced in the beginning of each chapter and the corresponding content is highlighted.

Abstract

The modern mining industry faces increasing challenges related to sustainability and raw material shortage that require additional efforts in research and development. A significant trend in underground mining is the movement towards zero personnel, which demands the full mechanization and subsequent automation of the mining process up to the use of fully autonomously operating robots. Future mining robots will require adapted excavation technologies to be capable of mining raw materials with less power and lower masses.

A review of excavation technologies has been conducted in order to perform preliminary evaluations of their potential applicability. Moreover, performance parameters such as the excavation rate and specific energy but also the expectable reaction forces have been estimated by using theoretical approaches on the example of a robot with a mass of 1500 kg.

The thesis is further discussing the predictability of the cutting forces of small, longitudinal part-face cutter heads in soft rock conditions. This includes a review of theoretical rock cutting models for estimating the cutting force of conical pick tools, experimental tests of a small, longitudinal part-face cutter head and assessing the applicability of single-pick rock cutting models to full-scale cutting operations. Experimental cutting tests of specimens with three different rock strengths (UCS = 16, 23 and 30 MPa) have been conducted successfully and the obtained results were taken to develop a sophisticated modelling approach to predict the cutting forces. Due to the comparatively small dimensions of the conical pick tools, major deviations between the single-pick cutting force models and measurement results could be found. Consequently, a dynamic model has been developed which is capable of including the kinematics of the pick cutting depth in the cutting force prediction. By a combination of the two new approaches, the cutting operation of a longitudinal part-face cutter head can be simulated. The results are highly satisfactory and showed a mean relative deviation of 7.2 % between the measured and simulated total cutting forces.

Eventually, conceptual designs of selected excavation technologies were developed that might be used in future works. These include three individual rock drilling systems, a part-face cutting tool, a high-pressure waterjet cutting tool and a hydrofracturing tool. The proposed concepts shall not be considered as full-fledged designs but shall provide a basis for future excavation systems of small-scale mining robots.

Kurzfassung

Die moderne Bergbauindustrie steht vor wachsenden Herausforderungen in Bezug auf Nachhaltigkeit und Rohstoffknappheit, die zusätzliche Anstrengungen im Bereich der Forschung und Entwicklung erfordern. Ein steigender Trend im Untertagebau ist die Entwicklung vollständig mechanisierter und automatisierter Prozesse bis hin zum Einsatz völlig autonomer Roboter. Künftige Bergbauroboter werden angepasste Abbautechnologien benötigen, um mit weniger Leistung und geringeren Massen eine ausreichende Produktivität zu garantieren.

Im ersten Schritt wurde eine Übersicht über diverse Abbautechnologien erstellt, um eine vorläufige Bewertung derer potenziellen Anwendbarkeit vorzunehmen. Darüber hinaus wurden Leistungsparameter, wie Abbaurate und spezifische Energie, aber auch die zu erwartenden Reaktionskräfte, mit Hilfe theoretischer Ansätze am Beispiel eines Roboters mit einer Masse von 1500 kg ermittelt.

Diese Arbeit befasst sich ferner mit der Vorhersagbarkeit der Schneidkraft von kleinen Längsschneidköpfen in weichem Gestein. Dies umfasst einen Überblick über theoretische Modelle zur Abschätzung der Schneidkraft einzelner Rundschaftmeißel, experimentelle Tests eines kleinen Längsschneidkopfes und die Bewertung der Anwendbarkeit von Einzelmeißel-Modellen auf die Berechnung der Schneidkräfte eines Längsschneidkopfes. Experimentelle Schneidversuche an Proben mit drei unterschiedlichen Gesteinsfestigkeiten (UCS = 16, 23 und 30 MPa) wurden erfolgreich durchgeführt und die erzielten Ergebnisse wurden zur Entwicklung einer Methodik zur Vorhersage der Schneidkräfte verwendet. Aufgrund der vergleichsweise kleinen Dimension der eingesetzten Rundschaftmeißel wurden große Abweichungen zwischen den Einzelmeißel-Modellen und den Messergebnissen festgestellt. Folglich wurde ein dynamisches Modell entwickelt, das den Effekt der sich verändernden Schnitttiefe eines Meißels in die Vorhersage der Schneidkraft einbeziehen kann. Die Simulationsmethodik liefert sehr zufriedenstellende Resultate und die Ergebnisse zeigten eine mittlere relative Abweichung von 7.2 % zwischen den gemessenen und simulierten Gesamtschneidkräften.

Schließlich wurden Konzepte für ausgewählte Abbautechnologien entwickelt: Mehrere Hartgesteinsbohrsysteme, ein kleinmaßstäbliches Teilschnittsystem, ein Hochdruckwasserstrahlschneidwerkzeug und ein weiteres System, welches mithilfe von unter Druck stehendem Wasser Gestein lösen kann. Diese vorgeschlagenen Konzepte sind nicht als vollwertige Entwicklungen zu betrachten, sondern sollen als Grundlage für zukünftige Abbausysteme für kleine Bergbau-Roboter dienen.

Contents

List of abbreviations

Abbreviation	Description
AR	Advance Rate
BTS	Brazilian Tensile Strength
CAI	Cerchar Abrasivity Index
DEM	Discrete Element Method
DTH	Down-the-hole
ER	Excavation Rate
IBR	Instantaneous Breaking Rate
ICR	Instantaneous Cutting Rate
LCH	Longitudinal Cutter Head
MTBM	Mini Tunnel Boring Machine
NCR	Net Cutting Rate
NPR	Net Production Rate
PR	Penetration Rate
RF	Reaction Force
RMR	Rock Mass Rating
ROP	Rate of Penetration
RQD	Rock Quality Designation
SE	Specific Energy
SID	Sump-in Depth
TBM	Tunnel Boring Machine
TCD	Total Cutting Depth
TCH	Transversal Cutter Head
TF	Thrust Force
UCS	Uniaxial/Unconfined Compressive Strength

1 Introduction

This chapter gives an introduction to robotics in mining, especially robots used for excavation and the accompanying technological challenges. The work in this thesis includes a review and an applicability assessment of selected excavation technologies for small-scale mining robots. Moreover, a major topic is the experimental testing of a small, longitudinal part-face cutter head and the subsequent development of an approach for simulating the cutting process. The thesis completes with propositions of conceptual design ideas of small-scale excavation tools.

1.1 Background

At this point in time, the world is confronted with challenges related to climate change and numerous undertakings are in process to pave the way to a sustainable future. The shortage of raw materials and the aim of more sustainable mining operations demand a rethinking of conventional approaches by inventing novel technologies which require sophisticated research and development efforts. To address these commitments, the use of fully automated machines and autonomous robots is being explored [17]. Small robots could be suitable for tasks in hazardous terrains, exploration of abandoned or flooded mines, and mining in difficult to access deposits. To meet the demands of future scenarios, existing technologies are required to be adapted and new approaches developed.

The design and technologies used in mining robots may differ significantly from conventional machines to achieve greater flexibility and mobility. Therefore, current mining technologies need to be re-evaluated to be capable of dealing with future obstacles. Numerous research and development projects are underway to develop robots for underground environments, which require new approaches and adaptations of commercial off-the-shelf (COTS) products due to their small size and limited power. [18]

It is worth noting that mobile robots are often characterized by a significantly lower mass (usually < 100 kg) [19], while mining machines are designed for high

performance and can weigh anywhere from 10 to over 100 tonnes, resulting in a substantial difference in mass and performance between the two types of machines. The classification of robot types and industrial mining machinery is presented in Figure 1.1.

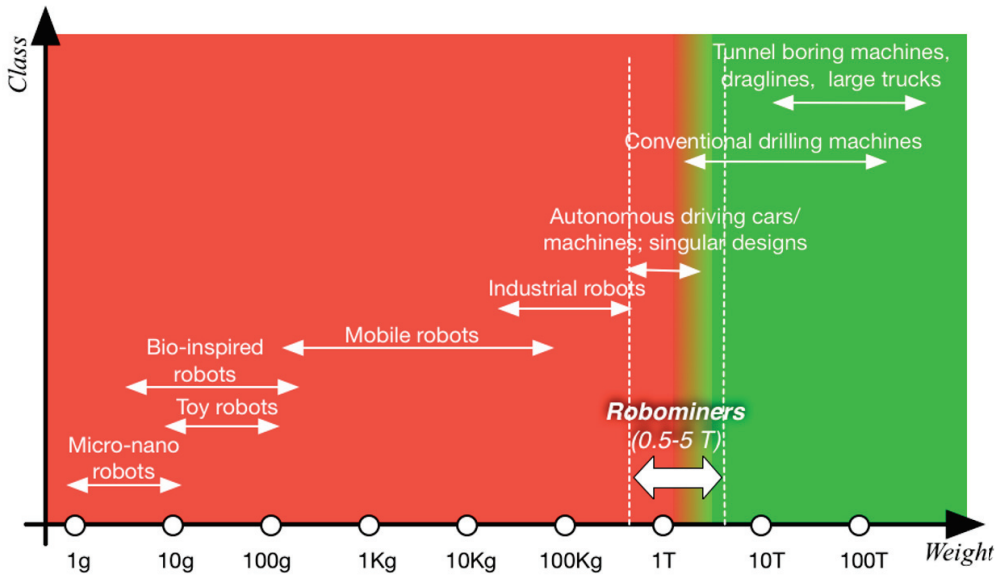

Figure 1.1: Classification of robots and mining equipment [20]

1.1.1 Limitations

Throughout this thesis, excavation systems are separated into drill and blast, mechanical, alternative and combined systems, with the first two being the most commonly used in modern mining. To ensure efficient and economical use, the mining system needs to meet a number of requirements, such as adequate advance and extraction performance, which are significantly influenced by the rock to be mined. Mechanical cutting systems have the great advantage of a continuous material excavation process, whereas drill and blast is applied where the rock strength exceeds the mechanical machine's capabilities.

In mechanical excavation systems, the interaction between an excavation tool and the rock causes reaction forces of which the carrier machine has to be capable of handling. The extent of these reaction forces varies depending on the excavation method and rock strength, whereas the maximum manageable force is highly depending on the machine mass. [2, 21]

Conventional, mechanical mining methods, such as part-face or full-face cutting methods, are subject to performance limitations. These limitations are primarily

imposed by the rock's strength and abrasivity as well as the machine's mass and power. While drill and blast remains a cost-effective approach to tunnelling and mining, it also implicates several significant drawbacks that cannot be overlooked. These disadvantages include safety concerns during stockpiling and transportation, the generation of toxic fumes and gases, as well as vibrations and noise and the complexity of automation. Moreover, legal restrictions regarding automated/autonomous blasting further compound these difficulties. To overcome these challenges, there is a growing trend towards the development of fully automated, continuous mining methods. Mechanical mining methods, such as part-face and full-face cutting systems, have emerged as crucial technologies that can serve as both heading and mining methods. However, these methods are severely limited, particularly part-face cutting machines (roadheaders), by rock strength and abrasivity. In contrast, full-face cutting machines with cutting discs are capable of penetrating higher rock strengths but have considerably less flexibility and mobility. Roadheaders are capable of cutting curves and junctions to some extent, whereas full-face cutting machines have substantially larger turning radii. [8, 22] Figure 1.2 depicts the mobility of mechanical heading and mining machines versus the uniaxial compressive strength of the rock to be excavated and shows a "gap" for new, alternative technologies.

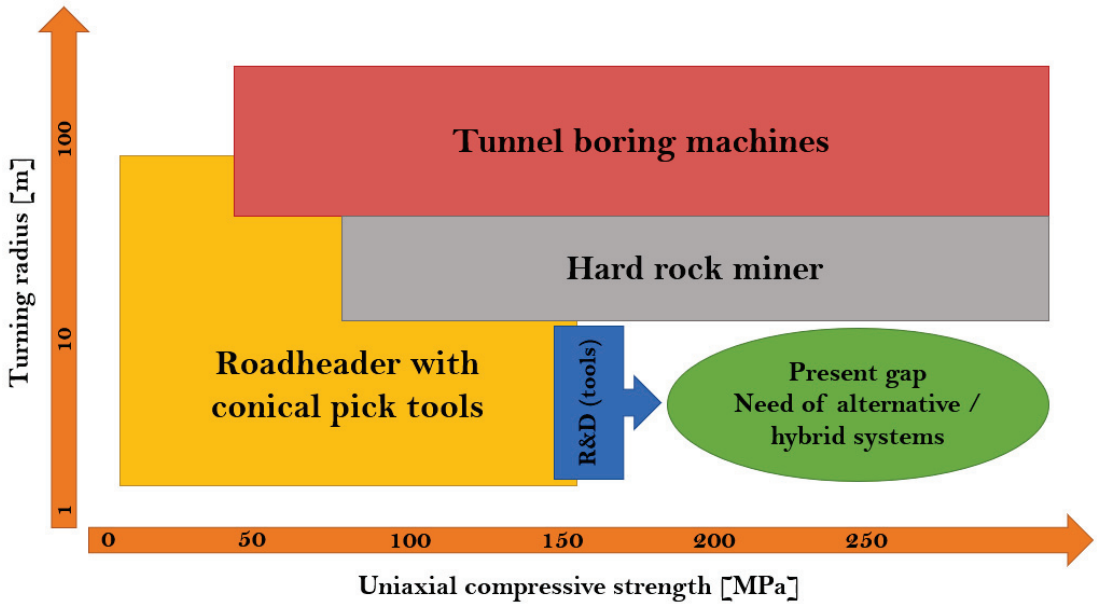

Figure 1.2: Limited mobility of mechanical excavation machines [4]

The issue described here also applies to smaller machines, but with far greater restrictions. This thesis deals with the challenges mentioned and tries to provide a guideline for the application of excavation systems in small-scale robots.

1.2 Research objective

This thesis aims for providing extensive information about the potential use of excavation systems in small, robotic mining machines. Hence, the main focus should be placed on determining maximum allowable specifications of excavation tools without exceeding the capabilities of the carrier machine. Enabling this, state-of-the-art technologies should be reviewed and assessed in terms of their applicability by analyzing performance indicators such as excavation rate, specific energy and expectable reaction forces.

Further on, a production tool system for a prototype of a small-scale mining robot should be developed and tested with a corresponding test setup. By taking advantage of the measurement data, the ascertained results should be compared to data reproduced with suitable approaches found in literature and a methodology for modelling the excavation process should be developed. This methodology shall be capable of predicting performance-related parameters.

The outcome of the applicability assessment should also be taken to outline conceptual designs of small-scale excavation tools for future small-scale mining robots.

Expected scientific contributions of this thesis are:

- Overview and applicability assessment of eligible excavation systems for small-scale mining robots.
- Determination of specified criteria, requirements and limitations to categorize selected excavation methods.
- Test setup to evaluate the performance of a small-scale excavation tool, integrated as production tool in a prototype of a robotic miner.
- Detailed understanding of the operating principle of this production tool and the resulting excavation forces.
- Modelling approach to predict performance-related parameters.
- Conceptual designs of potential excavation technologies used as production tools for future mining robots.

1.3 Outline of the thesis

In Chapter 2, a brief review of the state of the art of excavation systems is given. A detailed summary of various excavation methods can be found in Appendix A, particularly dealing with the potential application in small-scale mining robots and related developments are introduced. Selected excavation methods have undergone a detailed applicability assessment by utilizing approaches for estimating performance-related parameters. This part is presented in Chapter 3 and further parameter studies are given in Appendix B,.
Chapter 4 is dealing with the analysis of the performance of a small part-face cutter head. The development of a full-scale test setup and the testing methodology are covered within this chapter. The entirety of the test results are presented in Appendix C. In Chapter 5, a new approach for modelling part-face cutter heads to predict the cutting forces occurring in a cutting process is described. The content includes the review of profound rock cutting theories for single conical pick tools, the difficulties of upscaling to estimate the cutting forces of a full-scale cutter head and the development of a methodology which enables the process of simulating a longitudinal part-face cutter head's cutting behaviour. Extensive parameter studies and exemplary results can be found in Appendix D.
The verification and validation of the model have been conducted through several test cases. This part is discussed in Chapter 6 and continuative data is attached in Appendix E. After evaluating the applicability and feasibility of the presented excavation systems, selected conceptual propositions of small-scale excavation tools are depicted in Chapter 7.
Eventually, the overall conclusions are summarized in Chapter 8 and a suggested outlook is given in Chapter 9.

2 State of the art

The aim of this chapter is providing a brief review of state-of-the-art excavation technologies. The individual excavation methods including a preliminary assessment of the applicability as production tool system in a small-scale mining robot are described comprehensively in Appendix A. Further on, an overview of robot-like machinery applied in mining with tasks focused on excavation and exploration is given. Parts of the content have already been documented in [15].

2.1 Excavation technologies

This section summarizes established excavation technologies used in mining and tunnelling. In mining, the excavation of material can be performed by a variety of methods. Various technologies are used in the industry or have been tested in research and development projects and the individual excavation methods regarded in this thesis can be classified in four main categories: Drill and blast, mechanical excavation, alternative excavation and combined excavation (Figure 2.1).

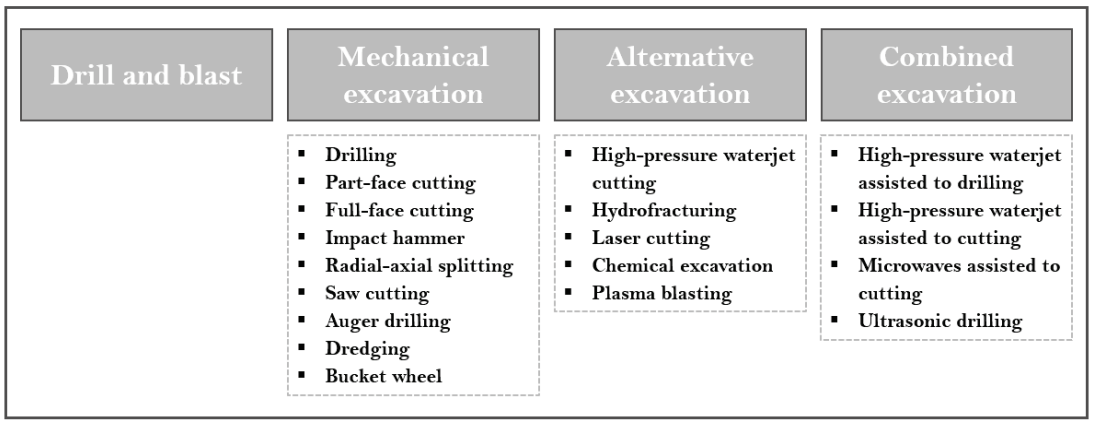

Figure 2.1: Classification of excavation methods

In the current mining industry, drill and blast and mechanical excavation state the two most prominent methods. Historically seen, drill and blast has been the

most popular method to excavate material because of its high efficiency, but the share of mechanical excavation is increasing due to new technologies which are able to penetrate hard rock material [23]. Advantages and disadvantages of each method are described in the corresponding sections in the appendix.
Further on, the urge of accessing new areas, excavating harder material with less energy input and using autonomously working machines have forced research and development to explore other technologies like alternative or combined excavation systems. Alternative excavation methods rely on different energy inputs such as high-pressure waterjet cutting, laser cutting or hydraulic fragmentation. Due to the high specific energy (amount of energy to excavate a unit volume of material) requirements, these methods are not economically applied at this point. Combined excavation systems are trying to exploit and merge the benefits of conventional and alternative systems to reduce energy needs and create more profitably working systems. [22, 24]

Following rock strength classes can be defined and are used throughout this thesis:

- UCS $<$ 30 MPa: Soft rock.
- 30 MPa $<$ UCS $<$ 70 MPa: Medium hard rock.
- 100 MPa $<$ UCS $<$ 200 MPa: Hard rock.
- UCS $>$ 200 MPa: Very hard rock.

Specific mining terms and abbreviations are used in this thesis, which are briefly explained below:

- UCS: Uniaxial or unconfined compressive strength in [MPa] – the compressive strength of rock.
- BTS: Brazilian tensile strength in [MPa] – the tensile strength of rock.
- Abrasivity or abrasiveness: The property of a rock that causes surface wear by friction to a tool.
- PR / ROP: Penetration rate / Rate of penetration in [cm/min], [cm/h], [m/min] or [m/h] – the speed at which a tool advances into the rock mass.
- AR: Advance rate in [m/h] or [m/d] – the progress or excavated length in tunnelling or mining per time unit (mostly hours or days).
- ER: Excavation rate in [m^3/h] – the excavated volume (cubic meters) per time unit (mostly hours).
- SE: Specific energy in [kWh/m^3] or [MJ/m^3] – the required energy to excavate a unit volume of rock (mostly m^3).

2.1.1 Drill and blast

Drill and blast is prominently applied in mining and tunnelling to excavate hard rock. The ability to excavate very hard rock with a high excavation rate per blast cycle is a crucial advantage over mechanical excavation [25]. Although this method is widely used in mining and tunnelling, there are some disadvantages which come along with it:

- Discontinuous operation.
- Creation of toxic fumes and gases and therefore need of a ventilation system.
- Noise, vibrations, fly-rock and risk by handling explosives.
- Additional working tasks and equipment required. [24]

A drill and blast cycle is basically consisting of several different tasks which can be seen in Figure 2.2.

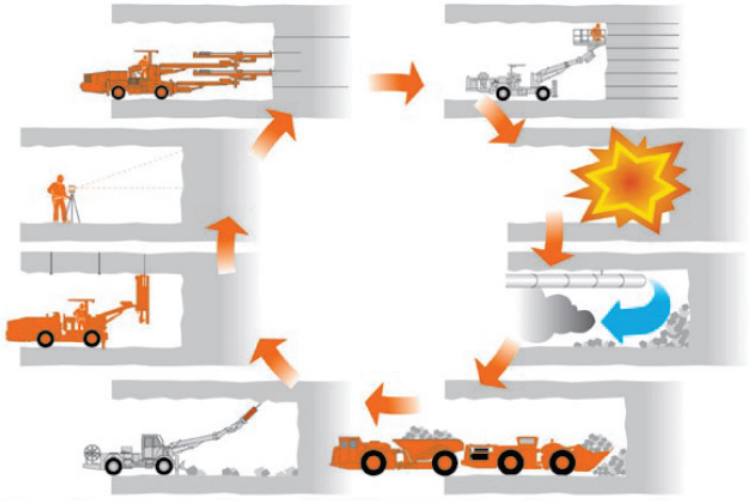

Figure 2.2: Drill and blast cycle [26]

Primary step is drilling the boreholes for the explosives with a drill jumbo or a drill rig. Those drilling machines are usually equipped with one or more rock drills. Drilling techniques such as top-hammer, down-the-hole-hammer or rotary drills are used [8]. This specific rock drilling types are described in Appendix A.2.1. The consecutive step is cleaning the boreholes followed by charging the explosives. After blasting happens, the air is ventilated to reduce the gas concentration. The excavated material is then hauled with a loader from the muck pile onto a truck and transported to a processing area. The newly created free surface needs to be scaled by rippers or mechanical cutting machines to remove loose material and

shape the tunnel geometry if undercut or overcut has been produced. The last step of a drill and blast cycle is stabilizing the roof with anchoring systems such as rock bolts. The cycle is then repeated, see [25] for details.
Advantages of drill and blast compared to mechanical excavation are:

- Generic applicability (soft to very hard rock).
- Flexible operation (suitable for various ground conditions).
- High production rate and high fragmentation grade. [24]

During the blasting process, different stresses are exerted to the rock. The boreholes are drilled parallel to a free face when blasting. The high stress intensity of a blast in a borehole results in the generation of a compressive stress wave through a crushed fractured zone surrounding the borehole. The radius of this zone is typically about twice the borehole diameter. Outside the shock zone is the transition zone where rock continues to crack but not be crushed. The radius of this zone is four to six times the borehole diameter. After the compressive stress wave passes through the transition zone, its state of stress intensity decreases as it enters the seismic zone. Rather than interacting with cracks in the rock, the fractures formed are extensions of the ones formed in the transition zones. The compressive stress wave is reflected back to the borehole at the free face as a tensile stress wave. Crack extension is promoted by the passage of the tensile stress. Because rock is weaker in tension than compression, this stress condition results in greater fracturing. [27]
A design of a development blast can be seen in Figure 2.3.

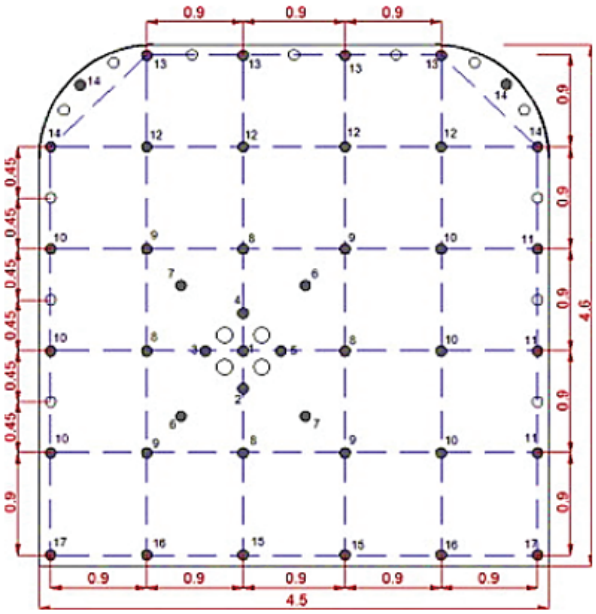

Figure 2.3: Design of development blast [27]

Development blasting is conducted to provide access for people and equipment to a stope. Horizontal access to a stope is provided by excavating an underground opening. These are termed drifts and cross-cuts and may be horizontal or inclined. Drifts provide access from the connection to surface to stope access. The cross-cuts provide access from the drifts to the stopes. To excavate a drift, drilling is normally conducted along the grade of drift being excavated from an opening. The drilling leaves a borehole that is perpendicular to the free face from where the drilling is conducted. Therefore, the compressive stress wave from the borehole would flow into the surrounding host rock and not reflect. [28]

To get the rock to fracture, a free face has to be excavated. This is conducted by including a burn cut when drilling the face. Burn cuts are begun by drilling large diameter holes along the grade of the drift. These large diameter holes are left unloaded. They provide the desired primary free face. Holes numbered 1 to 5 in Figure 2.3 are blasted in succession to form the first cut (burn cut). The pairs of holes 6 and 7 are then blasted in succession and the burn cut is formed. After the burn cut forms a free face, the sequences of holes 8-13 is actuated. [25]

Applicability to a small-scale mining robot

The most important feature is the capability of excavating larger amounts of very hard rock with one blast. Furthermore, a complete mechanization is state-of-the-art, however, a full automation of the charging process is a complex challenge to be mastered. Drilling is the most time-consuming step of drill and blast excavation. To keep the blast cycle to a minimum, the penetration rate of the drill and the number of boreholes are crucial. Drill and blast is a sophisticated and sensitive process - multiple, individual tools and working steps increase the efforts of rock excavation and need to be adjusted precisely. Advantages are the low reaction forces acting on the robot and the ability of excavating hard rock.

To excavate reasonable amounts of hard rock with the given boundary conditions, drill and blast is the option with the greatest potential for a future, small-scale mining robot. On the other hand, there are several aspects which make the use of drill and blast less attractive, such as: Tasks which demand various tools, challenging to be integrated in one robot, are required (Figure 2.4). The automation of the entire drill and blast cycle and minimization of risk of failure will be complex processes. Cleaning the borehole from debris before charging is necessary to position the explosives. Special explosives and igniters are required. Shock waves, vibrations and fly-rock create potential risks for the robot, especially under water. Scaling of tunnel surface and stabilization needs also be done to prevent rock bursts or collapses. [8]

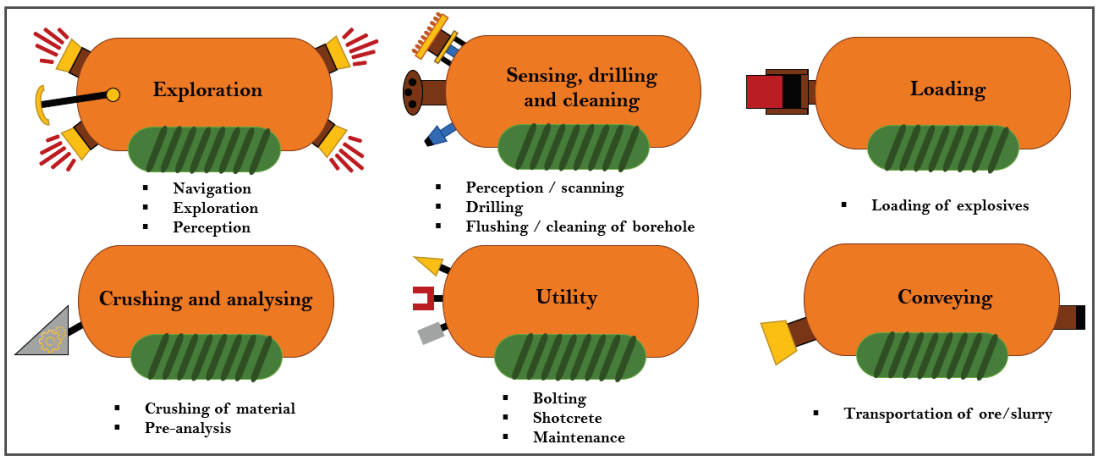

Figure 2.4: Drill and blast – Robot family [8]

Although drill and blast is the only option to operate in hard rock conditions due to the small size, low power and mass of a robot, the above mentioned aspects state obstacles which need to be overcome in a future scenario and therefore, drill and blast has not been considered for a detailed applicability assessment.

2.1.2 Mechanical excavation

Since the last few decades, there is an ongoing trend towards fully automated and mechanized systems, which led to an increase of the use of mechanical excavation systems in mining. Mechanical excavation systems include technologies which are loosening rock from the rock face entirely by mechanical energy input, such as pick and disc cutting methods, drilling or impact hammering. Besides drill and blast, mechanical excavation systems are the most applied excavation tools in underground mining scenarios due to their benefits [24, 29]. To the most common machines in the group of mechanical excavators belong: Roadheaders, tunnel boring machines, continuous miners, longwall drum shearers, borer miners, drill jumbos, impact hammers and bucket wheel excavators. Auger drills are applied in coal seam mining and rock cutting saws are mainly used in quarrying tasks [8].

Depending on the mechanical excavation technology, various rock cutting tools have been developed to cut rock. An overview chart of rock cutting tools is shown in Figure 2.5. [30]

Drag or conical pick tools are generally used for soft to medium hard rock with low abrasivity. Hard rock material requires machines equipped with disc or strawberry cutters [30].

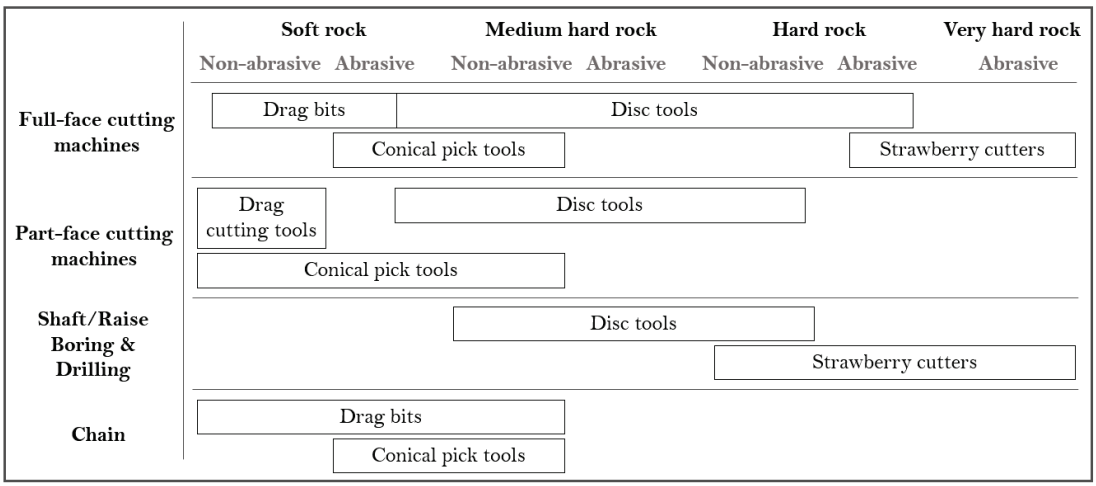

Figure 2.5: Classification of rock cutting tools (after [30])

In [24], *Bilgin* listed some general advantages of mechanical excavations compared to drill and blast:

- Continuous excavation process.
- Overall safer operation.
  - No explosive handling.
  - No vibration due to explosions.
  - No toxic gases.
- Uniform muck size with evenly distributed particle sizes.
  - Easier to haul and load.
  - No secondary breakage needed.
- Greater potential of selective mining.
  - Ore to waste rock ratio is generally more favourable.
- Higher production rate in good ground conditions.
- High potential for automation.

The cycle of drill and blast is presented in Figure 2.2 and can be compared to a tunnelling process of a roadheader, which is shown in Figure 2.6. The overall amount of required tasks in one cycle can be reduced to two main tasks: Excavation (ore, waste rock and profiling) combined with hauling/conveying and roof support [31]. The continuous process results in a higher and more efficient operation in soft to medium hard rock conditions [22, 24, 29].

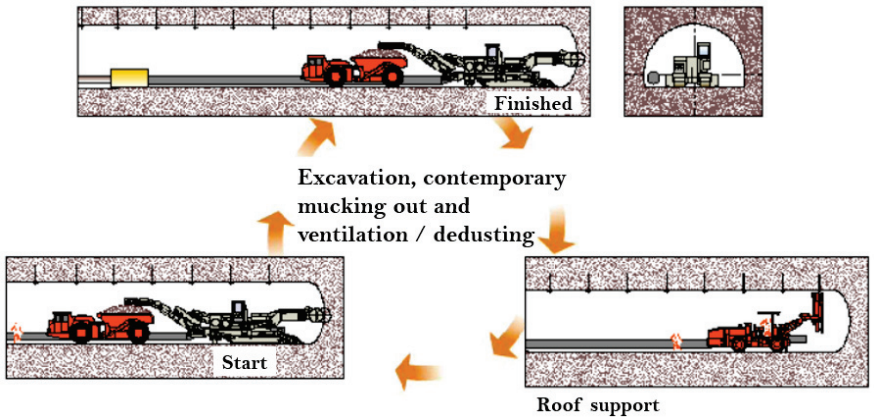

Figure 2.6: Tunnelling process of a roadheader [32]

Disadvantages of mechanical excavation systems compared to drill and blast are:

- Higher initial costs of machines, equipment and infrastructure.
- Less flexibility: Sensitive to ground conditions and cross-section shapes are limited.
- Less mobility: High turning radii and limited reach of production tool.
- Higher demand of maintenance due to wear.
- Inability to excavate hard rock. [24]

2.1.3 Alternative excavation

Alternative excavation methods cover all other excavation methods besides drill and blast and mechanical excavation systems. Compared to conventional methods, alternative excavation systems apply non-conventional techniques to excavate material such as fluid, electric, chemical or laser technologies. Conventional excavation systems, especially mechanical excavation systems, are limited by the rock strength and the high resulting reaction forces. [7]

Alternative excavation tools have been developed in terms of reducing those forces by using much more energy-dense technologies. Many lab tests with various alternative excavation tools have been conducted, but the major drawback is the high specific energy of such systems. They are – compared to mechanical excavation and drill and blast – much less efficient and require high power to extract only a fraction of rock as mechanical cutting systems. [10]

Hydrofracturing is an alternative excavation technique which combines two different tools: Mechanical rock drill creating the drillholes, and a high-pressure water

inducing tool which fractures the rock. The methodology is comparable to drill and blast, except the use of hydraulic energy to break the material. [33]
Similar to a radial-axial splitter, foam injection systems have also been investigated in the past. *Chapman* presented an indexing boom with controlled foam injection barrel and drill steel (Figure 2.7) [34].

Figure 2.7: Controlled foam injection barrel and drill steel [34]

Controlled foam injection rises several problems concerning the foam used to split the rock and is therefore not further evaluated: Environmental impact of foam, separation of foam and rock and transportation, processing and recycling of foam.

Thermal and laser excavation systems have been assessed in detail in [33]. By reason of their low efficiency and high energy input they won't be investigated further. In Figure 2.8, a laser drilling system is shown.

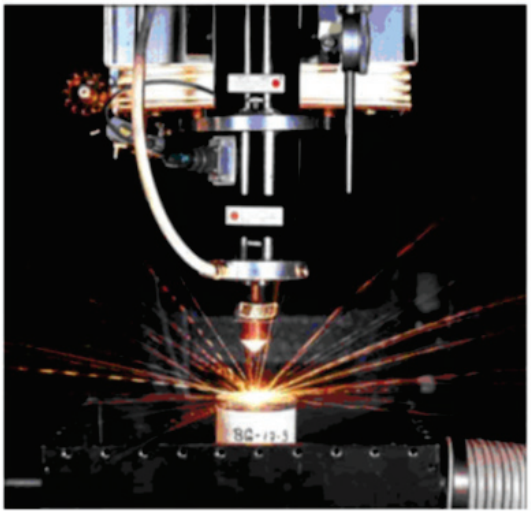

Figure 2.8: Laser drilling system on rock sample [33]

Small mining robots are even much more limited in terms of power and rock

strength, which means alternative excavation systems might be an interesting option as production tool systems due to their abilities to excavate harder and more abrasive rocks. Specific energy is also depending on the machine's power and alternative excavation systems will still be not as efficient as other methods, but the much lower reaction forces make them, besides drill and blast, attractive methods which could be applied in future mining scenarios including small mining robots targeting hard rock deposits. [8, 10, 33]

2.1.4 Combined excavation

Combined excavation methods utilize technologies from conventional (mechanical) and alternative excavation systems. Also known as hybrid excavation systems, those tools combine two different energy sources and aim to take advantage of both of them. A primary tool is applied to pre-weaken the rock to reduce the required excavation forces of the secondary rock excavation tool. [8, 21, 22]

Combined excavation tools purposely attempt to reduce the rock mass rating to increase the net production rate [33]. The rock mass rating describes the condition of the present geology and includes the uniaxial compressive strength, number and orientation of joints and condition of joint faces. Reducing the rock mass rating can be done with various methods which introduce crack networks and lower the rock strength, generate free surfaces or initiate additional stresses on the rock surface. [21]

Joy Global and *CRC Mining* have been working together on a novel combined excavation machine, equipped with an oscillating disc cutter called *DynaCut™* (Figure 2.9) and have also conducted cutting tests with an assisting 800 bar waterjet to support the cutting process. [21, 35]

Figure 2.9: *Joy Global* DynaCut machine © *Joy Mining* [35]

2.1.5 Applicability in selected rock conditions and conclusion

Following, a summary of the benefits and drawbacks of the presented excavation methods is given as well as an assessment of each's applicability in selected rock conditions. The following rock conditions have been defined with general geological risk factors and constraints:

- High lithostatic pressure (HLP): High principal stresses in vertical direction because of overburden.
- High shear stress (HSS): Displacements due to crossing of tectonic faults or shear zones and can lead to rock bursts.
- Friable or fractured rocks (FFR): Rocks of very low cohesion or tensile strength, which create instabilities and potential rock fall/bursts.
- Hard or tough rocks (HTR): Hard rock conditions or individual hard rock insertions.
- Heterogeneous rocks (HR): Contact of rock bodies of different strengths, which become planes of shear during deformation events.
- Faults and joints (FJ): Local zones of weakness, which may act as conduit for water or instabilities due to displacements.
- Inrush of water (IW): Intersection of mine with water bodies and creation of instabilities.
- Cavernous grounds (CG): Rocks of cohesive but water-soluble material can form caverns and eventually collapse.
- Seismic risks (SR): Displacements and/or energy release in form of seismic waves because of change in the stress field induced by mining.

In Table 2.1, the applicability of each excavation method in the selected rock conditions is described, whereas more detailed assessments of the finally selected excavation methods are in the corresponding sections in Chapter 3. This assessment is valid for a robotic miner with a mass of approximately 1-1.5 tons. A general risk are instabilities due to weak rock mass, displacements, faults and high principal stresses which can eventually lead to rock fall or rock bursts and in the worst case to a complete collapse of a tunnel or a mine. Those risks need to be mitigated in advance with the help of rock mechanics and certain technologies and should be reduced to a minimum. Machinery and equipment also should be capable

of withstanding certain smaller rock falls. Roof support should also be done if necessary.

Requirements and limitations of the investigated excavation methods are summarized in Table 2.2. For this assessment, the following parameters have been considered:

- Maximum uniaxial compressive strength of material to be excavated (UCS).
- Magnitude of expectable excavation forces (RF).
- Potential of downscaling to a small scale (SP).
- Requirement of auxiliary equipment (EQUIP).
- Requirement of maintenance (MAIN).
- Mobility and manoeuvrability (MM).
- Flexibility in terms of applicability to different rock/ground conditions (FLEX).
- Automation capability (AUT).
- Availability of commercial-off-the-shelf products (COTS).

According to the findings of the preliminary assessment of the excavation methods (discussed in Appendix A), the following technologies have been considered for an extensive analysis in Chapter 3: Rock drilling, part-face cutting, full-face cutting, impact hammer, high-pressure waterjet cutting and hydrofracturing.

Table 2.1: Applicability of excavation methods in selected rock conditions

	HLP	**HSS**	**FFR**	**HTR**	**HR**	**FJ**	**IW**	**CG**	**SR**
DB	Yes	Yes[2]	Yes[2]	Yes	Yes[2]	Yes[2,4]	Yes[2,4]	Yes[2,4]	Yes[2]
DRILL	Yes	Yes	Yes	Yes	Yes	Yes	Yes	Yes	Yes
PFC	Partially[1]	Partially[1]	Partially[1]	No	Partially[1]	Partially[1]	Partially[1]	Partially[1]	Partially[1]
FFC	No	No	No	No	No	No	No	No	No
IH	Partially[1]	Partially[1,2]	Partially[1,2]	No	Partially[1,2]	Partially[1,2]	Partially[1,2]	Partially[1,2]	Partially[1,2]
RAS	Partially[1]	Partially[1,2]	Partially[1,2]	No	Partially[1,2]	Partially[1,2,4]	Partially[1,2,4]	Partially[1,2,4]	Partially[1,2]
DR	Partially[1]	Partially[1]	Partially[1]	No	Partially[1]	Partially[1]	Partially[1]	Partially[1]	Partially[1]
BWE	No	No	No	No	No	No	No	No	No
SC	No	No	No	No	No	No	No	No	No
DWC	No	No	No	No	No	No	No	No	No
HPWJ	Yes[1]	Yes[1,2]	Yes[1,2]	Yes[1]	Yes[1,2]	Yes[1,2,3]	Yes[1,2,3]	Partially[1,2,3,6]	Yes[1,2]
HF	Yes[1]	Yes[1,2]	Yes[1,2]	Partially[1]	Yes[1,2]	Yes[1,2,3]	Yes[1,2,3]	Partially[1,2,3,6]	Yes[1,2]
PB	Yes	Yes[2]	Yes[2]	Yes[2]	Yes[2]	No[5]	No[5]	Partially[2,5]	Yes[1,2]
HPWJ-D	Yes	Yes	Yes	No	Yes	Yes[3]	Yes[3]	Yes[3,6]	Yes
HPWJ-C	Partially[1]	Partially[1]	Partially[1]	No	Partially[1]	Partially[1,3]	Partially[1,3]	Partially[1,3,6]	Partially[1,2]
M-C	Partially[1]	Partially[1]	Partially[1]	No	Partially[1]	No[5]	No[5]	Partially[1,5]	Partially[1,2]

DB - Drill and blast | DRILL - Drilling | PFC - Part-face cutting | FFC - Full-face cutting | IH - Impact hammer | RAS - Radial-axial splitting | DR - Dredging | BWE - Bucket wheel excavation | SC - Saw cutting | DWC - Diamond wire cutting | HPWJ - High-pressure waterjet cutting | HF - Hydrofracturing | PB - Plasma blasting | HPWJ-D - High-pressure waterjet assisted to drilling | HPWJ-C - High-pressure waterjet assisted to cutting | M-C - Microwaves assisted to cutting

[1]Highly depending on the rock strength.
[2]Uncontrolled rock falls/bursts and subsequent scaling (removal of loose material) required.
[3]Ambient water pressure needs to be exceeded by applied water pressure.
[4]Effect of ambient water needs to be taken into account.
[5]Not applicable in water.
[6]Use of water can create more instabilities.

Table 2.2: Requirements and limitations of excavation methods

	UCS	RF	SP	EQUIP	MAIN	MM	FLEX	AUT	COTS
DB	> 200 MPa	Low[3]	High	Yes[6,7,8,9]	Yes[12]	Medium	Medium[14]	Medium	Partly[16]
DRILL	> 200 MPa	Low	High	No[11]	Yes[12]	N/A[11]	Medium[5,14]	High[15]	Yes[16]
PFC	< 150 MPa	High	Medium[5]	Yes[7,8,9]	Yes[12]	Medium	Medium[5,14]	High[15]	Yes[17]
FFC	> 200 MPa	Very high	Low[5]	Yes[7,8,9]	Yes[12]	Low	High	High[15]	Yes[18]
IH	< 200 MPa	High	Medium[5]	Yes[7,8]	Yes[12]	High	Medium[5,14]	High	Yes[16]
RAS	< 100 MPa	High	Medium[5]	Yes[6,7,8,9]	Yes[12]	Medium	Medium[5,14]	Medium	Partially[1,2]
DR	< 50 MPa	N/A[4]	Low[5]	Yes[7,10]	Yes[12]	Low	Low[5]	N/A	No
BWE	< 50 MPa	N/A[4]	Low[5]	Yes[7]	Yes[12]	Low	Low[5]	High	No
SC	N/A[1,2]	N/A[1]	N/A[1]	N/A[1]	N/A[1]	N/A[1]	N/A[1]	N/A[1]	N/A[1]
DWC	N/A[1,2]	N/A[1]	N/A[1]	N/A[1]	N/A[1]	N/A[1]	N/A[1]	N/A[1]	N/A[1]
HPWJ	> 200 MPa	Low	High	Yes[7,9]	No[13]	High	High	High	Yes
HF	< 200 MPa	Medium	Medium[5]	Yes[6,7,8,9]	Yes[12]	Medium	Medium[5,14]	Medium	Partly[16]
PB	N/A[2]	Low[3]	High	Yes[6,7,8,9]	Yes[12]	Medium	Medium[5,14]	Medium	Partly[16]
HPWJ-D	> 200 MPa	Low	High	No[11]	Yes[12]	N/A[11]	Medium[5,14]	High	Partly[16]
HPWJ-C	N/A[2]	Very high	Medium[5]	Yes[7,8,9]	Yes[12]	Low	High	High	No
M-C	N/A[2]	Very high	Medium[5]	Yes[7,8,9]	Yes[12]	Low	High	High	No

UCS - Maximum UCS | RF - Mechanical reaction forces | SP - Scalability potential | EQUIP - Additional equipment/machinery required | MAIN - Maintenance effort | MM - Mobility and manoeuvrability | FLEX - Flexibility | AUT - Automation capability | COTS - Availability of COTS products in a small-scale

[1]Used for extraction and quarrying, not excavation.
[2]Likely hard to very hard rock. [3]Effect of blasting not considered. [4]Likely to be high.
[5]Limited by reaction forces.
Equipment for [6]Crushing, [7]Conveying, [8]Scaling, [9]Stabilization, [10]Storage. [11]If only used for exploration.
[12]Replacement of drill bit, pick tools, disc tools, chisel, cutting teeth/lips. [13]No wear of mechanical parts.
[14]Difficult in very soft/soil-type material.
[15]Automated machinery is already existing.
[16]Hand-held tools. [17]Small-scale part-face cutter heads as attachment tools. [18]Mini TBMs.

2.2 Robots in mining

In the past years, great efforts have been made to increase the application of automated machines not only in surface and underground mining, but also in subsea and extra-terrestrial mining [36]. Robotic systems shall help creating safer, more cost-effective and more productive mining operations [37].

In [36], *Marshall* defined primary technology drivers, which cause the rapid progress of automated machinery, robotic systems and robots in mining:

- Working environment: Minimization of infrastructure and personnel in harsh and remote ares [38].
- Labour shortage: Replacing of missing physical labour [39].
- Health and safety: Minimizing or excluding potential risks in deep mining conditions, complying legal regulations and dealing with growing equipment size.
- Equipment maintenance: Reduction of maintenance costs and machine failures [40, 41].
- Operational efficiency: Improving production times and overall mining efficiency.
- Sustainability: Decrease of power consumptions and CO_2 emissions.

Sustainability goals and the trend towards zero personnel are the main reasons for the progress in research and development of mining robots. Therefore, autonomously working robots will play a major role in future mining scenarios.

According to [42], the definition of a robot is:
"*Any automatically operated machine that replaces human effort, though it may not resemble human beings in appearance or perform functions in a humanlike manner. By extension, robotics is the engineering discipline dealing with the design, construction, and operation of robots.*"

Full automation of mining operations and processes, the application of robotic mining systems and integration of autonomous machines are already heavily performed, but the use of small-scale robots in mining is still an extremely pristine area [43]. Exemplary tasks for such robots could be maintenance, building of infrastructure, exploration, excavation, monitoring and search and rescue. Tunnelling and excavation is accompanied by high production rates in often unstable grounds and hard rock conditions and affords heavy-duty, high-performance machinery. The low power and low mass of small-scale robots are fundamental reasons which

will avert the replacement of conventional mining and tunnelling machines by miniature systems. [21]
Although, the potential use in small deposits, ultra-depths and difficult to access areas requires the development of suitable excavation systems [20].

2.2.1 Automated and autonomous machines in mining

Highly automated machines can be found almost everywhere in surface and underground mining, such machines have partly replaced human workforce in doing tasks like hauling, material transport and roadway development [37, 44]. Progressively increasing is also the number of autonomous vehicles (especially, loaders, trucks and blasthole drill systems [36]) which are highly sophisticated systems equipped with sensors for navigation, localization, control and perception.

2.2.1.1 Surface mining

Haul trucks are used for moving material from one location to another and are characteristically mobile and flexible to be able to drive in uneven terrain, steep slopes and tight curves. Automated haul trucks have been introduced in the last decade of the past century [45] and take usage of complex positioning systems [46] and self-awareness systems [47]. [36]
Fleet management is including technologies for positioning and production monitoring, and equipment task assignment. *Marshall* listed several commercial solutions, focus of ongoing research and highlighted points for improvement [36]. Hydraulic excavators, hydraulic shovels and electric rope shovels are machines which have been targeted for automation by improving systems design, monitoring and sensing tool-ground interaction. [36]
In [48], *Singh* has presented a comprehensive review already in 1997 and elaborated on this topic in [49]. Fully automated blasthole drill rigs with rotary or percussive rock drills have increased average tramming speeds and the overall efficiency. Other applications for robotic systems, tele-operated and remote-controlled are rock breakers, dozers and dragline excavators. [36]

2.2.1.2 Underground mining

The harsh environment and potential risks for human labour in underground mining are drivers for the implementation of robotic systems. Load-haul-dump machines (LHD), underground trucks and tramming systems generally can be

found with a high degree of automation, controlled remotely or partly working autonomously. [50]

Further on, applications of robotic systems take place in longwall mining [51] and loading of explosives [52]. Navigation underground has stated challenges due to inability of GPS use. Technologies such as radio frequency identification (RFID) [53], radio signals [54, 55], odometry [36], lidar [13] and aerial robots [56] are applied for underground navigation and localization. In [57], *Artan* gives a summary of commonly cited technologies.

2.2.2 Review of research and development

In the following, some exemplary developments of robots in mining environment or related scenarios are presented, including underground, subsea and extra-terrestrial applications [58] with focus on the individual excavation or extraction technology. Further concepts or analytical studies of robotic systems for mining, exploration or sampling are found in [59–65]. [36]

NASA Rassor

The regolith advanced surface systems operations robot (Rassor) has been developed for extra-terrestrial regolith excavation [66]. This robot is capable of manipulating, excavating, hauling and dumping of regolith by using two counter rotating bucket drums mounted onto a robotic platform (Figure 2.10).

Figure 2.10: NASA Rassor field test [66]

NASA Perseverance

The NASA Perseverance rover has been deployed in 2020 and landed on Mars in 2021. The main objectives are looking for habitability, seeking for signs of

past microbial life and catching samples of core rock and regolith, which shall be returned to Earth for analysis in the future. [67]

The design comprises robotic rover (Figure 2.11) equipped with a great variety of sensors such as cameras, x-ray lithochemistry instrument and radar imager for analysing the surface of the Mars and a bit carousel with 9 drill bits for surface analysis and sample acquisition [67].

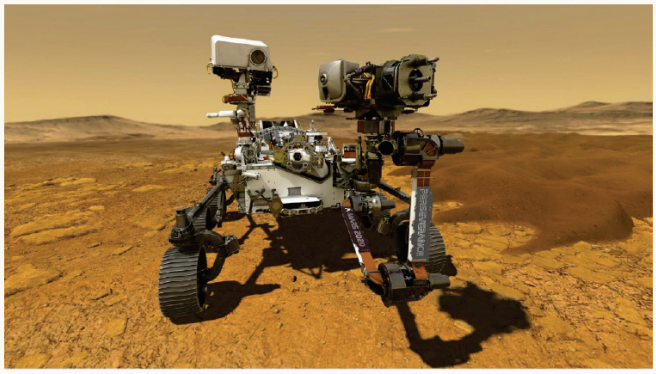

Figure 2.11: NASA Perseverance © *NASA* [67]

Viable Alternative Mine Operating System - ¡VAMOS!

In the process of the ¡VAMOS! project, a prototype of a remotely controlled mining machine has been designed and tested for the extraction of minerals in an underwater open-pit environment [68].

The robot is comprised of a tracked machine which is using a small, part-face cutter head as production tool and a material conveying system (Figure 2.12). The material is excavated, sampled with a rotating auger and the slurry is conveyed through a hydraulic transportation system to the surface. [69]

Figure 2.12: ¡VAMOS! machine © *LPRC* [70]

Tracked subsea trencher

A tracked trencher (Figure 2.13) for subsea operations, used for bury pipelines and cables with the help of jetting and cutting systems is introduced in [71].

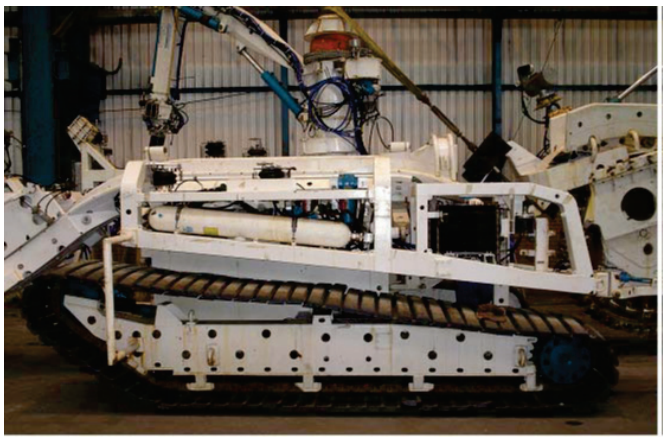

Figure 2.13: Tracked subsea trencher (T3) [71]

Underwater mining vehicle for the cobalt-rich crust

In [72], the design of a compact mining vehicle for subsea resource exploration is described. The prototype assembly's main parts build a tracked machine, a part-face cutter head and a hydraulic suction device (Figure 2.14).

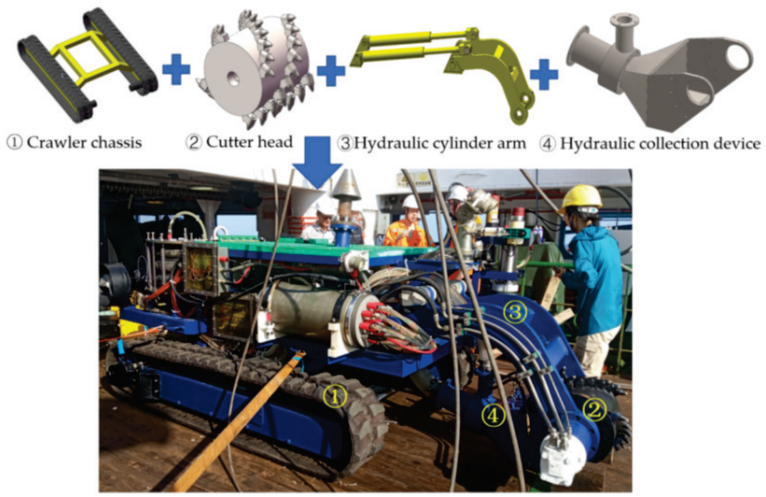

Figure 2.14: Underwater mining vehicle [72]

The machine has been successfully tested in a test tank excavating concrete with a uniaxial compressive strength of 60 MPa and in sea trials at different depths between 1000 and 2500 m. The locomotion, cutting and collection abilities could be proven. [72]

Robot for autonomous underground trenchless operations, mapping and navigation (BADGER)

The EU H2020 - BADGER project represents a feasibility study of the design and development of a subsurface robot (Figure 2.15), which is capable of navigating, drilling and manoeuvring through soil while mapping the subsurface. A rotating ultrasonic auger is applied to reduce the required force to drill through the subsurface. [73]

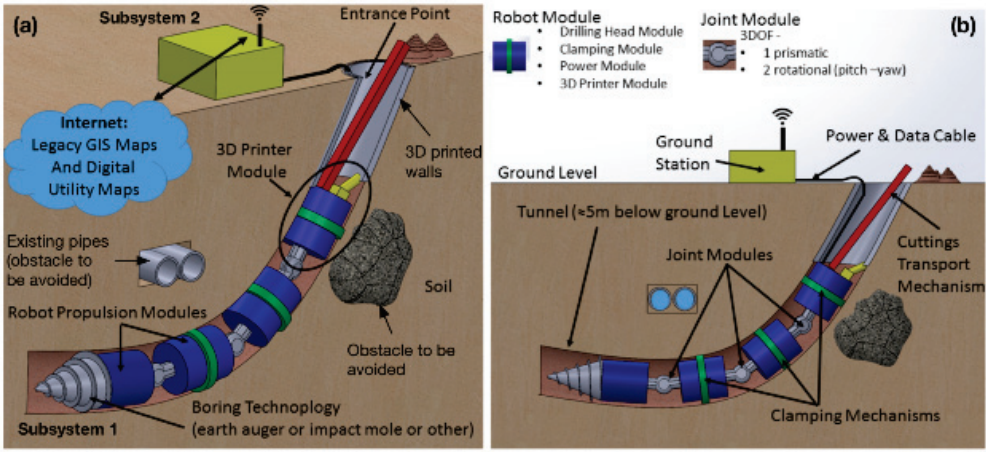

Figure 2.15: Schematic of the BADGER prototype [74]

Self-propelled jet technology machine

In [75], the concept of a self-propelled jet technology machine for flat mining horizons (Figure 2.16) is presented.

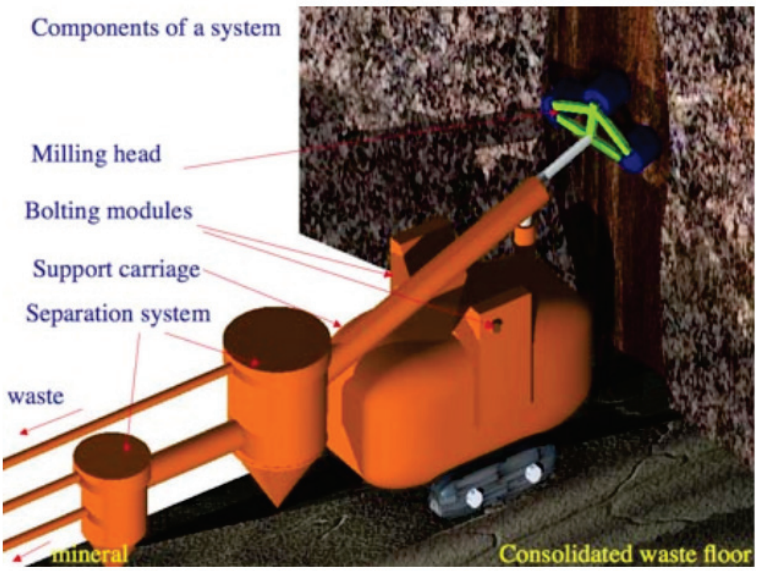

Figure 2.16: Concept of self-propelled jet technology machine [75]

3 Applicability assessment of selected excavation technologies

In this chapter, various analytical studies and investigations on the applicability of selected excavation methods are summarized. The conducted work is based on theoretical approaches found in primary literature. The content is partly documented in [15] and extended results, graphs and look-up tables are presented in Appendix B. Chosen excavation methods for further evaluation are:

- Rock drilling: Applied in drill and blast and hydrofracturing.
- Part-face cutting and full-face cutting.
- Impact hammer.
- High-pressure waterjet cutting.
- Hydrofracturing.

A standardized mass of a robot of 1500 kg and an available power for an excavation tool of 15 kW are assumed throughout this section. The results build initial points to evaluate and design production tool concepts for future mining robots.

3.1 Assessment of mechanical excavation systems

Within this section, performance parameters such as penetration rate, specific energy, excavation rate and reaction forces are evaluated with the help of empirical and analytical approaches found in corresponding literature. Furthermore, a review on available, small-scale commercial products is conducted.

3.1.1 Rock drilling

The review of rock drilling tools has shown that tophammer, rotary-percussive (down-the-hole-hammer) and rotary drilling are promising to be integrated into a

small mining robot. Typical applications would be exploration drilling and drilling of boreholes for explosives or a secondary rock fracturing process. In this section, the estimation of penetration rates, thrust forces and specific energies is made and the applicabilities of rock drills for a small-scale mining robot are assessed.

There are numerous models with which it is possible to calculate operational parameters using theoretically or empirically determined approaches. Different models are presented in [76–82].

In [83], an extensive study on the performance comparison of tophammer, rotary-percussive and rotary drills resulting of the work conducted in [84] is published. Tests of drilling several rock types with various parameters have been analysed and models for determining the penetration rate have been developed.

Equation 3.1 presents the obtained model for calculating the penetration rate of hydraulic tophammer drills [83].

$$PR_{TD} = 1.05 \cdot \frac{WOB^{0.824} \cdot n^{1.690}}{d_b^{2.321} \cdot \sigma_c^{0.610}} \tag{3.1}$$

PR_{TD}	Penetration rate of tophammer drill	$[m/min]$
WOB	Weight-on-bit	$[kg]$
n	Rotational speed	$[rpm]$
d_b	Bit diameter	$[cm]$
σ_c	Uniaxial compressive strength	$[MPa]$

The penetration rate for rotary-percussive drills can be estimated with Equation 3.2 [83].

$$PR_{RPD} = 3.24 \cdot \frac{(p_{op} \cdot d_p)^{0.826}}{R_c^{1.900}} \tag{3.2}$$

PR_{RPD}	Penetration rate of rotary-percussive drill	$[m/min]$
p_{op}	Operating pressure	$[bar]$
d_p	Piston diameter	$[mm]$
R_c	Schmidt hammer (N-type) rebound number	

Equation 3.3 shows the resulting approach of [83] for estimating the penetration rate of rotary drills.

$$PR_{RD} = 0.47 \cdot \frac{b_{pm}^{0.375}}{\sigma_c^{0.543} \cdot q^{0.093}} \tag{3.3}$$

PR_{RD}	Penetration rate of rotary drill	$[m/min]$
b_{pm}	Blow frequency	$[bpm]$
σ_c	Uniaxial compressive strength	$[MPa]$
q	Quartz content	[%]

Each individual model relies on different, but for each drilling technology characteristic parameters. The parameters used in the calculations are summarized in Table 3.1.

Table 3.1: Parameters used to calculate penetration rates, thrust forces and specific energies

(a) Tophammer drilling

b_{pm}	3000 bpm
q	0.1 %
P_{in}	15 kW
d_b	2.5 cm

(b) Rotary-percussive drilling

p_{op}	7 bar
d_p	25 mm
R_c	f(σ_c)
P_{in}	15 kW
d_b	2.5 cm

(c) Rotary drilling

WOB	1000 kg
n	300 rpm
P_{in}	15 kW
d_b	2.5 cm

For rotary-percussive drilling, the Schmidt hammer rebound number is derived from the uniaxial compressive strength of the test samples in [83] with Equation 3.4 by linear interpolation.

$$R_n(\sigma_c) = 42 + 0.374 \cdot (\sigma_c - 15.7) \tag{3.4}$$

Further on, the thrust force of a drill is calculated according to Equation 3.5.

$$F_{drill} = \frac{P_{in}}{PR \cdot 60} \cdot 1000 \tag{3.5}$$

Where F_{drill} is the thrust force in [N] and P_{in} is the input power in [kW].

Eventually, the formula of calculating the specific energy SE in [kWh/m^3] for a

drill with bit diameter d_b is presented in Equation 3.6

$$SE = \frac{P_{in}}{PR \cdot (\frac{{d_b}^2 \pi}{4})} \cdot 1000 \tag{3.6}$$

The penetration rates (Figure 3.1), thrust forces (Figure 3.2) and specific energies (Figure 3.3) are calculated for UCS between 10 and 200 MPa.

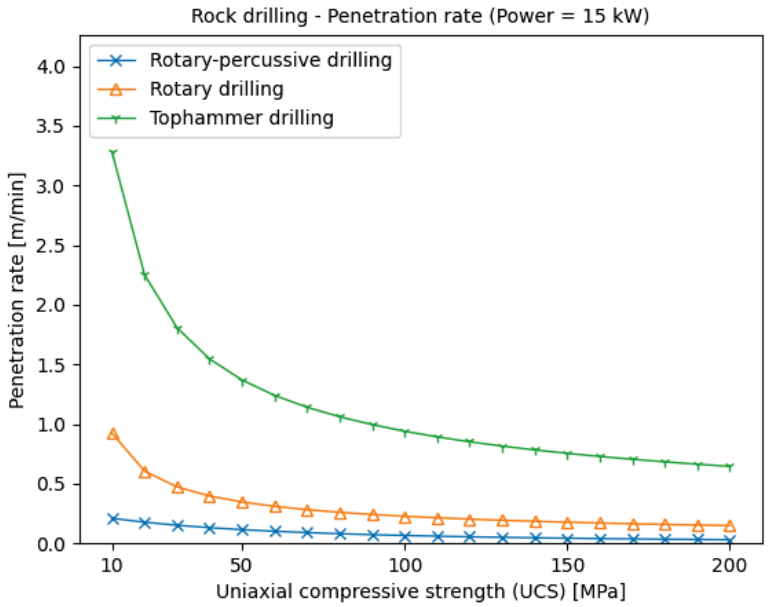

Figure 3.1: Rock drilling - Comparison of penetration rates

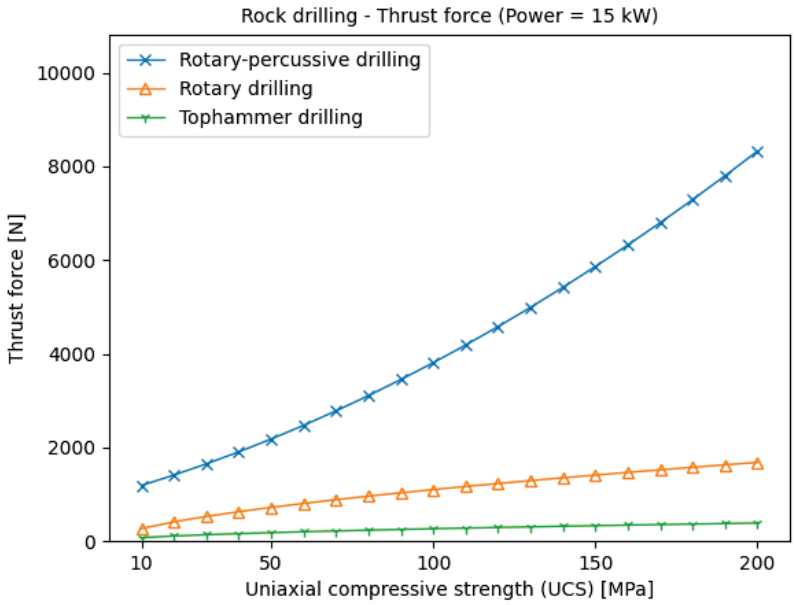

Figure 3.2: Rock drilling - Comparison of thrust forces

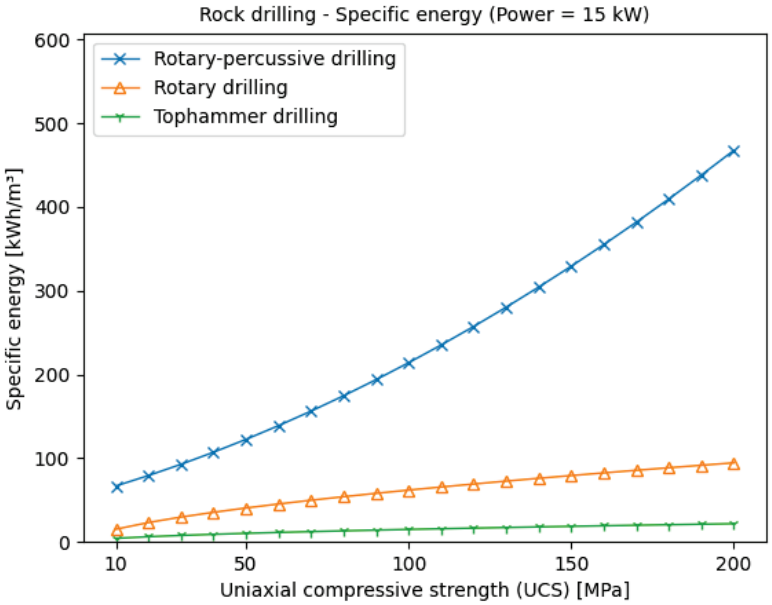

Figure 3.3: Rock drilling - Comparison of specific energies

Tophammer drilling exhibits the highest penetration rates followed by rotary and rotary-percussive drilling, whereas all show a decreasing trend with increasing uniaxial compressive strength.

Contrarily, the highest thrust force to penetrate the rock requires rotary-percussive drilling, which shows a progressively increasing behaviour. The thrust forces of rotary and tophammer drilling are much lower, both having a gradually increasing, but degressive behaviour. Those results have very good agreement with measured thrust forces in [76].

The calculated specific energies of the different drill systems show very high results. Because rock drilling tools are usually not used for excavation - only for exploration drilling, material sampling and borehole drilling - the specific energy is not a key performance indicator. In [24], specific energy levels in terms of efficiency is categorized. Mechanical excavation machines with specific energies above 20 MJ/m^3 (5.56 kWh/m^3) are considered to have very poor performance.

Researching commercial products provided an overview of suitable drilling tools and drill bits. Comparable tophammer drills (Figure 3.4) with drill bit diameters between 28 and 42 mm have been found [85, 86]. The smallest drill bits of oil-hydraulic rotary-percussive (DTH) drills available are between 70 and 100 mm [85] and of water-hydraulic drill bis between 60 and 115 mm [87] (Figure 3.5), all with similar feed length and mass.

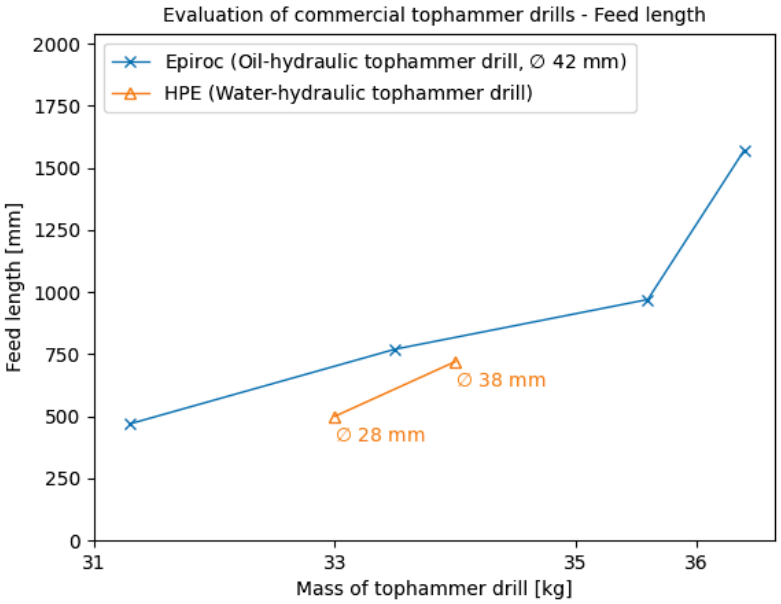

Figure 3.4: Tophammer drills - Commercial product comparison

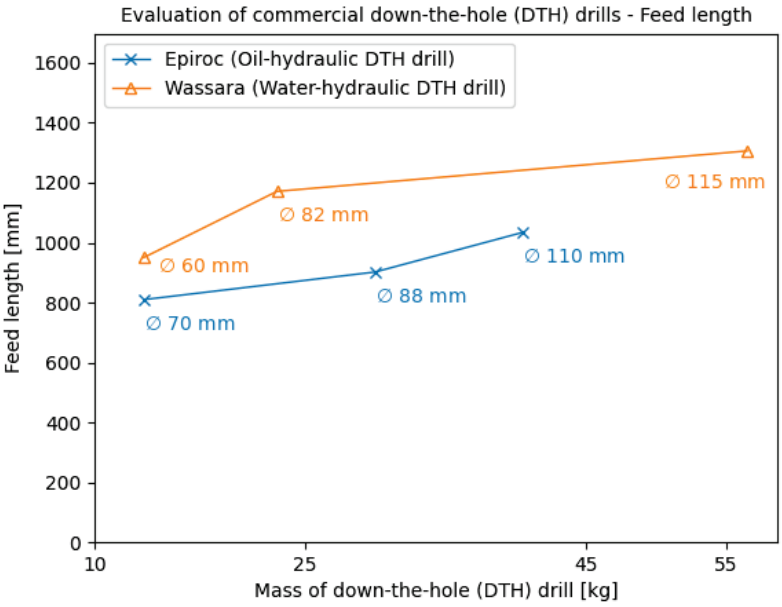

Figure 3.5: Rotary-percussive drills - Commercial product comparison

Extensive parameter studies on all rock drilling technologies, evaluating the influence of power-related parameters are appended in Appendix B.1.

3.1.2 Part-face cutting

Part-face cutting machines (especially roadheaders) are common machines in mining, tunnelling and roadway development. The performance is highly depending on the strength of the material to be cut. Therefore, models for predicting the instantaneous cutting rate are necessary in order to estimate the expectable performance in advance. The applicability assessment of a part-face cutting technology for a small-scale robotic miner is done in this section, concluding with a review on COTS products. Four different approaches of [24, 88–90] for calculating the instantaneous cutting rate *ICR* of roadheaders with transversal cutter heads are reviewed in this section. They all are simplified models and solely rely on the input power P_{in} (here chosen to be 15 kW) and the uniaxial compressive strength σ_c.

In the work published, *Balci* shows a statistical relationship between the specific energy *SE* and the mechanical rock properties [88]. On the basis of those conclusions, [88] formulated Equation 3.7 for calculating the *ICR*.

$$ICR_{Balci} = k \cdot \frac{P_{in}}{0.37 \cdot \sigma_c^{0.86}} \tag{3.7}$$

The approach of *Gehring* is shown in Equation 3.8 [90].

$$ICR_{Gehring} = k \cdot \frac{P_{in} \cdot \eta}{\sigma_c} \tag{3.8}$$

In both equations, k is a constant which is related to the efficiency of the system and usually assumed as 0.8 for roadheaders [88]. Additionally, [90] has considered the efficiency η of the cutter motor.

Kurosch investigated several cutting tests and developed a logarithmically fitted model (Equation 3.9) [89]. The model was validated for a roadheaders with cutter motor power of 132 kW and a linear correlation between instantaneous cutting rate and cutter motor power is assumed.

$$ICR_{Kurosch} = 75.7 - (14.3 \cdot \log \sigma_c) * (\frac{P_{in}}{132}) \tag{3.9}$$

A model which considers the discontinuities in rock formations has been proposed by *Bilgin* in [24], and the approach is shown in Equation 3.10.

$$ICR_{Bilgin} = 0.28 \cdot P_{in} \cdot (0.974)^{RMCI} \tag{3.10}$$

Where *RMCI* is known as the rock mass cuttability index in [MPa] and can be calculated after Equation 3.11 in which *RQD* is the rock quality designation of the rock mass in [%] [24].

$$RMCI = \sigma_c \cdot (\frac{RQD}{100})^{2/3} \tag{3.11}$$

Gehring developed an individual, simplified model for estimating the instantaneous cutting rate of roadheaders with longitudinal (LCH) and transversal (TCH) cutter heads, both shown in Equation 3.12 and Equation 3.13 [91].

$$ICR_{Gehring,LCH} = \frac{1739}{\sigma_c^{1.13}} \cdot (\frac{P_{in}}{230}) \tag{3.12}$$

$$ICR_{Gehring,TCH} = \frac{719}{\sigma_c^{0.78}} \cdot (\frac{P_{in}}{250}) \tag{3.13}$$

Equation 3.12 has been developed for longitudinal cutter heads having a cutter motor power of 230 kW and Equation 3.13 for transversal cutter heads having a cutter motor power of 250 kW [24].

The instantaneous cutting rates of the four approaches are calculated for UCS between 10 and 150 MPa and compared in Figure 3.6.

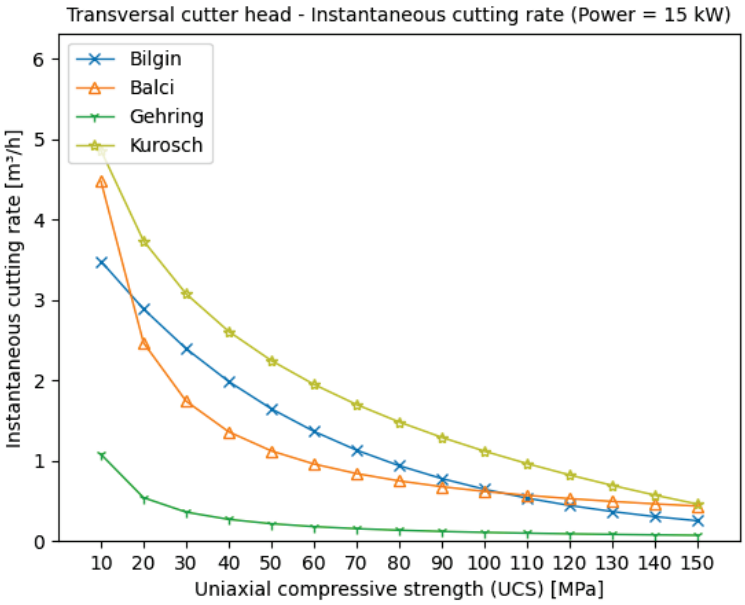

Figure 3.6: Comparison of approaches for calculating the instantaneous cutting rate of part-face cutting machines

The ICR models of [24], [88] and [89] provide similar results at reasonable magni-

tude, only the model of [90] results in lower instantaneous cutting rates. Although all results are in a reasonable range, quantifying them is not possible due to a lack of available data for cutter heads with such low input power.

Using Equations 3.12 and 3.13, the instantaneous cutting rates for LCH and TCH roadheaders are calculated and compared in Figure 3.7.

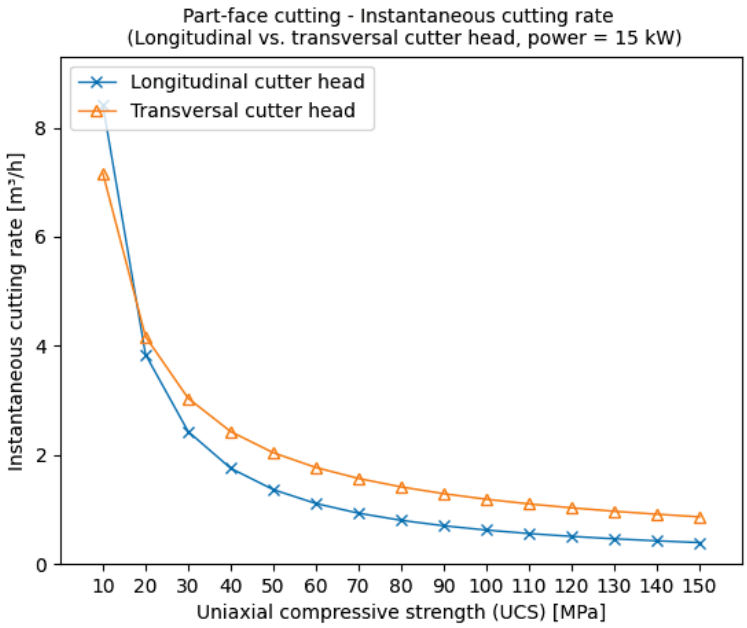

Figure 3.7: Instantaneous cutting rates of roadheader with LCH and TCH

According to the research done in Appendix A.2.2, transversal roadheaders exhibit higher cutting rates than longitudinal roadheaders. This statement is confirmed to by the results in the figure above.

The specific energy *SE* is often used to evaluate the efficiency of an excavation process. *Bilgin* states, for efficient part-face cutting operations the specific energy for good to moderate cutting performance shall be between 1.4-3.3 kWh/m^3, at the worst case it can rise up to 5.56 kWh/m^3 [24]. *SE* is a function of the cutter motor power and the instantaneous cutting rates and can be calculated after Equation 3.14.

$$SE = \frac{P_{in}}{ICR} \tag{3.14}$$

Specific energies of conventionally used axial and radial roadheaders are calculated with cutter motor power P_{in} of 15 kW and *ICRs* after Equations 3.12 and 3.13.

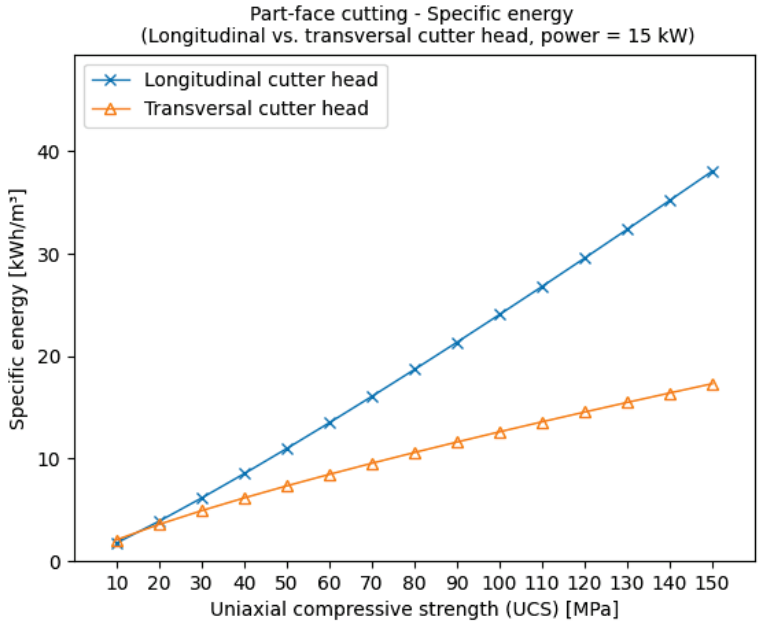

Figure 3.8: Specific energy of part-face cutting - LCH vs. TCH

Assessing the obtained results, both roadheader types with $P_{in} = 15$ kW have good to moderate performance in only very soft rock (< 30 MPa) conditions and do not deviate much. Above $\sigma_c = 30$ MPa, the offset between the two roadheader types is increasing, while TCH being more efficient.

Predicting the cutting force of part-face cutting machines is a complex topic and is elaborated in detail in Chapter 5. To estimate the cutting force of an exemplary cutter head, the theory of *Roxborough* [92] has been used (Equation 3.15).

$$F_c = \frac{16\pi d^2 \sigma_c \sigma_t^2}{(2\sigma_t + \frac{\sigma_c \cos\theta}{1+\tan\phi/\tan\theta})^2} \cdot n_{picks} \tag{3.15}$$

F_c	Cutting force	$[N]$
d	Pick cutting depth	$[mm]$
σ_c	Uniaxial compressive strength	$[MPa]$
σ_t	Tensile strength	$[MPa]$
θ	Semi-cone angle	$[°]$
ϕ	Friction angle	$[°]$
n_{picks}	Number of picks in contact	

For calculating the cutting force of a part-face cutter head, Equation 3.15 has

been taken with parameters listed in Table 3.2.

Table 3.2: Parameters for calculating the cutting force of part-face cutter heads

d	5 mm
σ_c	10 - 150 MPa
σ_t	1.5 - 15 MPa
θ	40°
ϕ	10°
n	7

The cutting force F_c depending on the uniaxial compressive strength σ_c is shown in Figure 3.9.

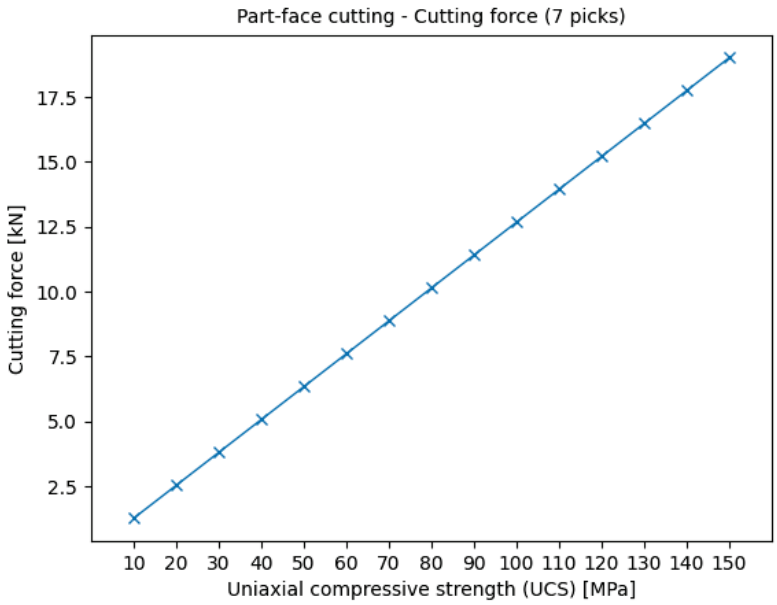

Figure 3.9: Cutting force of a part-face cutter head

The total cutting force F_c is greatly influenced by the magnitude of the uniaxial compressive strength and a linear relation between them is shown and the application of a cutter head in even medium hard rock conditions is questionable due to the high required cutting forces.

The relation between power and mass of an excavation tool follows basically an exponential trend, shown in Figure 3.10. A review of two different part-face cutter head attachment suppliers [85, 93] shows the same trend of increasing mass by using higher cutter head motor power. The installed power in a small mining robot is assumed between 15 and 40 kW, which results in production tool mass (mass of cutter head including motor, gearbox and all mechanical parts) between 30 and 500 kg.

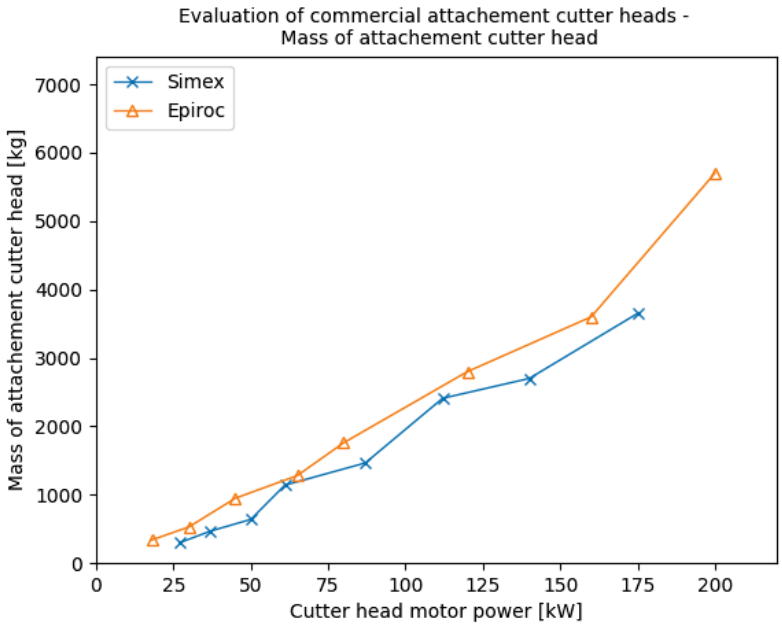

Figure 3.10: Correlation between power of cutter head motor and product mass

By elaborating on minimum requirements for the implementation of a part-face cutter head with specific mass, researching commercial products [85, 93] supports in estimating the minimum mass of the carrier machine (Figure 3.11).

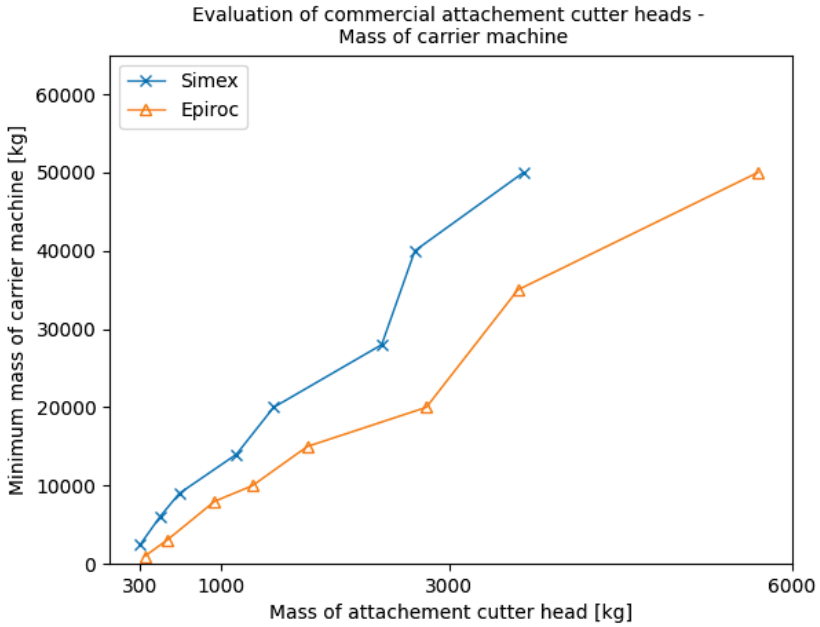

Figure 3.11: Correlation between product mass and carrier machine mass

The carrier machine (in this case the robot) needs a minimum mass of 700 kg for a production tool with a mass of 30 kg according to the product research.

Extensive studies of the influence of parameters on the instantaneous cutting rate, specific energy and cutting force of part-face cutting machines are presented in Appendix B.2.

3.1.3 Full-face cutting

The performance prediction of full-face cutting machines in tunnelling and roadway development is a key tool in preliminary feasibility studies. In order to assess the applicability of a full-face cutting technology for a small robot, methodologies for estimating operational parameters have been used and the extensive study is summarized in this section. Lastly, a review of commercial products is done. This content has already been partly published in [3].

In [94], *Rostami* published a model for performance prediction of TBMs and since then, the model has been improved in [95–102]. Further productivity and performance models for TBMs were found in [103–106].

The theoretical-empirical model introduced in [94, 97] uses rock properties and the geometry of the cutter head to calculate the net production rate, penetration rate and forces of TBMs. The assumption of a pressure distribution P_0 along the periphery of the disc cutter is assumed in order to estimate the forces acting on the machine. The pressure distribution is calculated with Equation 3.16 and Equation 3.17, where the constant C is typically 2.12. The tangential force F_t, normal force F_n and rolling force F_r (Figure 3.12) are then calculated with Equations 3.18, 3.19 and 3.20. The total jacking thrust F_{thrust} (Equation 3.21) is depending on the number of discs installed on the cutter head.

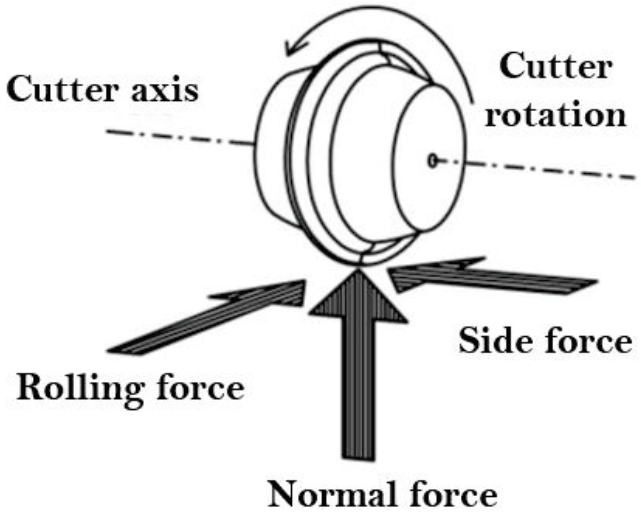

Figure 3.12: Forces on a disc cutting tool [97]

With the resulting torque T (Equation 3.22) and angular speed ω (Equation 3.23) the required power P for penetrating the rock is determined (Equation 3.24).

Eventually, the net production rate NPR and advance rate AR are predicted with Equation 3.26 and Equation 3.27. With the obtained net production rate it is possible to estimate the specific energy SE with the corresponding formula in Equation 3.28, where k is usually 0.8 for TBMs.

$$\phi = \cos^{-1}(\frac{r-p}{r}) \tag{3.16}$$

$$P_0 = C \cdot \sqrt[3]{\frac{s}{\phi\sqrt{r \cdot w}} \cdot \sigma_c^2 \cdot \sigma_t} \tag{3.17}$$

$$F_t = (\frac{P_0 \cdot \phi \cdot r \cdot w}{1+\phi}) \tag{3.18}$$

$$F_n = F_t \cdot \cos\frac{\phi}{2} \tag{3.19}$$

$$F_r = F_t \cdot \sin\frac{\phi}{2} \tag{3.20}$$

$$F_{thrust} = F_n \cdot n_{discs} \tag{3.21}$$

$$T = 0.3 \cdot d_m \cdot F_r \cdot n_{discs} \tag{3.22}$$

$$\omega = \frac{2\pi \cdot n}{60} \tag{3.23}$$

$$P = \omega \cdot T \tag{3.24}$$

$$A = \frac{d_m^2\pi}{4} \tag{3.25}$$

$$NPR = r \cdot n\pi \cdot A \tag{3.26}$$

$$AR = r \cdot n\pi \tag{3.27}$$

$$SE = k \cdot \frac{P}{NPR} \tag{3.28}$$

ϕ	Angle of contact area between rock and tool	$[rad]$
r	Disc radius	$[mm]$
p	Penetration per revolution	$[mm/rev]$
P_0	Pressure in crushed zone	$[N/mm^2]$
C	Constant	
s	Disc spacing	$[mm]$
w	Disc width	$[mm]$
σ_c	Uniaxial compressive strength	$[MPa]$
σ_t	Tensile strength	$[MPa]$
F_t	Tangential force	$[N]$
F_n	Normal force	$[N]$
F_r	Rolling force	$[N]$
F_{thrust}	Jacking thrust	$[N]$
n_{discs}	Number of discs	
T	Torque	$[Nm]$
d_m	Diameter of TBM	$[m]$
n	Rotational speed	$[rpm]$
ω	Angular velocity	$[s^{-1}]$
P	Power	$[kW]$
A	Cross-sectional area of TBM	$[m^2]$
NPR	Net production rate	$[m^3/h]$
AR	Advance rate	$[m/h]$
SE	Specific energy	$[kWh/m^3]$
k	Energy transfer ratio from the cutter head to the tunnel face	

The parameters in Table 3.3 have been used for the calculations below.

Table 3.3: Full-face cutting parameters

r	140 mm
s	40 mm
w	12 mm
C	2.12
k	0.8
P	15 kW
p	5 mm/rev
n	7.4 rpm
n_{discs}	9
d_m	1 m

The total jacking thrust F_{thrust} represents the force which is required to cut into the rock. Figure 3.13 shows the total jacking thrust (calculated according to Equation 3.21) for uniaxial compressive rock strengths between 10 and 200 MPa. Although, roller discs enable cutting hard rock material, they require very high cutting forces compared to other mechanical excavation tools [7], even at low strengths. Therefore, an application of a disc-cutting technology in a small-scale mining robot is considered to be unfeasible. In this studies, a small-scale full-face cutting machine is only considered to be used for tunnelling or roadway development, not mining.

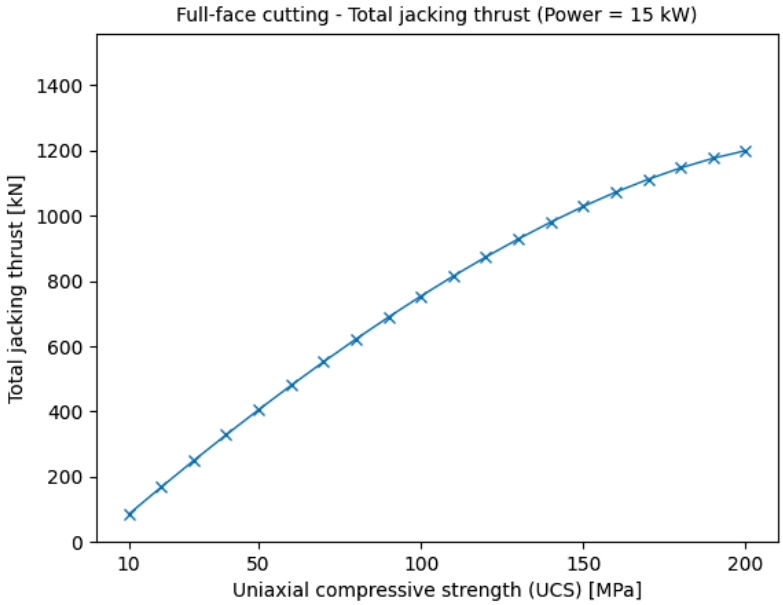

Figure 3.13: Full-face cutting - Total jacking thrust

Perhaps a similar technology as developed in [74] is worth evaluating for low

strength material, but the findings in [69] showed also the need of high thrust forces. Small tunnel boring machines and Mini TBMs (MTBM) are applied in special scenarios and the review of commercial products show similar thrust forces.

To assess the productivity of a 15 kW full-face cutting machine, the net production rate NPR (Figure 3.14) and the advance rate AR (Figure 3.15) have been determined, by assuming a rotational speed n of 7.4 rpm and a machine diameter d_m of 1 m.

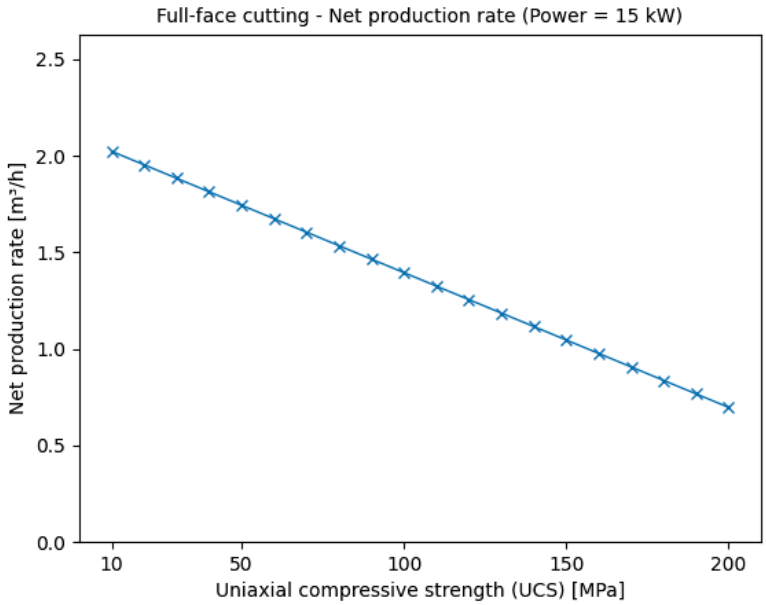

Figure 3.14: Full-face cutting - Net production rate

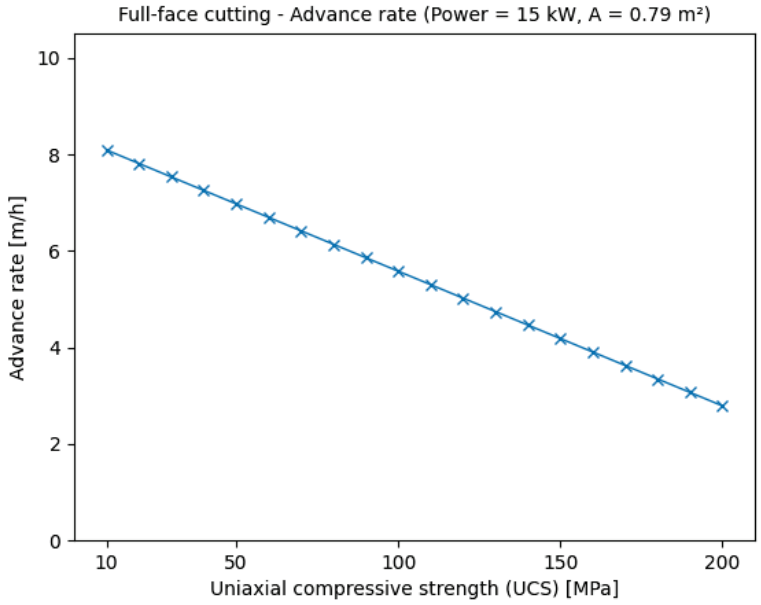

Figure 3.15: Full-face cutting - Advance rate

Both show a linearly decreasing trend with higher rock strengths, but theoretically satisfactory results, if the fact of the high jacking thrust is neglected.

The specific energy calculation is shown in Figure 3.16, and according to the classification of [24], a good to moderate performance is given at uniaxial rock strengths below 40 MPa. Again by not considering the inability of applying high enough jacking thrust.

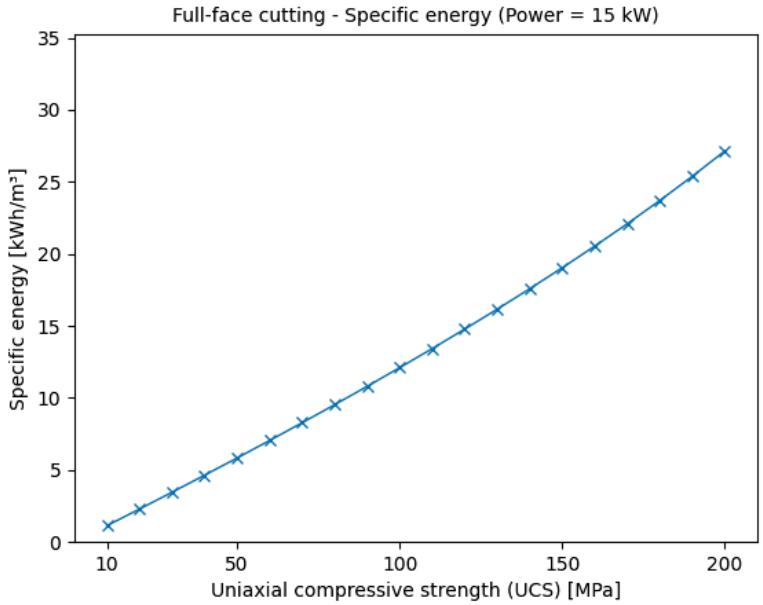

Figure 3.16: Full-face cutting - Specific energy

Herrenknecht provides a wide variety of machines with the pipe jacking technology. Models with an excavation diameter of up to 1.3 m are presented in Table 3.4. As explained by the manufacturer, there is no access to the cutter head and hydraulic drive is directly transferred to the machine from the power pack in the control container. The machines are completely remote-controlled and designed for soft ground, mixed ground and hard rock conditions by use of different cutter heads. Highly effective cone crushers facilitate the transportation of material via slurry pipes to an entrance shaft. [107]

The diameter of microtunnelling machines by *Robbins* ranges from 1 to 3 m [108]. Some of the models' specifications are inserted in Table 3.5. Comparing the two similar models of DN1000 and AVN1000XC of *Robbins* and *Herrenknecht* shows much higher torque and power capacities in the *Herrenknecht* model. *Robbins* does not provide smaller diameter machines ($<$ 1295 mm) for microtunnelling technology, but instead has another type of boring machines suitable for hard rocks called the small boring unit (SBU) [108].

Table 3.4: Technical features of selected *Herrenknecht* AVN machines [107]

Model	Excavation diameter [mm]	Revolution [rpm]	Torque [kNm]	Power [kW]	Mass [t]
AVN250XC	368	44	5.9	45	0.85
AVN300XC	410	27	5.9	45	0.95
AVN400XC	565	19	5.9	45	1.1
AVN500XC	665	15	5.9	45	3
AVN600XC	780	13	5.9	45	3.8
AVN700XC	875	11	5.9	55	4.4
AVN800XC	975	7.4	5.9	55	4.5
AVN1000XC	1295	5.4	5.9	75	7.6

Table 3.5: Technical features of selected *Robbins* microtunnelling machines [108]

Model	Excavation diameter [mm]	Revolution [rpm]	Torque [kNm]	Power [kW]
DN1000	1295	5	69	37
DN1200	1505	5	81	45
DN1500	1810	4	208	90
DN1800	2150	3	420	88
DN2000	2425	3	553	120

SBU-A (see Figure 3.17) is suitable for rock with UCS of 25 to 170 MPa with driving length of up to 150 m (bore diameter range of 0.6 to 1.8 m). It consists of a cutter head and a thrust bearing assembly that can be used with an auger boring machine (ABM). The muck removal can be done by auger, muck car or small conveyor belts. Mini-disc cutters are utilized for this machine. Main specifications of some small SBU-A machines are inserted in Table 3.6. [108]

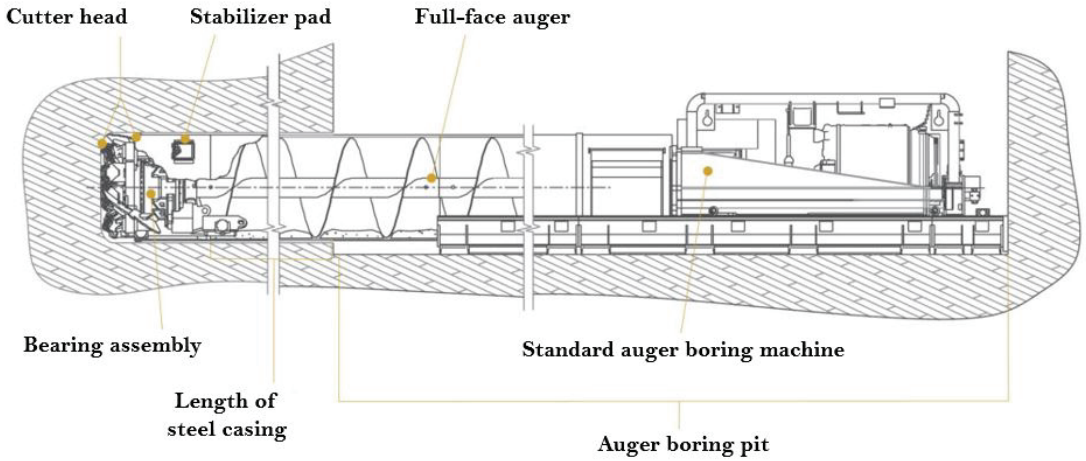

Figure 3.17: The SBU-A technology © *Robbins* [108]

Table 3.6 shows some specifications of small boring machines of the company Robbins [108].

Table 3.6: *Robbins* small boring machine (SBU-A) specifications [108]

Model	Excavation diameter [mm]	Torque [kNm]	Thrust [kN]	Approx. mass [t]	Approx. length [m]	Cutter size [inch]	No. of cutters
SBU-A 24	660	7.86 to 10.575	200 to 400	0.86	1	6.5	9
SBU-A 30	810	7.86 to 10.575	200 to 400	1.12	1	6.5	9
SBU-A 36	970	17.085 to 22.915	290 to 580	1.54 to 1.61	0.94	6.5 or 9.5	13
SBU-A 42	1120	26.17 to 34.98	380 to 760	1.72 to 2.25	0.93	6.5 or 9.5	16

The other type of SBU is called SBU-RC (remote controlled small boring unit), which is available in diameter range of 0.6-1.1 m and is a compact package with driving length of up to 150 m. It is the latest innovation of SBU for mixed ground and hard rock conditions which takes advantage of a continuous steering system run by the operator on the surface using a smart guidance system. Articulation cylinders are used for steering and further control of the line and grade is performed by stabilizer pads. Muck removal is conducted by a vacuum suction instead of using auger system at long distances. Moreover, these machines are capable of being pushed by pipe jacking systems or the ABM system. [108]

Table 3.7 summarizes the specifications of different small boring machine of the company *Robbins* [108].

Table 3.7: *Robbins* small boring machine (SBU-RC) specifications [108]

Model	Excavation diameter [mm]	Revolution [rpm]	Torque [kNm]	Thrust [kN]	Power [kW]	Approx. weight [t]	Approx. length [m]
SBU-RC 24	660	16	11.25	400	40	2.72	3
SBU-RC 30	813	16	11.25	445	40	3.99	3
SBU-RC 36	965	16	21.97	800	75	5.17	3.2
SBU-RC 42	1117	16	21.97	960	75	6.85	3.2

Thrust forces, torques and excavation diameters of the two similar machine types are further compared in Figure 3.18. Additional parameter studies of the parameters influencing the net production rate, specific energy and forces acting on a full-face cutting machine are presented in Appendix B.3.

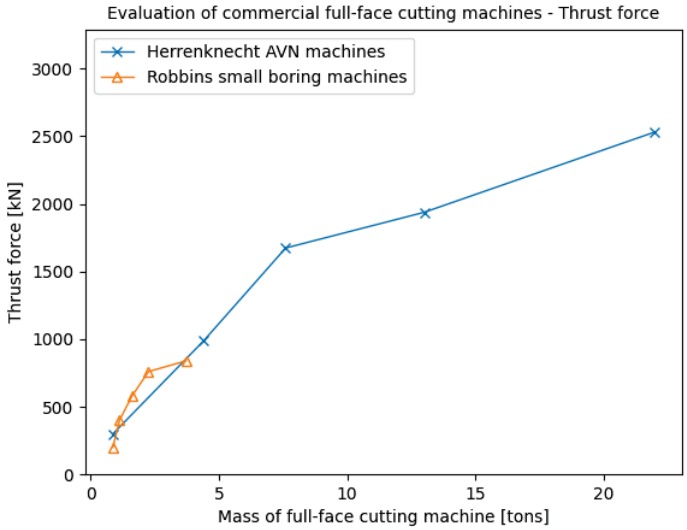

(a) Thrust force

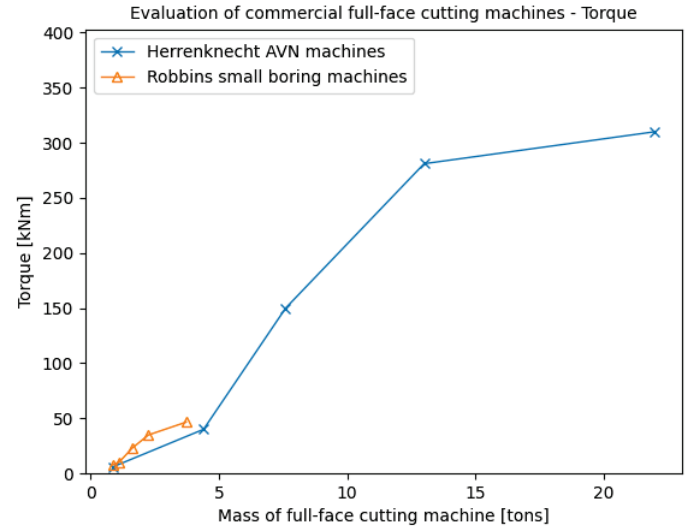

(b) Torque

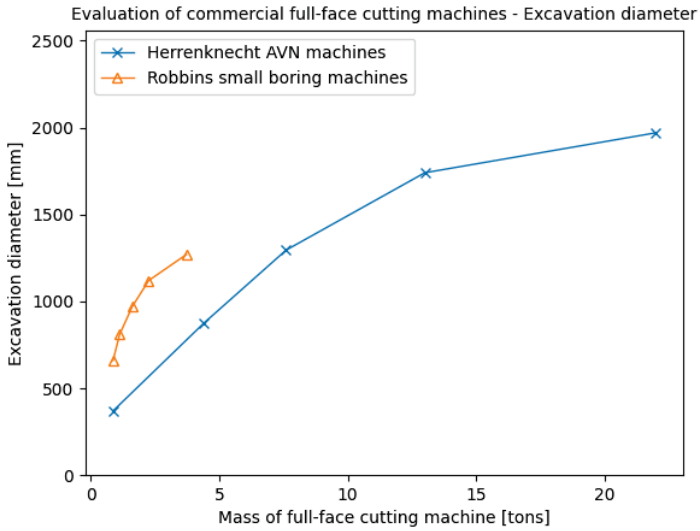

(c) Excavation diameter

Figure 3.18: Full-face cutting - Review of commercial products

3.1.4 Impact hammer

Impact hammers are mainly used as auxiliary tools in mining and tunnelling. Standalone impact hammers for excavation operations are not common because of the occurring wear, vibrations and overall comparatively poor performance, although some excavation applications are presented in [24] and [109]. The performance prediction of impact hammers was investigated extensively in [110–115] and the model has again been summarized in [24].
The performance prediction methodology of impact hammers, presented in [24], can be conducted with calculating the instantaneous breaking rate *IBR* (Equation 3.30), penetration rate *PR* (Equation 3.31) and specific energy *SE* (Equation 3.32).

$$RMCI = \sigma_c \cdot (\frac{RQD}{100})^{2/3} \tag{3.29}$$

$$IBR = 4.24 \cdot P \cdot RMCI^{-0.567} \tag{3.30}$$

$$PR = \frac{IBR}{A} \tag{3.31}$$

$$SE = \frac{P}{IBR} \tag{3.32}$$

$RMCI$	Rock mass cuttability index	$[MPa]$
RQD	Rock quality designation	$[\%]$
IBR	Instantaneous breaking rate	$[m^3/h]$
P	Power of impact hammer	$[kW]$
PR	Penetration rate	$[m/min]$
A	Cross-sectional area of tunnel	$[m^2]$
SE	Specific energy	$[kWh/m^3]$

In Figure 3.19, the instantaneous breaking rate of an impact hammer with 15 kW input power is calculated according to Equation 3.30. The calculations have been made with a rock quality designation of 50 %.

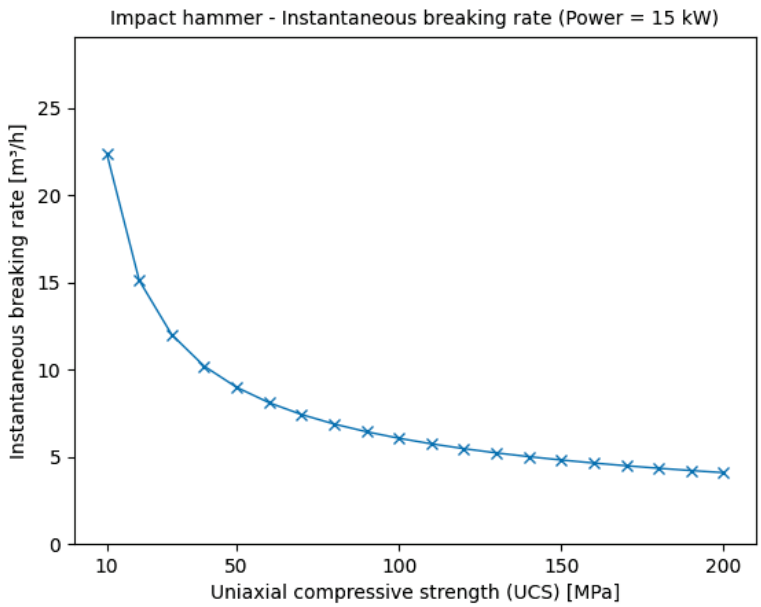

Figure 3.19: Impact hammer - Instantaneous breaking rate

Although the results show high instantaneous breaking rates, especially at low rock strengths, those results are considered to be only reachable in perfect conditions and difficult to achieve in reality [24].

Figure 3.20 shows the penetration rate (Equation 3.31) for a tunnel with an assumed tunnel cross-sectional area of 0.79 m^2 (circular cross-section with diameter d_t of 1 m).

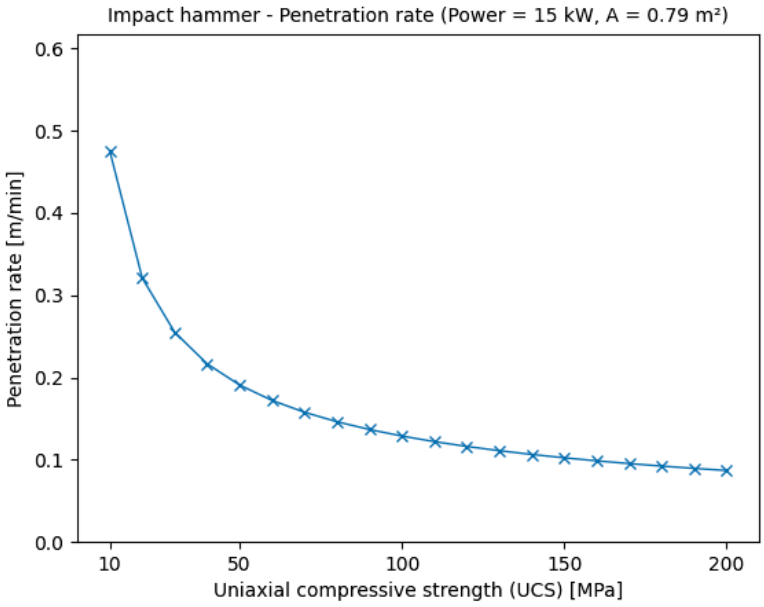

Figure 3.20: Impact hammer - Penetration rate

Again, the results are treated with great caution and do not consider any inhomogeneities. Note: The penetration rate is visualized in [m/min]. Due to the high instantaneous breaking rate, a comparably satisfying specific energy is reached at all strength levels (Figure 3.21).

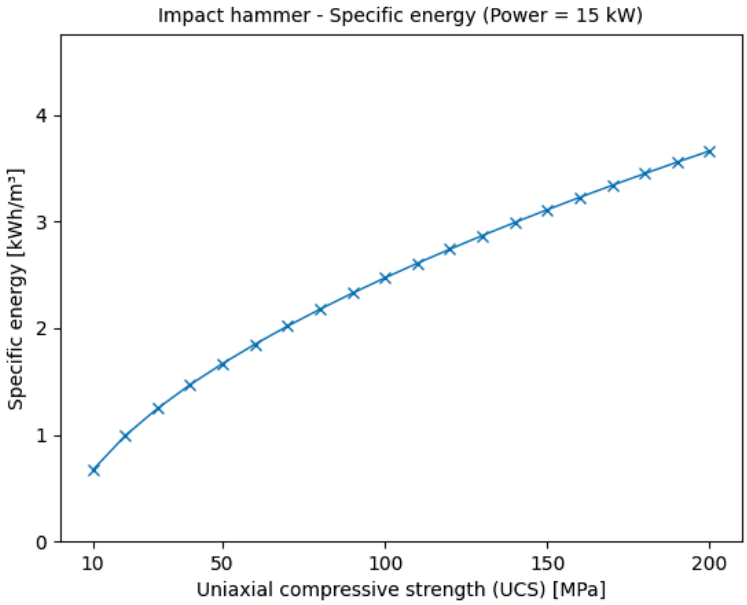

Figure 3.21: Impact hammer - Specific energy

Lastly, the impact hammer forces are calculated and illustrated in Figure 3.22, calculated after Equation 3.5.

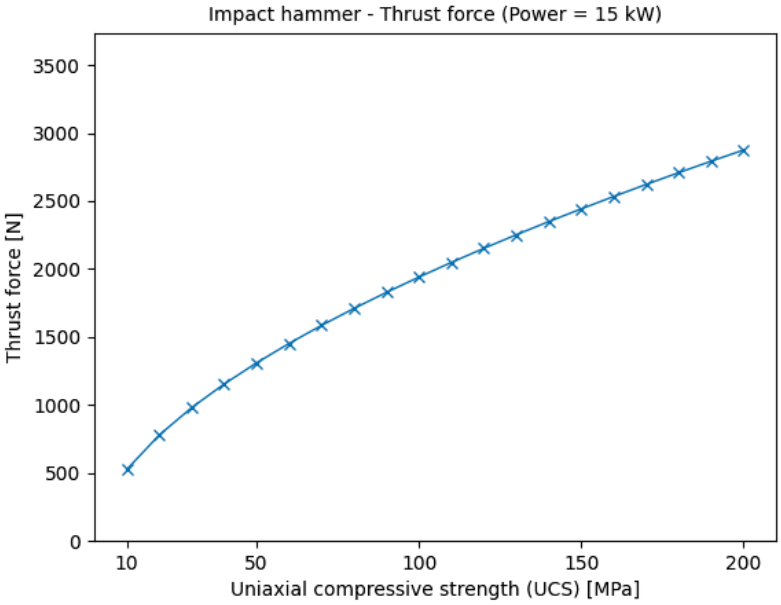

Figure 3.22: Impact hammer - Thrust force

Despite obtaining low impact hammer forces, the high vibrations due to the impacting motion of an impact hammer are classifying that excavation method as unfavourable. Additionally, the particle and muck size distribution cannot be controlled accurately and therefore it is no longer considered.

Nevertheless, a commercial product review has been conducted and impact hammers of two manufacturers [85, 116] have been compared (Figure 3.23).

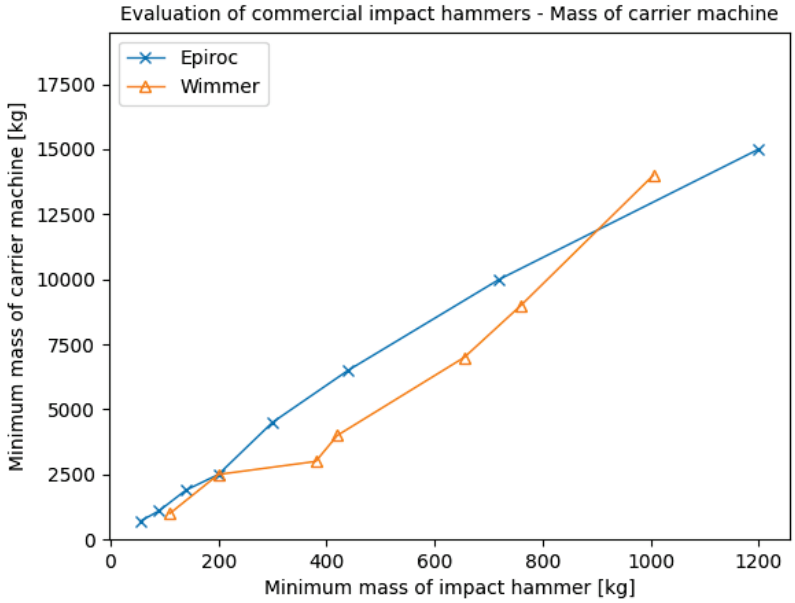

Figure 3.23: Impact hammer - Product research

On average, the mass of the carrier machine is ten times higher than the mass of the integrated impact hammer.

Additional parameter studies of the parameters influencing the instantaneous breaking rate, specific energy and impact hammer thrust force are presented in Appendix B.4.

3.1.5 Comparison

In this chapter, the calculated results are compared with each other in order to create look-up tables for the applicability of mechanical excavation systems for a small-scale mining robot with 15 kW of available power for an excavation tool.

The expected reaction force equals the applied drilling, cutting or thrust force. A comparison of the reaction forces is presented in Figure 3.24. For a better understanding, two individual plots have been created, one for single tool use and

one for multiple tool use. Single tool use encloses excavation tools with the least number of tools to be in contact with the rock.

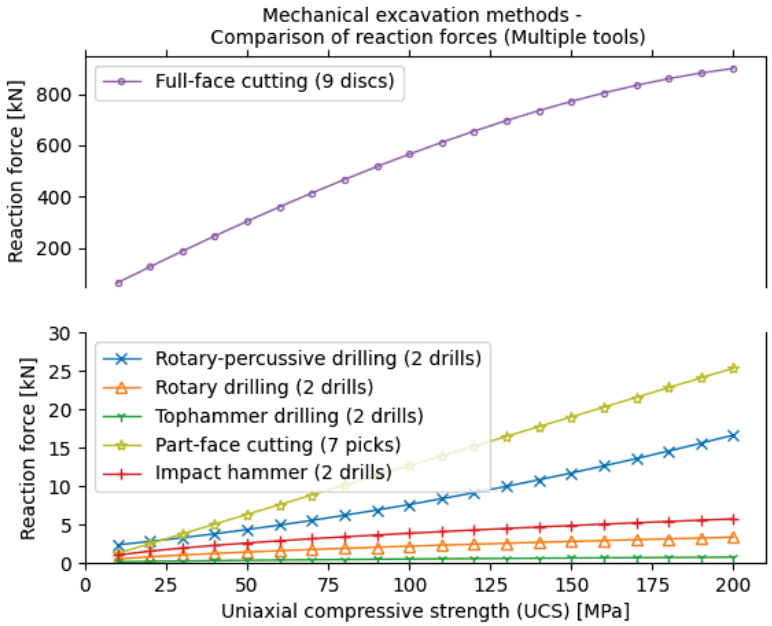

(a) Single tool use

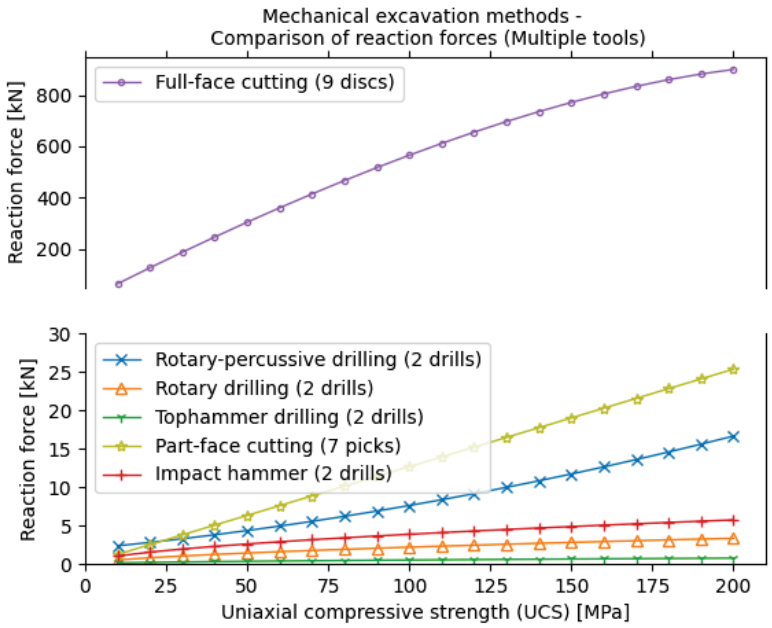

(b) Multiple tool use

Figure 3.24: Comparison of theoretical reaction forces

Although in reality, excavation with 1 pick of a part-face cutter head or 1 disc tool of a full-face cutter head would not happen, the force of a single tool is a good indicator for the applicability.

Figure 3.25 shows a comparison of the specific energies of the discussed mechanical excavation systems.

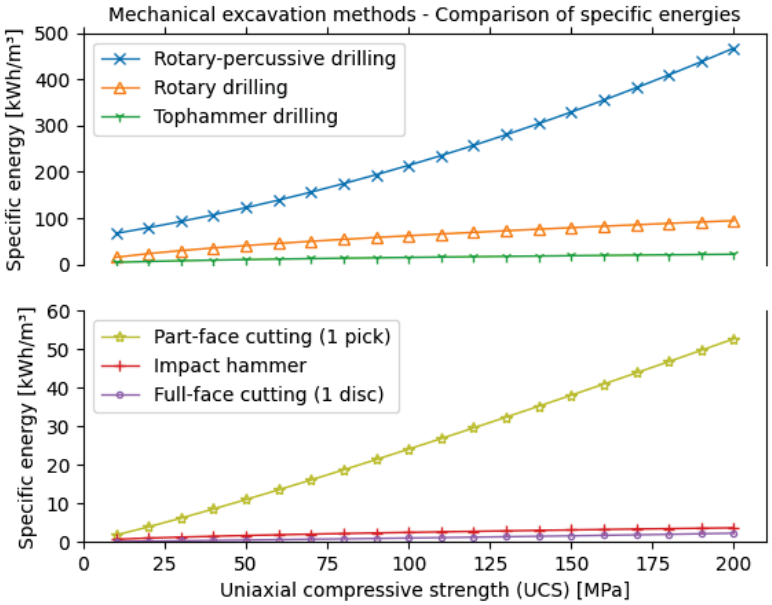

Figure 3.25: Comparison of specific energies

The penetration rates of the rock drilling systems and impact hammer are displayed in Figure 3.26 and the advance rates of part-face cutting and full-face cutting are shown in Figure 3.27.

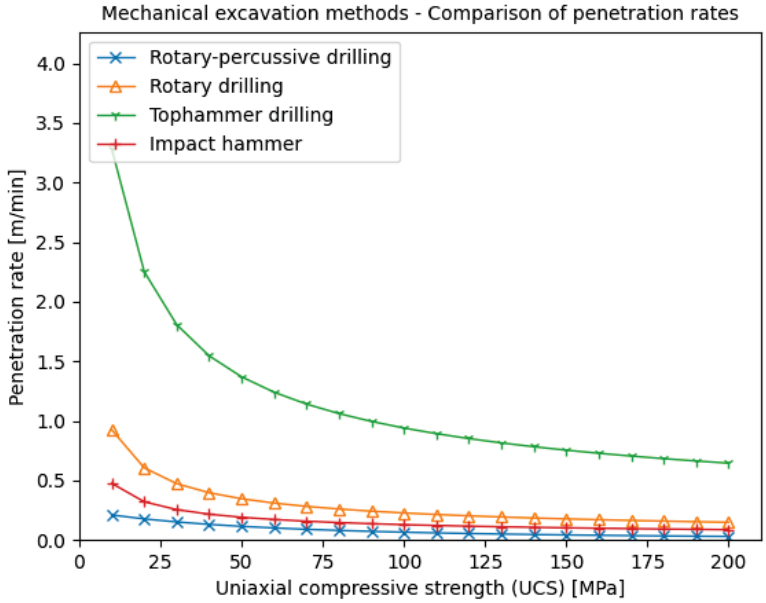

Figure 3.26: Penetration rates of rock drilling and impact hammer

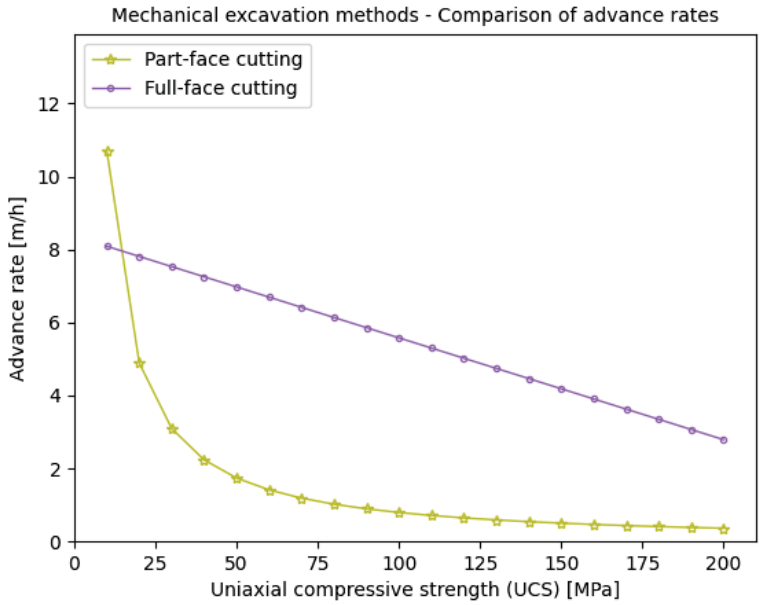

Figure 3.27: Advance rates of part-face cutting and full-face cutting

Penetration rates and advance rates have been split in two separate plots, because they describe two different parameters.

Figure 3.28 is comparing the excavation rates of part-face cutting, full-face cutting and impact hammering. Rock drilling is not considered as a pure excavation technology, for this reason, their results have not been taken into account.

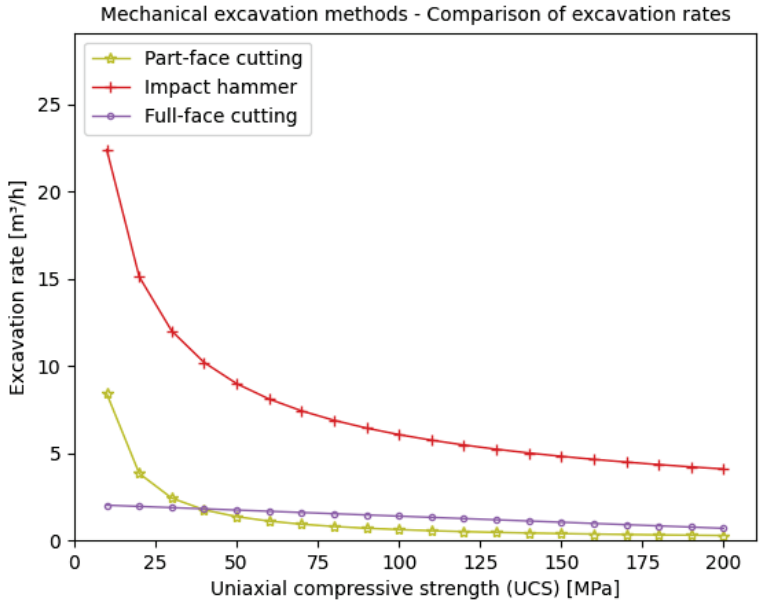

Figure 3.28: Excavation rates of part-face cutting, full-face cutting and impact hammer

3.1.6 Considerations of the integration of mechanical excavation systems in a small-scale robot

Some elements of this section have already been published in [4].

The economic efficiency of mechanical mining methods is strongly limited by the strength of the rock to be excavated. As previously discussed, the excavation process in mechanical mining methods requires high forces, which in turn act on the machine as reaction forces. Small mining machines (mining robots) have limited power and a comparatively low mass and can therefore only absorb low reaction forces. Aim of the in this section presented investigations is the analysis of maximum allowable reaction force and minimum required mass of a robot for the applicability of an individual excavation technology.

3.1.6.1 Traction forces of a small-scale robot

During the mining process, the interaction between the tool and the rock generates forces that needs to be lower than the traction forces of the machine. Depending on the undercarriage (type and material) and the subsoil material, different friction coefficients result [117]. Rubber tires or tracks are typically used as undercarriages of tunnelling and mining machines. In [118], unconventional concepts for locomotion of robots in harsh environments were considered. Findings from this work showed the potential of screw-type systems as locomotion system. Figure 3.29 compares the traction forces of the three mentioned variants for a robot with a total mass of 1500 kg.

The traction forces of a robot with track and tire systems have been calculated with Equation 3.33, whereas Equation 3.34 has been used for determining the traction forces of a robot with a screw system and Equation 3.35 for a robot with screw system and an additional gripping mode. A simplified model was assumed, with which the traction force was calculated using Coloumb's approach.

$$F_{tr} = m_{Robot} \cdot g \cdot \mu \tag{3.33}$$

$$F_{tr,screw} = m_{Robot} \cdot g \cdot \left(\frac{\sin\alpha + \mu\cos\alpha}{\cos\alpha - \mu\sin\alpha}\right) \tag{3.34}$$

$$F_{tr,screw*} = \left(m_{Robot} \cdot g + F_{gripping} \cdot n_{screws}\right) \cdot \left(\frac{\sin\alpha + \mu\cos\alpha}{\cos\alpha - \mu\sin\alpha}\right) \tag{3.35}$$

F_{tr}	Traction force of robot with tracks or tire system	$[N]$
$F_{tr,screw}$	Traction force of robot with screw system	$[N]$
m_{Robot}	Robot mass	$[kg]$
g	Gravitational acceleration on Earth	$[m/s^2]$
α	Thread leading angle of screw	$[°]$
$F_{tr,screw*}$	Gripping force of 1 screw	$[N]$
n_{screws}	Number of screws	

The parameters in Table 3.8 have been used for the calculations below.

Table 3.8: Friction coefficients for different surface materials [119, 120]

	Gravel, loose	Gravel road	Clay loam, wet	Sand, dry	Sand, wet	Concrete	Clay loam, dry	Ice
Tracks, screws	0.4	0.5	0.7	0.3	0.5	0.45	0.9	0.15
Tires	0.3	0.35	0.45	0.2	0.4	0.9	0.55	0.1

The traction forces of the three different locomotion systems have been calculated for different ground material (Figure 3.29).

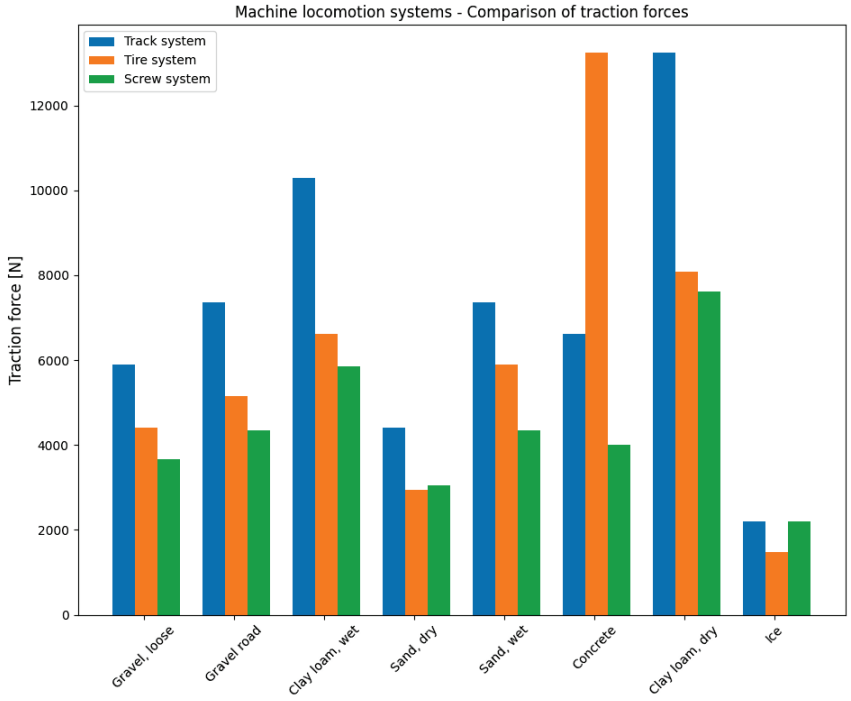

Figure 3.29: Comparison of traction forces of different systems [4]

Overall, track systems have the highest traction forces. However, a screw system can be used in a more versatile manner and can thus increase the flexibility and mobility of a robot. A symmetrical arrangement of an even number of screws in relation to the base body of the robot allows firstly a direction-independent and position-independent use and secondly, by applying an additional gripping force with the help of the screws, the traction forces can be significantly increased (Figure 3.30). A gripping force $F_{tr,screw*}$ of 10 kN has been assumed.

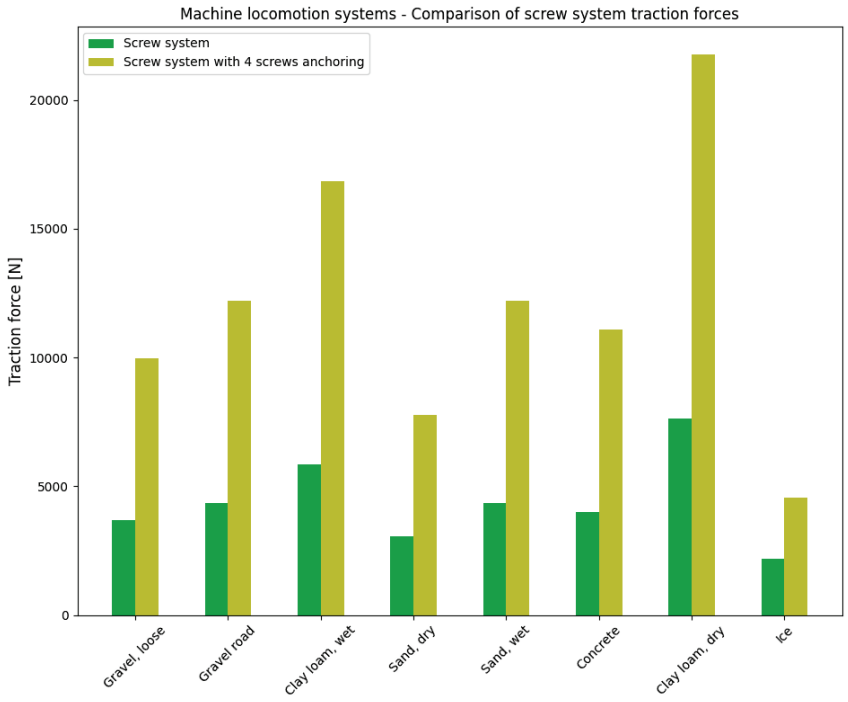

Figure 3.30: Traction forces of standard screw system and with additional gripping mode [4]

3.1.6.2 Reaction forces of mechanical excavation systems

To compare the traction forces with the theoretical reaction forces of excavation systems, the results of Section 3.1.5 are processed and presented in a simplified way.

In Figure 3.31, thrust forces (drilling, cutting and hammering forces) are compared for rotary drilling, part-face cutting, full-face cutting and impact hammer. The bar plots are respectively for 1 rotary drill, 1 pick tool, 1 disc tool and 1 impact hammer each for specified UCS levels. Rotary rock drilling has been chosen for further investigations, because it shows reasonable drilling forces, satisfactory penetration rates and, compared to tophammer and rotary-percussive drilling, does not induce vibrations due to a percussive motion. Note: The y-axis is in logarithmic scale.

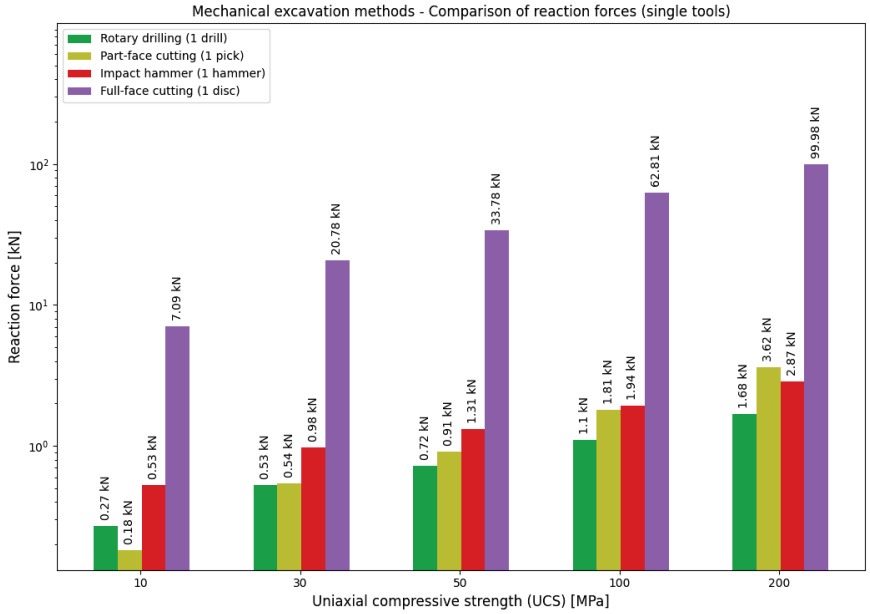

Figure 3.31: Reaction force of drilling (1 rotary drill), impact hammering (1 hammer), part-face cutting (1 pick) and full-face cutting (1 disc)

The results in Figure 3.31 are implying that a robot with 1500 kg will have issues using a part-face or full-face cutting tool.

Similar calculations have been made for 2 rotary drills, part-face cutter head with 7 picks in contact, full-face cutter head with 9 discs in contact and 2 impact hammers (Figure 3.32). Note: The y-axis is in logarithmic scale.

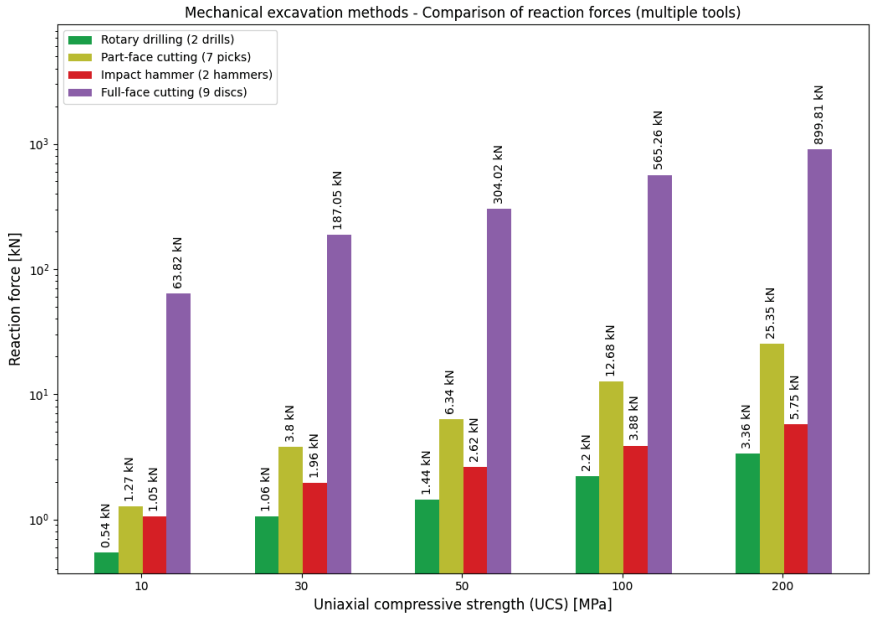

Figure 3.32: Reaction force of drilling (2 rotary drills), impact hammering (2 hammers), part-face cutting (7 picks) and full-face cutting (9 discs)

In conclusion:

- Using a rotary drill is causing reaction forces between 270 N for 10 MPa UCS and 1680 N for 200 MPa UCS.
- Reaction forces of an impact hammer are between 530 N for 10 MPa UCS and 2870 N for 200 MPa UCS.
- Part-face cutting with 7 picks in contact is leading to reaction forces between 1.27 kN for 10 MPa UCS and 25.35 kN for 200 MPa UCS.
- The highest reaction forces are caused by a full-face cutting technology with 9 discs in contact. Between 63 kN for 10 MPa UCS and 900 kN for 200 MPa UCS.

Further on, the reaction forces have been compared with the providable traction forces of a robot with a mass of 1500 kg. The traction force F_{screw} was calculated at 4.34 kN for the standard screw system and for gripping mode activated the traction force F_{screw*} is 12.2 kN.

In Figure 3.33, thrust forces of single tool calculations are compared to the calculated traction forces of a screw-driven robot. Note: The y-axis is in logarithmic scale. Multiple tool use can be seen in Figure 3.34.

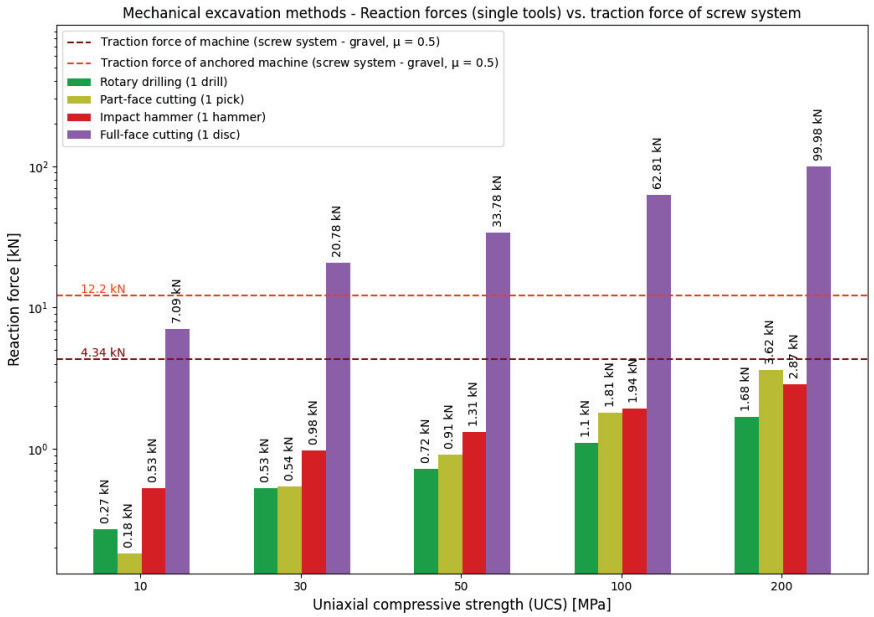

Figure 3.33: Reaction force vs. thrust force for drilling (1 rotary drill), impact hammering (1 hammer), part-face cutting (1 pick) and full-face cutting (1 disc)

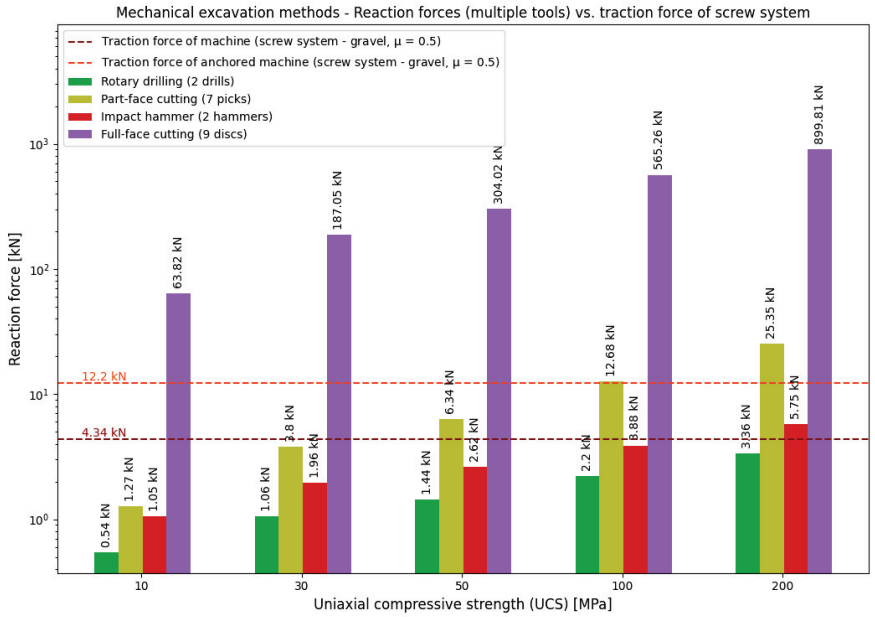

Figure 3.34: Reaction force vs. thrust force for drilling (2 rotary drills), impact hammering (2 hammers), part-face cutting (7 picks) and full-face cutting (9 discs)

Following conclusions can be made:

- Using a rotary drill is applicable up to 200 MPa UCS, even without gripping mode activated.
- Impact hammer is also feasible up to 200 MPa UCS with a standard screw-driven robot.
- The limit of part-face cutting with 7 picks in contact is below 100 MPa UCS. This seems questionable, due to the light mass of the robot and the comparison with industrial machinery. A comparable small pick cutting depth ($d = 5$ mm) has been chosen in the calculations, which means the cutting forces result in lower magnitude.
- According to the findings, an application of a full-face cutting system (9 discs) is not feasible at any rock strength.

Further investigations for track and rubber tire systems are appended in Appendix B.6.

3.1.6.3 Minimum masses of small-scale robots for applying mechanical excavation systems

Developing a small-scale robot with a certain excavation tool requires the dimensioning of the robot in a way that it can handle the reaction forces caused by the

tool-rock interaction. A crucial parameter is the minimum mass which is needed in order to excavate rock without anchoring the machine. Therefore, studies have been conducted to receive the minimum mass of a robot for a certain excavation method. The minimum masses for single tool excavation systems are shown in Figure 3.35 and Figure 3.36 presents the minimum masses for multiple tools in contact. Note: The y-axes are in logarithmic scale.

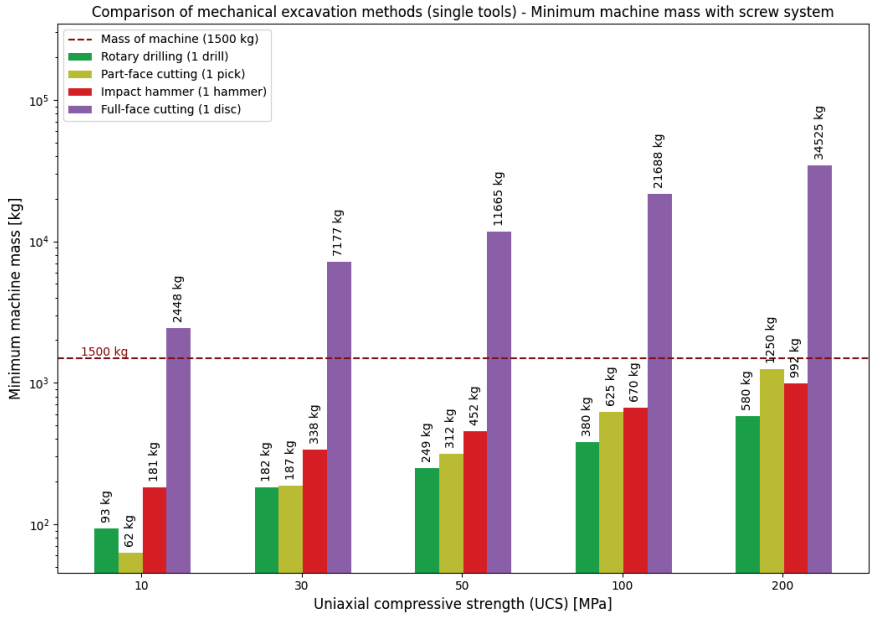

Figure 3.35: Minimum required robot mass for drilling (1 rotary drill), impact hammering (1 hammer), part-face cutting (1 pick) and full-face cutting (1 disc)

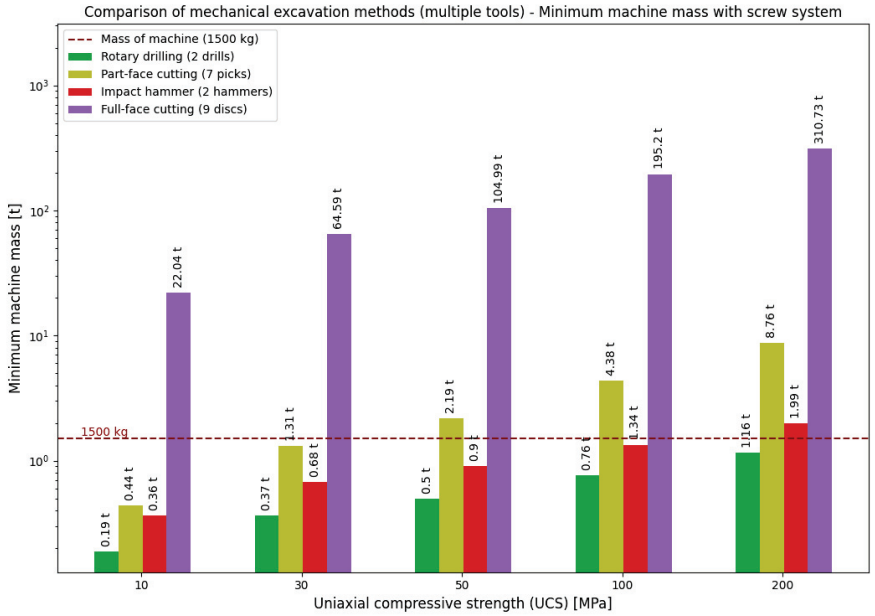

Figure 3.36: Minimum required robot mass for drilling (2 rotary drills), impact hammering (2 hammers), part-face cutting (7 picks) and full-face cutting (9 discs)

From the calculations these findings can be highlighted:

- Rotary drilling: Drilling into rock with 10 MPa UCS leads to a minimum mass of the robot of 93 kg and in using a rotary drill in a 200 MPa hard rock, the minimum robot mass increases to 580 kg.
- Impact hammer: The result for the minimum robot mass required for applying an impact hammer at 10 MPa UCS rock is 181 kg, whereas for 200 MPa UCS rock the minimum mass of a robot has to be 992 kg.
- Part-face cutting: A minimum robot mass of 440 kg is required to excavate rock with 10 MPa UCS and 8760 kg for 200 MPa UCS.
- Full-face cutting: For cutting rock with 10 MPa UCS, a minimum robot mass of 22 t is needed and for rock with 200 MPa UCS the calculated minimum mass is 310 t.

Extensive studies on traction forces of the three selected undercarriage systems, look-up tables for reaction forces and matrices for minimum masses are attached in Appendix B.6.

3.2 Assessment of alternative and combined excavation systems

The preliminary assessment in Chapter 2 and Appendix A suggested high-pressure waterjet cutting and hydrofracturing as potential excavation methods. These two technologies are assessed in terms of there rock excavation potential in this section.

3.2.1 High-pressure waterjet cutting

In Appendix A.3.1, the applications of pure waterjet cutting (PWJC) and abrasive waterjet cutting (AWJC) are described. Abrasive waterjet cutting is used in cutting material with higher strengths and has been used in some mining applications, presented in [121–124].

Various analyses have been conducted in the past, investigating the influence of high-pressure waterjet parameters (e.g. water pressure, abrasive feed rate, traverse speed or water flow rate) on the cutting characteristics [125–128]. Generally, a strong correlation between the cutting depth of a high-pressure waterjet and the uniaxial compressive strength of the rock to be cut can be outlined, as shown in [126, 129, 130].

In [131], *Oh* developed a simplified model for estimating the cutting depth depending on the UCS on the basis of cutting tests and parabolic regression. Subsequently, a model based on the kinetic energy of the waterjet was introduced in [132].

Further, more sophisticated models, but without the consideration of the jet energy diffusion have been published in [133–135].

The applicability of a high-pressure abrasive waterjet system by taking advantage of the model in [131] is evaluated in this section. The methodology includes analysing the cutting depth for different water pressures and rock strengths, and estimating the excavation rate and specific energy by processing the results. The cutting depth D_{WJ} can be estimated with Equation 3.36.

$$D_{WJ} = C_1 \cdot (\frac{\sigma_c}{1MPa})^{-C_2} \tag{3.36}$$

C_1 and C_2 are empirical constants and according to the data published in [131] show a linear correlation with the cutting depth. Therefore, the data has been used to create linear interpolation functions obtaining suitable values of C_1 and C_2

for different traverse speed and water pressure. The calculation of the excavation rate is made in compliance with Equations 3.37, 3.38 and 3.39. Obtaining the specific energy is done by using Equations 3.40 and 3.41.

$$A_{WJ} = \frac{d_n^2 \pi}{4} \tag{3.37}$$

$$V_{WJ} = A_{WJ} \cdot D_{WJ} \tag{3.38}$$

$$ER_{WJ} = \frac{V_{WJ}}{t_{exp}} \tag{3.39}$$

$$P_{WJ} = p_{WJ} \cdot Q_{WJ} \tag{3.40}$$

$$SE_{WJ} = \frac{P_{WJ} \cdot t_{exp}}{V_{WJ}} \tag{3.41}$$

σ_c	Uniaxial compressive strength	$[MPa]$
A_{WJ}	Cross-sectional area of waterjet	$[mm^2]$
C_1	Constant	$[MPa]$
C_2	Constant	
D_{WJ}	Cutting depth	$[mm]$
d_n	Focusing tube diameter	$[mm]$
V_{WJ}	Excavated volume	$[m^3]$
ER_{WJ}	Excavation rate	$[m^3/s]$
t_{exp}	Waterjet exposure time	$[s]$
P_{WJ}	Hydraulic power	$[W]$
p_{WJ}	Water pressure	$[bar]$
v_t	Traverse speed	$[mm/s]$
Q_{WJ}	Water flow rate	$[mm^3/s]$
SE_{WJ}	Specific energy	$[kWh/m^3]$

The corresponding cutting depths for five water pressure levels depending on the uniaxial compressive strength of the rock are depicted in Figure 3.37.

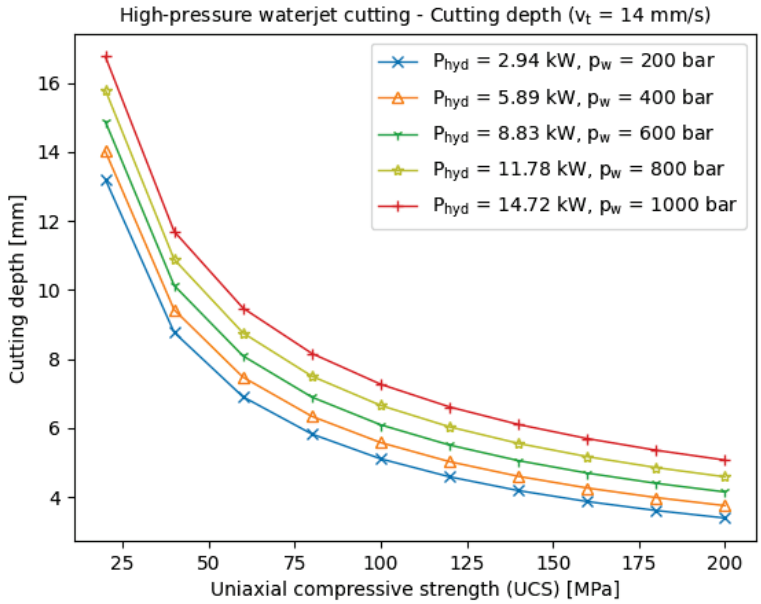

Figure 3.37: High-pressure waterjet cutting - Cutting depth

A shortcoming of this approach is the neglect of a minimum required pressure to be able to initiate erosion. *Hagan* described a threshold pressure p_{th} which need to be overcome in order to cut the rock (Equation 3.42) [136].

$$p_{th} = \frac{\sigma_c}{2} \tag{3.42}$$

The cuttability map in Figure 3.38 shows the maximum rock strength to be cut for certain waterjet pressures.

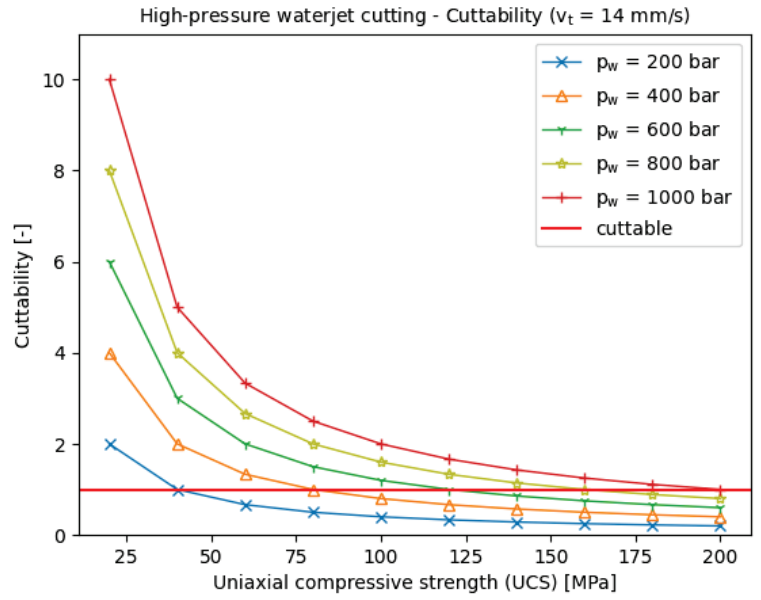

Figure 3.38: High-pressure waterjet cutting - Cuttability

If the cuttability is greater than 1, the application of a high-pressure waterjet with this water pressure is possible. Another visualization provides a plot in Figure 3.39, which shall facilitate a quick evaluation of the required water pressure.

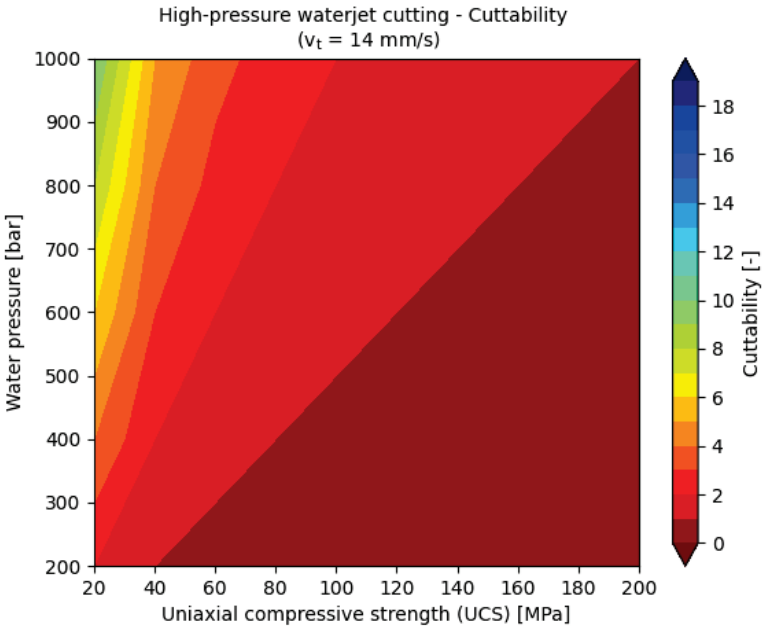

Figure 3.39: High-pressure waterjet cutting - Cuttability map

The cutting depth calculations in Figure 3.40 include the threshold pressure and point out the maximum UCS to be cut with the defined water pressure.

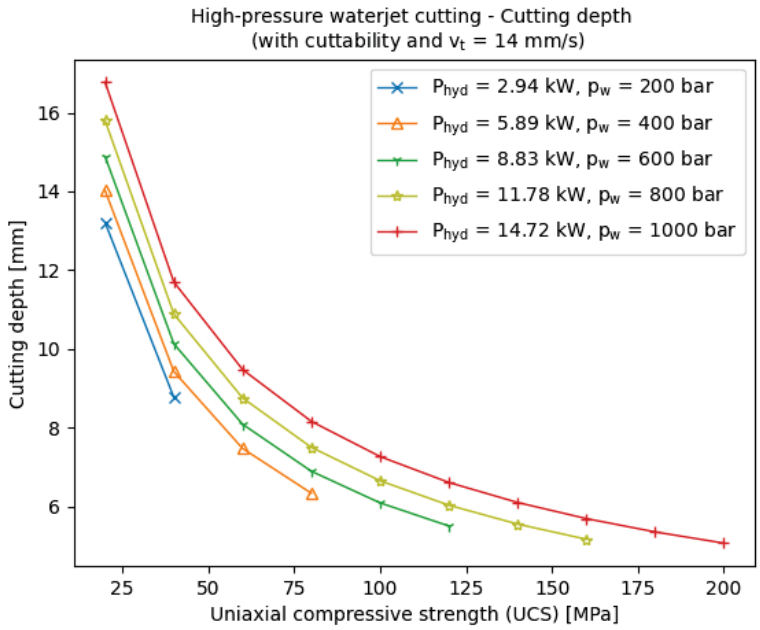

Figure 3.40: High-pressure waterjet cutting - Cutting depth (with cuttability)

Analysing the cutting depth results indicate a lower influence of the water pressure on the cutting depth than expected. The lowest possible water pressure shall be used for excavating rock. The excavation rates for different waterjets are displayed in Figure 3.41, considering the threshold pressure.

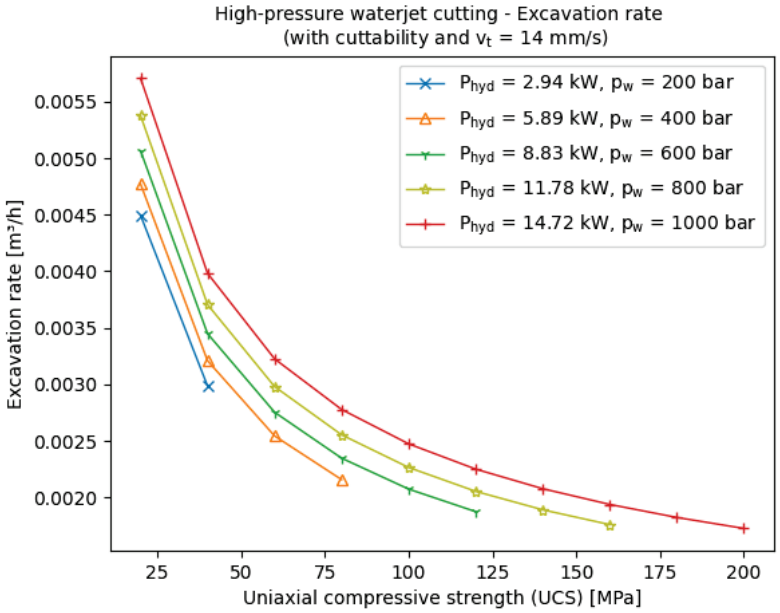

Figure 3.41: High-pressure waterjet cutting - Excavation rate (with cuttability)

The magnitude of the water pressure influences the excavation rate only slightly. The specific energy courses for the five water pressure levels (five hydraulic power levels) are plotted in Figure 3.42.

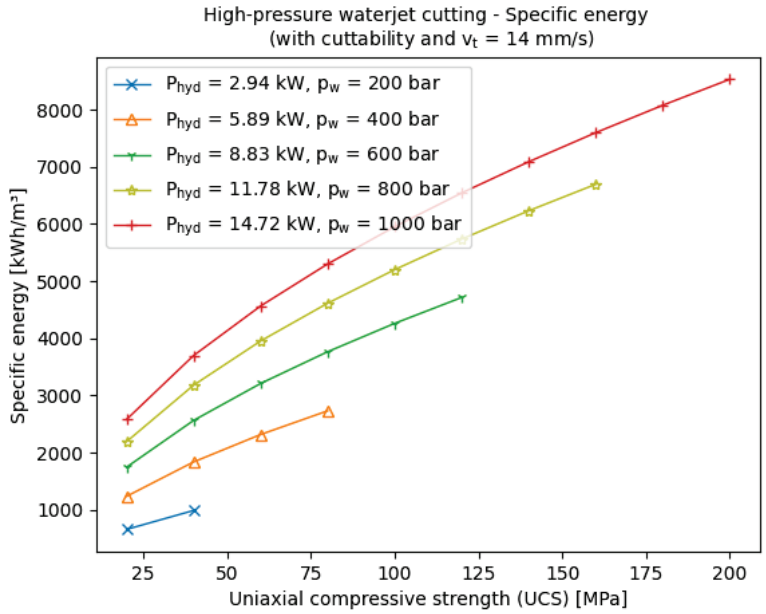

Figure 3.42: High-pressure waterjet cutting - Specific energy (with cuttability)

The specific energy of a high-pressure waterjet, especially compared to mechanical excavation systems, are far from being economical. Expectedly, employing a high-pressure waterjet for economical rock excavation is not feasible. The amount of material being excavated per time unit is negligibly small to use it as an excavation tool. However, the benefits of high-pressure waterjets (such as very low reaction forces and possibility of excavating hard rock) are providing the potential capabilities of an excavation tool concept for a small-scale robot. The low efficiency can be partly bypassed by combining multiple waterjets in order to excavate solid volumes of material. A conceptual idea is described in Section 7.4.

Extensive parameter studies on high-pressure waterjet cutting, evaluating the influence of performance-related parameters are attached in Appendix B.5.

3.2.2 Hydrofracturing

This section is dealing with the applicability of hydrofracturing. The methodology was developed and the simulations were conducted in [137]. Parts of the work are documented in [15]. *Narimani* used DEM simulation to analyse the feasibility of a hydraulic rock fracturing system for a small-scale mining robot by determining minimum hydraulic pressure to fracture the rock in specified borehole layouts.

The rock mass is modelled of tetrahedral blocks representing the rock particles to be formed with a borehole in the center (Figure 3.43).

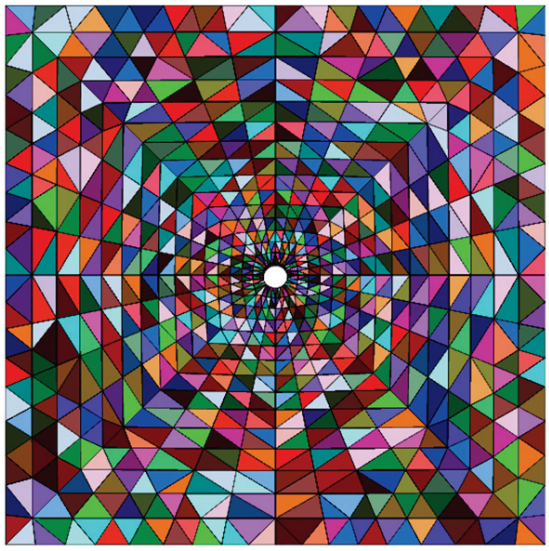

Figure 3.43: The simulation model for a single borehole simulations [137]

In this study, three different types of rocks representing soft, hard and very hard rocks (see Table 3.9) were investigated. Rock mechanics test results of granodiorite

from a previous study in [138], were employed. [15]
In addition, a harder rock is opted with the characteristics similar to a very hard granodiorite. The main difference of the other two rocks is that unlike Granodiorite 1 - which was calibrated based on laboratory tests - the other rocks are artificially made by varying the strength parameters. [137]

Table 3.9: Rock properties of the three rock types [137]

Rock type	σ_c [MPa]	σ_t [MPa]
Sandstone	43.8	3.2
Granodiorite 1	129.7	7.5
Granodiorite 2	218	10

Depending on the strength of the rocks, different pressure ranges paired with a certain flow rate were applied as the boundary conditions of the models. The pressure levels are in the range of 40 to 70 MPa and the total flow rates are limited from 1.3 to 5 l/s. During the simulations, pressure in one point in the sidewall of the borehole was monitored and the final pressure was recorded. In addition, the extension of the fractures were evaluated measured for each case. [137]
A closer examination of the fracture extension around the boreholes revealed that the fractures are divided into three major zones with highly densified cracks, moderately densified cracks and slightly densified cracks. Figure 3.44 shows the developed fractures associated with 50 MPa internal pressure and a total flow rate of 2 l/s. [137]

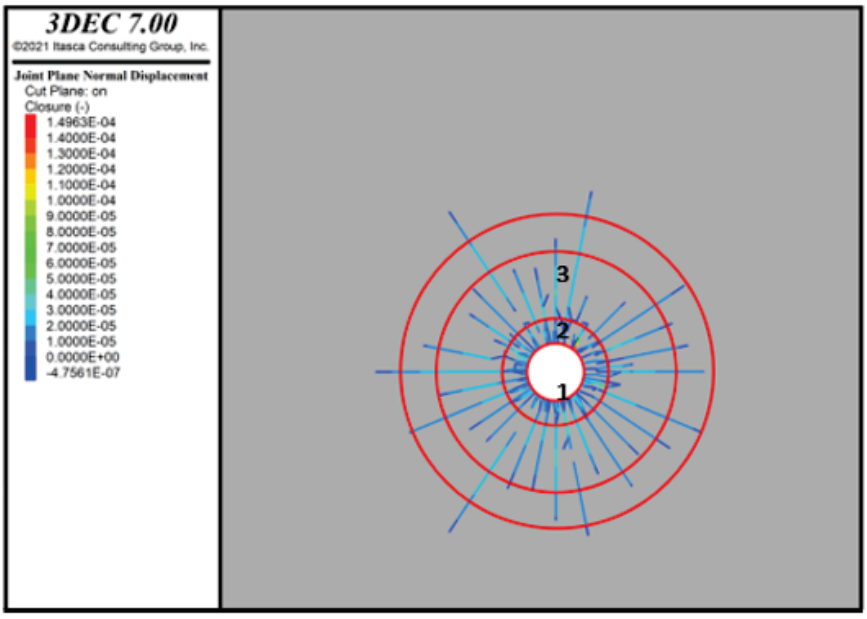

Figure 3.44: Distinction of fractures exceeding 10 μm (Granodiorite 1) [137]

The fractures are numbered from one to three with number three as the lowest fracturing density. [137]

- Zone 1: Highly densified cracks.
- Zone 2: Moderately densified cracks.
- Zone 3: Slightly densified cracks.

Some selected results of the distinction of fractures for different pressure levels are included in Appendix B.7.

The simulations have shown that similar to blasting, an initial free face is required. This was implemented by creating neighboring boreholes with 1 borehole being not pressurized. If high enough pressure is applied in a borehole and the crack propagation reaches the next free face (in this case an empty borehole), the rock is fractured and excavated. [137]

According to blasthole design patterns for small cross-sectional areas, a suitable borehole layout (Figure 3.45) has been designed in [137]. Two pilot holes are drilled in the middle of the pattern to provide an initial free face. The distance of the rest of boreholes will be higher as more free faces are created.
The distance between the boreholes d_1 and d_2 have been set to 60 mm and the borehole diameter d_b to 30 mm. [15, 137]

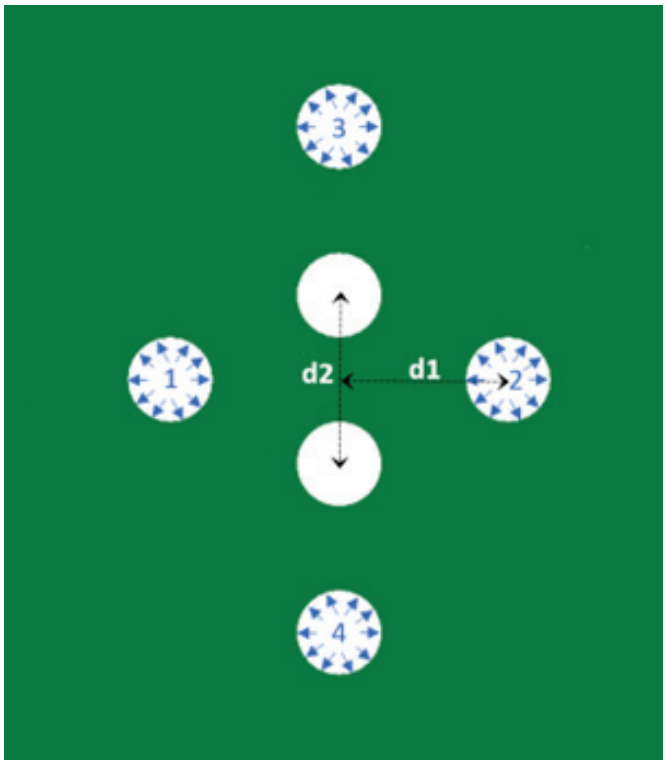

Figure 3.45: A suggested pattern of boreholes for multiple hydrofracturing [137]

Figure 3.46 presents the excavation process of hydrofracturing for a specified borehole design. The empty boreholes are created in the center and the neighboring boreholes a pressurized one after another. The minimum number of boreholes and distances between them are depending on the tunnel geometry and the rock properties.

The theoretical applicability of using hydrofracturing for rock excavation - similar to a rock blasting process - was shown in [137].

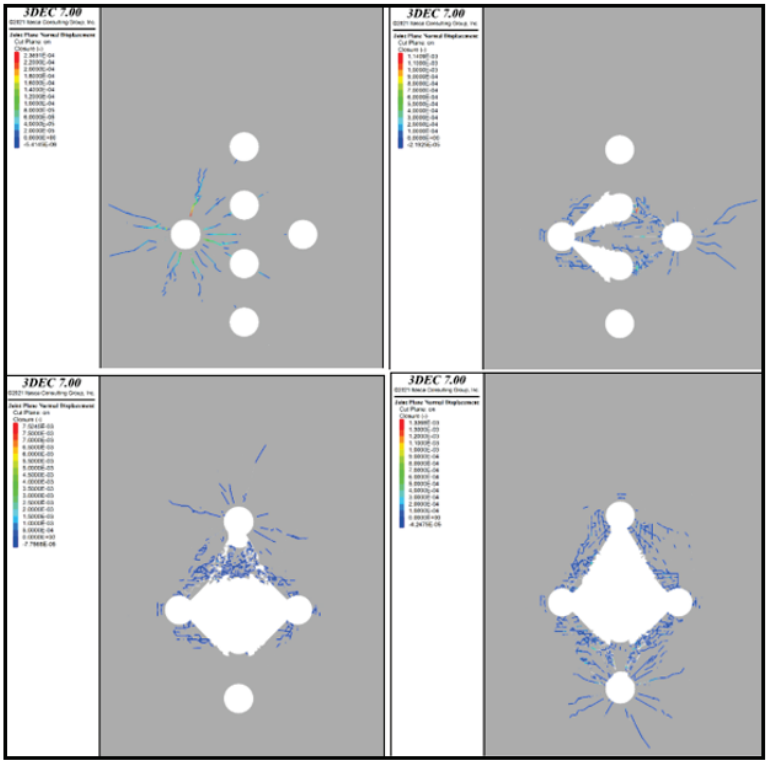

Figure 3.46: Fracture formation as a result of sequential hydrofracturing [137]

The results of the hydrofracturing cycles for excavating a layout as it is seen in Figure 3.46 are summarized in Table 3.10. The specifications of a hydrofracturing tool include the hydraulic pressure to apply internal pressure inside the borehole and a a corresponding flow rate.

Table 3.10: Hydrofracturing specifications for the three rock types [137]

Rock type	Internal pressure [MPa]	Flow rate [l/s]
Sandstone	44	2.69
Granodiorite 1	50	2.43
Granodiorite 2	55	2.63

3.3 Conclusion

Regarding the analyses, studies and investigations in Appendix A and Chapter 3, the following conclusions can be derived: Part-face cutting is a continuous excavation method with suitable performance in soft rock scenarios. The forces generated during the cutting process need to be handled by the robot. Lightweight robot means the magnitude of manageable forces is also low. Due to that finding, a concept of a small part-face cutter head has been developed for soft rock applications. The concept is presented in Section 7.2.

Full-face cutting is not applicable to a robotic miner in that small scale. The forces exerted onto the robot are far away from manageable with such small mass and low power. Machines with comparable power (Mini TBMs) weigh a multiple of the robot. This excavation method is not further used for concept development.

High-pressure waterjet cutting is a promising, alternative excavation method, especially for small-scale mining robots. The reaction forces are negligibly small and the potential of excavating hard rock is great. The overall production rate of the production tool is assumed to be less compared to mechanical excavation methods and the specific energy is high, making it a non-economical tool on a standalone basis. But the ability of easily and environmentally friendly excavating hard rock material is an attractive thought and a concept with a nozzle assembly is investigated in detail and presented in Section 7.4.

Combined excavation systems seem to have high potential for small, mobile mining machines. Those excavation methods cover different, explosive-free rock breaking methods, which combine a conventional (mechanical) tool with an alternative rock fracturing technique. In order to excavate hard rock material, the reaction forces are required to be kept at a manageable magnitude. Since drilling exhibits reasonable reaction forces (particularly rotary drilling), a combination of a rotary rock drilling system and a secondary rock fracturing tool (hydrofracturing) is suggested as an excavation tool for medium hard rocks. Concepts of different drilling tools and a hydrofracturing tool have been developed and are described in Section 7.1 according to the requirements and limitations. Using the conclusions of [137] - summarized in Section 3.2.2 - a hydrofracturing excavation tool has been developed on a conceptual basis and documented in Section 7.4.

The only excavation method which is not limited in terms of rock strength is drill and blast. Full automation of the DB cycle poses a challenge which needs to be overcome in future, and the potential risks need to be reduced to a minimum. Therefore, this method is excluded from the concept development.

4 Full-scale test of a small, longitudinal part-face cutter head

Evaluating suitable excavation technologies and investigating the applicability for certain mining scenarios provided a profound guideline for a selection of potential excavation tools for small-scale mining robots. The findings in Appendix A and Chapter 3 are taken in order to develop a production tool for a prototype of a small robotic miner (Figure 4.1). Due to the benefits of continuous excavation and availability of COTS products, a part-face cutting tool has been selected as excavation tool. This section describes the experimental tests of a small, longitudinal part-face cutter head.

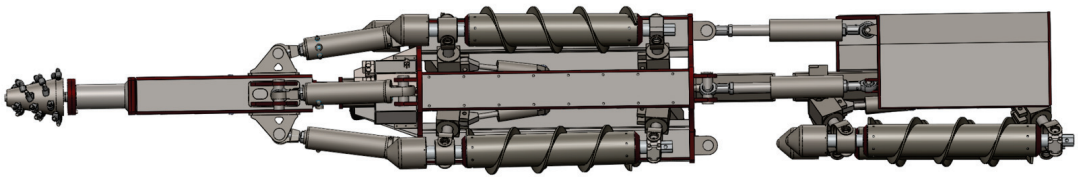

Figure 4.1: Prototype of small-scale mining robot © *ROBOMINERS Consortium*

A major part of the development of the production tool was testing the performance and defining capabilities and limitations. Prior to the concepting of the test setup, the boundary conditions and power requirements of the part-face cutter head have been defined. According to those parameters, the power system of the test rig has been conceptualized. The concept is explained in the following section.
Parts of this content are already documented in [11] and [14].

4.1 Design

The test setup was theoretically developed and the design is briefly described in the next paragraph. The 3D CAD model of the test setup can be seen in Figure 4.2.

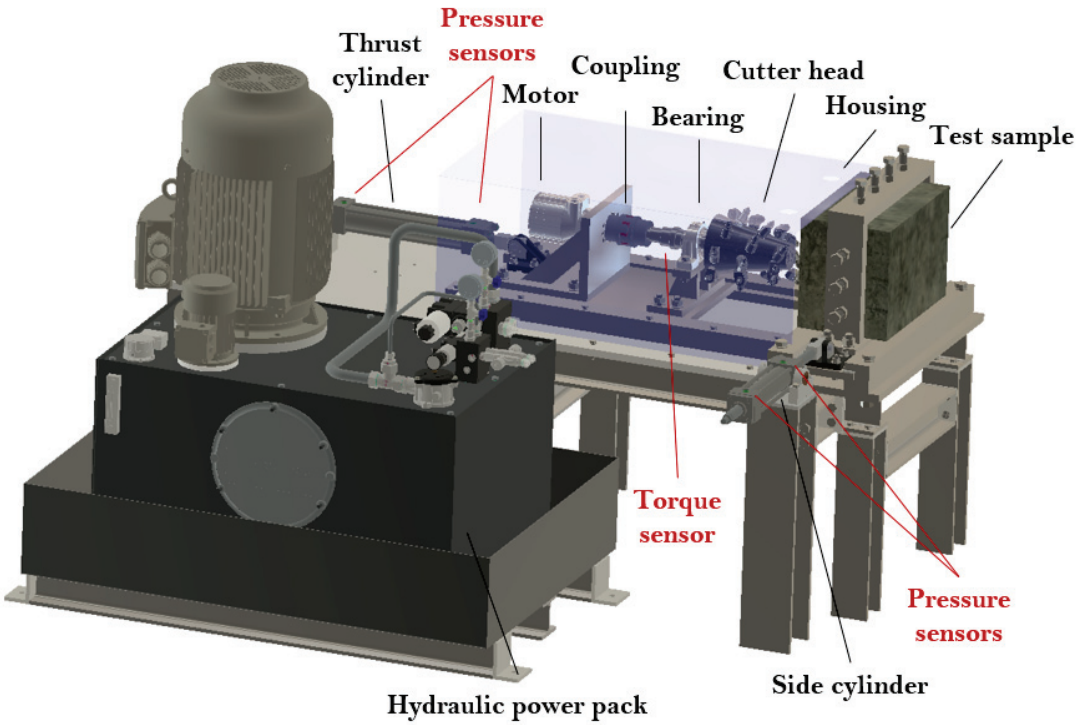

Figure 4.2: 3D model of cutter head test setup [11]

The production tool assembly is mounted on a linear movable sliding system which is connected to the thrust cylinder. The cutter head motor is an 18 kW oil-hydraulic motor and connected via a flexible coupling with the drive shaft. The rock samples are fixed inside a steel cage and can be pinned down with screws to hold it in place during the cutting tests. The side cylinder moves the test sample laterally to the cutter head, also called slewing. All components are made of structural steel to provide enough stability and rigidity. The hydraulic components are powered by a hydraulic power pack next to the test rig, which is controlled with a remote. The motor can be switched on/off and the cylinders actuated independently. The entire production tool is inside a housing which serves as dust preventer and is made out of safety glass to prevent fly-rock. Dust is produced during the cutting operation and a vacuum cleaner is used to keep visibility inside the housing clear. Cylinder forces are constantly measured with a continuous measurement system and the cutting torque is measured with a low-cost torque sensor.

4.2 Laboratory setup

The final setup of the test rig can be seen in Figure 4.3, Figure 4.4 and Figure 4.5.

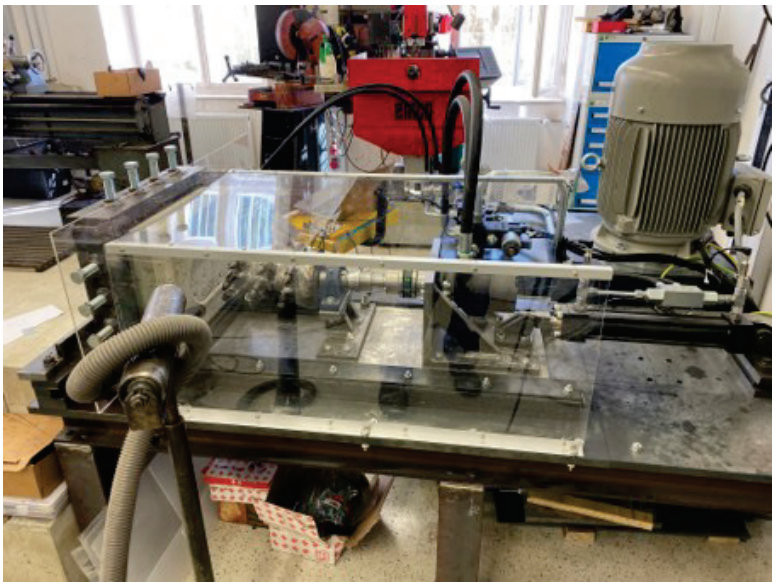

Figure 4.3: Cutter head test rig assembly

Various test samples have been created, which are described in Section 4.3. Those include standard concrete samples with different UCS and concrete samples with oilshale and limestone blocks inserted.

Figure 4.4: Cutter head test rig assembly with measurement system and rock samples

The main components include the main frame, part-face cutter head, cutter head

motor, thrust (axial) and slew (radial) cylinder, test sample cage, test specimen, hydraulic power pack and measurement instruments.

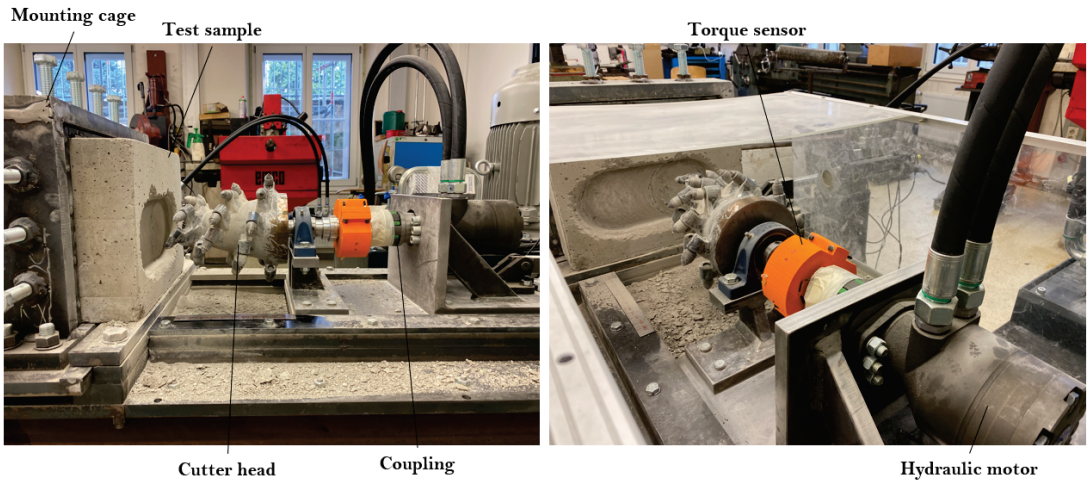

Figure 4.5: Components of the cutter head test rig assembly

The rotational speed of the cutter head motor as well as the cylinder speeds were controlled by proportional valves and kept at constant levels in the individual test scenarios.

4.2.1 Longitudinal cutter head

The cutter head (Figure 4.6) has been designed and manufactured by *Sandvik Mining and Construction* and can be considered as a small-scale version of a longitudinal roadheader's cutter head. The pick tools cut the rock and are orientated in 2 spirals on the cutter head.

Figure 4.6: Original cutter head with 23 picks

The original design of the cutter head included 23 picks. The picks are typically orientated in pairs with 180° angular offset, except the foremost pick, which was attached as a single pick. Due to its position, the most cutting work in a cutting cycle had to be performed by this pick.

After some initial cutting tests, major wear on pick 1 could be seen and a 24^{th} pick has been added (Figure 4.7), which is at 180° offset to pick 1 and allows to split the load between those two picks. The comparison of both designs is summarized in Section 4.3.

Figure 4.7: Adapted cutter head with 24 picks

4.2.2 Condition monitoring

During the experimental tests, a continuous observation of forces was required in order to classify the performance in different rock strength regimes. The parameters being measured were the forces required for moving the cutter head assembly axially and radially as well as the cutting torque and cutting force. Two low-cost *Arduino*-based measurement instruments have been developed.

4.2.2.1 Cylinder forces

The cylinder forces have been measured with 4-20 mA pressure sensors, and a signal processing system has been developed. The electrical signal is converted to a voltage between 0-5 V and constantly read by an *Arduino Uno*. The microcontroller is connected to a measurement laptop and a self-developed processing program allows to measure the hydraulic pressures and convert them to cylinder forces in real-time.

4.2.2.2 Cutting torque and cutting force

The cutting torque needed also to be measured during the entire cutting process to get feedback about the occurring cutting forces depending on the following parameters:

- Number of picks in contact / total sump-in depth.
- UCS of material.

A low-cost torque sensor has been developed, which measures the forces with 2 strain gauges in a Full-Wheatstone-Bridge system. The voltage difference is converted and amplified by an A/D-converter and read by an *Arduino Nano* microcontroller. The torque sensor is battery-powered and the data is written to a Micro-SD card. To obtain correct results it was necessary to calibrate the data processing code precisely.

The cutting torque has then be used to derive the cutting forces of the cutter head.

4.3 Test methodology

The performance of the cutter head has been tested by two predefined tests (see Figure 4.8):

- Axial cutting test: Cutting into the rock sample axially by actuating the thrust cylinder.
- Radial cutting test: Cutting into the rock sample radially by actuating the side cylinder and moving the rock sample.

For each test, the cylinder forces and cutting torque have been measured.

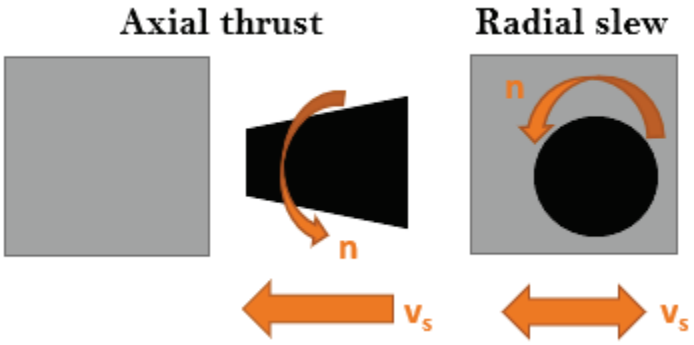

Figure 4.8: Illustration of cutting cycle [11]

The rotational speed of the cutter head has been set at a constant speed of n = 300 rpm, whereas two slew speed levels (v_s = 7 mm/s and 14 mm/s) have been used, further named as slow slew and fast slew. For each rock strength category, 5 test sets have been made to minimize statistical errors, summarized in Table 4.1.

Table 4.1: Test scenarios

	Rotational speed [rpm]	Slew speed [mm/s]
Slow slew	300	7
Fast slew	300	14

Depending on the cutting depth and the angular orientation of the cutter head, a certain number of picks is in contact with the rock. Each test specimen has been cut incrementally by increasing the total sump-in depth. The number of picks in contact increases linearly with the total-sump in depth.

4.3.1 Test samples

An example of a test sample can be seen in Figure 4.9. Various concrete samples (23 and 30 MPa UCS, further called B20 and B30 concrete), oilshale (16 MPa UCS) and limestone (60–80 MPa, not measured) have been created. In order to obtain compact samples, the oilshale and limestone samples have been cast inside a concrete block.

Figure 4.9: Test specimen - 400 x 230 x 300 mm (w x l x h)

The material properties of the test samples are presented in Table 4.2.

Table 4.2: Properties of test specimens

Test specimen	σ_c [MPa]	σ_t [MPa]	CAI
B20 concrete	23[1]	2.2[1]	2.08[2]
B30 concrete	30[3]	3.0[3]	2.08[3]
Oilshale	16[4]	1.6[4]	0.5[5]

[1]UCS and BTS test results documented in [139].
[2]CAI measurements conducted by [140].
[3]Assumed according to comparative values found in [141].
[4]UCS and BTS of oilshale tested and documented in [142].
[5]Experience based value.

4.3.1.1 Oilshale sample

To test the cutting performance in close-to-realistic conditions, rock samples with oilshale insertions have been created. Therefore, oilshale blocks (Figure 4.10) have been moulded into B20 concrete in different orientations and layers.

Figure 4.10: Oilshale block

A completely cut specimen after a full cutting test cycle can be seen in Figure 4.11.

Figure 4.11: Cut specimen with oilshale insertions

4.3.1.2 Mixed sample

Eventually, a mixed sample with oilshale and limestone insertions has been created to be able to test the cutting performance in soft to medium hard rock. The rock samples were extracted from an open-pit oilshale mine. The UCS of limestone has not been measured, but the sample provider assumed it to be between 60–80 MPa. The mixed sample is presented in Figure 4.12. Oilshale layers can be seen on the top and limestone insertions are visible on the front face.

Figure 4.12: Test specimen with oilshale layers and limestone insertions

4.3.2 Cutting tests

For each material sample, various cutting tests - separated in axial and radial cutting tests - have been made and cylinder forces and cutting torque have been measured. Figure 4.13 shows an entirely cut concrete sample with debris.

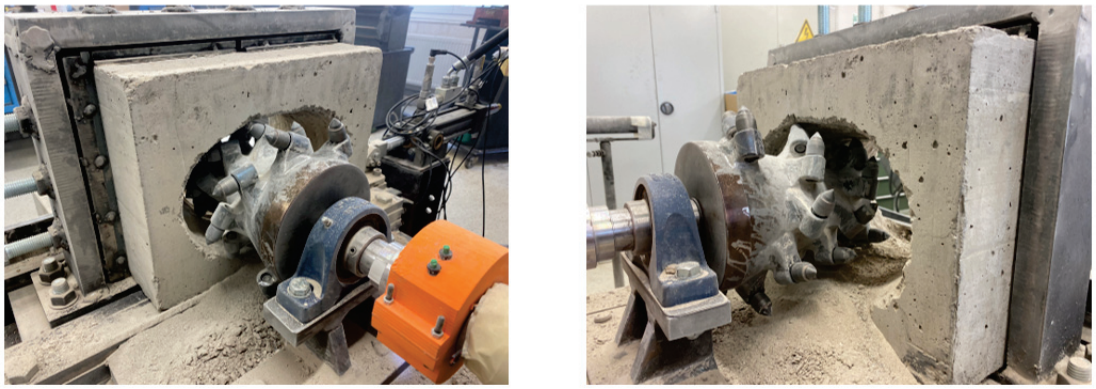

Figure 4.13: Cutting test of B20 concrete

Axial and radial cutting tests have been done alternating. A partly cut specimen with the cutting profile is shown in Figure 4.14. In this image, the number of picks in contact and the pick spacing between the picks can be seen well.

Figure 4.14: Partly cut test specimen

For a detailed assessment of the cylinder forces, a continuous monitoring and recording of the individual forces was desired. The measurement of the cylinder forces allowed the determination of force specifications for individual test specimens and UCS levels. An example of the raw cylinder forces is shown in Figure 4.15.

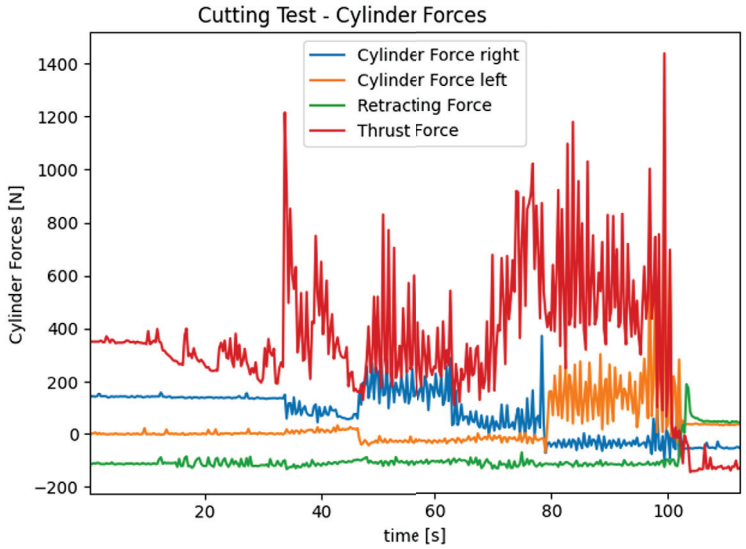

Figure 4.15: Measured cylinder forces before postprocessing

The raw forces have been postprocessed accordingly to obtain the thrust (axial) and slew (radial) forces of the cylinders, which define the required forces for

moving the cutting boom. Result plots with axial/radial force, cutting torque and cutting forces have been made for each test (Figure 4.16).

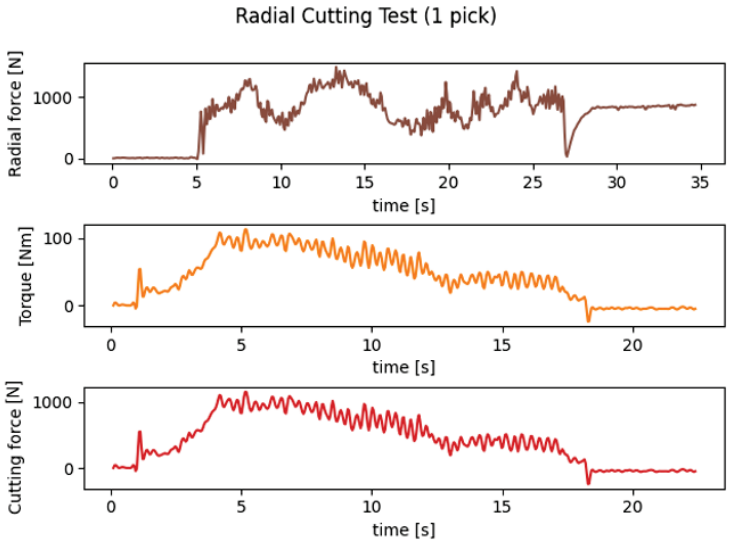

Figure 4.16: Postprocessed results

4.3.3 Adaption of cutter head

The cutter head design needed to be adapted due to major wear on pick 1 (Figure 4.17), caused by a few cutting cycles of B20 concrete. According to the B20 concrete's CAI value, the material is considered to be very abrasive [50]. Furthermore, the issue of having only 1 pick cutting the rock leads to an imbalance of the cutting force.

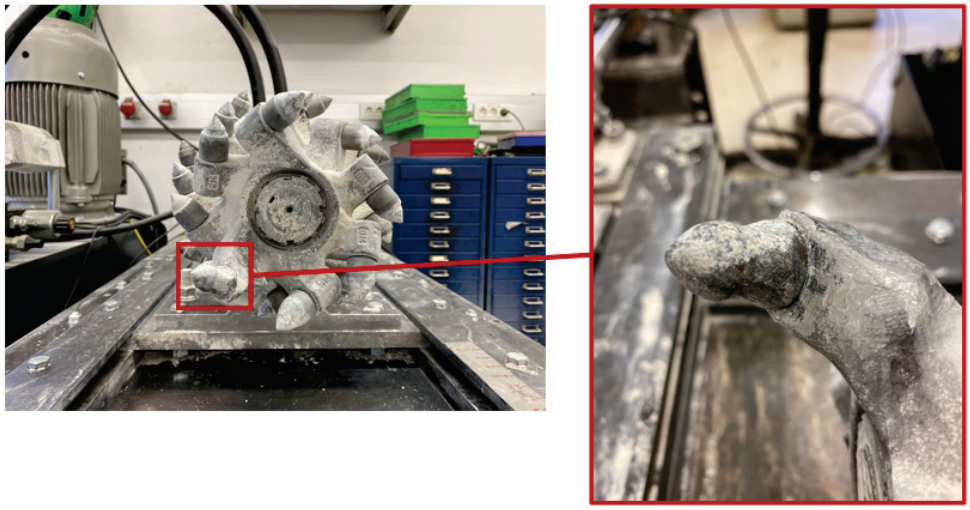

Figure 4.17: Significant wear of pick #1

This downside has been eradicated by adding another pick at the same axial position as pick #1 with 180° angular offset to obtain an opposing pick pair. Further advantages of attaching an additional pick are load sharing, improved cutting force balance and an overall smoother cutting operation. The original and adapted cutter head are shown in Figure 4.18.

Figure 4.18: Original (left) and adapted (right) cutter head

The advantage of the adapted cutter head over the original cutter head can be seen by much smaller measured force amplitudes. Further on, the processing software has been revised and improved to obtain higher resolution of the measurement data. An exemplary plot of the cutting torque and cutting force of adapted cutter head and updated software can be seen in Figure 4.19.

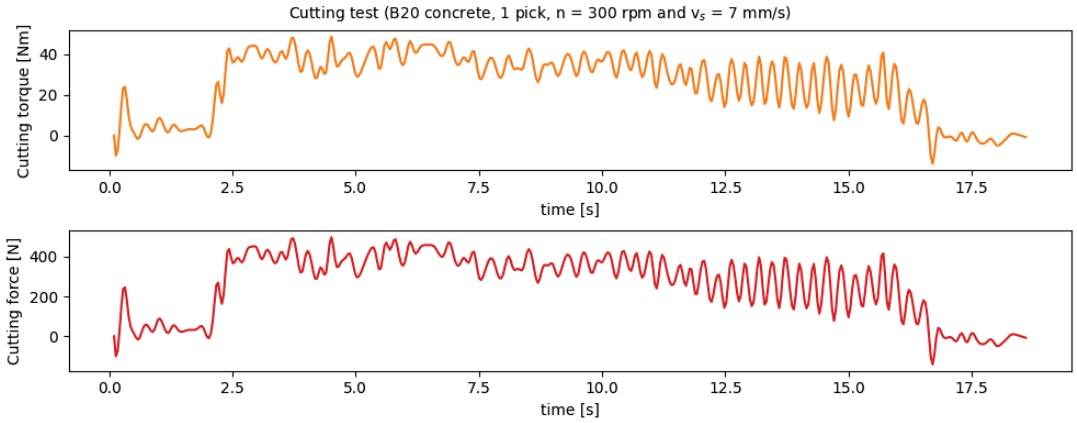

Figure 4.19: Exemplary measurements of cutting test [11]

4.4 Results

The results of the conducted cutting tests are summarized and analysed in this section. The results include axial force, radial force, cutting torque and cutting force of B20 concrete, B30 concrete and oilshale cutting tests.

All obtained measurement results are enclosed in Appendix C in processed and comprehensive mode of presentation, including statistical analyses.

4.4.1 Slow slew

This section concludes cutting tests with a constant rotational speed $n = 300$ rpm and a constant cylinder slew speed of $v_s = 7$ mm/s. For each test specimen type, 5 cutting cycles have been performed. A full cutting cycle consists of alternating axial and radial cutting tests with incrementally increasing sump-in depth until the cutter head is entirely in contact with the specimen. For every test specimen at least two full cutting cycles have been conducted.

4.4.1.1 Cylinder forces

The entirety of maximum measured axial forces and radial forces are depicted in Figure 4.20 and 4.21 respectively, whereas the dashed lines indicate the average values of each sump-in depth level.

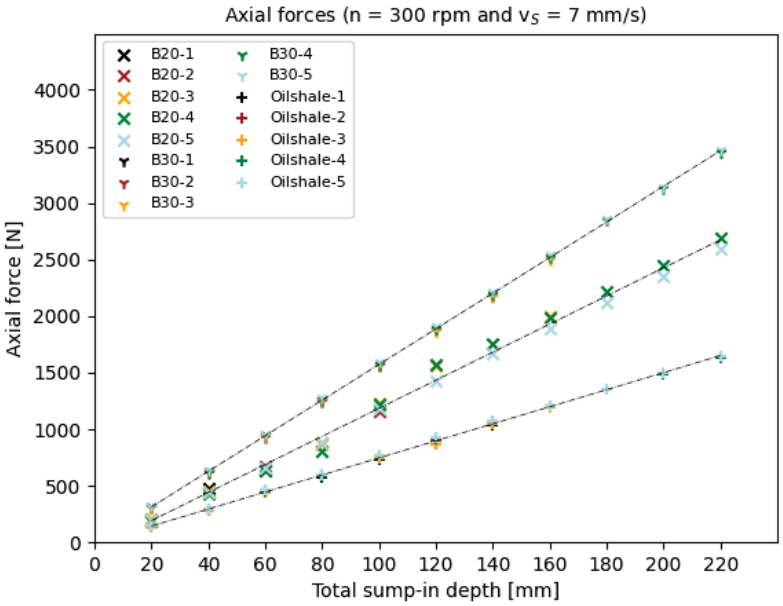

Figure 4.20: Slow slew - Axial forces

The minimum, maximum and average results of full sump-in cutting are outlined in Table 4.3 and Table 4.4.

Table 4.3: Slow slew - Summary of axial forces (full sump-in)

Test sample	$F_{a,min}$ [N]	$F_{a,max}$ [N]	$\overline{F_a}$ [N]
B20 concrete	2597	2690	2644
B30 concrete	3451	3467	3459
Oilshale	1636	1649	1643

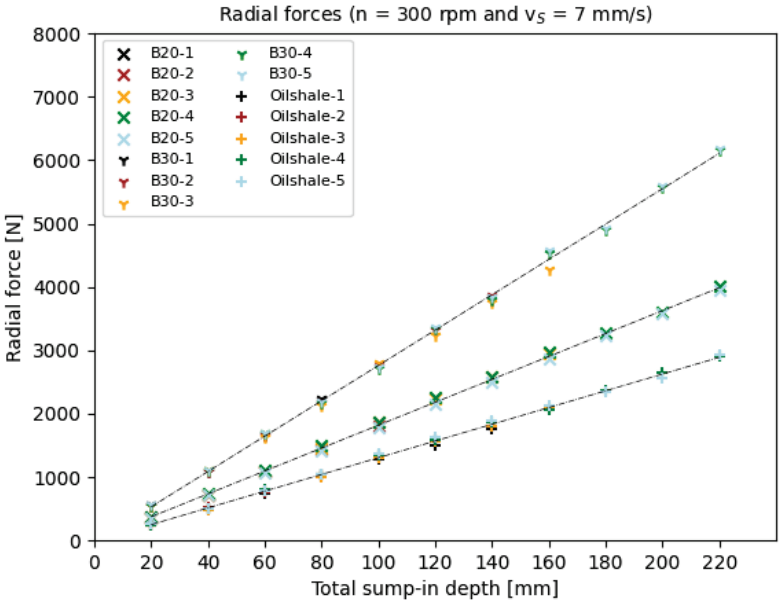

Figure 4.21: Slow slew - Radial forces

Table 4.4: Slow slew - Summary of radial forces (full sump-in)

Test sample	$F_{r,min}$ [N]	$F_{r,max}$ [N]	$\overline{F_r}$ [N]
B20 concrete	3952	4017	3985
B30 concrete	6152	6177	6165
Oilshale	2901	2924	2912

Both forces show a slightly degressive trend with increasing sump-in depth. This trend is evaluated to be plausible because of increasing number of picks in contact. The magnitude of the cylinder force is depending on the uniaxial compressive strength of the material, as expected. The higher the UCS of a specimen to be cut is, the higher are the required cylinder forces.

4.4.1.2 Cutting torque

The cutting torque measurements for all slow slew cutting tests are shown in Figure 4.22. This graph shows the maximum cutting torque of each individual cutting test which is acting on the cutter head drive shaft.

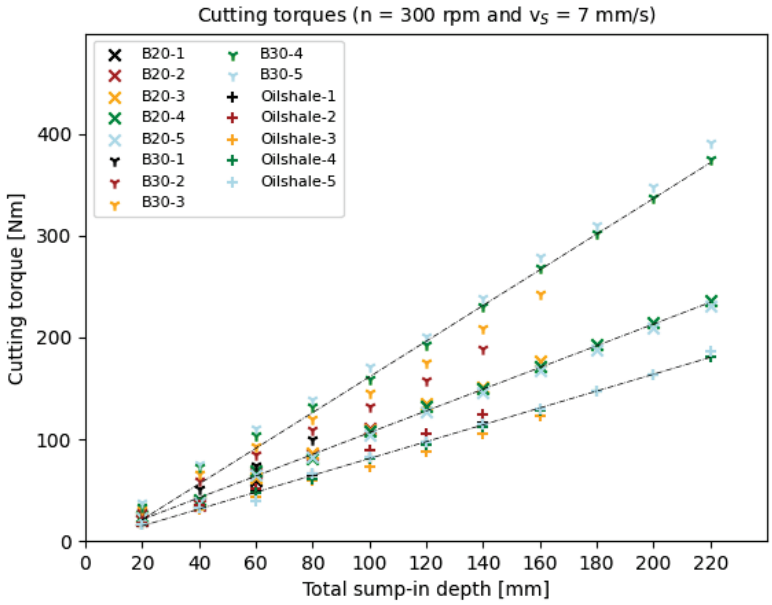

Figure 4.22: Slow slew - Cutting torques

Sufficient cutting torque needs to be provided by the cutter head motor in order to cut rock. Table 4.5 summarizes the minimum, maximum and average measured cutting torque for full sump-in cutting of each test sample.

Table 4.5: Slow slew - Summary of cutting torques (full sump-in)

Test sample	$T_{c,min}$ [Nm]	$T_{c,max}$ [Nm]	$\overline{T_c}$ [Nm]
B20 concrete	231	236	234
B30 concrete	375	392	384
Oilshale	181	187	184

Analysing the cutting torque measurement data, a linear correlation between the cutting torque and the uniaxial compressive strength of the test specimen can be recognized. The average cutting torque $\overline{T_{c,slow}}$ for slow slew can be estimated with Equation 4.1 below, whereas σ_c is the uniaxial compressive strength.

$$\overline{T_{c,slow}} = 1.1 \cdot \sigma_c - 1.5 \tag{4.1}$$

4.4.1.3 Cutting force

The cutting force can be derived from the measured cutting torque and the effective pick radii. The results are displayed in Figure 4.23.

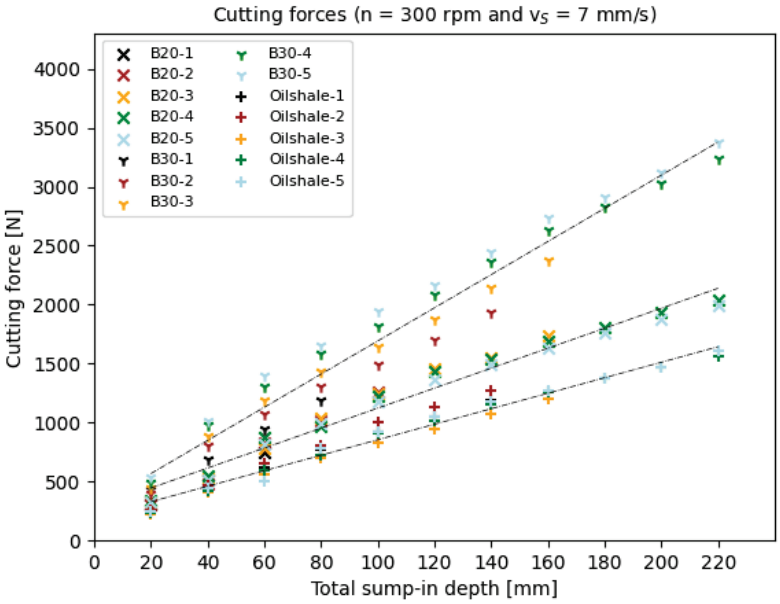

Figure 4.23: Slow slew - Cutting forces

The boundary values are summarized in Table 4.6 and a linear regression of the cutting force measurement depending on the UCS has been made and is graphically shown in Figure 4.24.

Table 4.6: Slow slew - Summary of cutting forces (full sump-in)

Test sample	$F_{c,min}$ [N]	$F_{c,max}$ [N]	$\overline{F_c}$ [N]
B20 concrete	1994	2037	2016
B30 concrete	3237	3384	3311
Oilshale	1563	1614	1588

The linear regression provides a satisfying approximation of the cutting force for different UCS values and the average cutting force $\overline{F_{c,slow}}$ for slow slew can be calculated with Equation 4.2, in which σ_c is the uniaxial compressive strength.

$$\overline{F_{c,slow}} = 16.6 \cdot \sigma_c - 19 \tag{4.2}$$

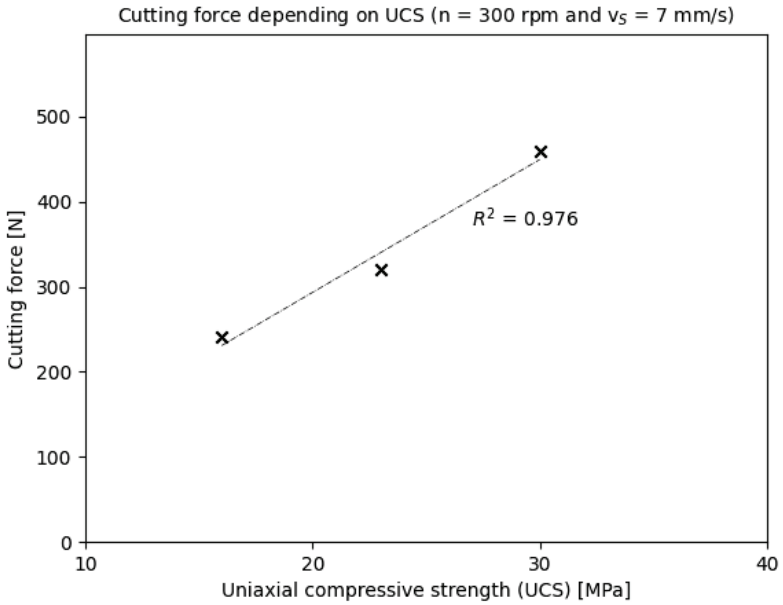

Figure 4.24: Slow slew - Cutting force assumption [11]

4.4.2 Fast slew

The fast slew test cases describe the compendium of cutting tests with a constant rotational speed $n = 300$ rpm and a constant cylinder slew speed of $v_s = 14$ mm/s.

Analogues to the slow slew test cases, cylinder forces and cutting torques have been measured. The resulting axial and radial forces as well as the cutting torque and cutting force are summarized in this section.

4.4.2.1 Cylinder forces

Axial thrust forces and radial slew forces are shown in Figure 4.25 and Figure 4.26. Because of the fast slew speed and resulting higher, maximum cutting depth of a single pick, a full sump-in of the cutter head could not be performed. The maximum available torque of the cutter head motor has been exceeded at some points and a constant slew motion could not be maintained.

In order to obtain consistent measurement results, the tests in which the slew speed had to be reduced were not taken into account for the analysis.

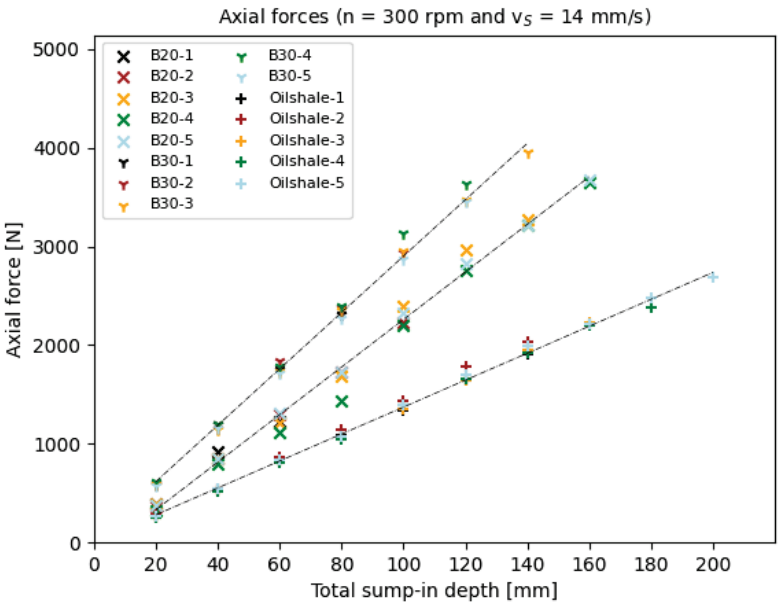

Figure 4.25: Fast slew - Axial forces

The maximum number of picks in contact n was 8 for the B20 concrete, 7 for the B30 concrete and 10 for the oilshale samples, used in Table 4.7 and Table 4.8 representing the maximum, minimum and average measured cylinder forces at maximum total sump-in depth.

Table 4.7: Fast slew - Summary of axial forces

Test sample	$F_{a,min}$ [N]	$F_{a,max}$ [N]	$\overline{F_a}$ [N]
B20 concrete (n = 8)	3653	3680	3666
B30 concrete (n = 7)	3955	3955	3955
Oilshale (n = 10)	2694	2694	2694

Table 4.8: Fast slew - Summary of radial forces

Test sample	$F_{r,min}$ [N]	$F_{r,max}$ [N]	$\overline{F_r}$ [N]
B20 concrete (n = 8)	5490	5586	5538
B30 concrete (n = 7)	6854	6854	6854
Oilshale (n = 10)	4610	4610	4610

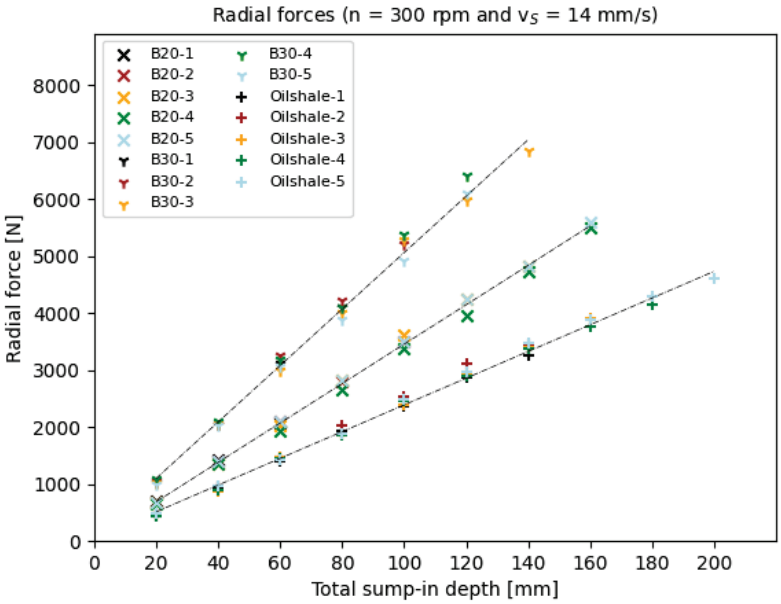

Figure 4.26: Fast slew - Radial forces

4.4.2.2 Cutting torque

Similarly to slow slew cutting tests, the cutting torque has been measured in various tests for B20 concrete, B30 concrete and oilshale (Figure 4.27).

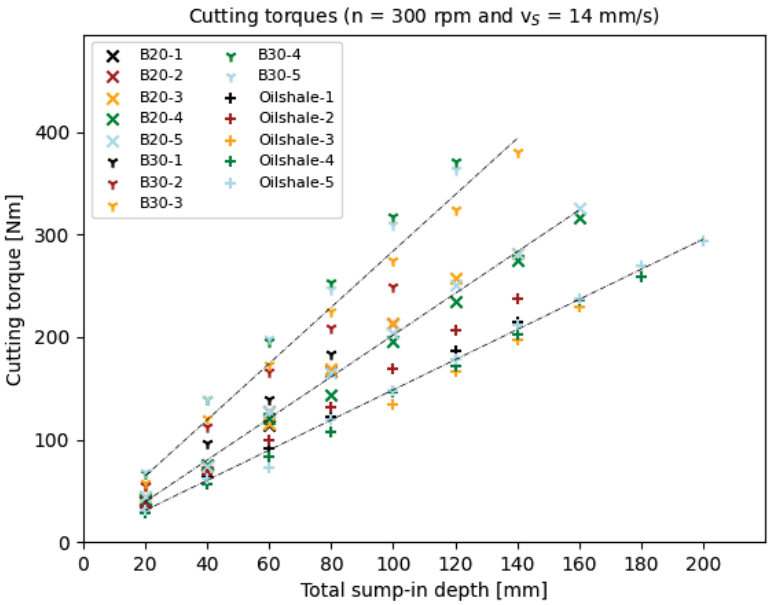

Figure 4.27: Fast slew - Cutting torques

Again, a slightly degressive trend of the cutting torque can be observed and due to the faster slew speed, the measured cutting torque is much higher compared to

the slow slew speed cutting test (Table 4.9).

Table 4.9: Fast slew - Summary of cutting torques

Test sample	$T_{c,min}$ [Nm]	$T_{c,max}$ [Nm]	$\overline{T_c}$ [Nm]
B20 concrete (n = 8)	317	326	321
B30 concrete (n = 7)	381	381	381
Oilshale (n = 10)	294	294	294

For $v_s = 14$ mm/s, the average cutting torque $\overline{T_{c,fast}}$ can be approximated with Equation 4.3 below.

$$\overline{T_{c,fast}} = 2.1 \cdot \sigma_c - 4.0 \tag{4.3}$$

4.4.2.3 Cutting force

The cutting force has been derived from the measured cutting torque and the results are shown in Figure 4.28.

Table 4.10 shows the maximum, minimum and average cutting forces for each individual test specimen.

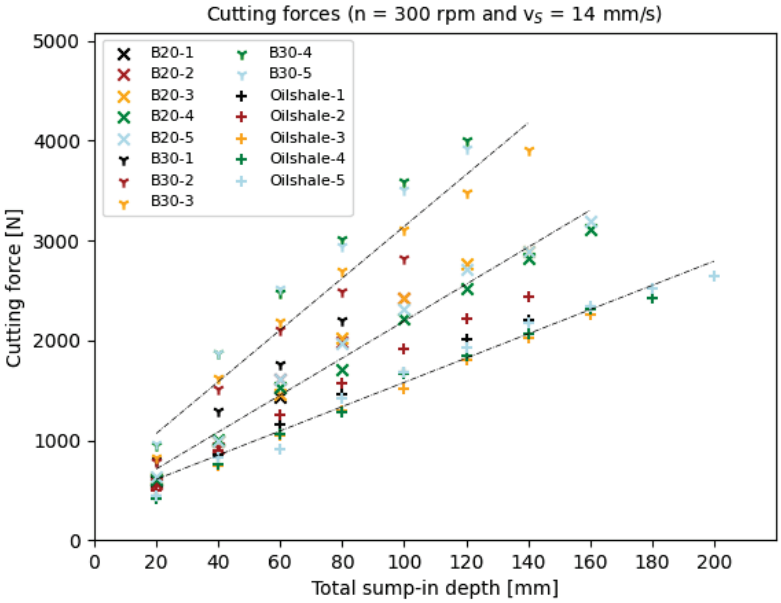

Figure 4.28: Fast slew - Cutting forces

Again, a linear regression provides the relation of the cutting force and the uniaxial compressive strength of the to be cut (Figure 4.29).

Table 4.10: Fast slew - Summary of cutting forces

Test sample	$F_{c,min}$ [N]	$F_{c,max}$ [N]	$\overline{F_c}$ [N]
B20 concrete (n = 8)	3107	3192	3149
B30 concrete (n = 7)	3911	3911	3911
Oilshale (n = 10)	2646	2646	2646

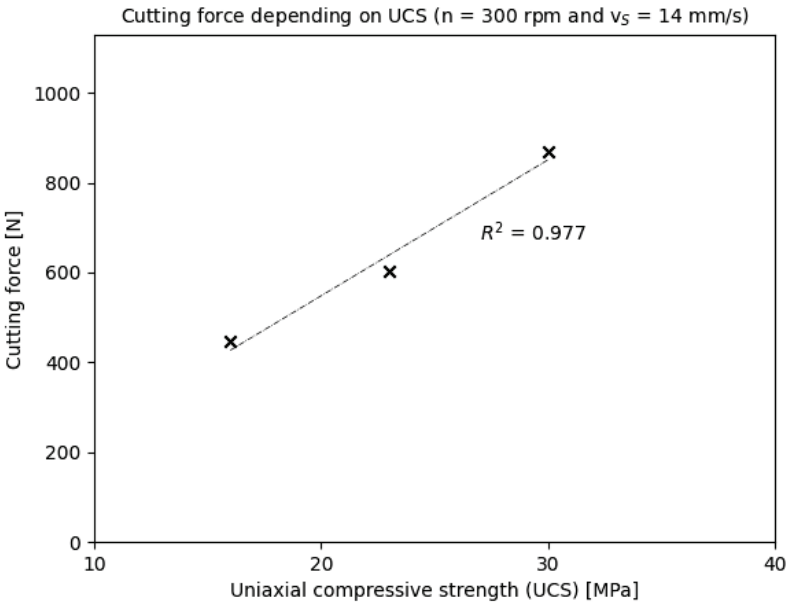

Figure 4.29: Fast slew - Cutting force assumption

Due to the linear behavior, the average cutting force $\overline{F_{c,fast}}$ for $v_s = 14$ mm/s can be estimated with Equation 4.4.

$$\overline{F_{c,fast}} = 30.3 \cdot \sigma_c - 57.4 \tag{4.4}$$

The conducted experimental tests served as analysis of forces acting on the longitudinal part-face cutter head and provided specifications for the application as production tool in a small mining robot prototype. The highlighted results shall be consulted for dimensioning of structural parts in the robot and limit the maximum UCS of a rock to be excavated.

4.5 Performance assessment

In order to assess the performance of the production tool, the excavation rate and advance rate are approximated in this section.

4.5.1 Excavation rate and advance rate

The prototype is supposed to be tested in an open-pit oilshale mine. The oilshale deposit is intersected by shallow limestone layers. Therefore, the excavation performance has been tested especially for oilshale samples.

The excavation rate is highly depending on the rock strength. The hardest rock which has been cut was limestone with an approximate UCS of 60-80 MPa. Cutting limestone was hardly possible, only with a discontinuous slew motion cutting tiny amounts of rock was feasible. Oilshale (UCS = 16 MPa) could be cut considerably faster.

The excavation rate has been calculated by measuring the excavated volume after a certain amount of time. In this case, 15 s cutting tests have been made and the average results for concrete, oilshale and limestone have been summarized. The advance rates have been assumed for a circular tunnel profile and calculated with a constant tunnel diameter of 1 m.

Concrete up to 30 MPa

- In 15 s a volume of approximately 6.5×10^{-4} m^3 (excavation rate is approximately 0.157 m^3/h) was excavated.
- The estimated advance rate is about 0.2 m/h.

Oilshale

- An excavation rate of maximum 0.8 m^3/h was achieved.
- The estimated advance rate in pure oilshale conditions is about 0.63 m/h.

Limestone

- The estimated excavation rate is difficult to estimate and not precise because of discontinuous cutting. A rough approximation of the excavation rate in limestone conditions is 0.01 m^3/h.
- Additionally, the high rotational speed and slow slew speed result in heavy dust generation.

The cutting tests showed an application limit of the part-face cutter head for rocks with maximum UCS of < 40 MPa to be able to excavate with a reasonable, continuous excavation and advance rate.

4.5.2 Particle size of excavated material

The particle size distribution is crucial for the conveying of the material. An even distribution is preferred to design a suitable transport method for the mined ore and host rock. The grain size is depending on rock strength, rock mass and rock formation as well as on rotational speed and slew speed of the part-face cutter head.

Concrete is a very compact material without greater fault zones, which results in very fine debris and dust formation (Figure 4.30), because initiated cracks hardly propagate in tough rocks. Oilshale typically tends to spall in chips and irregular particle sizes (Figure 4.31).

Figure 4.30: Debris of B20 concrete sample

Figure 4.31: Debris of oilshale sample

The layering of the oilshale inside the sample leads to a very difficult to estimate particle size distribution. Grain sizes up to 5 cm have been occurred regularly. Particles and dust of concrete and limestone could be easily removed with a standard vacuum cleaner, small oilshale particles too.

4.5.3 Wear of pick tools

The abrasivity of material is responsible for the grade of wear. The abrasivity is categorized with the cerchar abrasivity index.

- CAI concrete: = 2.08: Very abrasive and high wear of pick tools.
- CAI oilshale = 0.5: Little abrasive and very low wear of pick tools.

Figure 4.32 shows a new pick, a pick with minor wear (oilshale samples) and a pick with major wear (B20 concrete samples). Both worn picks have been inspected after cutting a volume of 0.01 m^3. The majorly worn pick is significantly reduced in diameter, but the tip angle has been kept in a good shape due to the self-sharpening character of the conical pick tool.

Figure 4.32: New pick (left), pick with minor wear (center) and pick with major wear (right)

In Figure 4.33, different stages of wear are presented. Starting with a new pick until a heavily worn conical pick tool.

Figure 4.33: Increasing wear on conical pick tools

The pick rotates inside the pick holder to get even wear and maintain a sharp tip. Heavy dust residue between pick and pick holder prevents a pick from rotating and generates one-sided wear. A one-sided worn pick has increased contact stresses and eventually increases the cutting forces. If a pick is worn, the neighbouring picks need to take over the cutting work. If tip height is reduced by approximately 5 mm, it is recommended to exchange the pick by a new one.

4.6 Conclusion

The following conclusions regarding the cutting efficiency and the overall performance can be derived from the cutting tests:

Cutting tests

- Conduct of cutting tests with test specimens of 23 MPa (concrete), 30 MPa (concrete) and 16 MPa (oilshale) UCS.
- Forces and torque are are linearly correlating with the uniaxial compressive strength of the material.
- The part-face cutter head is applicable in soft rock conditions, particularly at maximum UCS of 30 MPa in order to obtain relatively efficient excavation performance.

Performance

- Generally, no high performance is expected, because of low power and small mass of the test rig/robot. Slow advance and excavation rates are expected.
- Abrasive material leads to excessive wear of pick tools. (Usually, proportion of quartz is decisive. Concrete is very abrasive, oilshale is little abrasive).
- Loose/brittle material - especially with layers and fault zones - tends to break in larger chunks. Difficult to have evenly distributed grain size of excavated material.
- Oilshale
  - Irregular grain size of excavated material.
  - Satisfying excavation rate because of low uniaxial compressive strength.
- Limestone
  - Fine particles and heavy dust formation.
  - Poor excavation process because of high uniaxial compressive strength.

5 Modelling approach for predicting the cutting forces of part-face cutter heads

In order to be able to predict the cutting forces of a part-face cutter head, a combination of a kinematic model of the cutting process and a cutting force calculation approach is introduced. This chapter includes a review of existing rock cutting theories, the adaption and application of one theory and a developed methodology to calculate the dynamic cutting forces of a part-face cutter head. The content has already been published in [11] and extensive results are presented in Appendix D.

5.1 Theoretical background on part-face cutting

Subsequently, the theoretical background of mechanical cutting with focus on rock cutting with conical pick tools is outlined. A recapitulation of Appendix A.2.2 is done in greater detail. Standard mechanical cutting machines use cutting drums (continuous miners) or cutter heads (roadheaders) to excavate ore. Cutter heads are typically either transversal or longitudinal cutter heads. Transversal cutter heads exhibit a general higher efficiency, are capable of cutting harder rock compared to longitudinal cutter heads and therefore have become established as a prominent machines in mining and tunnelling. [15]

5.1.1 Longitudinal cutter head

A longitudinal cutter head has the rotation axis of the cutter head in-line with the boom axis (Figure 5.1). The picks are arranged in a spiral shape up to the front end of the drum [24]. The positions of the picks are precisely defined and have to be harmonized in order to generate a continuous excavation pattern without

interfering with each other and to excavate the entire cutting volume during slewing [14, 15].

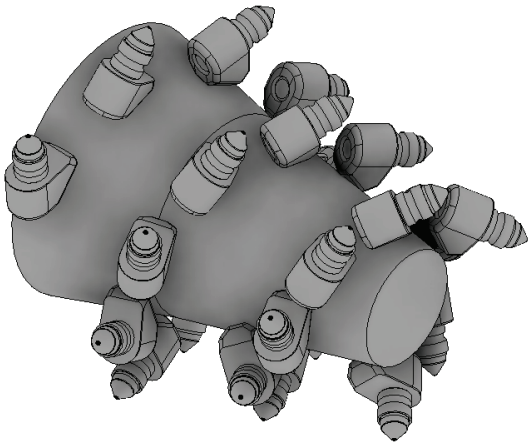

Figure 5.1: Longitudinal cutter head [11]

The design of the cutter head is highly depending on the material to be excavated, taking into account various rock properties, the overall rock mass rating and the specifications of the carrier machine.

5.1.1.1 Cutting process

Once the cutter head is in contact with the rock, the interaction between the cutter head with the rock can be distinguished in three contact types. The cutting depth of the pick changes with the rotation angle of the cutter head.

- Progressive cut: The pick cutting depth is increasing from a minimum ($\sim$ 0) to a maximum (Figure 5.2).

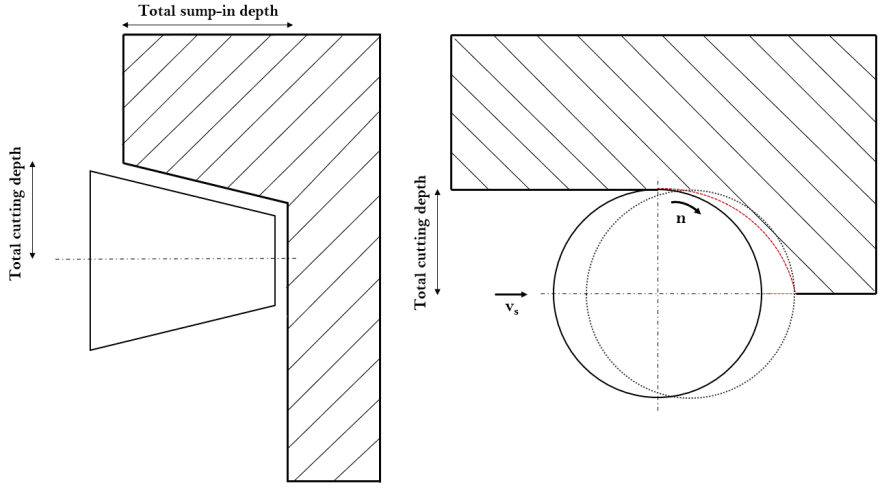

Figure 5.2: Progressive cutting (PC)

- Degressive cut: The pick cutting depth is decreasing from a maximum to a minimum (Figure 5.3).

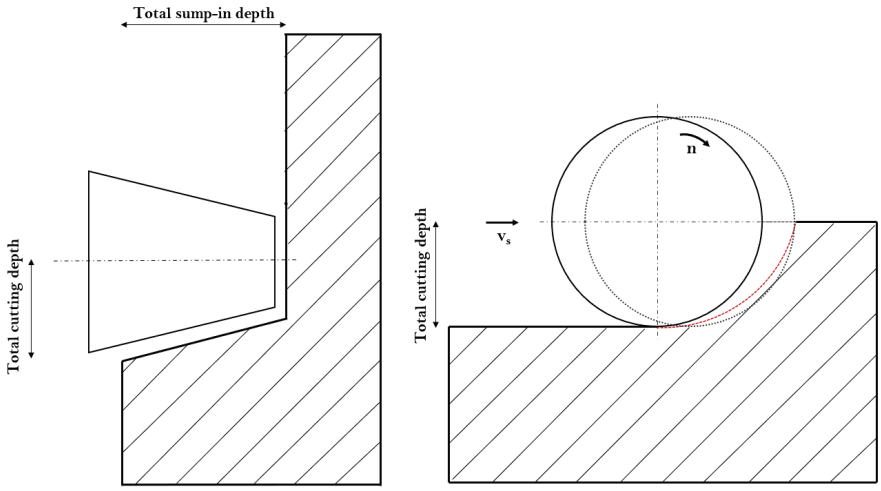

Figure 5.3: Degressive cutting (DC)

- Full contact cut: A combination of progressive cut and degressive cut (Figure 5.4).

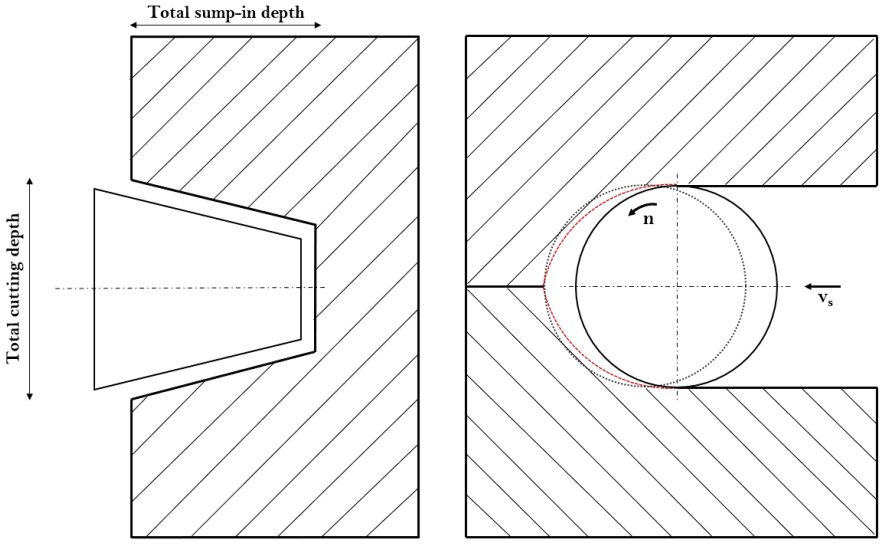

Figure 5.4: Full contact cutting (FCC)

The maximum cutting depth is also influenced by the total cutting depth *TCD* and the sump-in depth *SID* of the cutter head.

The work in this chapter and Chapter 6 is mainly focusing on the full contact cutting case, because the cutting tests described in Chapter 4 cover exclusively FCC.

5.1.2 Conical pick tools

Conical pick tools are the most commonly used pick tool type in part-face cutter heads. The picks applied in the tested part-face cutter head are a small-scale version, have a steel base body and the tip is made of hardened steel. The conical pick tool's shape and tip material quality can vary depending on the intended application. The pick tools are axially fixed inside a tool holder but are rotatable to enable a uniform wear profile. [24]

5.1.2.1 Pick forces

The resulting force acting on a pick can be separated into the cutting force F_c, the normal force F_n and the side force F_s. The cutting force is pointing in the direction of the pick's motion and is generally parallel to the cut surface. It is depending on the rock strength and responsible for chip formation in the rock mass. A threshold value needs to be exceeded to initiate cracks in the rock. [143, 144]

The normal force points towards the cutter drum and is perpendicular to the cutting force. It is also known as passive force, because it is applying pressure on the pick and pushing the machine away from the rock face. Consequently, it is a function of the contact area between the tip of the pick and the cut surface and a result of the frictional resistance of the rock.

The side force acts on the side of the pick. This force occurs, because the picks are not installed perpendicular to the rotation axis. The occurring forces and the corresponding geometrical angles are shown in Figure 5.5. [50]

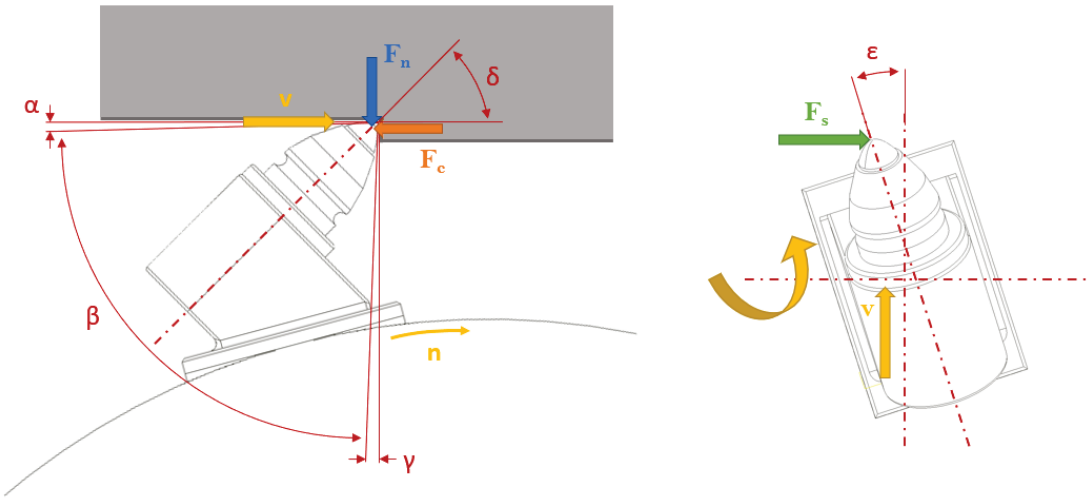

Figure 5.5: Conical pick tool - Forces and angles [11]

The pick orientation is described by the clearance angle α, the rake angle γ, the attack angle δ and the tilt angle ϵ, whereas the geometry of the pick tip is defined by the tip angle β [50, 145, 146].

The clearance angle α is defining the contact area between the pick and the rock surface, which influences the magnitude of the normal force. Increasing the clearance angle up to 10° can reduce the frictional resistance and lead to a decrease of the specific energy. Higher clearance angles tend to higher wear of the pick by flattening the tip. [145, 147]

The rake angle γ of a pick determines the nature of the load on the front side of its tip. When the rake angle is positive, the tip of the tool experiences compressive stress, while a negative rake angle increases the level of tensile stress. Negative rake angles can result in significant tensile stresses within the carbide tip, potentially leading to complete failure of the pick. [145, 147]

The attack angle δ ensures the provision of a sufficiently high cutting force. Attack angles range from 40° to 60°, depending on the cutter head design and rock to be cut [24, 143, 145]. Higher attack angles can lead to increased wear of the pick tip with consequent flattening, which eventually increases the normal force.

To obtain an evenly worn pick tip surface and keep the sharpness of a pick, the pick is supposed to rotate inside the pick holder. This is done by tilting the pick around it's symmetry axis by a specified tilt angle ϵ. When the pick leaves the cutting groove, a torque is applied and the pick is slightly turned around it's axis. [145, 146, 148]

The tip angle β, also called wedge angle, defines the geometry of the tip of the pick. A sharper angle allows cutting the rock more effortlessly, but generally used for cutting softer rock. Tip angles between 70° and 90° are used. If the strength of the rock increases, the risk of tip failure for sharp-angled tips increases leading to a decrease of the tip angle at higher rock strengths. [145, 149, 150]

5.1.2.2 Pick cutting depth and pick spacing

The part-face cutter head design parameters related to the pick tools are the pick cutting depth d and the pick spacing s. The pick cutting depth describes the depth which the pick breaks into rock during the cutting motion and the pick spacing indicates the distance between two neighbouring picks, both shown in Figure 5.6. [143, 145, 151]

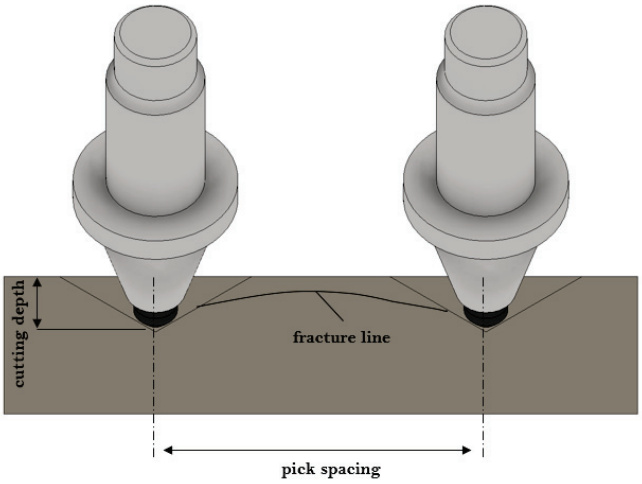

Figure 5.6: Pick cutting depth and pick spacing

The maximum achievable cutting depth is depending on the rock to be cut and the structural strength of a pick. If a pick indents a rock, cracks are initiated. If the distance of two neighbouring picks is small enough and the propagated cracks meet, the material breaks out. If the spacing is too large, remnant ribs will stay in place. Therefore an optimal pick cutting depth to pick spacing ratio needs to be found by single-pick cutting tests. [143, 145]

The relation between the pick cutting depth and the pick spacing is called rib breaking factor s/d and an illustration is seen in Figure 5.7. Generally it can be stated, that the larger the pick cutting depth is, the greater the pick spacing can be chosen. [24, 152]

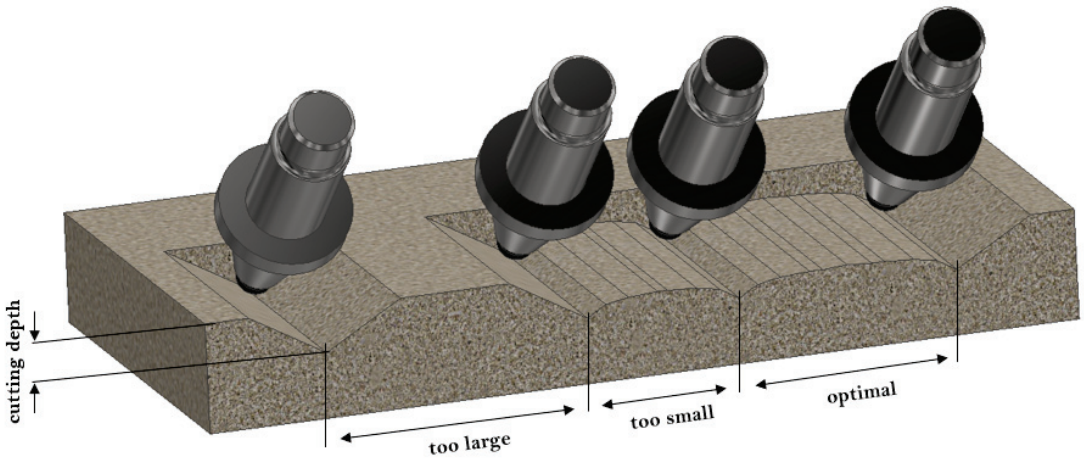

Figure 5.7: Influence of pick cutting depth on pick spacing

5.2 Simplified cutting force prediction model

Numerous single-pick cutting force estimation models have been developed over the last decades since the application of conical pick tools in mining has started. In the following section, the most known approaches are analysed and compared to the experimental test data.

5.2.1 Review of cutting force models for conical picks

Rock cutting theories for conical pick tools have been published in [153–156], but have not been taken into account for detailed investigations. A simulation approach using the DE method is presented in [157] and several methodologies for numerical simulations of the cutting process of part-face cutter heads could be found in [158–160].

In [161], *Yasar* extensively reviewed some rock cutting theories: *Lundberg* conducted the initial study on rock cutting/indentation with conical picks, following their usage on mechanical cutting machines [162]. It was found that the formation of radial cracks during indentation of conical picks occurs due to the rock's tensile strength being exceeded [162].

Evans proposed the first theory on the cutting of rock with conical picks in [163]. As per *Evans'* theory, when a conical pick is forced to indent into rock, it generates a hole underneath it, accompanied by the formation of radial compressive stresses. *Evans'* theory also suggests the presence of tensile stresses accompanying the radial compressive stresses, which open up the crack interface [163]. [161]

Theory of Evans

Evans' approach (Equation 5.1) is considering both the compressive strength σ_c and the tensile strength σ_t of the rock. The interaction between the pick and the rock is taken into account by the pick cutting depth d and the pick geometry is defined by the semi-cone angle θ (where, $\theta = \beta/2$). [163]

$$F_c = \frac{16\pi d^2 \sigma_t^2}{\sigma_c \cos^2 \theta} \tag{5.1}$$

The theory in [163] does not consider the effect of friction. Further on, the cutting force F_c is inversely proportional to the compressive strength and fails to attain a value of zero if the semi-cone angle θ reduces to zero. [161]

Theory of Roxborough

Additionally to *Evans'* theory, *Roxborough* included the effect of friction in his approach (Equation 5.2) [92]. This friction coefficient is represented as angle ϕ. ϕ typically has a value between 10° and 30°. [161]

$$F_c = \frac{16\pi d^2 \sigma_c \sigma_t^2}{(2\sigma_t + \frac{\sigma_c \cos\theta}{1+\tan\phi/\tan\theta})^2} \tag{5.2}$$

Theory of Goktan

Goktan stated a new hypothesis (Equation 5.2.1) which is aiming to overcome the shortcomings of [163]'s theory. [164]

$$F_c = \frac{4\pi d^2 \sigma_t \sin^2(\theta+\phi)}{\cos(\theta+\phi)} \tag{5.3}$$

None of the above mentioned theories considers the position of the pick relatively to the rock, which is usually described by the four pick angles but at least by the rake angle γ.

Theory of Goktan and Gunes

Goktan and Gunes elaborated the approach by including the rake angle γ (Equation 5.4). [165]

$$F_c = \frac{12\pi d^2 \sigma_t \sin^2[(90-\gamma)/2+\phi]}{\cos[(90-\gamma)/2+\phi]} \tag{5.4}$$

To understand the behaviour of the individual theories, the single-pick cutting forces depending on the uniaxial compressive strength have been calculated and visualized (see Figure 5.8).

It is important to note that for calculation, the tensile strength σ_t was chosen to be 10 % of the compressive strength σ_c. A clearly linear behaviour can be seen, which matches the experimental data. [24, 161]

Pick cutting depth d has been set to 5 mm, semi-cone angle θ to 80° for standard conical pick tools [165], friction angle ϕ to 10° [161] and the rake angle γ of the pick to -7° [165].

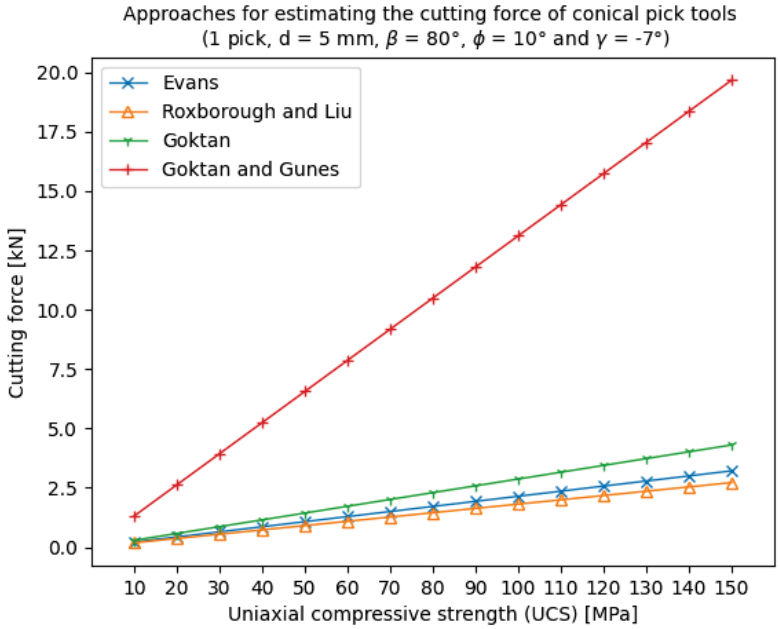

Figure 5.8: Comparison of cutting force estimation models [11]

Interestingly, the theories of *Evans*, *Roxborough* and *Goktan* provide cutting forces of similar magnitude, whereas the theory of *Goktan and Gunes* result in much higher magnitudes. This divergence is presented in Figure 5.9.

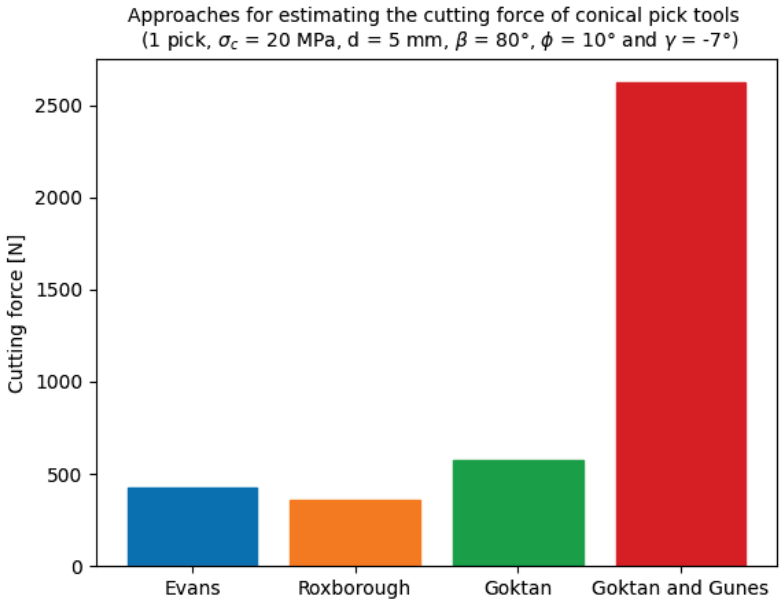

Figure 5.9: Comparison of cutting force estimation models - $\sigma_c = 20$ MPa [11]

Figure 5.10 shows the influence of the pick cutting depth on the cutting force. All models include a parabolic influence of the pick cutting depth, which make them highly sensitive to varying the pick cutting depth.

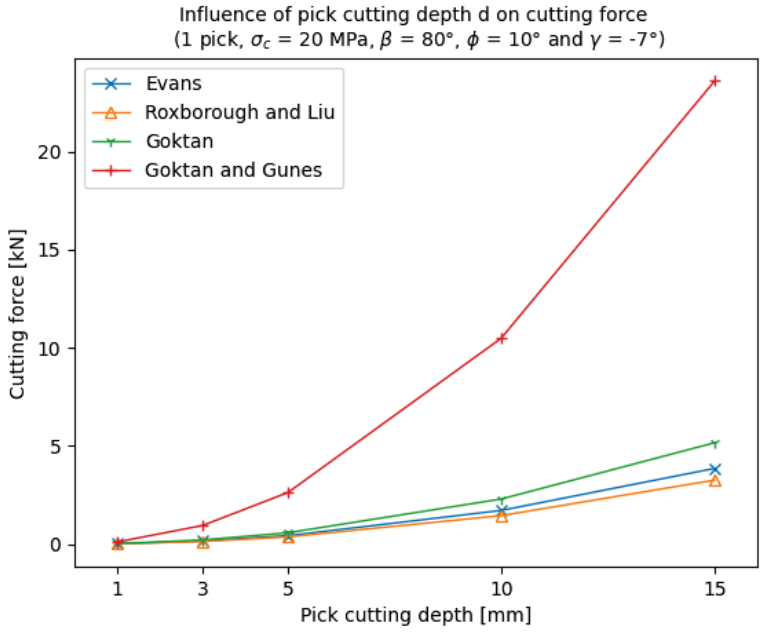

Figure 5.10: Influence of pick cutting depth on cutting force

It should be noted that the only theory regarding true conical pick cutting is *Evans'* study from 1984. All other models are simply modifications of *Evans'* theory. [161]

However, *Evans* developed his theory based on the concept of indentation rather than cutting, which does not accurately reflect the actual cutting conditions observed in laboratory or field settings with conical picks. [161]

A theory focused on the mechanics of conical pick cutting should take the cutting conditions into account more realistically [161].

Eventually, if the cutting forces of experimental data is extracted for different rock strengths, processed and with the help of linear regression, the cutting force depending on the uniaxial compressive strength (UCS) can be predicted (Equation 4.2).

Because the measurements have been made with a maximum UCS of 30 MPa, the results are treated very cautiously, but also a linear behaviour can be observed (see Figure 5.11).

Quantifying the obtained results is done in the next section by comparing the calculated cutting forces with the experimental results.

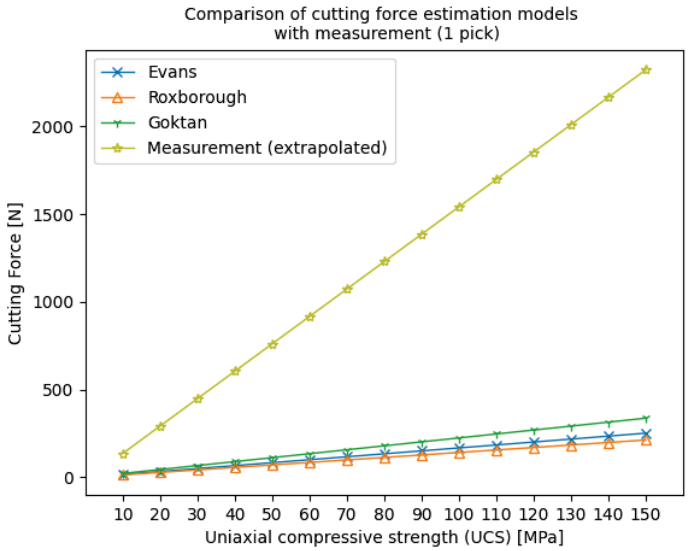

Figure 5.11: Comparison of cutting force estimation models with measurement depending on the UCS [11]

5.2.2 Modified single-pick cutting force model

In Figure 5.12, the cutting test data is compared with the obtained cutting forces from the individual rock cutting theories. Note: The cutting force resulting from the experimental data shows the maximum cutting force during a full pick rotation (180°). Due to the already very deviation of the resulting forces from the theory of *Goktan and Gunes* and the experimental results, the approach of [165] results was omitted for further comparison.

None of the calculated single-pick cutting forces show a similar magnitude as the measured cutting force, which are much higher than the cutting forces provided by the reviewed rock cutting theories. This might be attributable to the small-scale of the conical picks used in the experimental test. Although smaller picks have a significantly smaller contact area, which causes less friction, with the theories of [92, 163, 164] it is not possible to estimate the cutting forces for comparatively small cutting depths (< 5 mm).

Therefore, it is inevitable to introduce a scale factor for further use, which adapts the formula to small-scale conical pick tools.

Modified theory of Roxborough

Although, no hypothesis showed a good compliance with the experimental data, the formula of *Roxborough* is used and rearranged with an additional scale factor k to incorporate the smaller pick size (Equation 5.5). k needs to be calibrated for any pick dimension and in this case has been agreed on $k = 3.15$.

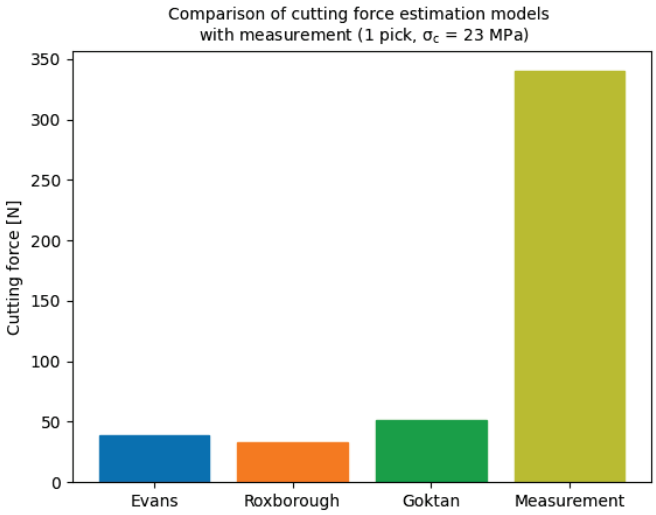

(a) B20 concrete [11]

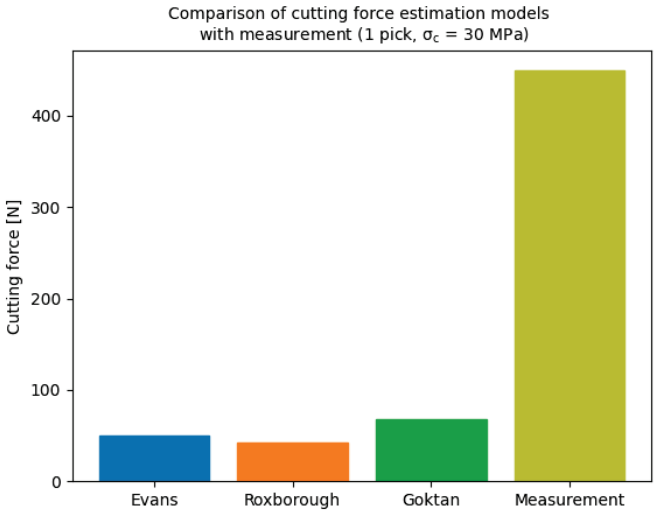

(b) B30 concrete

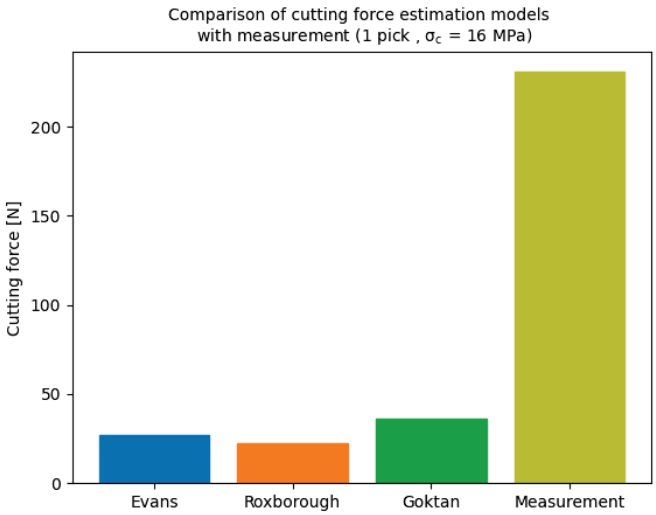

(c) Oilshale

Figure 5.12: Comparison of cutting force estimation models with measurement

$$F_c = k^2 \cdot \frac{16\pi d^2 \sigma_c \sigma_t^2}{(2\sigma_t + \frac{\sigma_c \cos\theta}{1+\tan\phi/\tan\theta})^2} \tag{5.5}$$

Comparing the modified theory with more experimental data shows very good agreement for soft rock conditions (see Figure 5.13).

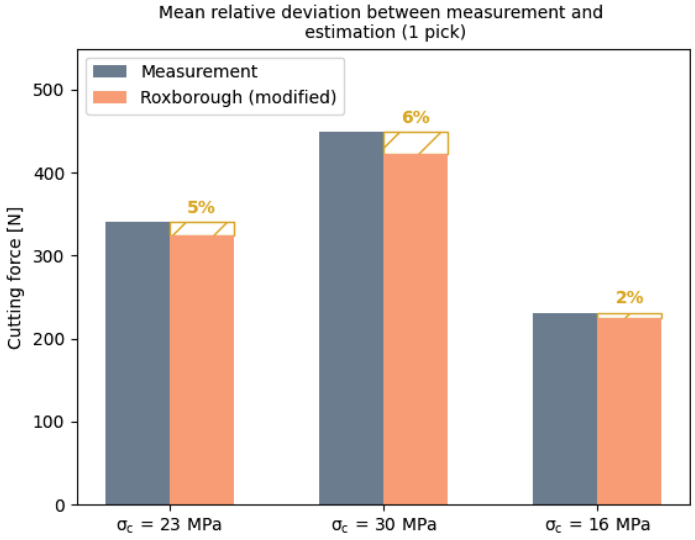

Figure 5.13: Comparison of modified *Roxborough* theory with measurement [11]

A better agreement on predicting the cutting force depending on UCS can be achieved with the modified model (Figure 5.14).

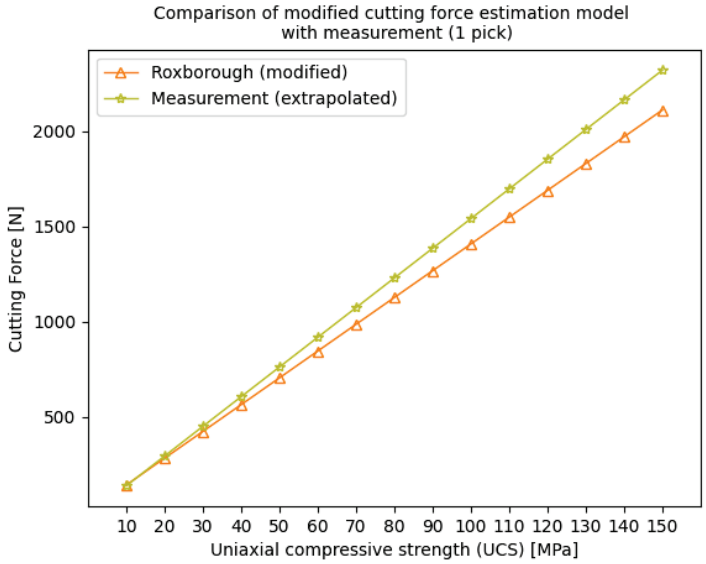

Figure 5.14: Comparison of modified *Roxborough* model with measurement

5.2.2.1 Limitations

The modified approach has some limitations: If the cutting models from the previous section are taken to calculate the total cutting force of a full-scale cutter head during a cutting operation, it is only possible by multiplying the single cutting force with the number of picks in contact (Equation 5.6).

$$F_{c,total} = F_c(d_{max}) \cdot n \tag{5.6}$$

That approach leads to a linear behaviour between the total sump-in depth of the cutter head and the total cutting force $F_{c,total}$. However, in reality, the cutting force is a function of the cutting depth of the pick (Equation 5.7).

$$F_{c,total} = \sum_{n=1} F_{c,n}(d_{\theta,n}) \tag{5.7}$$

The cutting depth of a pick is not constant throughout a contact cycle. Depending on the relative position, the rotation direction and slewing direction of the cutter head, the cutting depth of the pick is either increasing (progressive cut), decreasing (degressive cut) or a combination of both (full contact cut).

A detailed investigation on the behaviour of the cutting depth of a pick is done in Section 5.3. Figure 5.15a, 5.15b and 5.15c show the theoretical cutting forces of a cutter head depending on the total sump-in depth compared to the data obtained with the cutting tests.

The theoretical results show a linear increase of the cutting force (Equation 5.6), whereby the experimental data clearly shows a degressive behaviour of the total cutting force $F_{c,total}$. This phenomenon results from the overlapping contact paths of the individual picks.

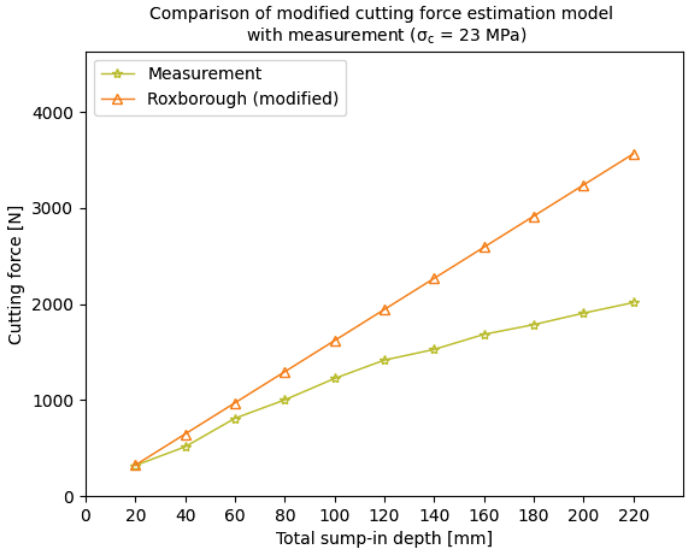

(a) B20 concrete [11]

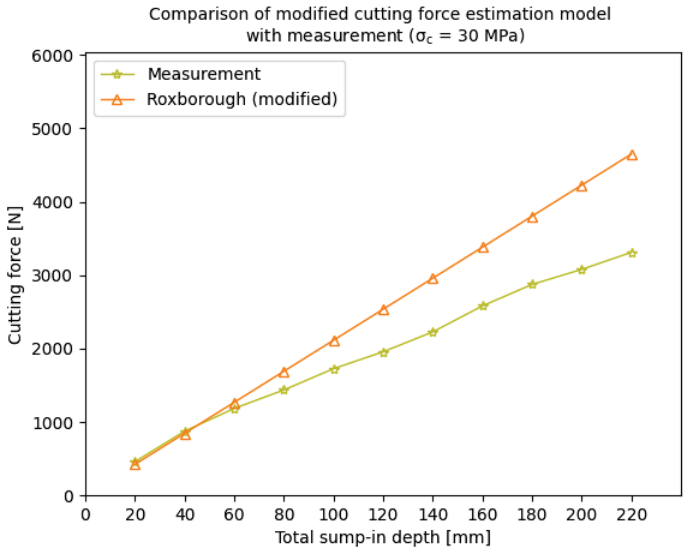

(b) B30 concrete

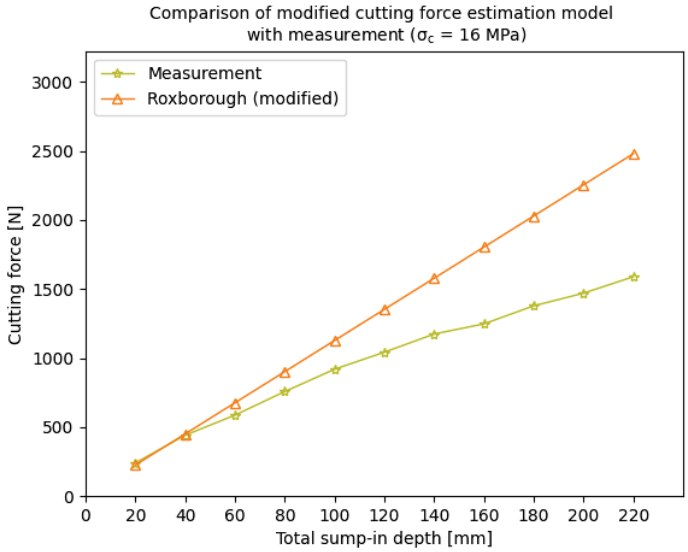

(c) Oilshale

Figure 5.15: Comparison of modified model with measurement

5.3 Part-face cutter head simulation model

A kinematic model of the pick cutting process has been developed to analyse the influence of the changing cutting depth of the pick on the cutting force. The results depicted in this section were obtained with arbitrary cutter head dimensions and pick specifications, in order to not publish any confidential data.

5.3.1 Configuration

In this case (see Figure 5.16), 24 picks are placed onto the surface of the cutter head, whereas they appear in pairs on 180° offset spirals. Figure 5.17 shows the pick orientation in a top view.

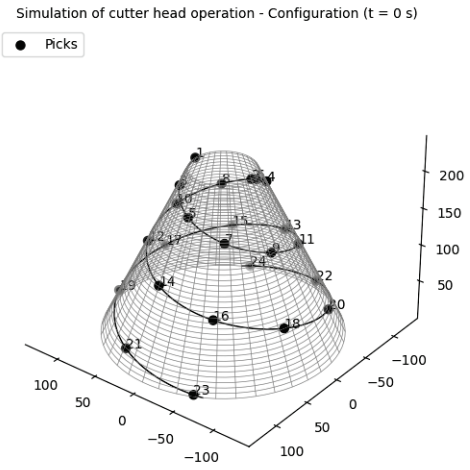

Figure 5.16: Simulation of cutting process - Configuration of cutter head [11]

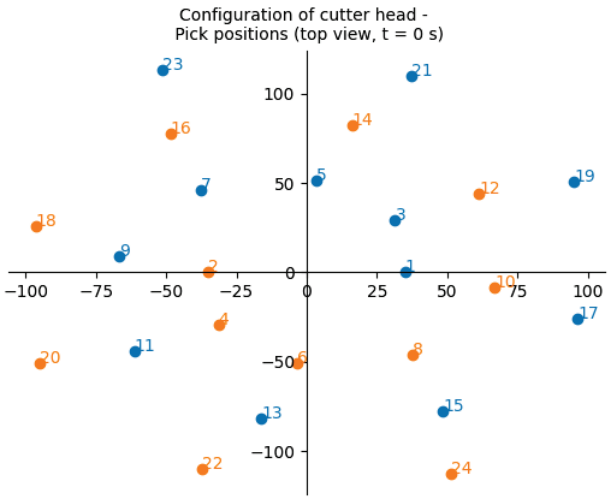

Figure 5.17: Simulation of cutting process - Configuration of pick positions

The experimental setup was mainly focusing on the FCC case. Each individual pick is in contact with the rock for 180°. Figure 5.18 shows the contact angle of the picks on the cutter head.

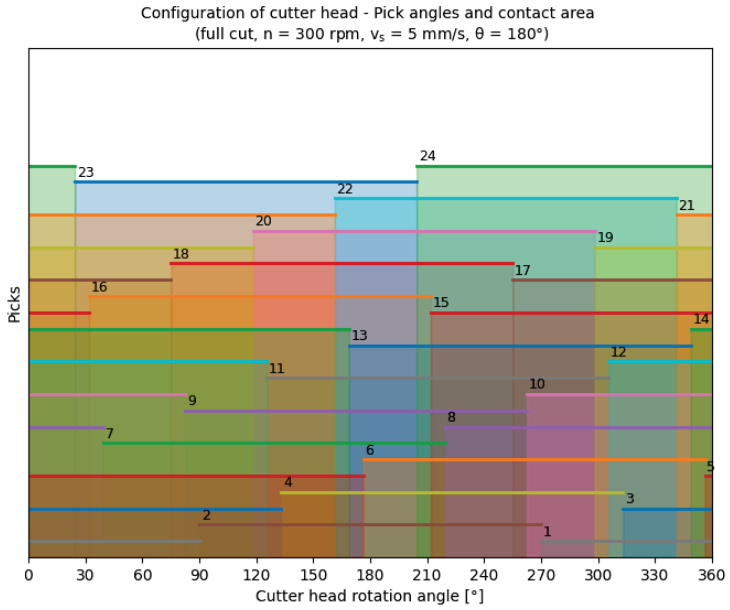

Figure 5.18: Simulation of cutting process - Configuration of pick contact angles [11]

Pick contact will further be used to define start and end time of a single pick's contact.

5.3.2 Consideration of the changing pick cutting depth

The pick cutting depth is a function of the rotation angle and the slew speed ($d = f(\theta, v_s)$). The pick kinematics are modelled with Equation 5.8.

$$p(t) : \begin{cases} x(t) = r \cdot \cos\theta + v_s \cdot t \\ y(t) = r \cdot \sin\theta \end{cases} \tag{5.8}$$

Where r defines the effective pick radius, θ the rotation angle and v_s the slew speed. The pick cutting depth d_θ is calculated according to Equation 5.9.

$$d_\theta = \sqrt{(x(t) - x_0)^2 + (y(t) - y_0)^2} \tag{5.9}$$

The cutting force F_c is calculated with the modified cutting force model (described in Section 5.2.2) and combined with the above equations incorporates a dynamic behavior ($F_c = f(\theta, v_s)$). The total cutting force $F_{c,total}$ of the cutter head is obtained by Equation 5.10, where n is an individual pick in contact.

$$F_{c,total} = \sum_{n=1} F_{c,n}(d_{\theta,n}) \tag{5.10}$$

Equation 5.11 describes the calculation of the total cutting torque $T_{c,total}$.

$$T_{c,total} = \sum_{n=1} F_{c,n}(d_{\theta,n}) \cdot r_{eff,n} \tag{5.11}$$

Where r_{eff} is the effective pick radius.

5.3.2.1 Cutting depth

In Figure 5.19, a simplified model of three picks in contact is seen, whereas the picks have an individual angular offset of 20°. The paths of the picks over the rotation angle is visualized and the profile of a full contact cut operation can be recognized on the basis of the pick cutting depth courses.

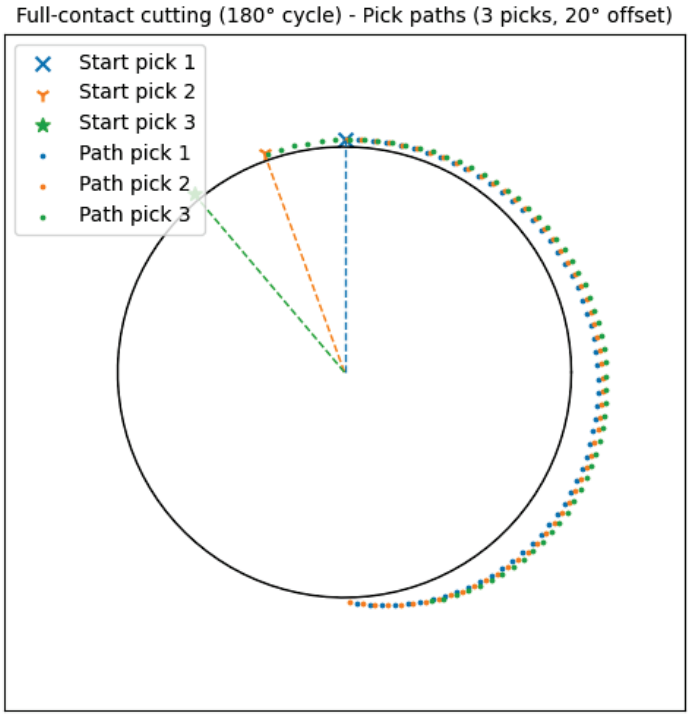

Figure 5.19: Full contact cut - Illustration of pick paths with horizontal slew [11]

According to Equation 5.9, the individual cutting depths are calculated and plotted over the rotation angle. The pick cutting depth is following a sinusoidal curve, which is in agreement with the data presented in [166]. A shift of the cutting depth maximum by 20° can be seen in Figure 5.20.

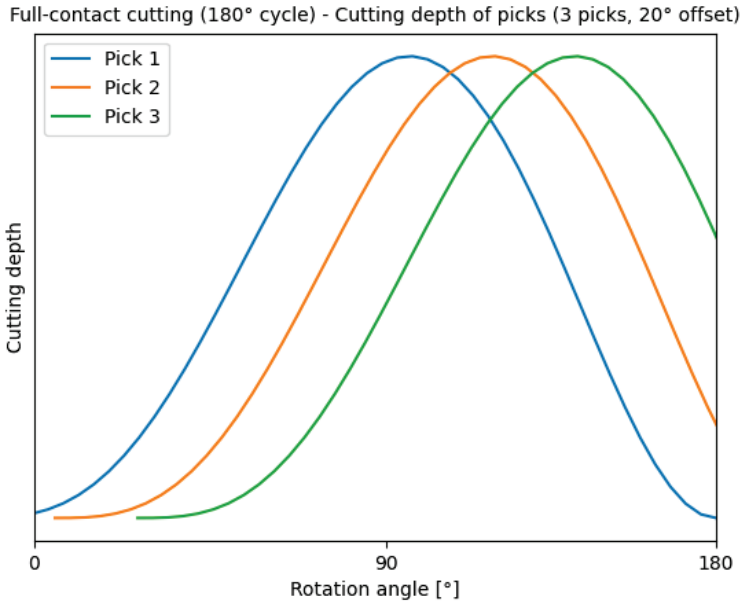

Figure 5.20: Cutting depth depending on rotation angle of pick [11]

For longitudinal cutter heads, the maximum cutting depth d_{max} of a single pick is defined by the interaction of the rotational speed and slew speed.

5.3.2.2 Cutting force

Once the single-pick cutting depths are determined for each time step, the cutting force can be computed with the Equation 5.12.

$$F_c = k^2 \cdot \frac{16\pi d_\theta^2 \sigma_c \sigma_t^2}{(2\sigma_t + \frac{\sigma_c \cos\theta}{1+\tan\phi/\tan\theta})^2} \tag{5.12}$$

The exemplary cutting forces of the three-pick model with the total cutting force $F_{c,total}$ are presented in Figure 5.21.

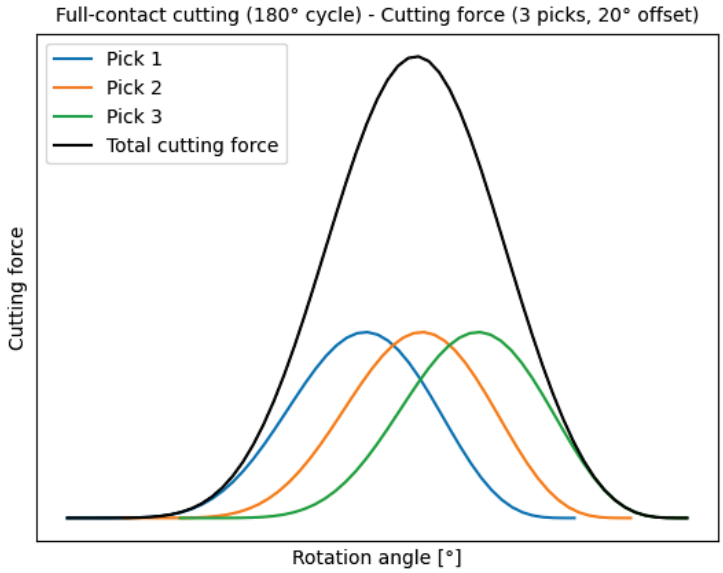

Figure 5.21: Cutting force depending on rotation angle of pick [11]

Comparing the dynamic behaviour of the cutting force with the cutting force resulting of a constant pick cutting depth, points out again the artificial altering of the total cutting force (Figure 5.22) when using a constant pick cutting depth. The discrepancy increases linearly with increasing number of picks in contact.

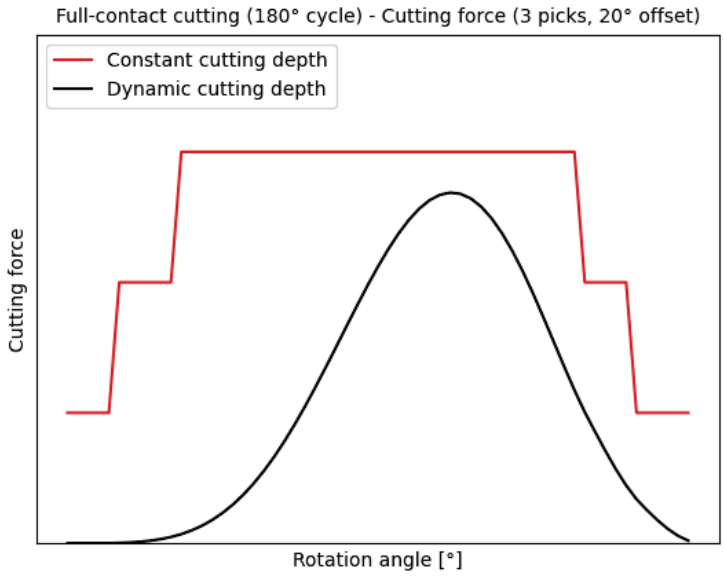

Figure 5.22: Comparison of constant and dynamic pick cutting depth

Hereby, the issue mentioned in Section 5.2.2.1 is overcome due to the dynamic characteristic of the cutting depth. In essence, the total cutting force $F_{c,total}$ is

not a linear multiple of the individual forces. Instead, $F_{c,total}$ is less than the value predicted with the upscaled single-pick theories. According to this information, the phenomenon of the degressive behaviour of the total cutting force determined in experimental tests can be modelled and verified.

5.3.3 Simulation

The developed methodology allows a dynamic modelling of a part-face cutter head including the pick positions, pick cutting depths, cutting forces and cutting torques. In the following, selected possibilities of this modelling approach are presented.

5.3.3.1 Cutting parameters

Additionally to the cutter head dimensions, the total cutting depth *TCD* and the sump-in depth *SID* are taken into account. With the rotational speed n, the slew speed v_s and the total cutting time t the cutter head movement can be modelled (Figure 5.23). The current picks in contact are highlighted.

This methodology allows a simulation of an entire cutting cycle or the displaying of parameters for very short contact times.

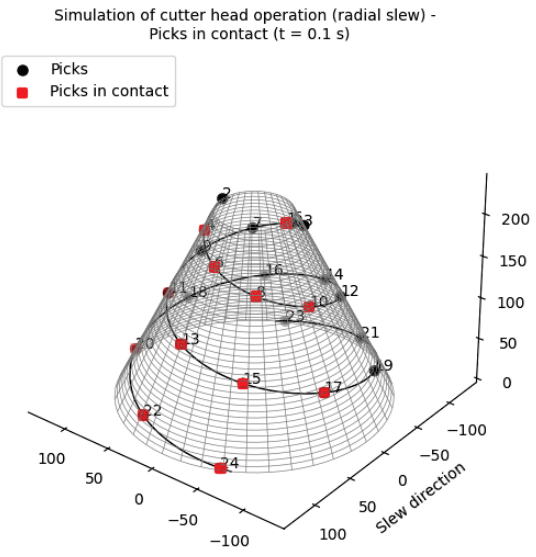

Figure 5.23: Simulation of cutter head

The calculation of the cutting depth of each individual pick and time step is done and exemplary results are visualized in Figure 5.24. The cutting forces and

cutting torques of the cutter head are calculated for each pick and time step and exemplary results are depicted in Figure 5.25 and Figure 5.26.

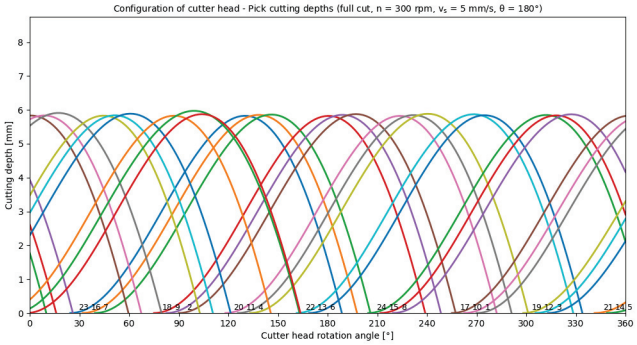

Figure 5.24: Pick cutting depths depending on rotation angle of cutter head [11]

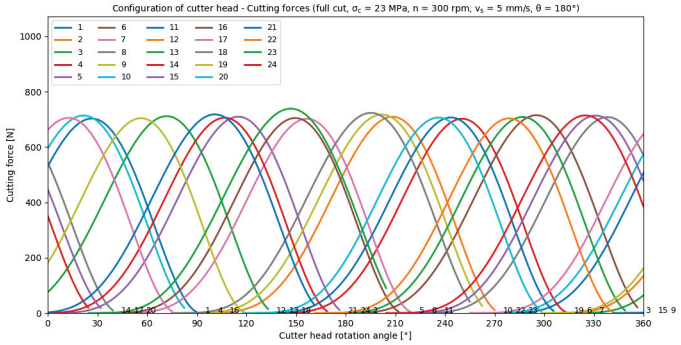

Figure 5.25: Pick cutting forces depending on rotation angle of cutter head

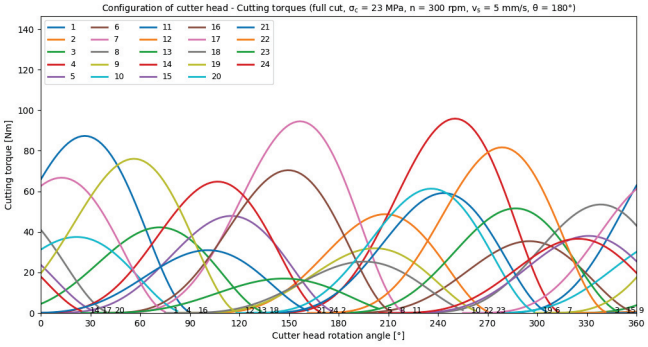

Figure 5.26: Pick cutting torques depending on rotation angle of cutter head

Examples for full cutting simulation, including the sump-in process (axial thrust) and slew motion, can be modelled. The cutting forces and cutting torques of a fictitious rock mass with slightly fluctuating uniaxial compressive strength can be seen in Figure 5.27. Assuming the rotational speed and slew speed are constant, the excavation rate can be determined by calculating the displaced rock volume.

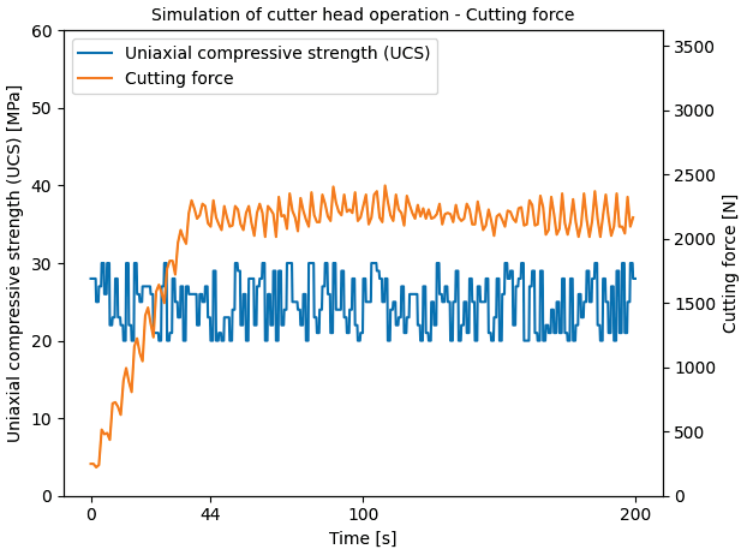

(a) Total cutting force

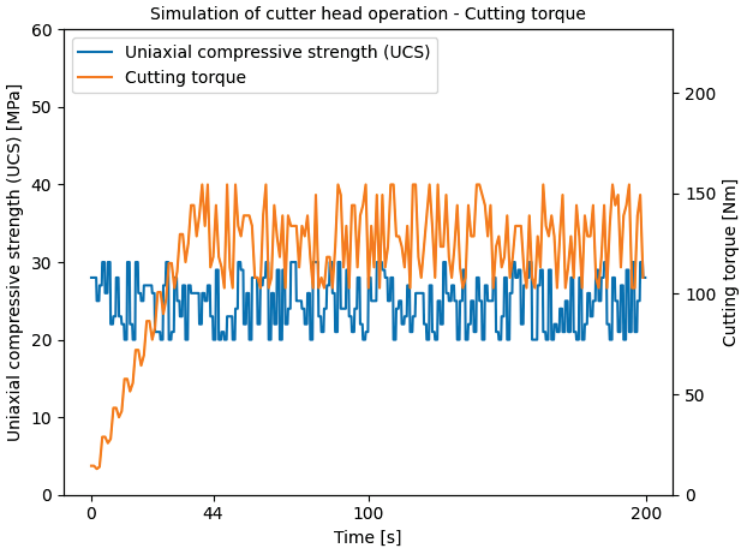

(b) Total cutting torque

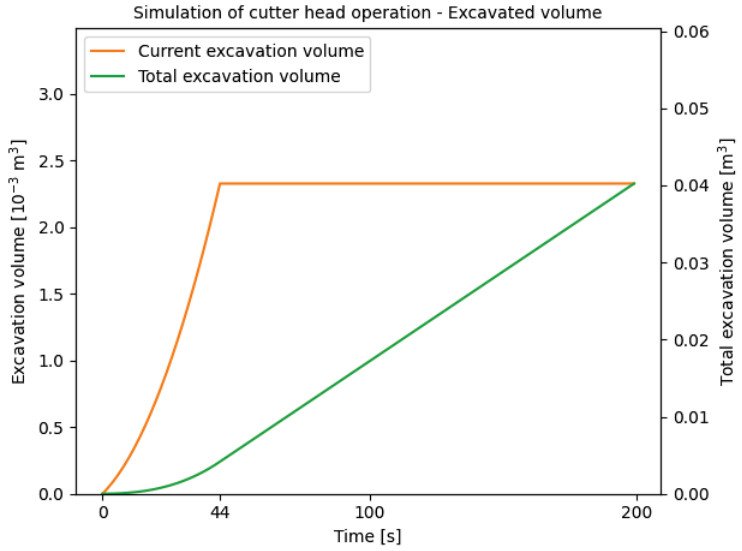

(c) Excavation rate

Figure 5.27: Simulation of a 200 s cutting cycle

5.3.3.2 Cutter head kinematics

Additional capabilities of the simulation methodology includes the modelling of the entire production tool kinematics with the boom dimensions (Figure 5.28).

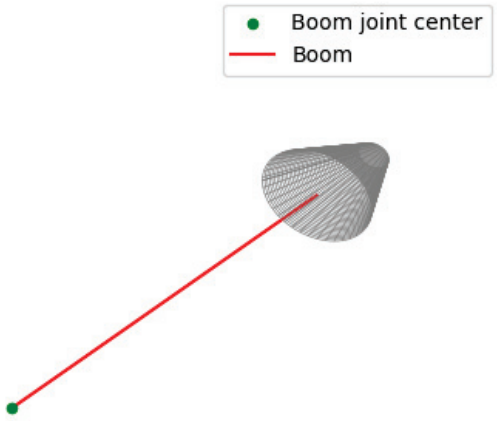

Figure 5.28: Longitudinal cutter head model [11]

Modelling the kinematics of the entire production tool system enables the opportunity to analyse potential excavation profiles by implementing the geometry and spatial limitations of the boom.

The illustrations in Figure 5.29 show the longitudinal part-face cutter head with the boom and 1 exemplary pick with its pick path. The rotational speed and slew speed are constant and a slew motion from left to right is defined. An arbitrary number of picks can be defined, but, for better visibility, the illustration of only 1 pick is shown.

Three different cutting conditions with positive and negative cutting height and consideration of a total cutting depth can be seen in Figure 5.30. Cutting height, sump-in depth and total cutting depth can be chosen arbitrarily to model progressive, degressive or full contact cutting of a longitudinal part-face cutter head. A selection of cutting conditions is displayed in Figure 5.31.

The modelling of a production tool using transversal cutter head is appended in Appendix D.

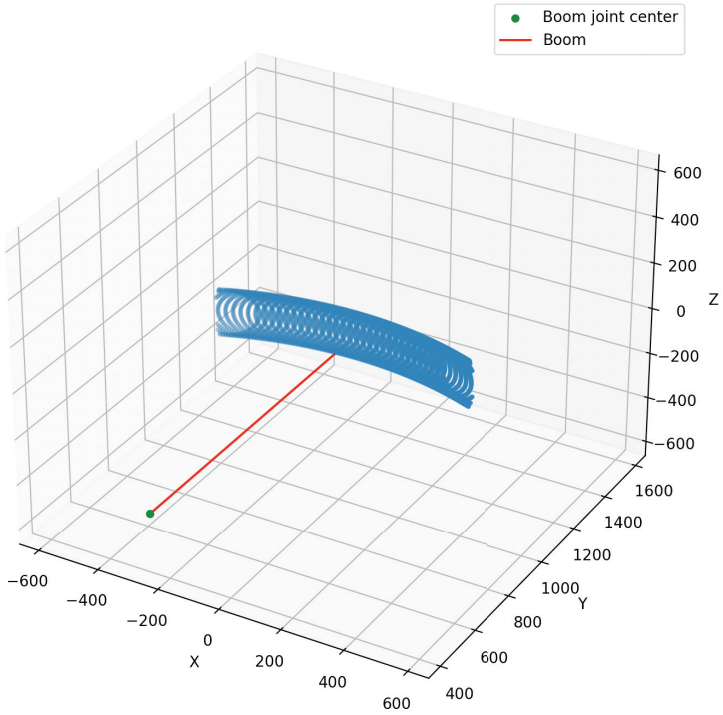

(a) Kinematic model

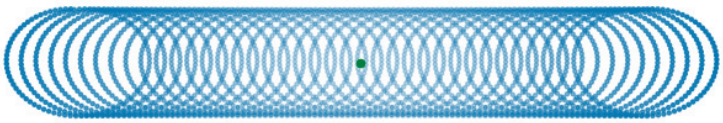

(b) Pick path

Figure 5.29: Longitudinal cutter head model - Full contact cutting

(a) Positive cutting height - 100 mm total cutting depth

(b) Negative cutting height - 100 mm total cutting depth

(c) Full contact cutting

Figure 5.30: Longitudinal cutter head model - Pick cutting kinematics

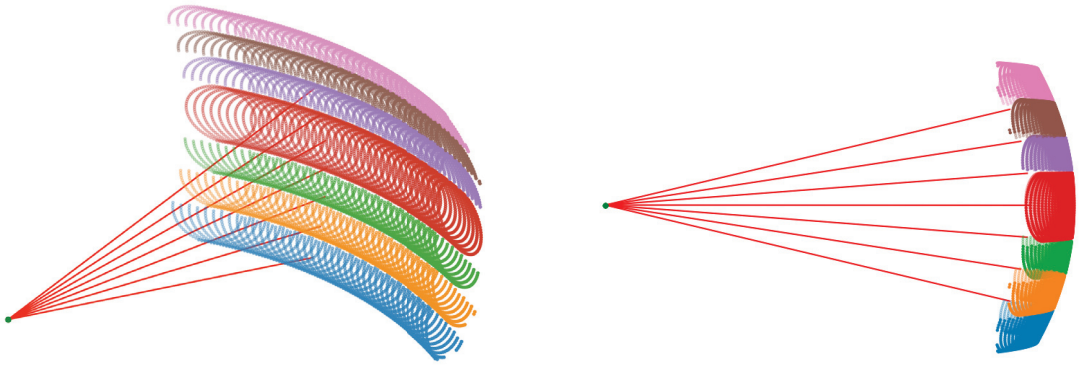

(a) Tunnel profile **(b)** Tunnel profile - side view

Figure 5.31: Longitudinal cutter head model - Combined 1 pick cutting kinematics

6 Verification and validation

The developed simulation model in Chapter 5 was validated with the data acquired in the experimental tests (Chapter 4). Validating the model required a processing of the measurement data and is hereafter discussed in detail for the B20 concrete cutting tests. Further validation has been performed for B30 concrete and oilshale tests, each with slew speed $v_s = 7$ mm/s and 14 mm/s. Main validation parameters were the cutting force and cutting torque, whereby the validation results of the cutting torque are attached in Appendix E due to the linear relation between the cutting force and cutting torque. Some parts of the content covered in this section have already been published in [11] and extended results, graphs and look-up tables are presented in Appendix E.

6.1 Objective

The aim of the subsequent process is the validation of the developed methodology for the simulation of the nonlinear total cutting force of a longitudinal cutter head as the experimental tests have shown. To verify and validate the cutting force model, the results of the cutting tests presented in Chapter 4 have been used. In these cutting tests, test sample have been cut in a cyclical process. Pre-defined levels of total sump-in depths have been established and the total sump-in depth for each test has been controlled with the axial thrust. For each level, the maximum cutting torque $T_{c,total}$ has been measured and the total cutting force $F_{c,total}$ has been derived from it.

6.2 Slow slew

6.2.1 B20 concrete

The comparison of cutting test and simulation is shown in Figure 6.1a. The total cutting force is displayed for specified total sump-in depth levels. The arithmetic

average total cutting forces of the maximum measured forces from 5 cutting tests are depicted and opposed with the simulation results. The comparison shows satisfying agreement with the experimental data. Especially, the nonlinear increase of the total cutting force could be simulated in a realistic behavior. Another comparison has been done for the total cutting force as a function of number of picks in contact (see Figure 6.1b). Again, the simulation shows the same trend as the experimentally obtained data. The absolute deviations are marginal and overall, the simulation shows highly satisfactory results.

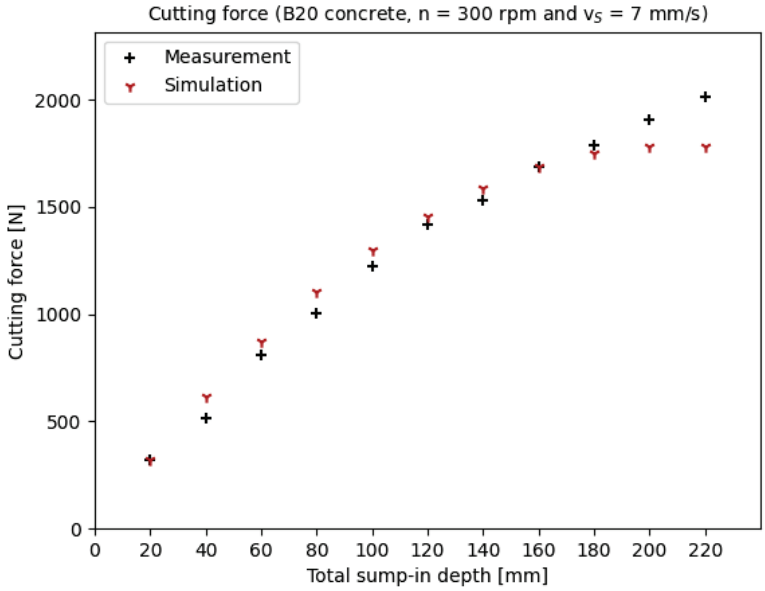

(a) Cutting force depending on total sump-in depth of cutter head [11]

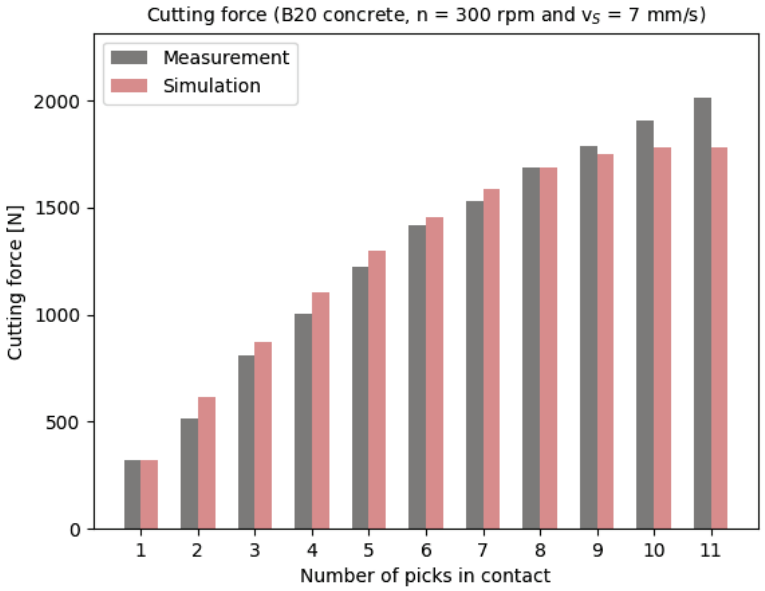

(b) Cutting force depending on number of picks in contact [11]

Figure 6.1: Slow slew - Validation of simulated cutting forces (B20 concrete)

6.2.2 B30 concrete

Figure 6.2 shows the comparison of the simulation results and the experimental data of the B30 concrete test specimen. Similar to the B20 concrete analysis, the nonlinear trend of the total cutting force could be proven (Figure 6.2a) and the absolute deviations of the cutting forces (Figure 6.2b) at the individual total sump-in depth levels are low.

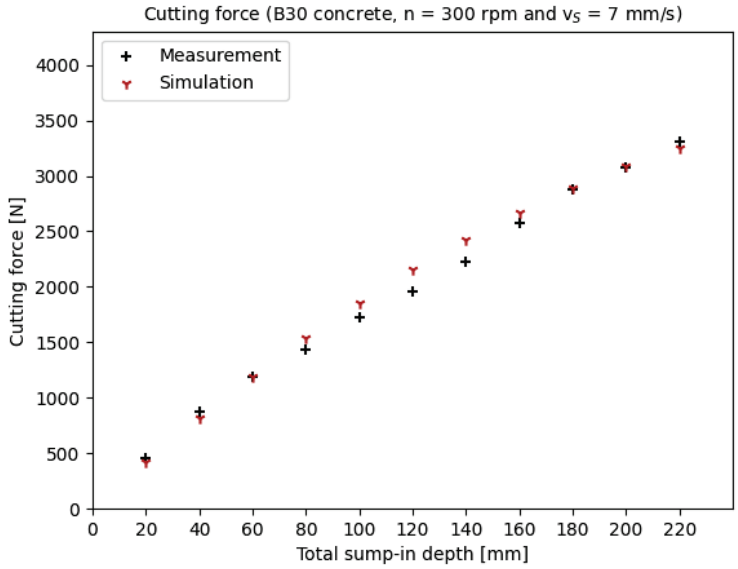

(a) Cutting force depending on total sump-in depth of cutter head

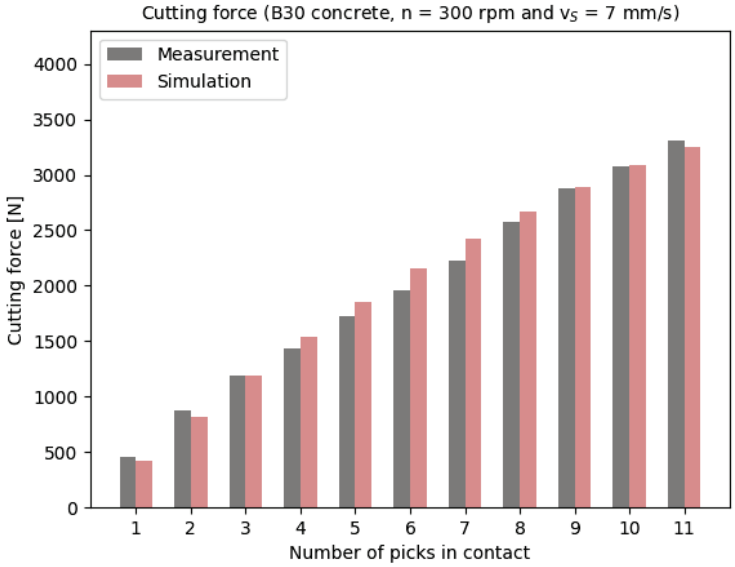

(b) Cutting force depending on number of picks in contact

Figure 6.2: Slow slew - Validation of simulated cutting forces (B30 concrete)

6.2.3 Oilshale

The nonlinear trend of the total cutting force could be successfully proven for the oilshale test specimen (Figure 6.3a), although the absolute deviations of the total cutting force are satisfactory at smaller total sump-in depths and increasing at higher sump-in depths (Figure 6.3b).

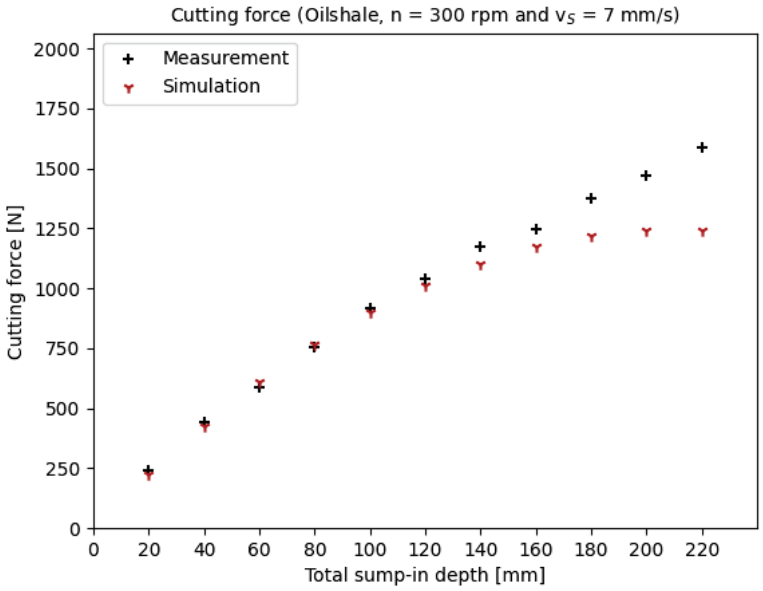

(a) Cutting force depending on total sump-in depth of cutter head

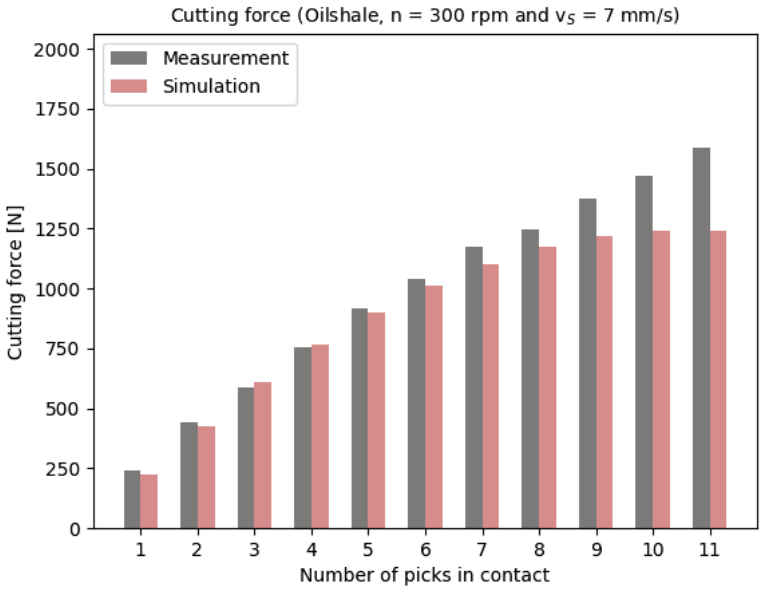

(b) Cutting force depending on number of picks in contact

Figure 6.3: Slow slew - Validation of simulated cutting forces (oilshale)

6.2.4 Analysis of deviation between experimental tests and simulation

The deviations between the results of the simulation model and the experimental data are investigated in detail in this section.

6.2.4.1 Cutting force

In Figure 6.4, the mean relative deviations between measurement and simulation are shown for the three different test sample types.

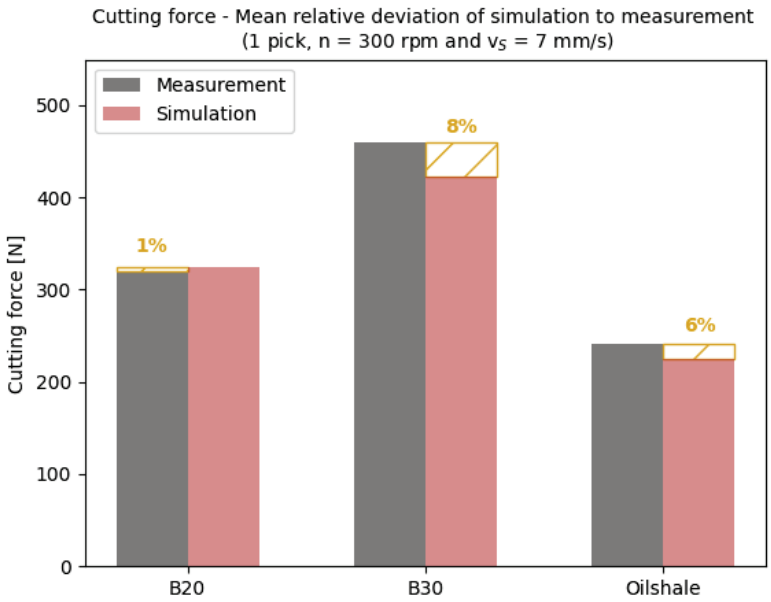

Figure 6.4: Slow slew - Cutting force for the three test sample types [11]

A maximum mean relative deviation of 8 % for the B30 concrete sample could be found, whereas the minimum mean relative deviation between measurement and simulation is 1 % for the B20 concrete sample.

The linear regression conducted in Section 4.4.1.3 (Equation 4.2) provides an approach for estimating the cutting force for different UCS values.

This equation can be exploited to show the trend also for higher uniaxial compressive strength regions. Compared with the cutting forces calculated with the modified single-pick cutting theory, the extrapolated data shows again good conformity (see Figure 6.5).

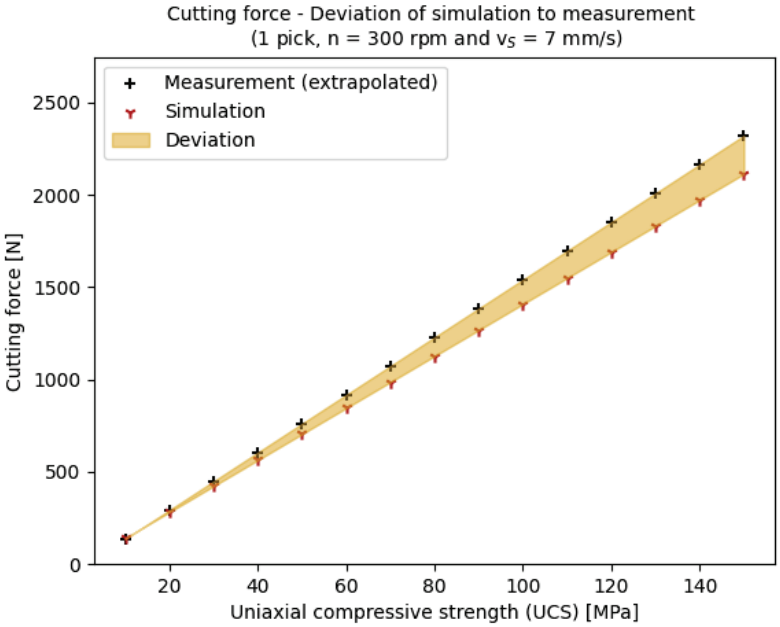

Figure 6.5: Slow slew - Cutting force comparison depending on UCS [11]

Although it is important to mention that the cutting forces above the maximum uniaxial compressive strength of the test sample types need to be assessed with caution. The relative deviations between extrapolated data and simulation are presented in Figure 6.6.

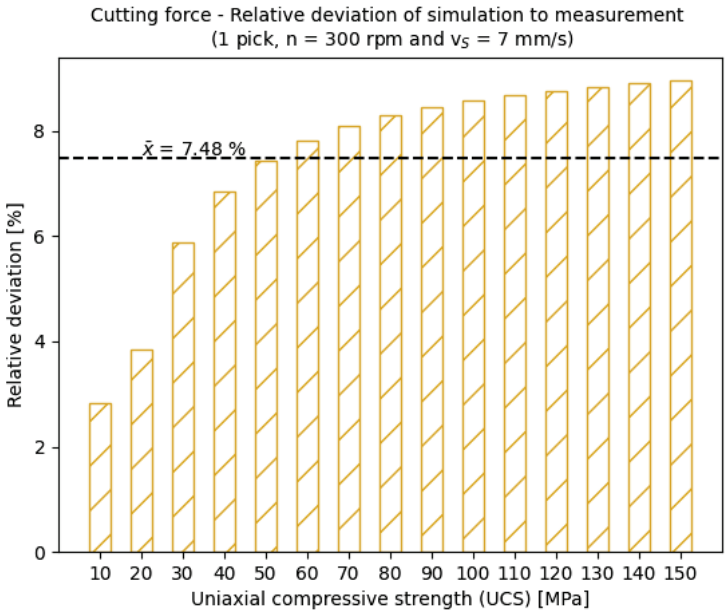

Figure 6.6: Slow slew - Relative deviation of cutting force depending on UCS [11]

The relative deviations provide good results for uniaxial compressive strengths

between 10 and 40 MPa, whereas above the threshold, the magnitudes are higher but still reasonable. A mean relative deviation of 7.48 % can be recognized.

6.2.4.2 Specific energy

Additionally, the specific energy of the cutting tests has been calculated according to Equation 6.1 and Equation 6.2 and compared to the specific energy estimation approach described in Section 3.1.2 (see Figure 6.7). The measured excavation rate ER has been discussed in Section 4.5.

$$P_{in} = T_c \cdot \omega \tag{6.1}$$

$$SE = \frac{P_{in}}{ER} \tag{6.2}$$

P_{in}	Power	$[kW]$
T_c	Measured cutting torque	$[Nm]$
ω	Angular velocity	$[s^{-1}]$
SE	Specific energy	$[kWh/m^3]$
ER	Excavation rate	$[m^3/h]$

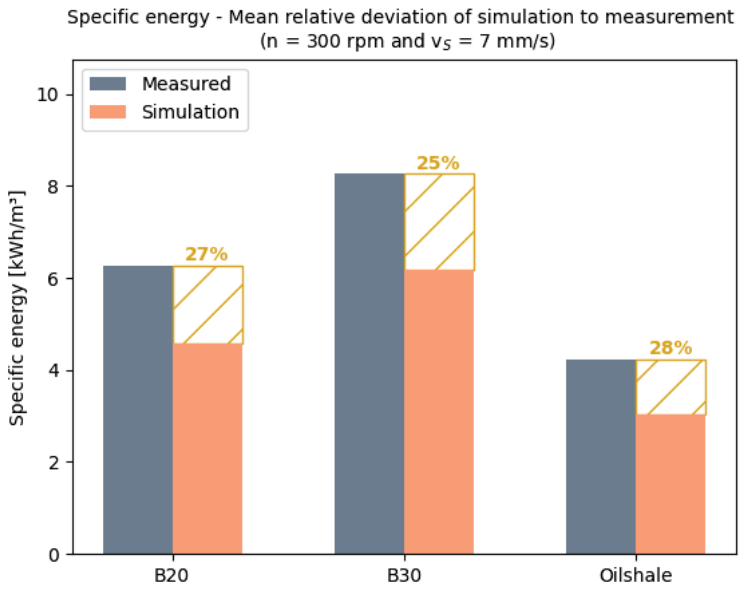

Figure 6.7: Slow slew - Specific energy depending on UCS of test specimens

As expected, the simulation results are lower than the measured specific energy. The simulation does solely represent ideal conditions (homogeneous rock mass). Deviations of almost 30 % between the simulation and measurement are recognized.

Due to the linear behaviour of the specific energy with increasing UCS, a linear regression has been made. The specific energy SE_{slow} can be approximated with Equation 6.3 and is shown in Figure 6.8.

$$SE_{slow} = 0.3 \cdot \sigma_c - 0.4 \tag{6.3}$$

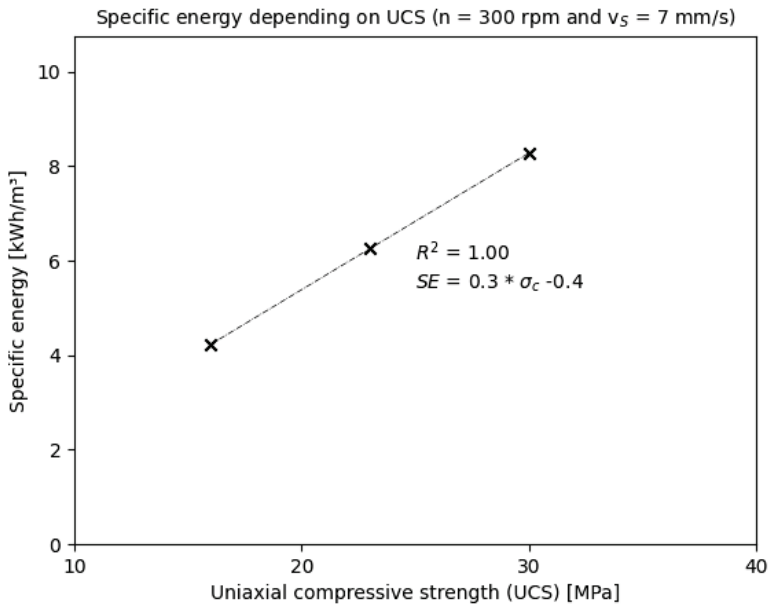

Figure 6.8: Slow slew - Linear regression of specific energy

6.3 Fast slew

Similar to Section 6.2, the developed model is further tested for the fast slew test case and the result validation is described in this section.

6.3.1 B20 concrete

The nonlinear behaviour of the total cutting force could be modelled very well (Figure 6.9a) and the absolute deviations between the simulated cutting forces and the measured cutting forces are very satisfactory (Figure 6.9b).

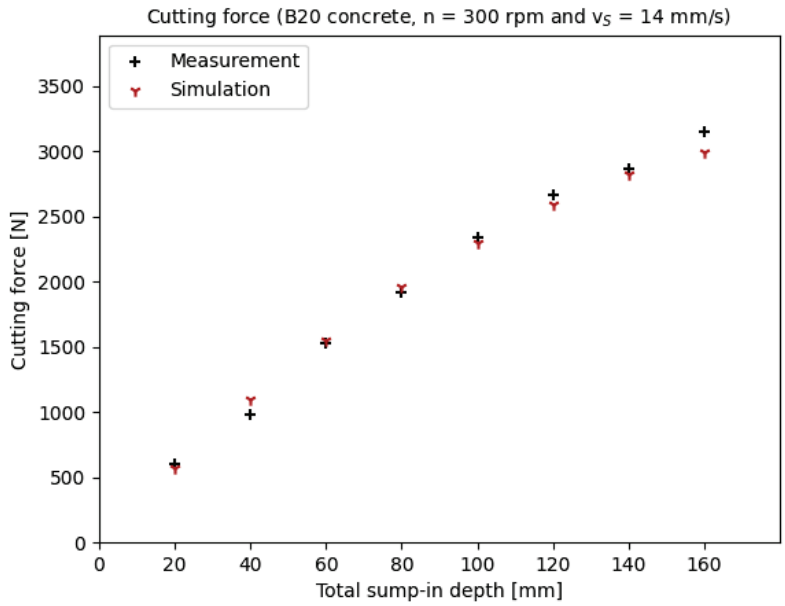

(a) Cutting force depending on total sump-in depth of cutter head

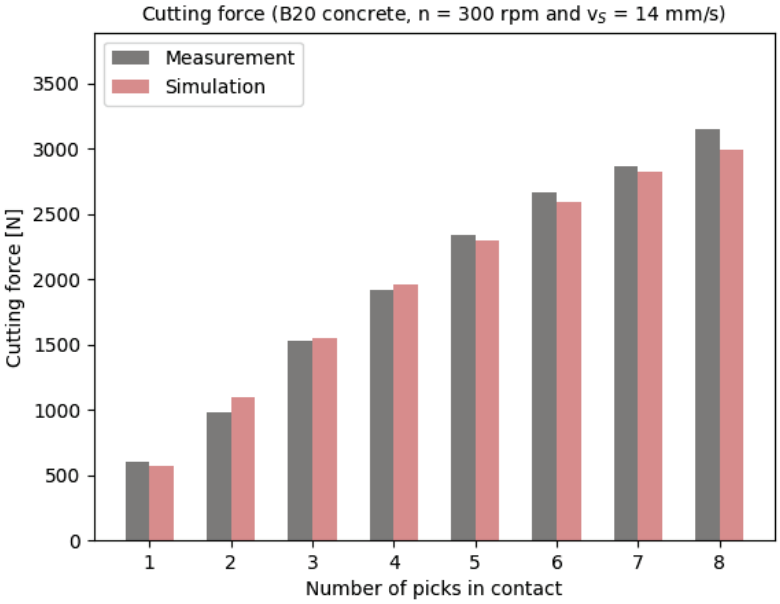

(b) Cutting force depending on number of picks in contact

Figure 6.9: Fast slew - Validation of simulated cutting forces (B20 concrete)

6.3.2 B30 concrete

Figure 6.10a shows the course of the cutting force for B30 concrete at increasing total sump-in depth levels. A similar nonlinearity is seen in both scatter plots. The absolute deviations between the total cutting force are highly satisfactory (Figure 6.10b).

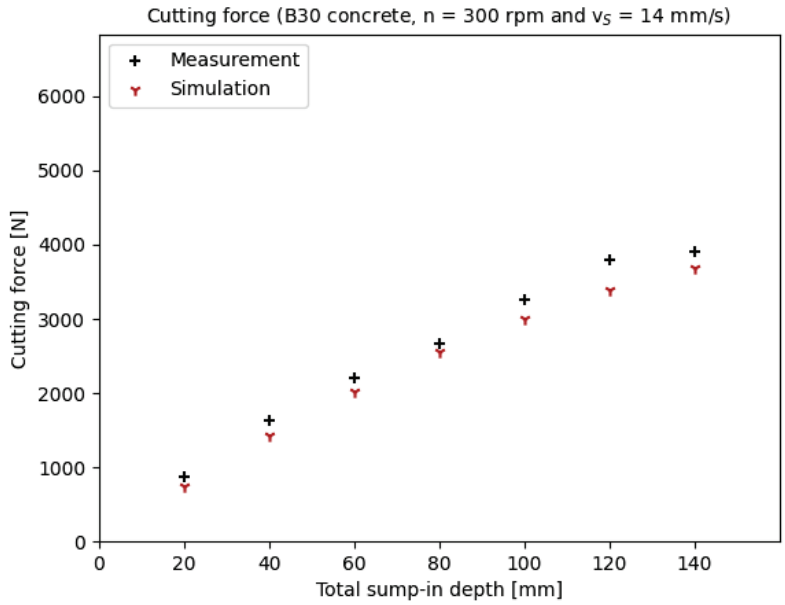

(a) Cutting force depending on total sump-in depth of cutter head

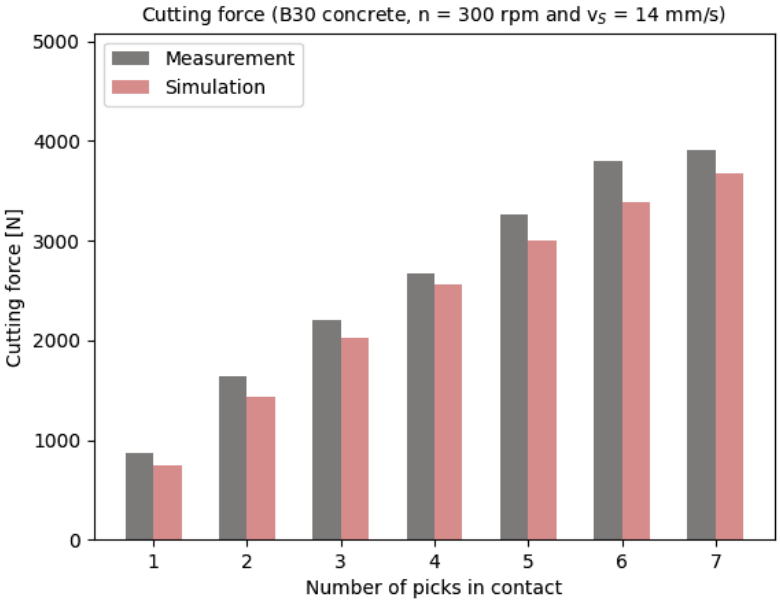

(b) Cutting force depending on number of picks in contact

Figure 6.10: Fast slew - Validation of simulated cutting forces (B30 concrete)

6.3.3 Oilshale

The fast slew oilshale cutting results are opposed with the simulation data in Figure 6.11a. The simulation data agrees very well with the measured cutting forces, except at greater total sump-in depth levels the deviation becomes greater (Figure 6.11b).

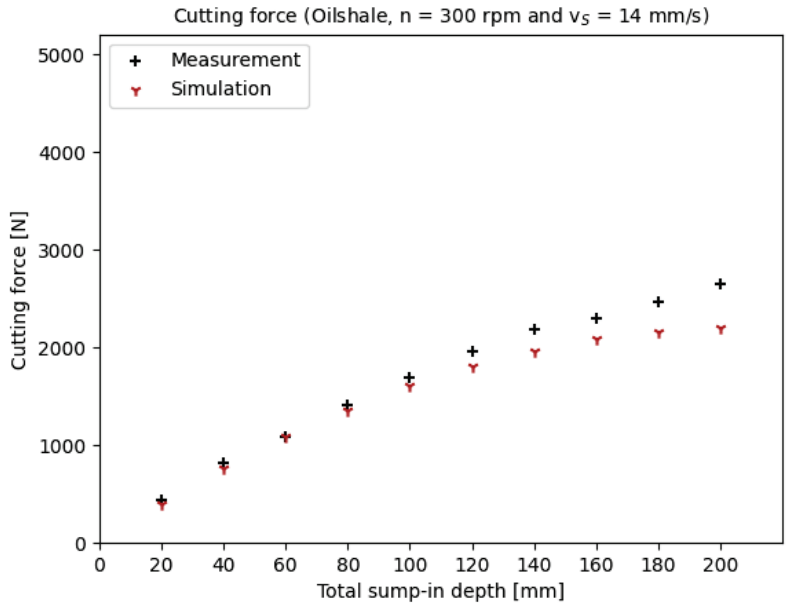

(a) Cutting force depending on total sump-in depth of cutter head

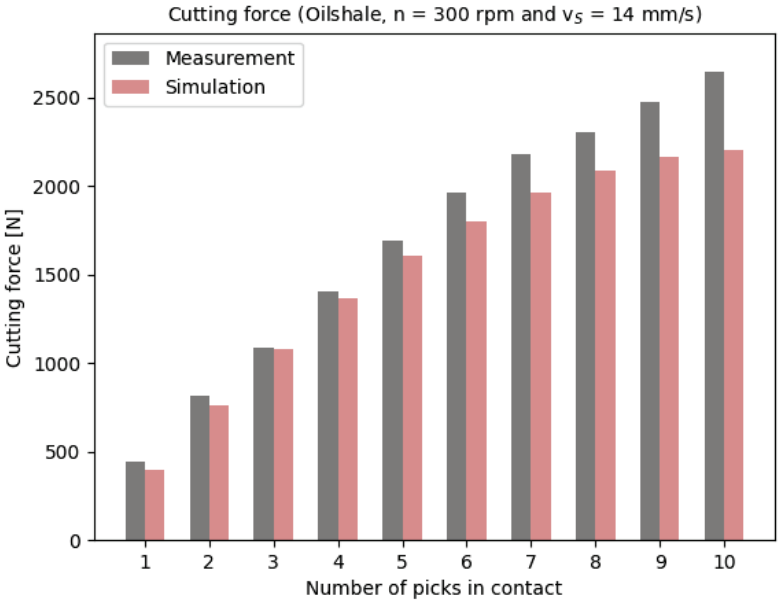

(b) Cutting force depending on number of picks in contact

Figure 6.11: Fast slew - Validation of simulated cutting forces (oilshale)

6.3.4 Analysis of deviation between experimental tests and simulation

The absolute and relative deviations between measurement and simulation of fast slew test cases are evaluated in this section.

6.3.4.1 Cutting force

In Figure 6.12, the mean relative deviations between measurement and simulation are shown for the three test specimens.

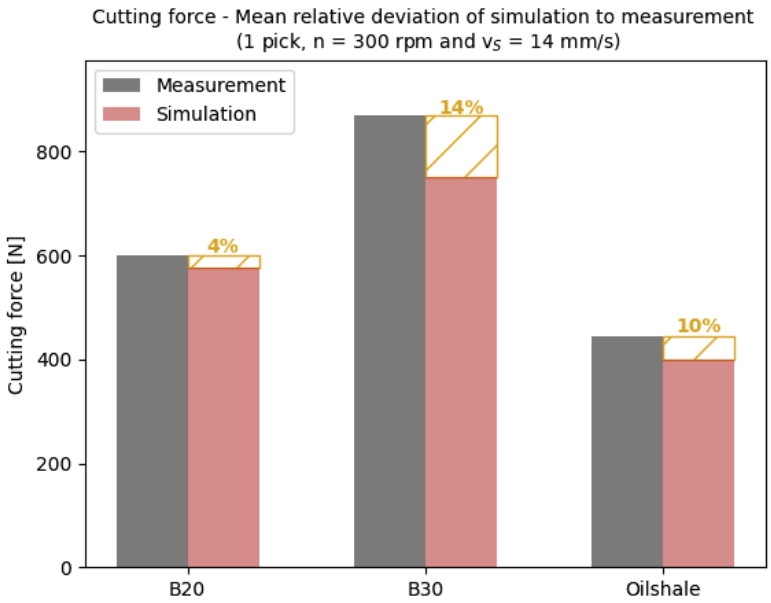

Figure 6.12: Fast slew - Cutting force for the three test sample types

A maximum mean relative deviation of 14 % for the B30 concrete sample could be found, whereas the minimum mean relative deviation between measurement and simulation is 4 % for the B20 concrete sample.

The linear regression of the measured cutting forces in Section 4.4.1.3 (Equation 4.4) provides an equation for approximating the cutting force for different UCS values.

This equation can be used to estimate the trend also for higher uniaxial compressive strength regions. Compared with the cutting forces calculated with the modified single-pick cutting theory, the extrapolated data shows again good conformity (see Figure 6.13).

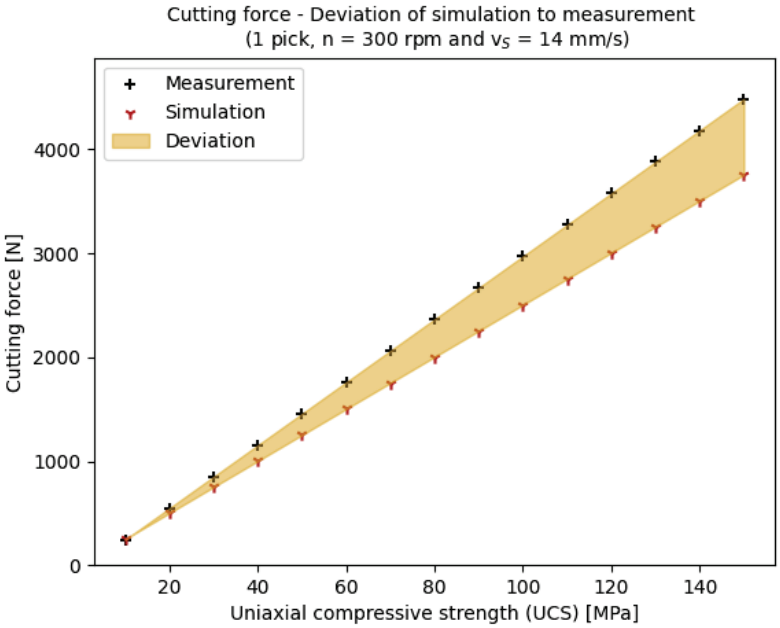

Figure 6.13: Fast slew - Cutting force comparison depending on UCS

Although it is important to mention that the cutting forces above the maximum uniaxial compressive strength of the test sample types need to be assessed with caution. The relative deviations between extrapolated data and simulation are presented in Figure 6.14.

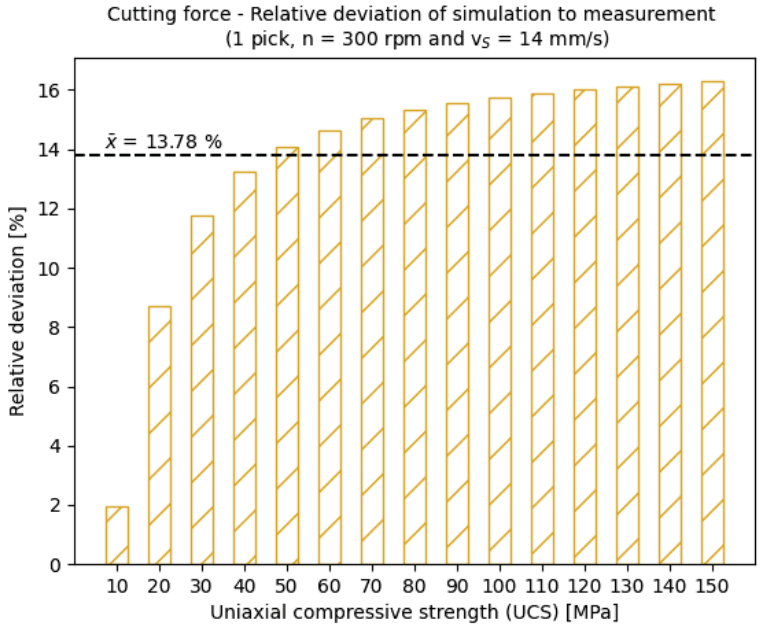

Figure 6.14: Fast slew - Relative deviation of cutting force depending on UCS

The relative deviations provide good results for uniaxial compressive strengths between 10 and 20 MPa, whereas above the threshold the magnitudes are satisfac-

tory but noticeably higher. A mean relative deviation of 13.78 % is significantly higher than in the slow slew cutting validation.

6.3.4.2 Specific energy

The specific energies for the three specimens have been calculated with Equation 6.1 and Equation 6.2 and compared to the theoretical specific energies determined with the approach presented in Section 3.1.2. The comparison is shown in Figure 6.15.

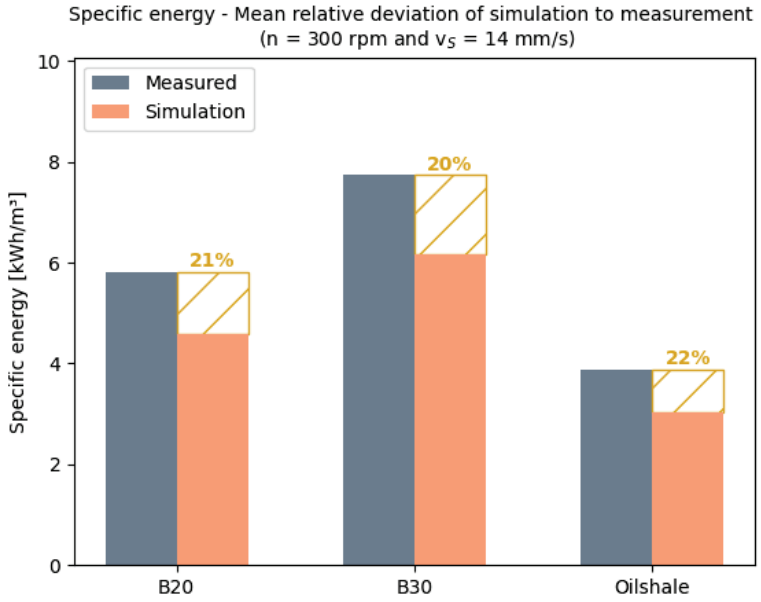

Figure 6.15: Fast slew - Specific energy depending on UCS of test specimens

The measurement results are higher than the calculated specific energy. Deviations of 20-22 % between the simulation and measurement are observed. A linear regression has again been conducted. The specific energy SE_{fast} can be estimated with Equation 6.4 and is shown in Figure 6.16.

$$SE_{fast} = 0.3 \cdot \sigma_c - 0.5 \tag{6.4}$$

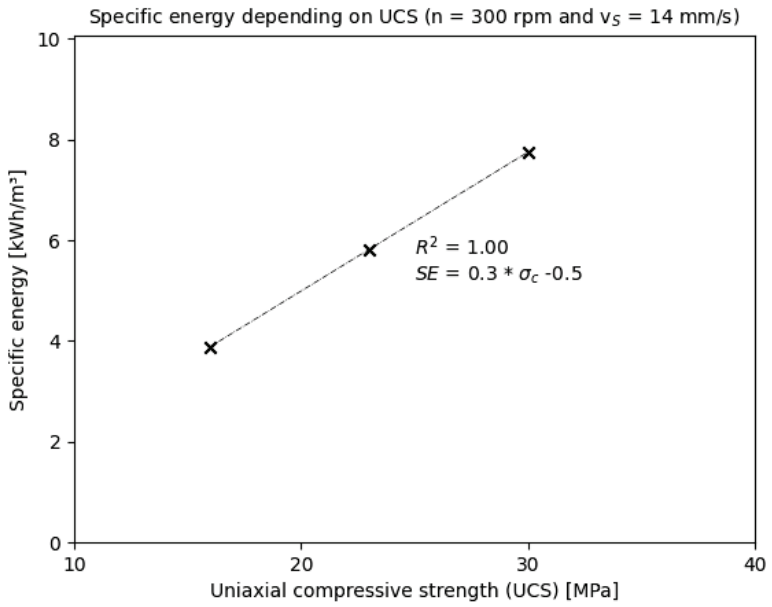

Figure 6.16: Fast slew - Linear regression of specific energy

6.4 Conclusion

In summary, the following conclusions can be drawn: The model is able to predict the total cutting force of a small, longitudinal part-face cutter head as well as the total cutting force progression at increasing total sump-in depth levels, specifically for soft rock. The deviations of the simulated results for slow slew are a maximum of 8 %, whereas they amount to a maximum of 14 % for fast slew. However, the correctness of the cutting force is of subordinate importance. Much more important is the validation of the ability to reproduce the dynamic character of the cutting process. The modelling of the variable pick cutting depth makes it possible to take the individual cutting forces of the single pick tools in contact into account.

Further validation results for the cutting torque can be found in Appendix E. These are not explained separately, as the linear relationship between the cutting force and the cutting torque would not lead to different conclusions.

In the future, it would be interesting to test this model for other part-face cutter heads and rock strengths to validate the developed modelling approach.

7 Conceptual designs of selected excavation tools

In the last chapter, the conclusions and results of the previous chapters are used to develop conceptual ideas of potential production tool systems for different scenarios. The presented concepts shall be considered as initial approaches for further detailed conceptualization and not as full-fledged developments. Parts of this chapter have already been documented in [15].

7.1 Rock drilling tools

Rock drilling tools are used in general only as a primary tool to drill boreholes for explosives or as an auxiliary tool used in a rock fragmentation process. Also, exploration drilling to receive material samples count to the most important use cases. In the following, three different rock drilling concepts are presented. They shall be applicable up to a uniaxial compressive strength of 200 MPa.

Tophammer drill

Figure 7.1 shows a concept of a tophammer drill system. A tophammer drill is usually powered by an oil-hydraulic hammer which applies a rotatory motion and a percussive force on the drill string, which allows penetrating higher rock strengths than rotary drilling.

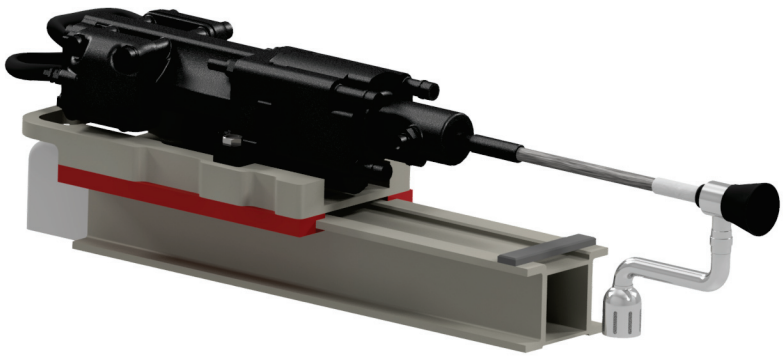

Figure 7.1: Tophammer rock drill - Concept

The drill bit is crushing the material and the debris is flushed out of the borehole either by water or by air. For material analysis, a funnel has also been integrated at the front end which is shrouding the drill bit. The water flushes the material through the collector pipe and the material is than separated in a filtering system or can be further pumped to a material analysis module.
The parts of the tophammer rock drill concept are described in Figure 7.2.

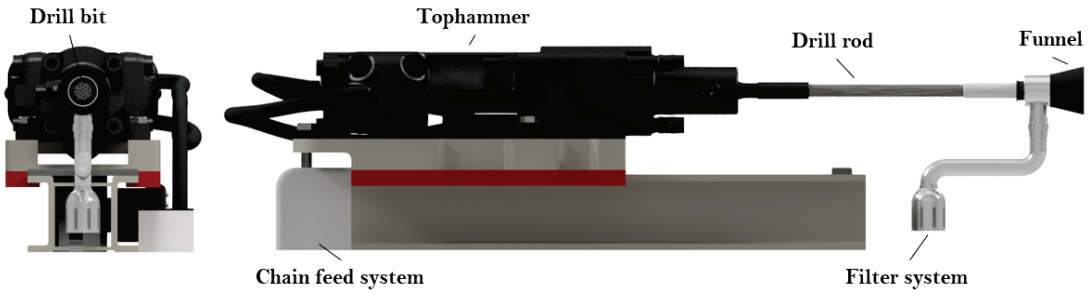

Figure 7.2: Tophammer rock drill - Parts

The *Doofor DF430X* tophammer [167] is implemented as hydraulic hammer. The specifications of the tophammer drilling tool are summarized in Table 7.1.

Table 7.1: Specifications of tophammer rock drilling tool

Percussion power	5 kW
Percussion pressure	120 bar
Percussion oil flow rate	45 l/min
Hammer torque	100 Nm
Hammer oil flow rate	10 - 15 l/min
Mass of hammer	41 kg
Drill rotation speed	200 – 300 rpm
Drill hole diameter	28 mm
Drill hole length	300 mm
Penetration rate	< 1 m/min
Drilling force	< 4 kN
Total mass	approx. 150 kg

Rotary-percussive (down-the-hole-hammer) drill

Down-the-hole-hammer drills have the great advantage over tophammer drills that the percussive motion is applied at the very front of the drill string. Figure 7.3 shows the concept of a rotary-percussive rock drilling system. This concept includes a water-hydraulic DTH hammer, a water-hydraulic motor and a water-hydraulic cylinder. Debris is flushed out by water in this case. The overall specifications of the rotary-percussive drilling tool are shown in Table 7.2.

Figure 7.3: Water-hydraulic rotary-percussive rock drill - Concept

Figure 7.4 is presenting the DTH drill concept. The thrust force is applied by a water-hydraulic cylinder. The *Wassara W50* hammer [87] serves as DTH hammer, water-hydraulic motor (M15) and thrust cylinder are both taken from *The Water Hydraulics Company* [168].

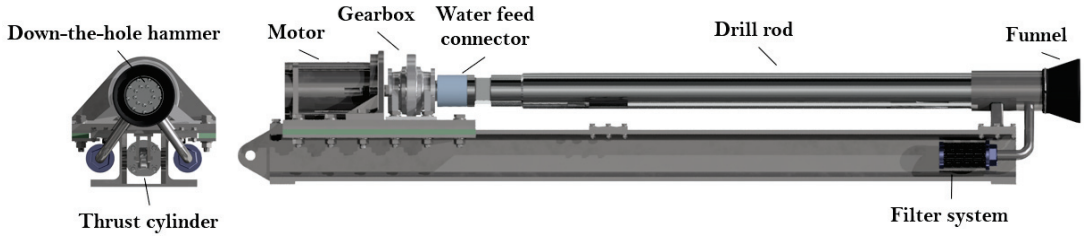

Figure 7.4: Water-hydraulic rotary-percussive rock drill - Parts

Rotary drill

The concept of a rotary drilling tool is presented in Figure 7.5 and with its part description in Figure 7.6. The drill is again powered by a water-hydraulic motor with a 1:20 reduction gearbox.

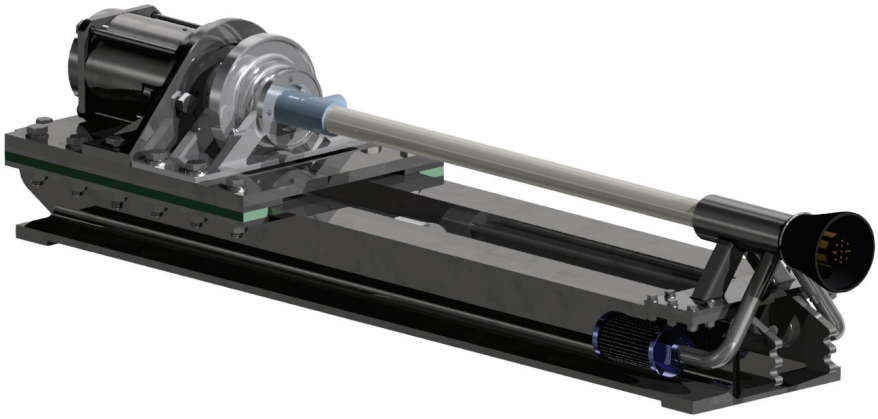

Figure 7.5: Rotary rock drill - Concept

Table 7.2: Specifications of rotary-percussive rock drilling tool

DTH hammer length	950 mm
Bit diameter	60 mm
Water pressure of hammer	50 - 170 bar
Water consumption of hammer	40 - 150 l/min
Weight of hammer	13.5 kg
Water consumption of motor	72 l/min
Water pressure of motor	160 bar
Motor rotation speed	4000 rpm
Mass of motor	6 kg
Gearbox ratio	1:20
Drill rotation speed	100 – 200 rpm
Drill hole diameter	60 mm
Drill hole length	300 mm
Penetration rate	$<$ 1 m/min
Drilling force	$<$ 6 kN
Total mass	approx. 70 kg

Table 7.3 shows the specifications of the rotary drilling tool concept.

Table 7.3: Specifications of rotary rock drilling tool

Motor rotation speed	4000 rpm
Gearbox ratio	1:20
Drill rotation speed	200 rpm
Drill hole diameter	30 mm
Drill hole length	300 mm
Penetration rate	$<$ 1 m/min
Drilling force	$<$ 10 kN
Total mass	approx. 50 kg

Thrust force is applied by a water-hydraulic cylinder and again, a material collector system - including a funnel, piping and two filtering systems - is integrated to collect the debris for analysis.

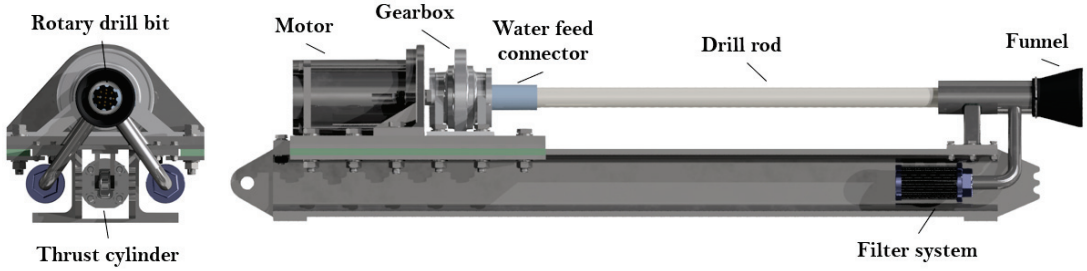

Figure 7.6: Rotary rock drill - Parts

In Table 7.4, the applicability of rock drilling systems in selected rock conditions is described in more detail.

Table 7.4: Applicability of rock drilling systems to selected rock conditions

Rock condition	Applicability
High lithostatic pressure	Yes. The high lithostatic pressure is not to considered as a problem. Required thrust forces can be significantly higher, but stability issues should not be a concern.
High shear stress	Yes. Careful selection of borehole positions and borehole layout to prevent unexpected displacements or rock bursts.
Friable or fractured rocks	Yes. Can be beneficial because of decreased thrust forces and higher penetration speeds, but borehole positions and layouts need also be chosen precisely.
Hard or tough rocks	Yes. Higher thrust forces and lower penetration speeds are to be expected.
Heterogeneous rocks	Yes. Thrust forces and penetration speeds will vary. Also, wear of the drill bit can be significantly higher if abrasive rock is encountered. Borehole positions and layout need to be chosen to minimize risks and exploit the weaknesses of the rock mass.
Faults and joints	Yes. Careful selection of borehole positions and borehole layout to prevent unexpected displacements or rock bursts.
Inrush of water	Yes. Careful selection of borehole positions and borehole layout to prevent or minimize inrush of water. Water per se not considered as a problem.
Cavernous grounds	Yes. If borehole is flushed with water, additional water can dissolve the material. Therefore, air flushing would be better to be applied in this case.
Seismic risks	Yes. Careful selection of borehole positions and borehole layout to prevent unexpected displacements or rock bursts.

7.2 Part-face cutting tool

Part-face cutting has the main advantage of a continuous excavation of material and giving a robot a greater flexibility. The performance is greatly depending on the rock to be excavated. Test specimens with uniaxial compressive strengths up to 40 MPa are considered to be potentially excavated, as shown by cutting tests in Chapter 4. The conducted performance analysis has been the starting point of the conceptual design process. Figure 7.7 shows the concept of water-hydraulically powered part-face cutting tool.

Figure 7.7: Part-face cutting tool - Concept

The individual parts of the excavation systems are described in Figure 7.8. A 17.5 kW water-hydraulic motor shall provide the cutting power for the cutter head. The desired rotation speed of the cutter head is about 300 rpm, which requires the use of a gearbox. A gearbox with a ratio of 1:15 has been selected, to be able to run the water-hydraulic motor on full speed while still having enough torque to provide high enough cutting forces. Depending on the abrasiveness of the material, the picks will wear down and need to be replaced after a certain cut volume. The coupling between the gearbox output shaft and the driving shaft of the cutter head allows minimum axial, radial and angular displacements, which will occur due to the high forces acting on the drive shaft.

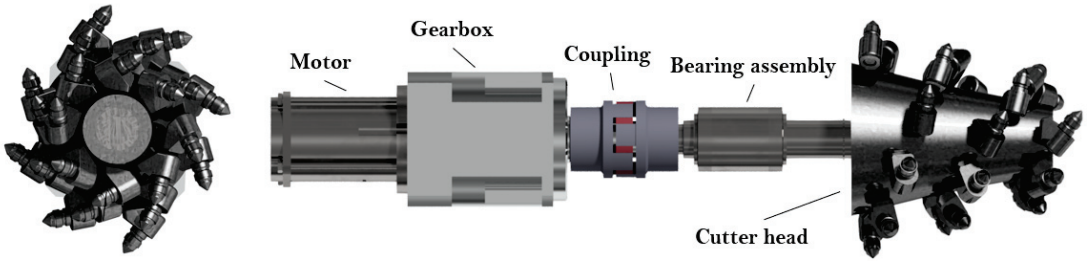

Figure 7.8: Part-face cutting tool - Parts

In Figure 7.9, the longitudinal cutter head can be seen in front and side view.

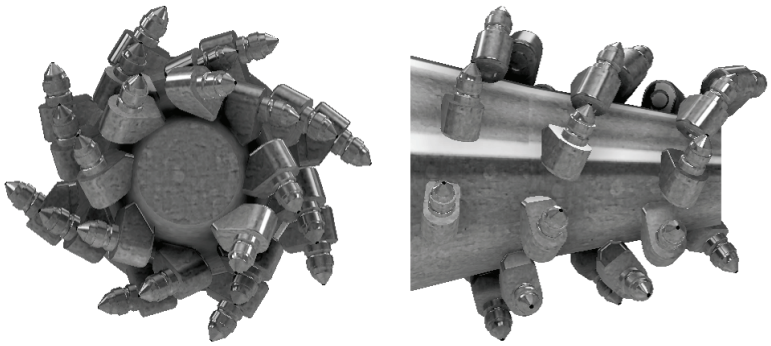

Figure 7.9: Longitudinal cutter head

The water-hydraulic motor will be driven at maximum speed which is between 4000–4500 rpm. The chosen gearbox has a ratio of 1:15, which allows a maximum torque of 675 Nm and reduces the rotation speed to 300 rpm. The specifications of the part-face cutting tool are summarized in Table 7.5.

Table 7.5: Specifications of part-face cutting tool

Power of water-hydraulic motor	17.5 kW
Motor rotation speed	4000 rpm
Gearbox ratio	1:15
Cutter head rotation speed	300 rpm
Cutter head torque	400 Nm
Max. cutting force (16 MPa UCS)	1600 N
Max. cutting force (30 MPa UCS)	3400 N
Total mass	50 kg
Excavation rate (16 MPa UCS)	< 0.8 m^3/h
Excavation rate (30 MPa UCS)	< 0.16 m^3/h

In Table 7.6, the applicability of a part-face cutting tool in selected rock conditions is described in more detail.

Table 7.6: Applicability of part-face cutting systems to selected rock conditions

Rock condition	Applicability
High lithostatic pressure	Partially. Possible, if rock strength doesn't exceed cutter head performance.
High shear stress	Partially. Possible, if rock strength doesn't exceed cutter head performance. Tectonic faults can facilitate excavation, because of weaknesses in the rock mass. Stability issues need to be assessed in advance and potential roof support applied.
Friable or fractured rocks	Partially. Possible, if rock strength doesn't exceed cutter head performance. Friable rocks can facilitate excavation, because of weaknesses in the rock mass. Stability issues need to be assessed in advance and potential roof support applied.
Hard or tough rocks	No. Generally, hard rocks cannot be excavated with a cutter head in that scale.
Heterogeneous rocks	Partially. Possible, if rock strength doesn't exceed cutter head performance. Weaker rocks will facilitate excavation, because of lower rock strength. Stability issues need to be assessed in advance and potential roof support applied. Performance will vary.
Faults and joints	Partially. Possible, if rock strength doesn't exceed cutter head performance. Local zones of weakness will facilitate excavation, because of weaker rock mass. Stability issues need to be assessed in advance and potential roof support applied. Water per se is not considered as a problem. Can make material more cohesive and caulk the picks.
Inrush of water	Partially. Possible, if rock strength doesn't exceed cutter head performance. Stability issues need to be assessed in advance and potential roof support applied. Water per se is not considered as a problem. Can make material more cohesive and caulk the picks.
Cavernous grounds	Partially. Possible, if rock strength doesn't exceed cutter head performance. Stability issues need to be assessed in advance and potential roof support applied. Water per se is not considered as a problem. Can make material more cohesive and caulk the picks.
Seismic risks	Partially. Possible, if rock strength doesn't exceed cutter head performance. Stability issues need to be assessed in advance and potential roof support applied.

7.3 High-pressure waterjet cutting tool

High-pressure waterjets can cut hard material without any significantly high reaction forces. Waterjets are usually taken to make precise cuts, but if arranged in a certain layout and mounted onto a manipulator, a continuous excavation tool can be developed. As shown in Section 3.2.1, the specific energy of high-pressure waterjets is poor and the amount of water required is high. Nevertheless, the idea of using high-pressure waterjets as a standalone excavation tool has been assessed due to the advantages if applied in a small-scale mining robot and investigated with a subsequent feasibility study.

A study of different waterjet arrangements is shown in Figure 7.10. The total amount of installed power shall not exceed 15 kW and the water flow per nozzle is held constant at 0.205 l/s:

- 1 high-pressure waterjet with 270 MPa water pressure: $<$ 400 MPa UCS.
- 2 high-pressure waterjet with 130 MPa water pressure: $<$ 250 MPa UCS.
- 3 high-pressure waterjet with 90 MPa water pressure: $<$ 170 MPa UCS.
- 5 high-pressure waterjet with 55 MPa water pressure: $<$ 100 MPa UCS.
- 10 high-pressure waterjet with 30 MPa water pressure: $<$ 50 MPa UCS.

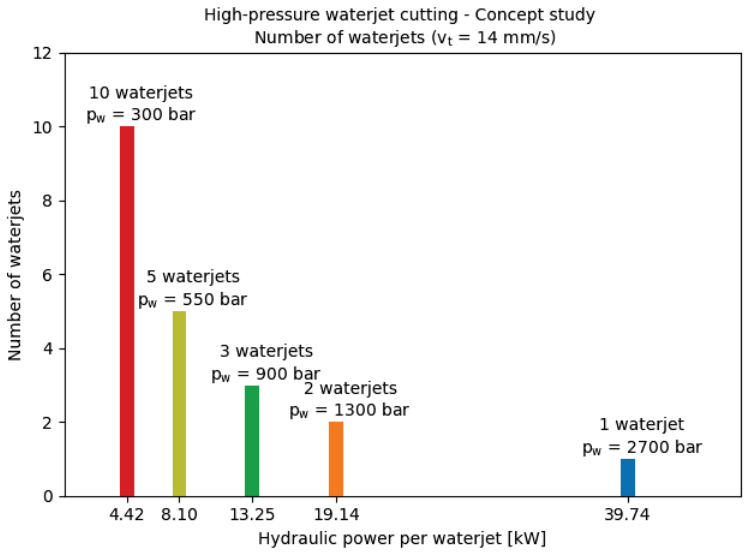

Figure 7.10: Feasible number of high-pressure waterjets with specified water pressure

Similar to the calculations conducted in Section 3.2.1, Figure 7.11 shows the cutting depths for the individual waterjets by taking into account the threshold

pressure for each rock strength.

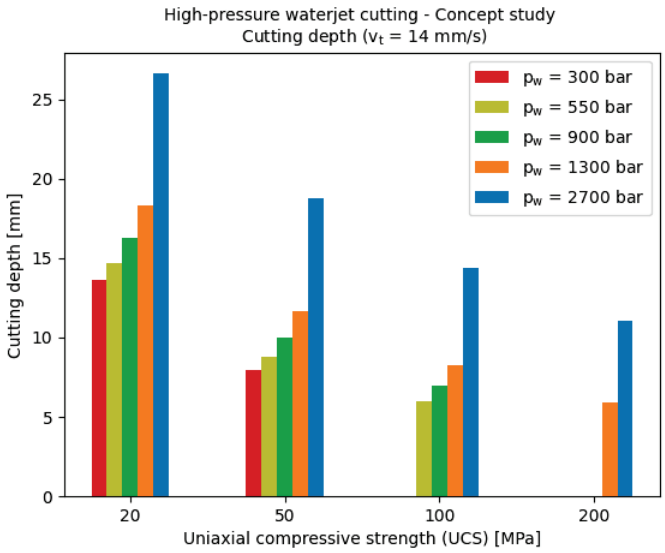

Figure 7.11: Cutting depths of combinations of high-pressure waterjets including threshold pressure

Based on the obtained results, a 5-waterjet arrangement has been selected and a conceptual design has been created. This enables cutting of medium hard rock with bearable power consumption. The concept of a high-pressure water jet cutting tool is presented in Figure 7.12.

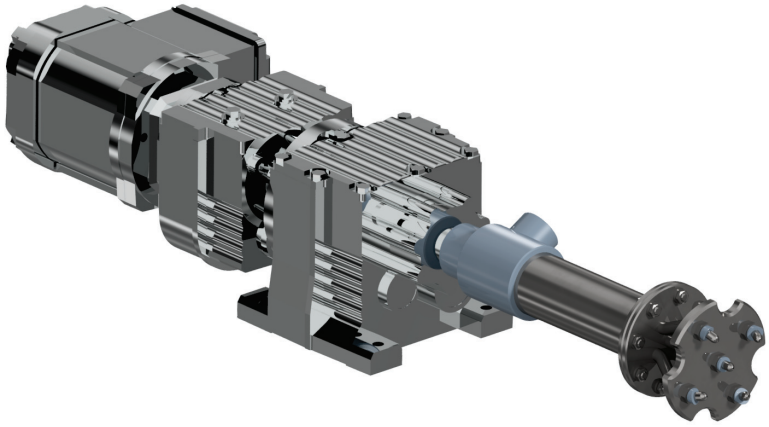

Figure 7.12: High-pressure waterjet cutting tool - Concept

The waterjets are mounted on a rotating shaft and orientated in a manner that the waterjets overlap each other in an intersection point exactly at the corresponding cutting depth. The rotation of the shaft allows the waterjet to cut a cone-shaped block of fractured rock. The water feed coupling is flushing high-pressure water from a water pump system to the nozzles through the hollow shaft. By moving the

shaft (mounted on a boom) this tool can be used to continuously excavate material. The center waterjet shall help to reduce the particle size of the excavated material. By increasing the power, this system can be upscaled easily. The components of the high-pressure waterjet cutting tool are shown in Figure 7.13.

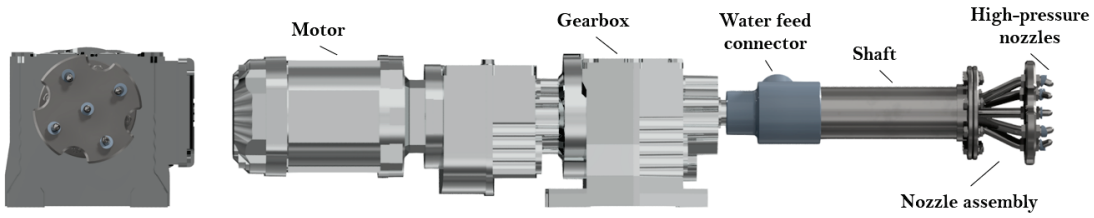

Figure 7.13: High-pressure waterjet cutting tool - Parts

The specifications of the high-pressure waterjet cutting tool are summarized in Table 7.7.

Table 7.7: Specifications of high-pressure waterjet cutting tool

Rotation speed	8 rpm
Traverse speed of waterjet	14.1 mm/s
Cutting depth of waterjet (20 MPa UCS)	15 mm
Cutting depth of waterjet (100 MPa UCS)	6 mm
Water pressure	550 bar
Water flow per nozzle	0.25 l/s
Water flow rate	61.5 l/min
Total weight	20 kg
Excavation rate (20 MPa UCS)	< 0.025 m^3/h
Excavation rate (100 MPa UCS)	< 0.01 m^3/h

The excavation process is sketched in Figure 7.14.

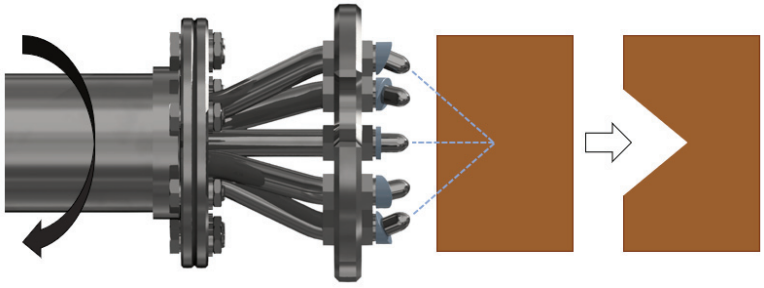

Figure 7.14: Excavation process of high-pressure waterjet cutting tool

In Table 7.8, the applicability of high-pressure waterjet systems in selected rock conditions is described in more detail.

Table 7.8: Applicability of high-pressure waterjet systems to selected rock conditions

Rock condition	Applicability
High lithostatic pressure	Yes. Water pressure is depending on the rock strength. Installed power limits the maximum pressure.
High shear stress	Yes. Water pressure is depending on the rock strength. Installed power limits the maximum pressure. Tectonic faults can facilitate excavation, because of weaknesses in the rock mass. Stability issues need to be assessed in advance and potential roof support applied.
Friable or fractured rocks	Yes. Water pressure is depending on the rock strength. Installed power limits the maximum pressure. Friable rocks can facilitate excavation, because of weaknesses in the rock mass. Stability issues need to be assessed in advance and potential roof support applied.
Hard or tough rocks	Yes. Water pressure is depending on the rock strength. Installed power limits the maximum pressure. Excavation performance will be decreased when hard rocks are encountered.
Heterogeneous rocks	Yes. Water pressure is depending on the rock strength. Installed power limits the maximum pressure. Weaker rocks will facilitate excavation, because of lower rock strength. Stability issues need to be assessed in advance and potential roof support applied. Performance will vary a lot.
Faults and joints	Yes. Water pressure is depending on the rock strength. Installed power limits the maximum pressure. Local zones of weakness will facilitate excavation, because of weaker rock mass. Stability issues need to be assessed in advance and potential roof support applied.
Inrush of water	Yes. Water pressure is depending on the rock strength. Installed power limits the maximum pressure. Stability issues need to be assessed in advance and potential roof support applied. Water per se is not considered as a problem. Distance of high-pressure waterjet cutting tool to the rock face may be decreased due to additional friction by contact with ambient water and water pressure needs to exceed the ambient water pressure.
Cavernous grounds	Partially. Stability issues need to be assessed in advance and potential roof support applied. Additional water can dissolve the material, which also needs to be taken into account. Water per se is not considered as a problem. Distance of high-pressure waterjet cutting tool to the rock face may be decreased due to additional friction by contact with ambient water and water pressure needs to exceed the ambient water pressure.
Seismic risks	Yes. Water pressure is depending on the rock strength. Installed power limits the maximum pressure. Stability issues need to be assessed in advance and potential roof support applied.

7.4 Hydrofracturing tool

The numerical simulations of hydrofracturing have shown a great potential in hard rock applications [137]. Therefore, two conceptual ideas of such a fracturing tool combined with a rotary rock drilling tool have been developed. Idea of this fragmentation method is using pressurized water inside a sealed borehole to fracture the rock by exceeding its strength. In the first stage, boreholes are generated with a water-hydraulically powered rotary drill, afterward the rock fragmentation tool pressurizes water inside those boreholes to fracture the rock similar to blasting.

Two concepts have been developed which can execute the hydrofracturing process. The downside of this excavation technology is the great amount of water which firstly needs to be provided and eventually has to be removed from the excavation point.

Rotary drill with a water-hydraulic cylinder as pressurizing tool
The boreholes are continuously filled with water and eventually the water pressure will be increased by exerting a pressure with a water-hydraulic cylinder onto the water column inside the drillhole. The fracturing tool needs to be anchored or held in place with high enough counter forces to prevent the reaction forces from pushing the tool away from the rock face. If the pressure inside the borehole is high enough to exceed the rock strength, the rock will fracture.

The combined rock fracturing tool is shown in Figure 7.15.

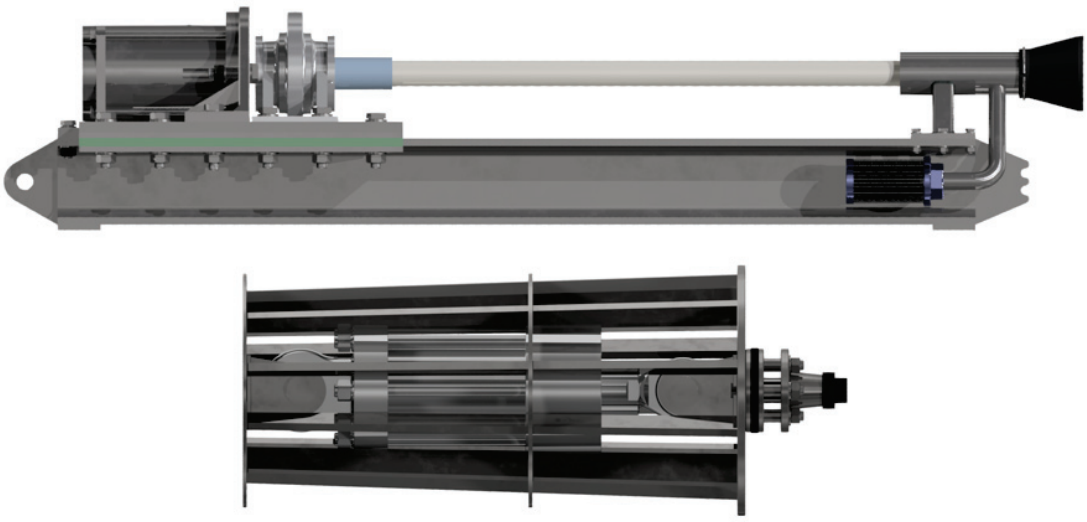

Figure 7.15: Hydrofracturing tool 1 - Concept

In Figure 7.16, the first rock fracturing system 1 is shown.

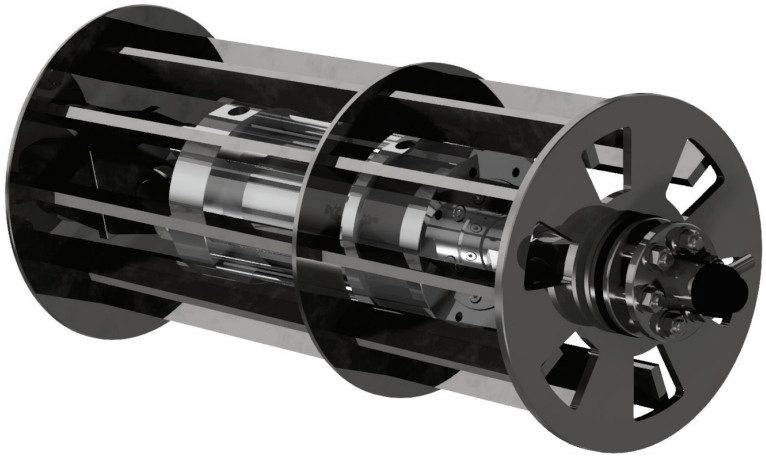

Figure 7.16: Rock fracturing tool 1 - Concept

The rock fracturing system 1 consists of a water-hydraulic cylinder, which is connected to a pressurizing part. This pressurizing part is in contact with the rock face and a funnel is inserted into the borehole. Water from a water pump is pumped through this pressurizing part and the borehole is sealed by the outer part of the funnel. If stroke is applied to the cylinder, a sliding pin, which is sliding inside the pressurizing part, is pushed onto the water column inside the borehole.

The components of the rock fracturing tool 1 are presented in Figure 7.17.

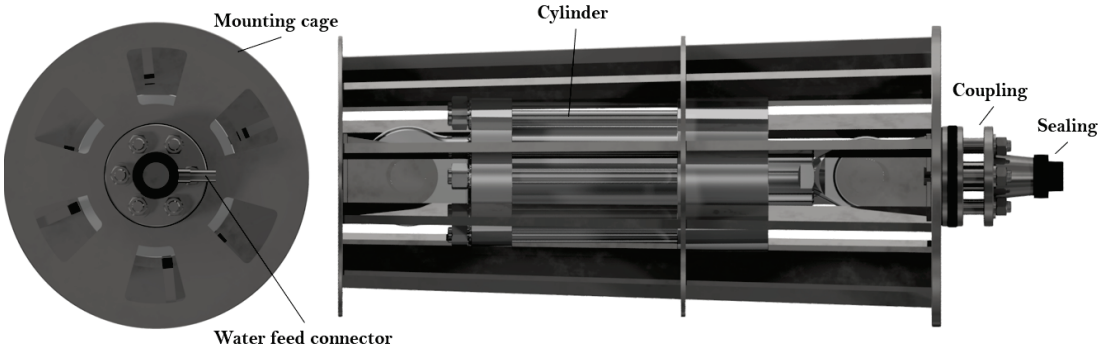

Figure 7.17: Rock fracturing tool 1 - Parts

Until now, this technology is not existing in practice and to assess feasibility in more detail, it is recommended to test this equipment with a simplified approach in a laboratory environment in the first stage. High cylinder forces, particularly for hard rock material, are limiting the applicability in a small-scale mining robot.

Further on, the sealing of the pressurized borehole will state a major obstacle.

Similar to blasting and radial-axial splitting, this should fracture the rock until

the pressure wave reaches the next free face. The methodology is sketched in Figure 7.18.

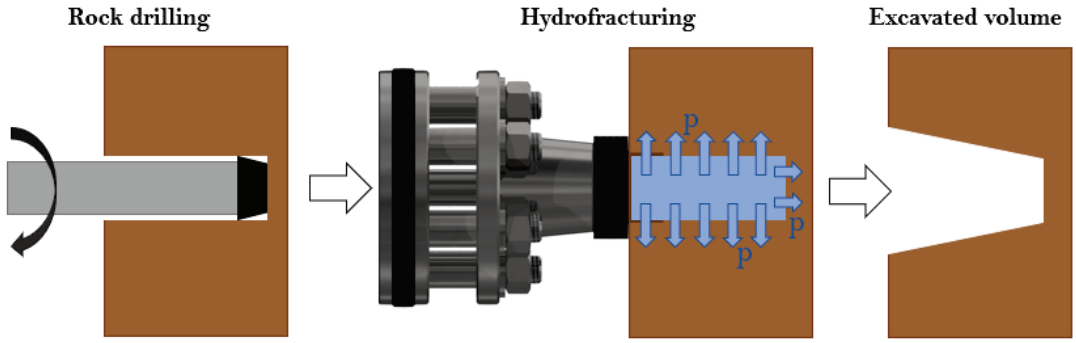

Figure 7.18: Hydrofracturing tool 1 - Excavation process

The specifications of the hydrofracturing tool are summarized in Table 7.9. The excavation rate can hardly be estimated in this case due to the multiple tasks included in the fracturing process. Number of boreholes defines the total drilling time and therefore has a major influence on the excavation rate. Pressurizing and fracturing the rock can not be quantified in this stage of development.

Table 7.9: Specifications of hydrofracturing tool

Motor rotation speed	4000 rpm
Gearbox ratio	1:20
Drill rotation speed	200 rpm
Drill hole diameter	30 mm
Drill hole length	300 mm
Penetration rate	< 1 m/min
Drilling force	< 10 kN
Water pressure	55 MPa
Water flow rate	2.63 l/min

Rotary drill with a high-pressure water pump and a pressure chamber as pressurizing tools

The second conceptual design (Figure 7.19) is similar to the first one, except the rock fracturing system is designed in a different way to not have any mechanical components which exert a force to pressurize the water inside a borehole.

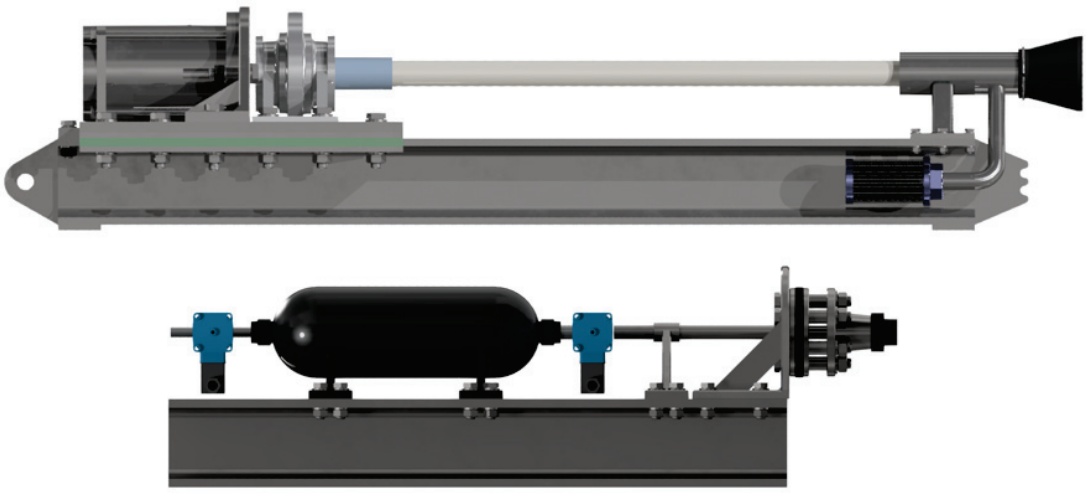

Figure 7.19: Hydrofracturing tool 2 - Concept

In Figure 7.20, the second rock fracturing system 2 is shown. The pressurization will be done by a high-pressure water pump and a pressure tank.

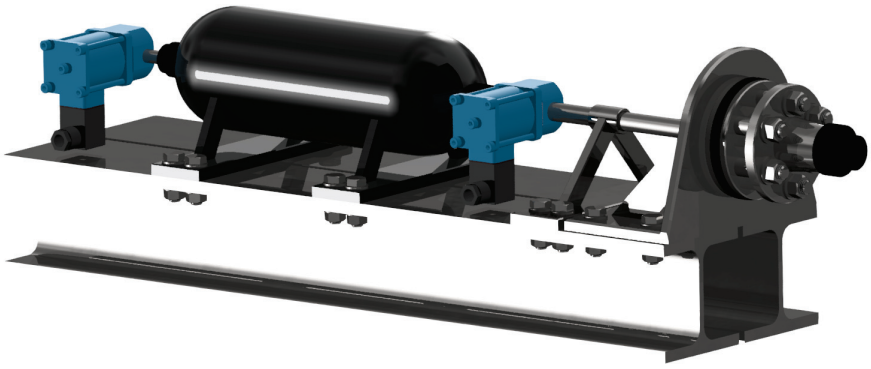

Figure 7.20: Rock fracturing tool 2 - Concept

High-pressure water is pumped from a separate high-pressure water pump and stored inside a small puffer tank. Afterward, the water is released by a high-pressure check valve into the borehole. The water is released within a fraction of time and the water is pushed inside the empty pre-drilled borehole and fractures the rock.

The components of the rock fracturing tool 2 are presented in Figure 7.21.

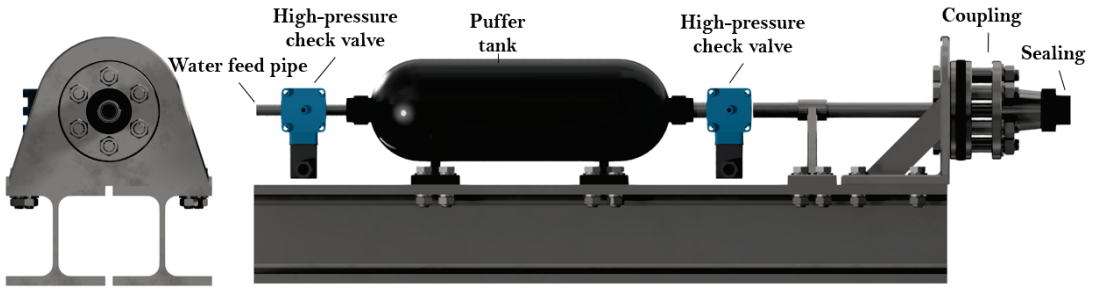

Figure 7.21: Rock fracturing tool 2 - Parts

By creating a borehole pattern design, similar to blasting and pressurizing each borehole consecutively, an entire mining cycle can be conducted (Figure 3.46 in Section 3.2.2). The advantages of this excavation technology compared to standard drill and blast are: Environmentally friendly (no use of oil), little to no vibrations, low power requirements, no generation of toxic fumes.

In Table 7.10, the applicability of hydrofracturing systems in selected rock conditions is analysed in more detail.

Table 7.10: Applicability of hydrofracturing systems to selected rock conditions

Rock condition	Applicability
High lithostatic pressure	Yes. Water pressure is depending on the rock strength. The high lithostatic pressure is not to considered as a problem. Required thrust forces of the drill can be significantly higher, but stability issues should not be a concern. Water pressure is depending on the rock strength. Installed power limits the maximum pressure.
High shear stress	Yes. Careful selection of borehole positions and borehole layout to prevent unexpected displacements or rock bursts. Tectonic faults can facilitate excavation, because of weaknesses in the rock mass. Required thrust forces of the drill can be significantly higher when harder rock is encountered.
Friable or fractured rocks	Yes. Water pressure is depending on the rock strength. Careful selection of borehole positions and borehole layout to prevent unexpected displacements or rock bursts. Friable rocks can facilitate excavation, because of weaknesses in the rock mass. Required thrust forces of the drill can be significantly higher when harder rock is encountered.
Hard or tough rocks	Partially. Water pressure is depending on the rock strength. Thrust force of rock drill will be significantly high. Installed power and water pressure are decisive for the overall efficiency.
Heterogeneous rocks	Yes. Water pressure is depending on the rock strength. Careful selection of borehole positions and borehole layout to prevent unexpected displacements or rock bursts. Weaker rocks can facilitate excavation, because of weaknesses in the rock mass. Required thrust forces of the drill can be significantly higher when harder rock is encountered.
Faults and joints	Yes. Water pressure is depending on the rock strength. Careful selection of borehole positions and borehole layout to prevent unexpected displacements or rock bursts. Local zones of weakness can facilitate excavation, because of weaknesses in the rock mass. Required thrust forces of the drill can be significantly higher when harder rock is encountered.
Inrush of water	Yes. Water pressure is depending on the rock strength. Careful selection of borehole positions and borehole layout to prevent unexpected displacements or rock bursts. Water per se is not considered as a problem. Water pressure needs to exceed the ambient water pressure.
Cavernous grounds	Partially. Water pressure is depending on the rock strength. Careful selection of borehole positions and borehole layout to prevent unexpected displacements or rock bursts. Additional water can dissolve the material, which also needs to be taken into account. Water per se is not considered as a problem. Water pressure needs to exceed the ambient water pressure.
Seismic risks	Yes. Water pressure is depending on the rock strength. Careful selection of borehole positions and borehole layout to prevent unexpected displacements or rock bursts. Installed power limits the maximum pressure.

8 Summary

The contribution of this thesis is the analysis of excavation technologies with respect to their applicability in future small-scale mining robots. After a preliminary overview of current excavation technologies and a review of the state of the art, selected technologies were subjected to further investigation.

Based on analyses, studies, and investigations conducted, the following conclusions can be derived. These statements refer to the application for small-scale mining robots, particularly for machines < 5000 kg. Part-face cutting is a continuous excavation method that demonstrates suitable performance in soft rock scenarios. The forces generated during the cutting process need to be managed by the robot and a light robot implies lower magnitude of manageable forces. Full-face cutting is not applicable for a robotic miner in a small scale. The forces exerted on the robot exceed its manageable capacity due to its low mass and power. Machines with comparable power, such as Mini TBMs, weigh significantly more than a robot. Therefore, full-face cutting was not considered for further concept development. High-pressure waterjet cutting is an alternative excavation method with high potential particularly for small-scale mining robots. The reaction forces associated with this method are negligible, and it has great potential for excavating hard rock. However, the overall production rate of the waterjet cutting tool is assumed to be lower compared to mechanical excavation methods, and the specific energy required is high, making it economically non-viable as a standalone tool. Nevertheless, the ability to easily and environmentally friendly excavate hard rock material is an attractive prospect. Combined excavation systems show high potential for small, mobile mining machines. These systems involve different rock fracturing methods that do not rely on explosives and combine conventional (mechanical) tools with alternative rock fracturing techniques. Rotary rock drilling exhibits bearable reaction forces, and therefore, a combination of a rotary rock drilling system and a secondary rock fracturing (hydrofracturing) is proposed as an excavation tool for medium-hard rocks. The only excavation method that is not limited by rock strength is drill and blast. However, full automation of the drill and blast cycle poses challenges that need to be addressed in the future and

the associated risks need to be minimized. Therefore, this method was excluded from the concept development.

Detailed investigations of excavation technologies have been conducted to perform preliminary evaluations of their potential applicability. Performance parameters such as excavation rate, specific energy, and expected reaction forces have been estimated using empirical or analytical approaches. The limitations and minimum requirements of selected excavation technologies were determined using a robot with a mass of 1500 kg as an example, considering the maximum uniaxial compressive strength of the rock to be excavated. Further on, look-up tables and extended results have been provided in order to facilitate a justified decision about the implementation of a certain excavation technology.

Experimental tests - with constant rotation speed of 300 rpm and slew speed levels of 7 and 14 mm/s - of a small, longitudinal part-face cutter head were conducted with test specimens of different uniaxial compressive strengths (UCS), including concrete (23 MPa and 30 MPa) and oilshale (16 MPa), in order to assess the applicability and performance of a small-scale mechanical cutting tool. The forces and torque during cutting showed a linear correlation with the UCS of the material and a nonlinear correlation with the number of picks in contact. The part-face cutter head is suitable for soft rock conditions, particularly for rock with UCS below 40 MPa, to achieve relatively efficient excavation performance. However, due to the low power and small mass of the test rig/robot, slow advance and excavation rates are expected. Excavation rates of maximum 0.8 m^3/h have been achieved in soft rock conditions. Additionally, abrasive materials cause excessive wear on pick tools, with concrete being highly abrasive and oilshale being little to non-abrasive. Loose and brittle materials, especially those with layers and fault zones, tend to break in larger chunks, resulting in uneven grain size distribution of the excavated material. In oilshale cutting tests, irregular grain size was observed, but the excavation rate remained satisfactory due to the low UCS. In limestone cutting tests, poor excavation performance was obtained due to the high UCS, resulting in the production of fine particles and heavy dust formation.

A main part was developing a methodology for predicting the total cutting force and cutting torque of a part-face cutter head. Rock cutting theories typically are limited to single conical pick tools. Specified approaches have been reviewed and compared to the measurement data for single picks in contact. Owing to the relatively small dimensions of the conical pick tools, significant disparities were observed between the cutting force models for single picks and the actual measurements. To address this issue, a single-pick rock cutting theory was adapted

and the cutting forces for single-pick cutting were verified. However, extrapolating this approach to predict cutting force and cutting torque for a full-scale cutter head necessitates disregarding the influence of variable cutting depth during the cutting operation. This leads to artificially elevated cutting forces and the inability of modelling the nonlinear behaviour of the cutting force with increasing sump-in depth of the cutter head. Consequently, a dynamic model was developed to incorporate this effect into the prediction of the cutting force. By combining these two approaches, it becomes feasible to simulate the cutting operation of a longitudinal part-face cutter head.

The model can accurately forecast the total cutting force of a small, longitudinal part-face cutter head, as well as the progression of the cutting force as the total sump-in depth increases, specifically for soft rock conditions. The maximum deviations in the simulated results for slow slew operations were 8 %, while for fast slew operations, they reached a maximum of 14 %. Nevertheless, the accuracy of the cutting force is of secondary importance compared to the validation of the model's ability to replicate the dynamic nature of the cutting process. Incorporating the variable pick cutting depth into the model enables the consideration of individual cutting forces exerted by each pick tool in contact. Moreover, the methodology allows modelling the kinematics of a production tool assembly including the boom and the cutter head by considering the spatial dimensions.

Eventually, conceptual designs of excavation technologies for certain rock conditions have been developed: three rock drilling tools for medium to hard rock, a water-hydraulically powered part-face cutting tool for excavating rocks below 40 MPa UCS, two types of hydrofracturing tools for mining medium hard rock and a high-pressure waterjet cutting tool for the excavation of hard rock.

9 Outlook

In order to test the applicability of certain small-scale excavation tools, laboratory and field tests are necessary. Small-scale mining robots equipped with mechanical cutting systems are intended to provide an opportunity to conduct research on the maximum bearable reaction forces. The application of alternative excavation tools could show the potential in hard rock conditions. Therefore, preliminary tests of prototypes of a continuous high-pressure waterjet cutting tool and a hydrofracturing tool are proposed.

Further on, it is necessary to test the cutting force prediction model for other part-face cutter heads and higher rock strengths in order to validate the methodology. The methodology could then be used for quick and reliable assessment of the expectable cutting forces of a cutter head in various operating scenarios. Additionally, a novel rock cutting theory, in particular for small-scale conical pick tools would be beneficial, taking into account the pick geometry and orientation as well as the interaction between the pick and rock by considering dynamic effects. This could be achieved by laboratory cutting tests with a divergent set of parameters combined with machine learning algorithms or with the help of numerical simulations (FE- or DE-simulations).

List of Figures

List of Tables

Bibliography

[1] Berner, M. and Sifferlinger, N. A. “HORIZON 2020 - ROBOMINERS: Entwicklung eines bio-inspirierten modularen Bergbau-Roboters”. In: *Stein & Kies (Mitgliederzeitschrift - Forum mineralische Rohstoffe)* 167 (2020). DOI: 10.34901/mul.pub.2023.154.

[2] Berner, M. and Sifferlinger, N. A. “H2020 – ROBOMINERS”. In: *BHM Berg- und Hüttenmännische Monatshefte* 166.2 (2021), pp. 59–63. ISSN: 0005-8912. DOI: 10.1007/s00501-020-01074-y.

[3] Narimani Dehnavi, R. and Berner, M. “Analysing the Feasibility of a Full-face Cutting Machine for the Robominers Project”. In: *BHM Berg- und Hüttenmännische Monatshefte* 166.2 (2021), pp. 64–69. ISSN: 0005-8912. DOI: 10.1007/s00501-021-01082-6.

[4] Berner, M. and Sifferlinger, N. A. “Abbautechnologien für zukünftige, mobile Bergbau-Roboter”. In: *BHM Berg- und Hüttenmännische Monatshefte* 167.2 (2022), pp. 76–83. ISSN: 0005-8912. DOI: 10.1007/s00501-022-01194-7.

[5] Leitner, J., Berner, M., and Sifferlinger, N. A. “Statusbericht – H2020-ROBOMINERS und M30 Projekttreffen”. In: *BHM Berg- und Hüttenmännische Monatshefte* 167.2 (2022), pp. 84–86. ISSN: 0005-8912. DOI: 10.1007/s00501-022-01193-8.

[6] Berner, M. and Sifferlinger, N. A. “Status of the H2020-ROBOMINERS Prototype”. In: *BHM Berg- und Hüttenmännische Monatshefte* 168.2 (2023), pp. 45–55. DOI: 10.1007/s00501-023-01318-7.

[7] Berner, M., Sifferlinger, N. A., and Moser, P. “Reduction of personnel in exposed areas, safety devices and early steps towards robots in mining”. In: *Proceedings of the International Future Mining Conference 2019* (2019), pp. 29–33. DOI: 10.34901/mul.pub.2023.155.

[8] Berner, M. and Sifferlinger, N. A. "Analysis of Excavation Methods for a Small-scale Mining Robot". In: *Proceedings of the International Symposium on Automation and Robotics (ISARC)*. Kitakyshu, Japan (Online Conference), 2020, pp. 481–490. DOI: 10.22260/ISARC2020/0067.

[9] Berner, M. and Sifferlinger, N. A. "Assessment of excavation technologies for a small-scale mining robot and development of future concepts". In: *Proceedings of the International Future Mining Conference 2021*. Australia (Online Conference), 2021, pp. 98–100. DOI: 10.34901/mul.pub.2023.156.

[10] Berner, M. and Sifferlinger, N. A. "Need of Alternative Excavation Tools for Mining Robots". In: *Proceedings of the 18th International Conference on Mineral Processing and Geometallurgy*. Vol. 18. Santiago de Chile, Chile (Online Conference), 2022, pp. 270–281. DOI: 10.34901/mul.pub.2023.157.

[11] Berner, M., Sifferlinger, N. A., and Gerer, R. "On the predictability of the cutting forces of small, longitudinal cutter heads". In: *Proceedings of the 15th International Symposium of Continuous Surface Mining 2023*. Freiberg, Germany, 2023, p. 14. DOI: 10.34901/mul.pub.2023.158.

[12] Henley, S. et al. *ROBOMINERS deliverable D2.2: Conceptual mining strategies and report on studies of bottlenecks and other limiting factors*. Ed. by ROBOMINERS Consortium. 2021.

[13] Burlet, C. et al. *ROBOMINERS deliverable D6.1: Miner perception report*. Ed. by ROBOMINERS Consortium. 2022.

[14] Berner, M., Sifferlinger, N. A., and Gerer, R. *ROBOMINERS deliverable D6.5: Develop a small-scale excavation tool system for the selective mining demonstrator based on COTS*. Ed. by ROBOMINERS Consortium. 2022.

[15] Berner, M., Sifferlinger, N. A., and Narimani Dehnavi, R. *ROBOMINERS deliverable D6.4: Production tools conceptualization and research at AT TRL-3*. Ed. by ROBOMINERS Consortium. 2022.

[16] Pinkse, T. et al. *ROBOMINERS Deliverable D5.4: Mining analogues & upstream/downstream mining processes*. Ed. by ROBOMINERS Consortium.

[17] Hiltz, R. *Taking a step into the robotic future*. 2020. URL: https://www.miningmagazine.com/innovation/news/1387411/taking-step-into-the-robotic-future (visited on 09/14/2023).

[18] European Commission. *Horizon 2020 Environment and resources data hub: H2020 - ROBOMINERS*. 2019. URL: https://sc5.easme-web.eu/?p=820971 (visited on 09/14/2023).

[19] Siciliano, B. and Khatib, O. *Springer Handbook of Robotics*. Springer Handbooks. Springer Berlin Heidelberg, 2008. ISBN: 978-3-540-30301-5.

[20] European Commission. *ROBOMINERS Proposal SEP-210520664: Resilient Bio-inspired Modular Robotic Miners / ROBOMINERS*. Ed. by European Commission. 2018.

[21] Sifferlinger, N. A. "Roboter im Bergbau – wo liegt der Bedarf?" In: *BHM Berg- und Hüttenmännische Monatshefte* 166.2 (2021), pp. 53–58. ISSN: 0005-8912. DOI: 10.1007/s00501-021-01079-1.

[22] Sifferlinger, N. A., Hartlieb, P., and Moser, P. "The Importance of Research on Alternative and Hybrid Rock Extraction Methods". In: *BHM Berg- und Hüttenmännische Monatshefte* 162 (2) (2017), pp. 58–66. ISSN: 0005-8912. DOI: 10.1007/s00501-017-0574-y.

[23] Heiniö, M. *Rock Excavation Handbook for Civil Engineering*. Sandvik Tamrock, 1999.

[24] Bilgin, N., Copur, H., and Balci, C. *Mechanical Excavation in Mining and Civil Industries*. Taylor and Francis Group, LLC, 2014. ISBN: 978-1-4665-8475-4.

[25] Darling, P. *SME Mining Engineering Handbook*. 3rd ed. Society for Mining, Metallurgy, and Exploration, Inc. (SME), 2011. ISBN: 978-0-87335-2642.

[26] Ahtola, U. et al. *Rock Excavation Handbook*. 1999.

[27] Zou, D. *Theory and technology of rock excavation for civil engineering*. Springer, 2018. ISBN: 978-981-10-1989-0.

[28] Spathis, A. T. and Gupta, R. N. *Tunneling in Rock by Drilling and Blasting*. CRC Press and Taylor and Francis Group, LLC, 2012. ISBN: 978-0-415-62141-0.

[29] Rostami, J. "Mechanical Rock Breaking". In: *SME Mining Engineering Handbook*. Ed. by P. Darling. Society for Mining, Metallurgy, and Exploration, Inc. (SME), 2011, pp. 417–434. ISBN: 978-0-87335-2642.

[30] Rostami, J. "Rock cutting tools for mechanical mining". In: *SME annual Meeting, Denver, Colorado, Society of Mining Metallurgy and Exploration Inc.* 2001.

[31] Krzysztof, K. "Hard rock mining – cutting or disk tools". In: *IOP Conference Series: Materials Science and Engineering* 545.1 (2019), p. 11. DOI: 10.1088/1757-899X/545/1/012019.

[32] Sifferlinger, N. A. “Stand der mechanischen Löseverfahren im Bergbau”. In: *BHM Berg- und Hüttenmännische Monatshefte* 167.2 (2022), pp. 43–51. ISSN: 0005-8912. DOI: 10.1007/s00501-022-01195-6.

[33] Hassani, F. *Review of explosive-free rock breakage: Technologies and expertise*. Ed. by McGill University. 2009.

[34] Chapman, Y. and Graham, C. “Controlled foam injection progress towards automated hard rock excavation”. In: *Proceedings of the 5th International Symposium on Mining Science and Technology*. 1999, p. 39.

[35] International Mining. *DynaCut technology achieving breakthroughs - International Mining*. 2015. URL: https://im-mining.com/2015/12/17/dynacut-technology-achieving-breakthroughs/ (visited on 09/14/2023).

[36] Marshall, J. et al. “Robotics in Mining”. In: *Springer Handbook of Robotics*. Springer International Publishing, 2016, pp. 1549–1576. ISBN: 978-3-319-32552-1. DOI: 10.1007/978-3-319-32552-1_59.

[37] Corke, P. et al. “Mining Robotics”. In: *Springer Handbook of Robotics*. Springer Berlin Heidelberg, 2008, pp. 1127–1150. ISBN: 978-3-540-30301-5. DOI: 10.1007/978-3-540-30301-5_50.

[38] Zlotnikov, D. “Mining in the extreme”. In: *CIM Magazine* 7.5 (2012), pp. 50–56.

[39] Cross, P. *Recent Trends in Output and Employment*. Statistics Canada Ottawa, 2007.

[40] Vagenas, N., Runciman, N., and Clément, S. R. “A methodology for maintenance analysis of mining equipment”. In: *International Journal of Surface Mining, Reclamation and Environment* 11.1 (1997), pp. 33–40.

[41] Gustafson, A. et al. “Production and maintenance performance analysis: manual versus semi-automatic LHDs”. In: *Journal of Quality in Maintenance Engineering* 19.1 (2013), pp. 74–88.

[42] Moravec, H. P. *Robot*. 2023. URL: https://www.britannica.com/technology/robot-technology (visited on 09/14/2023).

[43] Nanda, S. K. et al. “Application of robotics in mining industry: A critical review”. In: *Mining Technology-Extraction, Beneficiation for Safe & Sustainable Development, Indian Mining & Engg. Journal, Mine TECH* 10 (2010), pp. 108–112.

[44] B. Siciliano et al., eds. *Field and Service Robotics*. Springer Tracts in Advanced Robotics. Berlin, Heidelberg: Springer Berlin Heidelberg, 2010. ISBN: 978-3-642-13407-4. DOI: 10.1007/978-3-642-13408-1.

[45] Chadwick, J. "Autonomous mine truck". In: *Mining Magazine* 175.5 (1996), pp. 287–288.

[46] Barnes, J. "A new positioning technology for high precision indoor and outdoor positioning". In: *Proceedings of the 16th Int. Tech. Meeting of the Satellite Division of the US Inst. of Navigation*. 2003.

[47] Bastos, G. S. et al. "A single-dependent agent approach for stochastic time-dependent truck dispatching in open-pit mining". In: *Proceedings of the 14th International IEEE Conference on Intelligent Transportation Systems (ITSC)*. IEEE. 2011, pp. 1057–1062.

[48] Singh, S. "State of the art in automation of earthmoving". In: *Journal of Aerospace Engineering* 10.4 (1997), pp. 179–188.

[49] Singh, S. *State of the Art in Automation of Earthmoving*. Tech. rep. Carnegie Mellon University, 2002, p. 19.

[50] Sifferlinger, N. A. *Excavation Engineering - Mechanical Excavation*. Ed. by Chair of mining engineering and mineral economics. Leoben, Austria, 2022.

[51] Mitchell, G. "Longwall mining". In: *Australasian coal mining practice* (2009), pp. 340–373.

[52] Bonchis, A. et al. "Robotic explosive charging in mining and construction applications". In: *IEEE Transactions on Automation Science and Engineering* 11.1 (2013), pp. 245–250.

[53] Bartsch, E., Laine, M., and Andersen, M. *The application and implementation of optimized mine ventilation on demand (OMVOD) at the Xstrata Nickel Rim South Mine, Sudbury, Ontario*. 2010.

[54] Ralston, J., Hargrave, C., and Hainsworth, D. "Localisation of mobile underground mining equipment using wireless Ethernet". In: *Proceedings of the 40th IAS Annual Meeting*. Vol. 1. IEEE. 2005, pp. 225–230.

[55] Atia, M. et al. "Bayesian Filtering Based WiFi/INS Integrated Navigation Solution for GPS-Denied Environments". In: *Navigation* 58.2 (2011), pp. 111–125.

[56] Papachristos, C. et al. "Autonomous navigation and mapping in underground mines using aerial robots". In: *Proceedings of the 2019 IEEE Aerospace Conference*. IEEE. 2019, pp. 1–8.

[57] Artan, U., Marshall, J., and Lavigne, N. "Robotic mapping of underground mine passageways". In: *Mining Technology* 120.1 (2011), pp. 18–24.

[58] Mueller, R. P. "A Review of Extra-Terrestrial Regolith Excavation Concepts and Prototypes". In: *Earth and Space 2022* (2022), pp. 321–331.

[59] Vu, M. T. et al. "A study on an up-milling rock crushing tool operation of an underwater tracked vehicle". In: *Proceedings of the Institution of Mechanical Engineers, Part M: Journal of Engineering for the Maritime Environment*. Vol. 233. 1. SAGE Publications Sage UK: London, England, 2019, pp. 283–300.

[60] Vu, M. T. et al. "Analytical design of an underwater construction robot on the slope with an up-cutting mode operation of a cutter bar". In: *Applied Ocean Research* 86 (2019), pp. 289–309. ISSN: 0141-1187. DOI: 10.1016/j.apor.2019.02.019.

[61] Watanabe, Y. et al. "Research and Development of a Self-Walking Vertical Mining System Using DTH Drilling Unit and the Scale Model Test". In: *Proceedings of the International Conference on Offshore Mechanics and Arctic Engineering*. American Society of Mechanical Engineers. 2019.

[62] Kamprowski, R. "The use of underwater robots in searching for rare earth elements". In: *Wykorzystanie dronów i robotów w systemach bezpieczeństwa*. 2022, pp. 163–175. ISBN: 978-83-66740-37-2.

[63] Wei, H. et al. "Review on bioinspired planetary regolith-burrowing robots". In: *Space Science Reviews* 217 (2021), pp. 1–39.

[64] Lopes, L. et al. "UNEXMIN: an innovative approach for mineral exploration in flooded mines." In: *Geophysical Research Abstracts*. Vol. 21. 2019.

[65] Wang, T. et al. "Progress in the development of small-celestial-body anchoring robots". In: *Nature Astronomy* (2023), pp. 1–11.

[66] Mueller, R. P. et al. "Regolith Advanced Surface Systems Operations Robot (RASSOR)". In: *Proceedings of the 2013 IEEE Aerospace Conference*. 2013, pp. 1–12. DOI: 10.1109/AERO.2013.6497341.

[67] NASA. *Mars 2020 Perseverenance Launch Press Kit*. 2020. URL: https://www.jpl.nasa.gov/news/press_kits/mars_2020/download/mars_2020_launch_press_kit.pdf.

[68] Winkelman, M., Dijxhoorn, D., and Marcus, O. "Novel Solution for Mining Minerals:¡VAMOS!" In: *Proceedings of the Western Dredging Association Dredging Summit & Expo '18, Norfolk, VA, USA*. 2018, pp. 25–28.

[69] Bakker, E., Zibret, G., and Rainbird, J. “The ¡VAMOS! Sustainable Underwater Mining Solution”. In: *European Geologist* 44 (2017).

[70] La Palma Research Centre. *¡VAMOS!* 2023. URL: https://www.lapalmacentre.eu/portfolio-item/vamos/ (visited on 09/14/2023).

[71] Morgan, N. et al. “Tracked Subsea Trencher Mobility And Operation In Soft Clays”. In: *International Ocean and Polar Engineering Conference* (2007).

[72] Chao, X. et al. “A Compact Design of Underwater Mining Vehicle for the Cobalt-Rich Crust with General Support Vessel Part A: Prototype and Tests”. In: *Journal of Marine Science and Engineering* 10 (2022), p. 135. DOI: 10.3390/jmse10020135.

[73] Firstbrook, D. et al. *Ultrasonic Auger for Narrow-Gauge Borehole Drilling*. 2018. DOI: 10.1109/ULTSYM.2018.8579687.

[74] H2020 - Badger. 2018. URL: https://badger-robotics.eu/ (visited on 09/14/2023).

[75] Saperstein, L. W. et al. *Breakthrough energy savings with waterjet technology*. Tech. rep. Univ. of Missouri, Columbia, MO (United States), 2007.

[76] Abu Bakar, M. Z., Butt, I. A., and Majeed, Y. “Penetration Rate and Specific Energy Prediction of Rotary–Percussive Drills Using Drill Cuttings and Engineering Properties of Selected Rock Units”. In: *Journal of Mining Science* 54.2 (2018), pp. 270–284. ISSN: 1062-7391. DOI: 10.1134/S106273911802363X.

[77] Cheniany, A. et al. “An estimation of the penetration rate of rotary drills using the Specific Rock Mass Drillability index”. In: *International Journal of Mining Science and Technology* 22.2 (2012), pp. 187–193.

[78] Kim, D.-J. et al. “Design study of impact performance of a DTH hammer using PQRSM and numerical simulation”. In: *Journal of Mechanical Science and Technology* 33 (2019), pp. 5589–5602.

[79] Adebayo, B. and Akande, J. M. “Analysis of button bit wear and performance of down-the-hole hammer drill”. In: *Ghana Mining Journal* 15.2 (2015), pp. 36–41.

[80] Depouhon, A., Denoël, V., and Detournay, E. “Numerical simulation of percussive drilling”. In: *International Journal for Numerical and Analytical Methods in Geomechanics* 39.8 (2015), pp. 889–912.

[81] Bu, C. et al. “Numerical simulation of impact on pneumatic DTH hammer percussive drilling”. In: *Journal of Earth Science* 20.5 (2009), p. 868.

[82] Wang, Y. et al. “Impact dynamics of a percussive system based on rotary-percussive ultrasonic drill”. In: *Shock and Vibration* 2017 (2017).

[83] Kahraman, S. “Rotary and percussive drilling prediction using regression analysis”. In: *International journal of rock mechanics and mining sciences* 36.7 (1999), pp. 981–989.

[84] Kahraman, S. “The development of a model to obtain suitable drilling and blasting conditions in open pit mines and quarries”. Istanbul Technical University, 1997.

[85] Epiroc. 2023. URL: `https://www.epiroc.com/` (visited on 09/14/2023).

[86] HPESA. *Underground mining equipment*. 2023. URL: `https://www.hpesa.com/` (visited on 09/14/2023).

[87] LKAB Wassara. *DTH drills*. 2023. URL: `https://www.wassara.com/en/` (visited on 09/14/2023).

[88] Balci, C. et al. “Estimation of optimum specific energy based on rock properties for assessment of roadheader performance”. In: *SAIMM - Journal of The South African Institute of Mining and Metallurgy* 104 (2004), pp. 633–642.

[89] Kurosch, T. and Plinninger, R. J. “Roadheader Excavation Performance - Geological And Geotechnical Influences”. In: *Proceedings of the 9th ISRM Congress* (1999).

[90] Gehring, K. H. “Modern roadheader technology for tunnel excavation”. In: *Proceedings of Tunnel Maq*. 2000, pp. 1–14.

[91] Gehring, K. “A cutting comparison”. In: *Tunnels and Tunnelling* 21.11 (1989).

[92] Roxborough, F. F. and Liu, Z. C. “Theoretical considerations on pick shape in rock and coal cutting”. In: *Proceedings of the Sixth Underground Operator’s Conference* (1995), pp. 189–193.

[93] Simex. *Cutter heads*. 2023. URL: `https://www.simex.it/en-gb/products/tf-cutter-heads` (visited on 09/14/2023).

[94] Rostami, J. and Ozdemir, L. “A New Model for Performance Prediction of Hard Rock TBMs”. In: *Proceedings of the Rapid Excavation and Tunneling Conference*. 1993.

[95] Rostami, J., Ozdemir, L., and Neil, D. M. "Performance prediction: a key issue in mechanical hard rock mining". In: *International Journal of Rock Mechanics and Mining Sciences and Geomechanics Abstracts* 32.4 (1995).

[96] Rostami, J., Ozdemir, L., and Nilson, B. "Comparison between CSM and NTH hard rock TBM performance prediction models". In: *Proceedings of the Annual Technical Meeting of the Institute of Shaft Drilling Technology, Las Vegas*. 1996, pp. 1–10.

[97] Rostami, J. "Development of a force estimation model for rock fragmentation with disc cutters through theoretical modeling and physical measurement of crushed zone pressure". 1997.

[98] Rostami, J. "Hard rock TBM cutterhead modeling for design and performance prediction". In: *Geomechanik und Tunnelbau: Geomechanik und Tunnelbau* 1.1 (2008), pp. 18–28.

[99] Hassanpour, J., Rostami, J., and Zhao, J. "A new hard rock TBM performance prediction model for project planning". In: *Tunnelling and Underground Space Technology* 26.5 (2011), pp. 595–603.

[100] Farrokh, E., Rostami, J., and Laughton, C. "Study of various models for estimation of penetration rate of hard rock TBMs". In: *Tunnelling and Underground Space Technology* 30 (2012), pp. 110–123.

[101] Rostami, J. "Study of pressure distribution within the crushed zone in the contact area between rock and disc cutters". In: *International Journal of Rock Mechanics and Mining Sciences* 57.No. 3 (2013), pp. 172–186. ISSN: 1365-1609. DOI: 10.1016/j.ijrmms.2012.07.031.

[102] Rostami, J. "Performance prediction of hard rock Tunnel Boring Machines (TBMs) in difficult ground". In: *Tunnelling and Underground Space Technology* 57.3 (2016), pp. 173–182. ISSN: 0886-7798. DOI: 10.1016/j.tust.2016.01.009.

[103] Oraee, K. and Salehi, B. "Calculation Optimum Advance Rate and Productivity on TBM Tunneling-A case study in Iran". In: *Proceedings of the International Conference on Tunnelling & Trenchless Technology,* The Institution of Engineers-Malaysia. 2011.

[104] Wang, R. et al. "A mechanical method for predicting TBM penetration rates". In: *Arabian Journal of Geosciences* 13 (2020), pp. 1–15.

[105] Shen, X. et al. "A New Calculation Method of Cutterhead Torque Considering Shield Rolling Angle". In: *Applied Sciences* 12.1 (2021), p. 396.

[106] Jing, L.-j. et al. “A TBM advance rate prediction method considering the effects of operating factors”. In: *Tunnelling and Underground Space Technology* 107 (2021), p. 103620.

[107] Herrenknecht. 2023. URL: https://www.herrenknecht.com/de/ (visited on 09/14/2023).

[108] Robbins. 2023. URL: https://www.robbinstbm.com/ (visited on 09/14/2023).

[109] Tuncdemir, H. “Impact hammer applications in Istanbul metro tunnels”. In: *Tunnelling and Underground Space Technology* 23.3 (2008), pp. 264–272.

[110] Dincer, T. “The effect of some rock properties on the performance of roadheaders and impact hammers”. Istanbul Technical University, 1990.

[111] Aksoy, C. “Performance prediction of ımpact hammers by block punch ındex for weak rock masses”. In: *International Journal of Rock Mechanics and Mining Sciences* 46.8 (2009), pp. 1383–1388.

[112] Ocak, I. and Bilgin, N. “Comparative studies on the performance of a roadheader, impact hammer and drilling and blasting method in the excavation of metro station tunnels in Istanbul”. In: *Tunnelling and Underground Space Technology* 25.2 (2010), pp. 181–187.

[113] Bilgin, N., Yazici, S., and Eskikaya, S. “A model to predict the performance of roadheaders and impact hammers in tunnel drivages”. In: *ISRM International Symposium-EUROCK 96* (1996).

[114] Bilgin, N. et al. “Cutting Performance of Jack Hammers and Roadheaders in Istanbul Metro Drivages”. In: *World Tunnel Congress* 97.1 (1997), pp. 455–460.

[115] Bilgin, N., Dincer, T., and Copur, H. “The performance prediction of impact hammers from Schmidt hammer rebound values in Istanbul metro tunnel drivages”. In: *Tunnelling and Underground Space Technology* 17 (2002), pp. 237–247. ISSN: 0886-7798.

[116] Wimmer. *Hydraulikhämmer*. 2023. URL: https://www.wimmer.info/de/produkte/hydraulikhaemmer/ (visited on 04/07/2023).

[117] Kunze, G., Göhring, H., and Jacob, K. *Baumaschinen, Erdbau- und Tagebaumaschinen*. 1st ed. Wiesbaden: Springer Fachmedien Wiesbaden, 2002. ISBN: 978-3-528-06628-4. DOI: 10.1007/978-3-663-09352-7.

[118] Kruusmaa, M. and Godon, S. *ROBOMINERS deliverable D1.2: New bio-inspired locomotion strategies concepts for mining environments*. Ed. by ROBOMINERS Consortium. 2020.

[119] MacAllister Rentals. *Track vs Wheeled Equipment: Which Type of Machine Should I Rent?* 2017. URL: https://www.macallisterrentals.com/track-vs-wheeled-equipment-type-machine-rent/ (visited on 09/14/2023).

[120] Cole, B. N. "Inquiry into Amphibious Screw Traction". In: *Proceedings of the Institution of Mechanical Engineers*. Vol. 175. 1. 1961, pp. 919–940. DOI: 10.1243/PIME_PROC_1961_175_060_02.

[121] Momber, A. "The kinetic energy of wear particles generated by abrasive–water-jet erosion". In: *Journal of Materials Processing Technology* 83.1-3 (1998), pp. 121–126.

[122] Lu, Y. et al. "Hard rock drilling technique with abrasive water jet assistance". In: *International Journal of Rock Mechanics and Mining Sciences* 60 (2013), pp. 47–56.

[123] Oh, T.-M., Cho, G.-C., and Ji, I.-T. "Effects of free surface using waterjet cutting for rock blasting excavation". In: *Journal of Korean Tunnelling and Underground Space Association* 15.1 (2013), pp. 49–57.

[124] Cho, G.-C. and Oh, T.-M. *Excavation system using a water jet, and excavation method using the same*. US Patent No. 9,140,122. 2015.

[125] Hood, M., Nordlund, R., and Thimons, E. "A study of rock erosion using high-pressure water jets". In: *International Journal of Rock Mechanics and Mining Sciences & Geomechanics Abstracts* 27.2 (1990), pp. 77–86.

[126] Momber, A. and Kovacevic, R. "Test parameter analysis in abrasive water jet cutting of rocklike materials". In: *International Journal of Rock Mechanics and Mining Sciences* 34.1 (1997), pp. 17–25.

[127] Agus, M. et al. "Optimization of abrasive-workpiece matching". In: *BHR group conference series publication*. Vol. 41. 2000, pp. 171–182.

[128] Karakurt, I., Aydin, G., and Aydiner, K. "An experimental study on the depth of cut of granite in abrasive waterjet cutting". In: *Materials and Manufacturing Processes* 27.5 (2012), pp. 538–544.

[129] Singh, M. M. and Huck, P. J. "Correlation of rock properties to damage effected by water jet". In: *Proceedings of the 12th US Symposium on Rock Mechanics (USRMS)*. 1970.

[130] Summers, D. A. "Water Jet Cutting Related to Jet & Rock Properties". In: *Proceedings of the 14th US Symposium on Rock Mechanics (USRMS)*. 1972.

[131] Oh, T.-M. and Cho, G.-C. "Characterization of effective parameters in abrasive waterjet rock cutting". In: *Rock mechanics and rock engineering* 47 (2014), pp. 745–756.

[132] Oh, T.-M. and Cho, G.-C. "Rock Cutting Depth Model Based on Kinetic Energy of Abrasive Waterjet". In: *Rock Mechanics and Rock Engineering* 49.3 (2016), pp. 1059–1072. ISSN: 0723-2632. DOI: 10.1007/s00603-015-0778-y.

[133] El-Domiaty, A. and Abdel-Rahman, A. "Fracture mechanics-based model of abrasive waterjet cutting for brittle materials". In: *The international journal of advanced manufacturing technology* 13 (1997), pp. 172–181.

[134] Wang, J. "Predictive depth of jet penetration models for abrasive waterjet cutting of alumina ceramics". In: *International Journal of Mechanical Sciences* 49.3 (2007), pp. 306–316.

[135] Aydin, G., Karakurt, I., and Aydiner, K. "Prediction of the cut depth of granitic rocks machined by abrasive waterjet (AWJ)". In: *Rock mechanics and rock engineering* 46 (2013), pp. 1223–1235.

[136] Hagan, P. "The cuttability of rock using a high pressure water jet". In: *Proceedings of the Western Australian conference on mining geomechanics*. 1992, pp. 8–10.

[137] Narimani Dehnavi, R. *A DEM numerical simulation approach to investigate the feasibility of hydrofracturing as excavation technology for a small-scale mining robot*. Ed. by Chair of mining engineering and mineral economics. Leoben, Austria, 2021.

[138] Collins, B. D. et al. *Rock strength properties of granitic rocks in Yosemite Valley, Yosemite National Park, California*. 2020. DOI: 10.3133/ds1126.

[139] Kirl, M. *UCS and BTS Test Report*. Ed. by Chair of mining engineering and mineral economics. Leoben, Austria, 2022.

[140] Krainz, J. and Marek, M. *Cerchar Test Report*. Ed. by Chair of Subsurface Engineering. Leoben, 2022.

[141] Li, C., Kristjansson, G., and Høien, A. "Critical embedment length and bond strength of fully encapsulated rebar rockbolts". In: *Tunnelling and Underground Space Technology* 59 (2016), pp. 16–23. DOI: 10.1016/j.tust.2016.06.007.

[142] Dagrain, F. *Mechanical characterization a rock sample of Estonian bituminous shale*. Ed. by Stone Assistance SPRL. Viemme, Belgium., 2021.

[143] Vorona, M. “Optimierung des Schneidprozesses und Prognose der relevanten Arbeitsgrößen bei der Gesteinszerstörung unter Berücksichtigung des Meißelverschleißes”. PhD thesis. TU Bergakademie Freiberg, 2012.

[144] Shao, W. “A study of rock cutting with point attack picks”. PhD thesis. University of Queensland, School of Mechanical and Mining Engineering, 2016.

[145] Grafe, B. “Cutting Force Component-Based Rock Differentiation Utilising Machine Learning”. PhD thesis. TU Bergakademie Freiberg, 2022.

[146] Sun, Y. and Li, X. “Slant angle and its influence on rock cutting performance”. In: *Advances in Civil Engineering* (2018).

[147] Sobek, P. “Ermitteln Sie anhand der internationalen Fachliteratur sowie aus Schnittversuchen mit Rundschaftmeisseln verschiedenen Typs die für die Einsätze von Ausleger-Teilschnittmaschinen innerhalb des Erzbergbaues der DDR günstigste Meisselgeometrie”. PhD thesis. TU Bergakademie Freiberg, 1987.

[148] Keller, A. “Prognose von Aktivierungsparametern für die maschinelle Gewinnung hochfester Gesteine”. PhD thesis. TU Bergakademie Freiberg, 2020.

[149] Quang, P. V. “Beitrag zur Staubentstehung und -verhütung bei spanender Gesteinszerstörung”. PhD thesis. TU Bergakademie Freiberg, 2007.

[150] Zhou, W. et al. “The effect of geometries and cutting parameters of conical pick on the characteristics of dust generation: Experimental investigation and theoretical exploration”. In: *Fuel Processing Technology* 198 (2020), p. 12.

[151] Roxborough, F. F., King, P., and Pedrocelli, E. J. “Tests on the cutting performance of a continuous miner”. In: *Journal of the South African Institute of Mining and Metallurgy* (1981).

[152] Bilgin, N. et al. “The performance of a roadheader in high strength rock formations in Küçüksu tunnel”. In: *Materiały konferencyjne. 31th ITA-AITES World Tunnel Congress, Instanbul*. 2005.

[153] Kuidong, G., Du Changlong, J. H., and Songyong, L. “A theoretical model for predicting the Peak Cutting Force of conical picks”. In: *Frattura ed Integrità Strutturale: Annals* (2014).

[154] Wang, Z. et al. “Investigation of the Influence of Cutting Parameters on Conical Pick Cutting Performance and Rock Damage”. In: *Machines* 10.11 (2022), p. 17. DOI: 10.3390/machines10111034.

[155] Duan, M. et al. “Peak Cutting Force Estimation of Improved Projection Profile Method for Rock Fracturing Capacity Prediction with High Lithological Tolerance”. In: *Coatings* 12.9 (2022), p. 17. DOI: 10.3390/coatings12091306.

[156] Yasar, S. “A general semi-theoretical model for conical picks”. In: *Rock Mechanics and Rock Engineering* 53.6 (2020), pp. 2557–2579. DOI: 10.1007/s00603-020-02078-3.

[157] Rojek, J. et al. “Discrete Element Modelling of Rock Cutting”. In: *Computer Methods in Material Science*. Vol. 25. 2011, pp. 247–267. ISBN: 978-94-007-0734-4. DOI: 10.1007/978-94-007-0735-1_10.

[158] Tiryaki, B., Ayhan, M., and Hekimoglu, O. Z. “A new computer program for cutting head design of roadheaders and drum shearers”. In: *Proceedings of the 17th International Mining Congress and Exhibition of Turkey–IMCET*. 2001, pp. 655–662.

[159] Li, X. et al. “Study on roadheader cutting load at different properties of coal and rock”. In: *The Scientific World Journal* (2013), p. 8. DOI: 10.1155/2013/624512.

[160] Liu, Z. et al. “Experimental and numerical investigation of roadheader for breaking rock containing predrill holes”. In: *Energy Science & Engineering* 8.7 (2020), pp. 2511–2526. DOI: 10.1002/ese3.682.

[161] Yasar, S. and Yilmaz, A. O. “Drag pick cutting tests: A comparison between experimental and theoretical results”. In: *Journal of Rock Mechanics and Geotechnical Engineering* 10.5 (2018), pp. 893–906. ISSN: 1674-7755. DOI: 10.1016/j.jrmge.2018.02.007.

[162] Lundberg, B. “Penetration of rock by conical indenters”. In: *International Journal of Rock Mechanics and Mining Sciences & Geomechanics Abstracts* 11.6 (1974), pp. 209–214. ISSN: 0148-9062. DOI: 10.1016/0148-9062(74)90127-2.

[163] Evans, I. “A theory of the cutting force for point-attack picks”. In: *International Journal of Mining Engineering* 2.1 (1984), pp. 63–71. ISSN: 0263-4546. DOI: 10.1007/BF00880858.

[164] Goktan, R. M. “A suggested improvement on Evans’s cutting theory for conical bits”. In: *Proceedings of the Fourth International Symposium on Mine Mechanization and Automation*. Vol. 1. 1997, pp. 57–61.

[165] Goktan, R. M. and Gunes, N. "A semi-empirical approach to cutting force prediction for point-attack picks". In: *Journal of the South African Institute of Mining and Metallurgy* 105.4 (2005), pp. 257–263.

[166] Pajer, J., Pfeifer, M., and Kurth, F. *Tagebaugroßgeräte und Universalbagger*. Verlag Technik, 1971.

[167] Doofor Inc. 2023. URL: https://doofor.com/ (visited on 09/14/2023).

[168] The Water Hydraulics Company. URL: https://www.waterhydraulics.co.uk/ (visited on 09/14/2023).

[169] Restner, U. and Plinninger, R. J. "Rock Mechanical Aspects of Roadheader Excavation". In: *Proceedings of the ISRM Regional Symposium*. 2015. ISBN: 978-3-9503898-1-4.

[170] ASTM International. *ASTM D7012-14, Standard Test Methods for Compressive Strength and Elastic Moduli of Intact Rock Core Specimens under Varying States of Stress and Temperatures*. Tech. rep. 2017, p. 9. DOI: 10.1520/D7012-14E01.

[171] Sifferlinger, N. A. *Excavation Engineering - Mechanical Excavation*. Ed. by Chair of mining engineering and mineral economics. Leoben, 2022.

[172] ASTM International. *ASTM D3967-95a, Standard Test Method for Splitting Tensile Strength of Intact Rock Core Specimens*. Tech. rep. 2001, p. 3. DOI: 10.1520/D3967-16.

[173] Skawina, B. "Comparison of mechanical excavation and drilling: A discrete event simulation approach". MA thesis. 2013, p. 72.

[174] Rostami, J. and Hambley, D. F. "Blasthole Drilling". In: *SME Mining Engineering Handbook*. Ed. by P. Darling. Society for Mining, Metallurgy, and Exploration, Inc. (SME), 2011, pp. 435–441. ISBN: 978-0-87335-2642.

[175] Marshall, T. C. "A comparison between hydraulic and pneumatic rockdrills". In: *Journal of the South African Institute of Mining and Metallurgy* (1975), pp. 181–184.

[176] Song, C.-H. et al. "Development of lab-scale rock drill apparatus for testing performance of a drill bit". In: *International Journal of Precision Engineering and Manufacturing* 16.7 (2015), pp. 1405–1414. ISSN: 2234-7593. DOI: 10.1007/s12541-015-0185-z.

[177] Bruce, D. A., Lyon, R., and Swartling, S. "The history of down-the-hole drilling and the use of water-powered hammers". In: *Association of State Dam Safety Officials Annual Conference, Providence, RI, September* (2013), pp. 8–12.

[178] Drüppel, E. "Entwicklung eines Konzeptes für die schneidende Gewinnung im Salzstein". PhD thesis. Technische Hochschule Aachen, 2010.

[179] Sandvik Mining and Rock Technology. 2023. URL: https://www.rocktechnology.sandvik/en/ (visited on 09/14/2023).

[180] Vogt, D. "A review of rock cutting for underground mining: past, present, and future". In: *Journal of the Southern African Institute of Mining and Metallurgy* 116 (2016), pp. 1011–1026. DOI: 10.17159/2411-9717/2016/v116n11a3.

[181] Restner, U., Pichler, J., and Reumueller, B. "New technologies extend the range of applications of roadheaders". In: *Symposium on Innovations in Tunnelling, Swiss Federal Institute of Technology Zurich* (2007).

[182] The Pipe Jacking Association. 2022. URL: http://www.pipejacking.org/ (visited on 09/14/2023).

[183] Jiangtu. *What is Hydraulic Breaker and How Does It Work?* 2021. URL: https://jtexcavator.com/blog/what-is-hydraulic-breaker-and-how-does-it-work.html (visited on 09/14/2023).

[184] Yamamoto. 2023. URL: http://www.yamamotorocksplitter.com/products/ (visited on 09/14/2023).

[185] Paraszczak, J. and Planeta, S. "Feasibility of narrow vein mining using a mechanical rock splitter". In: *Mine Planning and Equipment Selection* 1 (2003), pp. 415–422.

[186] Anderson, S. J. and Swanson, D. E. *Capability Evaluation of the Radial-axial Splitter*. U.S. Department of the Interior, Bureau of Mines, 1987.

[187] McQueen, A., Suedel, B., and Wilkens, J. "Review of the Adverse Biological Effects of Dredging-induced Underwater Sounds". In: *WEDA J Dredging* 17.1 (2019), pp. 1–28.

[188] Royal IHC. *Cutter heads*. 2023. URL: https://www.royalihc.com/dredging/dredging-equipment/cutter-heads (visited on 09/14/2023).

[189] Thyssenkrupp. *Barracuda: Der Kompakt-Schaufelradbagger*. 2023. URL: https://www.thyssenkrupp-industrial-solutions.com/de/produkte-und-services/mining-systems/schaufelradbagger/barracuda (visited on 09/14/2023).

[190] Noen, A. *Bucket wheel excavator (K 100) - NOEN, a.s.* 2013. URL: https://www.noen.cz/en/reference/kr400lk-bucket-wheel-excavator-k-100/ (visited on 09/14/2023).

[191] Rasti, A., Adarmanabadi, H. R., and Sahlabadi, M. R. "Effects of controllable and uncontrollable parameters on diamond wire cutting performance using statistical analysis: a case study". In: *Rudarsko-geološko-naftni zbornik* 36.4 (2021), pp. 21–32. DOI: 10.17794/rgn.2021.4.3.

[192] BFT Pumps. *General Waterjet Cutting Information*. 2022. URL: https://en.bft-pumps.com/waterjet-cutting/general/ (visited on 09/14/2023).

[193] Ohlsson, L. "The Theory and Practice of Abrasive Water Jet Cutting". PhD thesis. Luleå tekniska universitet, 1995.

[194] Ciccu, R. *Water jet in rock and mineral engineering*. Tech. rep. Department of Mining and Minerals Engineering University of Cagliari. Cagliari, Italy, 2019.

[195] Gauert, C. et al. "A progress report on ultra-high-pressure waterjet cutting underground: the future of narrow reef gold and PGE mining". In: *Journal of the South African Institute of Mining and Metallurgy* 113 (2013), pp. 441–448.

[196] Henriques, T. V. L. D. *Rock cutting with high-pressure water jets*.

[197] Lopez-Pacheco, A. *Jet boring takes off at Cigar Lake*. 2023. URL: https://magazine.cim.org/en/technology/jet-boring-takes-off-at-cigar-lake/ (visited on 09/14/2023).

[198] Cameco. *Mining Methods*. 2023. URL: https://www.cameco.com/businesses/mining-methods (visited on 09/14/2023).

[199] Guo, B., Liu, X., and Tan, X. "Hydraulic Fracturing". In: *Petroleum Production Engineering*. Ed. by B. Guo, X. Liu, and X. Tan. Elsevier, 2017, pp. 389–501. ISBN: 978-0-7506-8270-1. DOI: 10.1016/B978-0-12-809374-0.00014-3.

[200] Kollé, J. J. and Fort, J. A. "Application of dynamic rock fracture mechanics to non-explosive excavation". In: *Proceedings of the 29th U.S. Symposium on Rock Mechanics (USRMS)*. 1988.

[201] Cuderman, J. F. et al. *Multiple fracturing technique for enhanced gas recovery*. Tech. rep. Sandia National Labs., Albuquerque, NM (USA), 1981.

[202] Cuderman, J. F. and Northrop, D. A. "A Propellant-Based Technology for Multiple-Fracturing Wellbores To Enhance Gas Recovery: Application and Results in Devonian Shale". In: *SPE Production Engineering* 1.02 (1986), pp. 97–103. ISSN: 0885-9221. DOI: 10.2118/12838-PA.

[203] Schmidt, R. A., Warpinski, N. R., and Cooper, P. W. "In Situ Evaluation Of Several Tailored-Pulse Well-Shooting Concepts". In: *SPE Unconventional Gas Recovery Symposium*. SPE, 1980. DOI: 10.2118/8934-ms.

[204] Swift, R. P. and Kusubov, A. S. *Technique for studying multiple fractures produced at intermediate loading rates*. Tech. rep. California Univ., Livermore (USA). Lawrence Livermore Lab, 1980.

[205] Kolle, J. J. and Fort, J. A. "Application of dynamic rock fracture mechanics to non-explosive excavation". In: *Proceedings of the 29th U.S. Symposium on Rock Mechanics (USRMS)*. 1988.

[206] Frangakis, T. "The development and testing of a water-pulse rock breaking system". In: *5th International Symposium on Mine Mechanization and Automation*. 1999.

[207] Nantel, J. and Kitzinger, F. "Plasma Blasting Techniques". In: *Proceedings of the Third International Symposium on Rock Fragmentation by Blasting*. 1990, pp. 79–82.

[208] Nantel, J. *The status of plasma blasting technology*. Tech. rep. CAMIRO Mining Division, 2006.

[209] Liu, S., Li, H., and Chang, H. "Drilling Performance of Rock Drill by High-Pressure Water Jet under Different Configuration Modes". In: *Shock and Vibration* (2017), pp. 1–14. ISSN: 1070-9622. DOI: 10.1155/2017/5413823.

[210] Kollé, J. J. "A comparison of water jet, abrasive jet and rotary diamond drilling in hard rock". In: *Tempress Technologies Inc* (1999), pp. 1–8.

[211] Liu, S. et al. "Experimental Investigation of Hard Rock Breaking Using a Conical Pick Assisted by Abrasive Water Jet". In: *Rock Mechanics and Rock Engineering* 53.9 (2020), pp. 4221–4230. ISSN: 0723-2632. DOI: 10.1007/s00603-020-02168-2.

[212] Songyong, L., Junfeng, C., and Xiaohui, L. "Rock Breaking by Conical Pick Assisted with High Pressure Water Jet". In: *Advances in Mechanical Engineering* 6 (2014), p. 868041. ISSN: 1687-8140. DOI: 10.1155/2014/868041.

[213] Ciccu, R. and Grosso, B. “Improvement of Disc Cutter Performance by Water Jet Assistance”. In: *Rock Mechanics and Rock Engineering* 47.2 (2014), pp. 733–744. ISSN: 0723-2632. DOI: 10.1007/s00603-013-0433-4.

[214] Ciccu, R. et al. “Rock disintegration using water jet-assisted diamond tools”. In: *Proceedings of 10th American water jet conference*. 1999, pp. 14–17.

[215] Kotwica, K. “Hard Rock Mining Using Disk Tools Supported by High-Pressure Water Jets in the Aspect of Reducing Energy Consumption”. In: *Energies* 14 (2021), p. 2595. DOI: 10.3390/en14092595.

[216] Baumann, L. “Versuche mit Hochdruckwasserstrahlen an einer Tunnelbohrmaschine”. In: *Glückauf* 116 (1980), pp. 1113–1117.

[217] Hartlieb, P. and Grafe, B. “Experimental Study on Microwave Assisted Hard Rock Cutting of Granite”. In: *BHM Berg- und Hüttenmännische Monatshefte* 2 (2017), pp. 77–81. ISSN: 0005-8912. DOI: 10.1007/s00501-016-0569-0.

[218] Whittles, D., Kingman, S., and Reddish, D. “Application of numerical modelling for prediction of the influence of power density on microwave-assisted breakage”. In: *International Journal of Mineral Processing* 68.1-4 (2003), pp. 71–91. ISSN: 0301-7516. DOI: 10.1016/s0301-7516(02)00049-2.

A Appendix - State of the art

A.1 Excavation principles

Parts of the content have already been documented in [15]. To understand the principles of rock fragmentation, it is required to summarize common characteristics which describe the mechanical and physical behaviour of rock. The rock strength defines the resistance to failure under load and it is a mechanical property which can be separated into uniaxial compressive strength (UCS) and brazilian tensile strength (BTS). Combined with the cuttability of the rock, which includes the excavation operation and the tool characteristics, the rock mass rating (RMR) can be assessed. [169]

General mechanical properties, classified by [26], are:

- Strength.
  - Resistance to fail under compressive, tensile or shear stress.
  - Effect of confining pressure, temperature, strain rates, fluid pressure and specimen size on strength properties.
- Deformability.
  - Resistance to change of shape or volume.
  - Elastic and thermal expansion constants.
- Hardness.
  - Resistance to a local (surface) failure by indentation or scratching.
- Fracture toughness.
  - Resistance to fracture propagation.
- Coefficient of friction.
  - Resistance to sliding of two bodies with planar surfaces in contact.

- Crushability and millability.
  - Resistance to comminution (reduction of a substance to a powder).
- Extractability.
  - Resistance to fragmentation and disruption by different extraction processes and ability of rock to induce wear on mechanical tools.

The uniaxial compressive strength is a general rock characteristic and it is the most applied parameter for describing the rock strength in material extraction processes [24].

Figure A.1 shows a standard UCS test sample and the schematic UCS test. Test samples are usually cylindrical objects with same height as diameter and a minimum of 5 tests is recommended to obtain reliable results. Within the test, a gradually increasing load onto the specimen is applied until the sample fails.

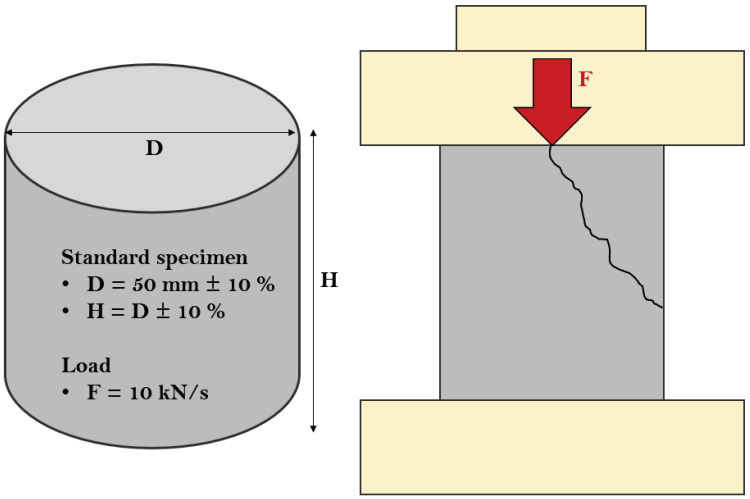

Figure A.1: Standardized UCS Test

With the resulting load-deformation graph, the UCS value σ_c of the material can be calculated (Equation A.1), in which F_{max} is the failure load and A is the cross-sectional area of the test sample [170]. Other material characteristics such as the strain ϵ and the fracture energy W_f can be determined [171].

$$\sigma_c = \frac{F_{max}}{A} \tag{A.1}$$

The tensile strength σ_t of a rock is mainly obtained through an indirect material test. The brazilian tensile strength (BTS) test applies a load perpendicular onto a

circular cross-section of a cylindrical probe until the sample fails indirectly under tensile stress, see Figure A.2. [24, 171]

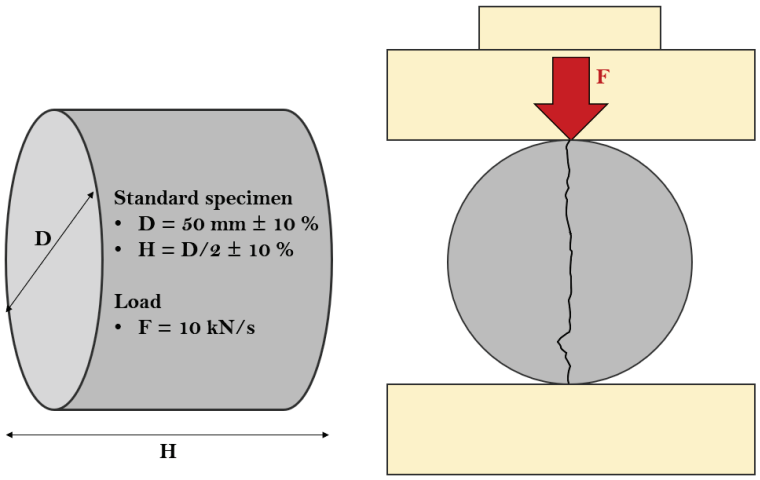

Figure A.2: Standardized BTS Test

Equation A.2 shows the calculation of the tensile strength σ_t, where F_{max} is the maximum applied load, H the length and D the diameter of the sample [172].

$$\sigma_t = \frac{2F_{max}}{\pi HD} \tag{A.2}$$

The abrasivity of a rock is described by the cerchar abrasivity index (CAI) and used for predicting and assessing the grade of wear of mechanical tools. The CAI is measured by pulling a 90° conical steel pin 1 cm across the untouched surface of a test sample in 1 s (Figure A.3). The CAI equals ten times the diameter of the worn tip. Lower CAI means generally less abrasive and less wear. [24, 171]

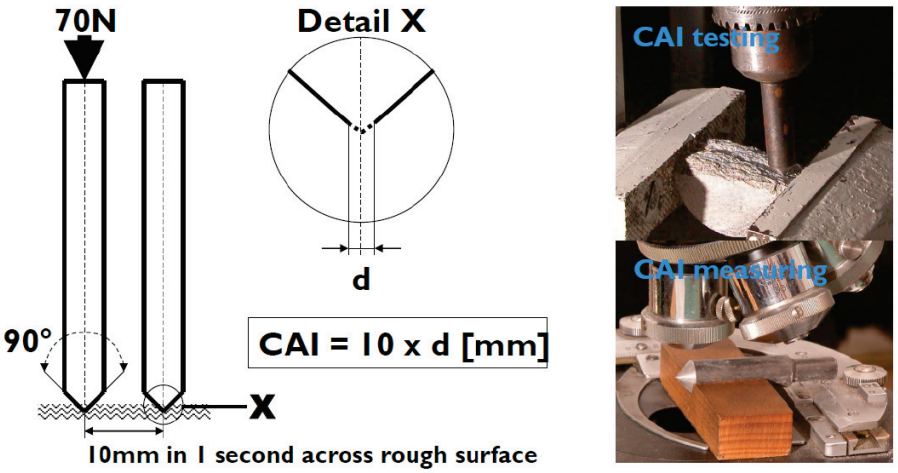

Figure A.3: Standardized CAI Test [171]

For mechanical excavation tools, a relation between UCS and CAI can be stated to provide regions of economical cuttability, see Figure A.4. Rock within the economic area is supposed to be able to be excavated economically without excessive effort and wear.

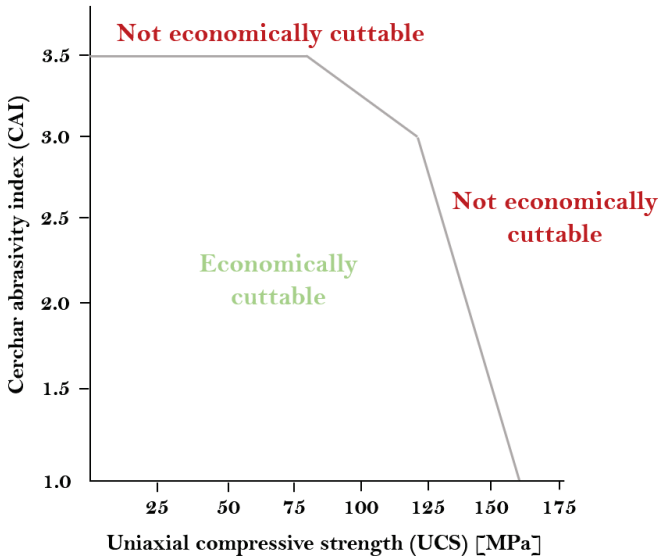

Figure A.4: Definition of economical cuttability (after [171])

A.2 Mechanical excavation

A.2.1 Rock drilling

Rock drilling on its own is not a mechanical excavation method used to excavate rock, but it is an important part in a drill and blast operation for drilling the boreholes and also used for exploration tasks [25] - as well as in surface (Figure A.5 left) and underground (Figure A.5 right) operations.

Basically, there are three main drilling technologies which all take us of similar parts (see Figure A.6) [173]:

- Tophammer drilling.
- Rotary-percussive (down-the-hole-hammer) drilling.
- Rotary drilling.

The primary energy input source can either be hydraulic, electric or pneumatic. A piston inside the drill is used as a prime mover and converts the energy from the input source to mechanical energy for actuating the entire drill system. Shank

adapter and rod transmit the rotary-percussive or pure rotary motion to a drill bit which penetrates the rock.

Figure A.5: Surface drilling rig (left) and underground drill jumbo (right)
© *Epiroc* [85]

Depending on the position of the piston – either it is on the top or the bottom of the drill string – the drilling tool is called tophammer (Figure A.6, left) or down-the-hole-hammer (Figure A.6, center) respectively. Rotary drilling (Figure A.6, right) only transmits torque throughout the drill string. [174–176]

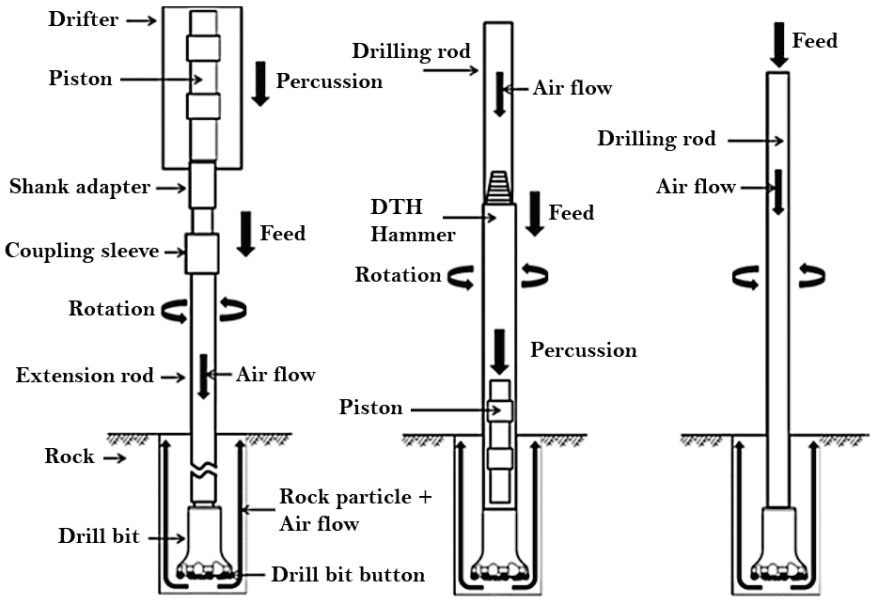

Figure A.6: Tophammer drilling (left), rotary-percussive (down-the-hole-hammer) drilling (center) and rotary drilling (right) [176]

Drilling into hard rock rock with a uniaxial compressive strengths of up to 300 MPa is possible [174].

Tophammer drilling

The piston in tophammer drilling is placed at the top of the drill string and accelerates inside the rock drill and strikes the drill rod in a percussive motion. This percussive motion is usually generated by a hydraulically or pneumatically actuated piston. This creates a stress wave throughout the entire drill string until the drill bit hits the rock. [174]

Combined with a rotatory motion, the drill penetrates into the rock. The diameter of such drill holes can go up to 150 mm. Advantage of this version of a rock drill is the simple access to the components, because the main parts which need to be maintained are on the top. On the other side, if the borehole is getting deeper, the distance between the hammer and the drill bit is getting larger which results in a decrease of efficiency. [176]
An exemplary tophammer without the drill rod and drill bit can be seen in Figure A.7.

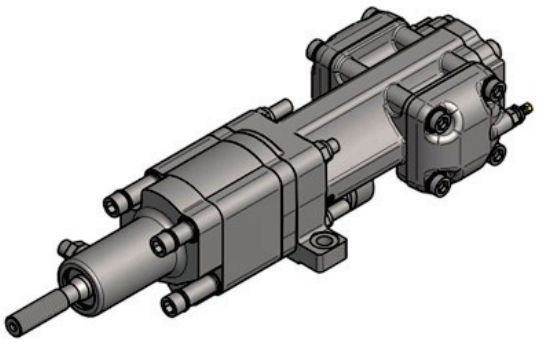

Figure A.7: Tophammer drill © *Doofor* [167]

Rotary-percussive drilling (Down-the-hole-hammer drilling)

Rotary-percussive drilling or down-the-hole (hammer) - short DTH - drilling, is a rock drilling method where the piston is directly behind the drill bit and not on top of the drill string (Figure A.8). The drill rod only transmits the rotatory motion. The piston is either actuated oil-hydraulically, pneumatically or in special applications water-hydraulically. [174]

Benefit of this assembly is a much higher efficiency compared to tophammer drilling due to the short distance between the piston and the drill bit. Disadvantage due to that design is that in case of maintenance the entire drill string needs to be pulled out or in worst case the hammer is left behind inside the drill hole. [174]

Figure A.8: Rotary-percussive drill [174]

In Figure A.9, a water-hydraulically driven rotary-percussive drill is shown.

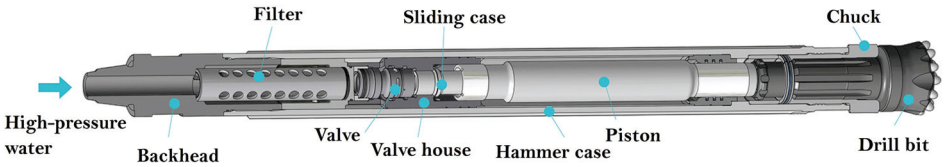

Figure A.9: Water-hydraulic rotary-percussive drill © *LKAB Wassara* [87]

Rotary drilling

Large diameter drill holes are typically made by rotary drilling systems. A motor (electric or hydraulic) applies a torque on the top of the drill string. A tricone or drag bit (Figure A.10) is mounted on the end of the drill string. [174, 176]

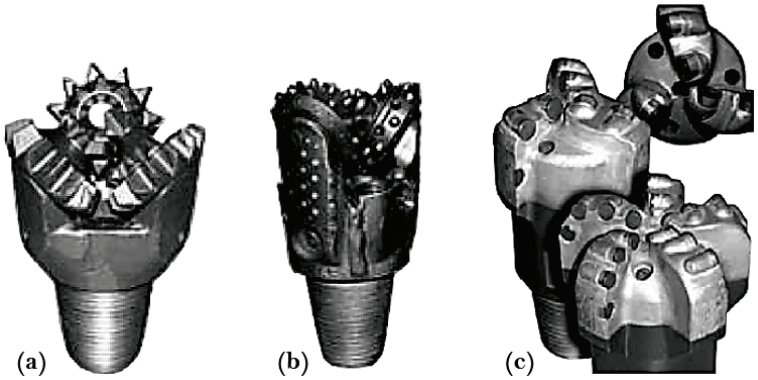

Figure A.10: Types of rotary drill bits: (a) Milled-tooth tricone bit, (b) TC insert tricone bit and (c) PDC insert drag bit. [174]

In [177], *Bruce* made the basic statements:

- Tophammer drilling is economic in rocks of all types with drill bit diameters up to about 12 cm. It has lower feed force and torque requirements and typically moderate flush pressure and flow demands (both for air and water).
- Rotary-percussive drilling is typically preferred in medium to hard rock materials for holes with diameter above 10 cm. High pressure and high volume flushing media are required, whereas feed and torque requirements are relatively low.

- Rotary drilling is economic within various hole diameters in soft to medium hard rocks. This method requires high bit load (feed or thrust force) and high rotary torque.

Applicability to a small-scale mining robot
Drilling in general creates low reaction forces – even at high rock strengths - compared to other mechanical excavation systems, but it is not economic to use it as a standalone excavation unit, because of its low production rate, except for exploration purposes and material analysis. Due to the fact that drilling is part of drill and blast and often an auxiliary tool for other excavation technologies (e.g. radial-axial splitting and hydrofracturing), the applicability of rock drilling systems has been investigated and the findings are documented in Section 3.1.1.

A.2.2 Part-face cutting

Part-face cutting machines are mining machines which excavate the material continuously in layers. Two part-face cutting machine types - roadheader and continuous miner - are presented in this chapter.

Roadheader
Roadheaders are part-face cutting machines used in underground mining or tunnelling scenarios, where the favourable ground conditions provide advantages over drill and blast. Those machines carry a rotating cutter head mounted on a boom in the very front which is excavating the material (Figure A.11). [178]

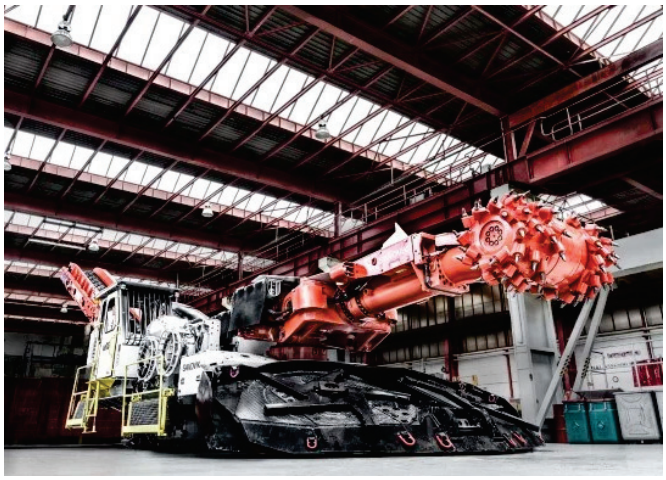

Figure A.11: Transversal roadheader © *Sandvik* [179]

They can be classified in transversal (radial) and longitudinal (axial) roadheaders, depending on their respective cutter head design (Figure A.12 and Figure A.13).

In transversal roadheaders, the cutter head axis is perpendicular to the boom that the reaction forces act in the direction of the cutting arm. As a result, radial roadheaders have a lower deadweight requirement than axial roadheaders. In the case of a longitudinal roadheader, the cutter head rotates in the extension of the cutting boom and therefore generates forces that act perpendicular to the cutting arm. If one relates that with the long lever arm, the mass of the cutter head has a negative effect on the required mass of the roadheader. [29]

The excavation rate of a roadheader is depending on its size (mass), power and material to be excavated. Radial roadheaders with a transverse cutter head are mostly used for mining of rocks with UCS values of more than 90 MPa, but at maximum up to 120 MPa [24]. In some special applications, uniaxial compressive strengths up to 150 MPa could be excavated [22]. Axial roadheaders have good performances at soft to medium hard rock material and are popular machines in the coal and salt mining industry [178].

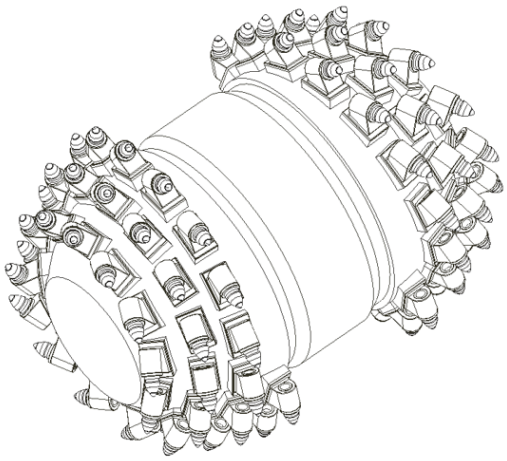

Figure A.12: Transversal (radial) cutter head

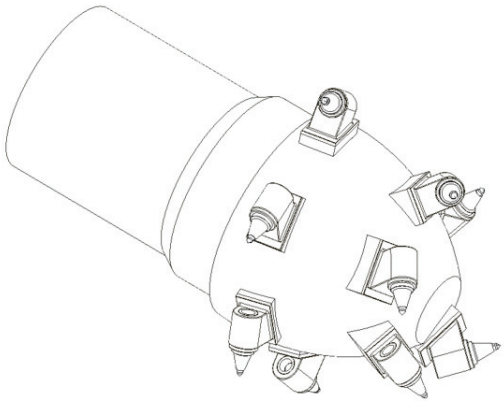

Figure A.13: Longitudinal (axial) cutter head

According to [24, 26] both roadheader types exhibit various advantages and disadvantages:

- The cutting direction of the cutter head has a major influence on the stability of the machine during the cutting process. Roadheaders with a transversal cutter head are more stable than roadheaders with a longitudinal cutter head with similar mass and power, because the direction of the cut is face-orientated.
- At transversal cutter heads, the greater part of the reaction force resulting from the cutting operation is towards the machine.
- Pick layout is easier on longitudinal cutter heads because cutting and slewing movement are in the same direction.
- Transversal roadheaders are less affected by inconsistent rock conditions and are able to cut harder rocks.
- Longitudinal roadheaders can be controlled more precisely and have a higher performance in profiling.

Continuous miner

A continuous miner (Figure A.14) is a machine with a single rotating cutting drum, moveable only in vertical direction, similar to a roadheader with a transversal cutter head, but without the ability to slew the drum in horizontal direction. The continuous miner is mainly used in coal, salt or potash mines and the entire width of the machine is covered by the drum. The geometry of the drum limits the machine to cutting a rectangular profile with approximately the same width as the drum [180]. To be able to manoeuvre the machine inside a tunnel, the cutting drum can be extended in width to excavate a marginal greater cross-section.

Figure A.14: Continuous Miner © *Sandvik* [179]

Comparing the cutting drum design, continuous miners are similar to roadheaders. They use drag bits or conical pick tools mounted on a rotating drum.

Conical pick tools

The conical pick tool (Figure A.15) is up to this date the most commonly applied rock cutting tool, besides disc cutters. The shape and dimension depend on the rock strength of the material to be excavated. [30]

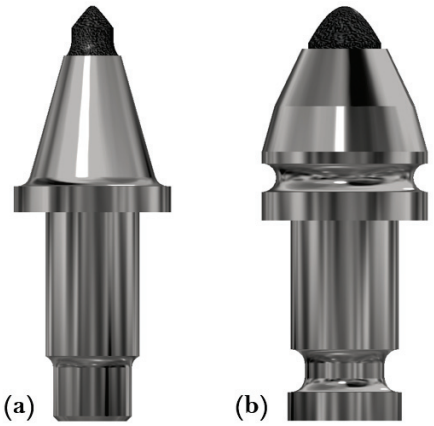

Figure A.15: Conical pick tool for: (a) Soft rock and (b) Hard rock.

The pick tools are fixed in a tool holder and are able to rotate about their axis to keep their sharpness. Highly abrasive rocks lead to excessive wear of the tools [31]. Hence, the specific pick consumption (SPC) is often used as performance indicator [181]. Specialized cooling systems and decreasing the cutting speed are measures for reducing the wear rate [89].

Applicability to a small-scale mining robot

A small-scale mining robot would afford a downscaled cutter head. Standard part-face cutting machines are already limited in terms of rock strength. Consequently, a robotic-miner equipped with a part-face cutter head would possess very restricted capabilities, although the advantages of the system could be beneficial for certain soft rock scenarios. Due to the low power and mass of a mining robot, an axial cutter head could be a potential production tool for the excavation of soft rock material. This is discussed in greater detail in Section 3.1.2 and Chapter 4.

A.2.3 Full-face cutting

Full-face cutting machines are cylindrical tunnelling machines with usually great lengths and are comprised of a rotating cutter head in the front, a cutter head support, a main frame, a thrust system including grippers and thrust cylinders and a material conveying system. These machines are using roller tools to penetrate into the rock face. [30]
Compared to conventional drill and blast, mechanical excavation has many advantages: Higher advance rates in sound rock mass conditions, less damage to the excavation profile, lower ventilation requirements and generally safer excavation conditions are some of the most prominent merits. Full-face cutting machines cut the entire cross-section of the rock face at the same time. Most of the full-face machines form a circular excavation [25]. Tunnel boring machines are capable of boring through a diverse range of geological conditions and rock with a uniaxial compressive strength above 200 MPa is possible [30].

Tunnel, shaft and raise boring machines as well as microtunnelling are the typical full-face cutting machines applied in underground mining. The part-face cutting machines engage only a part of the excavation tool, which provides the unique capability of creating non-circular excavation profiles. Comparing full-face cutting machines with other methods can be done by consideration of various criteria. Table A.1 contains some of the most important features for comparing full-face cutting with drill and blast and part-face cutting. [22, 24]

Table A.1: Individual comparison of full-face cutting with drill and blast and part-face cutting

Criterion	Compared to drill and blast	Compared to part-face cutting
Safety	Higher safety.	Generally safer.[1]
Selective excavation	Higher production/excavation rates in favourable ground conditions (higher economic benefits, early mining of high-grade ore, earlier job completion).	
Muck or mineral fragmentation quality and haulage	Uniform muck size (easy muck/excavated material haulage, no secondary breakage of large rock chunks, lower crushing and mineral processing costs).	Equivalent.[2]

Continuity of operation	Continuous operation (not periodic, conducive to automation, excavation-loading-ground supporting simultaneously).	Equivalent.[3]
Cuttable ground types	Not applicable in very hard and abrasive rocks.	Wider range of rock strength compared to part-face cutting.
Ground disturbance	Less overbreak, less scaling-support requirement, minimized maintenance, superior ground control in jointed/broken rocks.[4]	Equivalent.
Environment adaptability	More environment-friendly operation (no blast vibrations, no blasting ventilation required).	Equivalent.
Flexibility	Less flexibility on working conditions, very sensitive to ground conditions, limited opening cross-sectional area and shapes and usually not able to cut low turnoff radii, difficult adaptability to a working mine design.	
Mobility	Very large and heavy machines with low mobility from one face to another.[5]	
Maintenance	In hard and abrasive rocks, frequent maintenance of the machine might be necessary.	Less accessibility to the cutter head face and harder maintenance operation.
Capital cost	Higher initial/capital costs.	Equivalent or higher depending on the conditions.

[1]In unstable ground conditions, shields make part-face cutting machines as safe as full-face cutting machines.
[2]The capability of slurry transportation is an advantage in some full-face cutting machines.
[3]Part-face cutting machines can also be equipped with simultaneous support installation.
[4]It should be noted, that in deep underground excavation (overstressed hard rocks), blasting is deemed as an effective method for releasing a part of the stored energy in the rock mass. Thus, the ground disturbance caused by blasting could be a positive fact in deep mining conditions.
[5]There are unique technologies where the manoeuvrability of the full-face cutting machines is improved significantly. For instance, the boxhole boring machines (BBM) can excavate short length and small diameter openings in highly strengthened rocks.

The high specific energy requirements of these methods are obstacles on the way of their application in the industry. Among different full-face cutting machines, some are capable to be applied in small diameters: Tunnel boring machines (TBMs), pipe jacking and the boxhole boring machines (BBM). TBMs are manufactured in several types: Gripper TBMs, single shield TBMs, double shield TBMs, slurry TBMs and the most recent developed machines (mixshield and multimode TBMs). Each type can be selected based on the geological conditions of the ground. Except for gripper TBM types and double shield TBMs, other types of TBMs require segmental lining installation for providing the thrust forces and pushing the entire machine. Nevertheless, the segmental lining in stable grounds need not necessarily be a complete ring and depending on the cutting force requirements, the floor segment might suffice for providing the thrust forces. All of the TBMs work exclusively in man-entry mode, although the excavation diameter could go down to 1.5 m. [24]

The machines implementing the pipe jacking technology (Figure A.16) can be divided into two main categories of methods with the possibility of working in man-entry mode up to 4.8 m and the other category of non-man entry mode also called microtunnelling down to 0.4 m in diameter. With the slurry mode, almost all the ground conditions from soft ground, heterogeneous ground and hard rocks can be excavated using this method. Unlike tunnel boring machines, the pipe jacking methods take advantage of concrete pads inside entry shafts to produce the reaction forces for excavation, pushing the whole machine forward and compensating against the ground and water pressure on the tunnel face in unstable grounds. [24, 102]

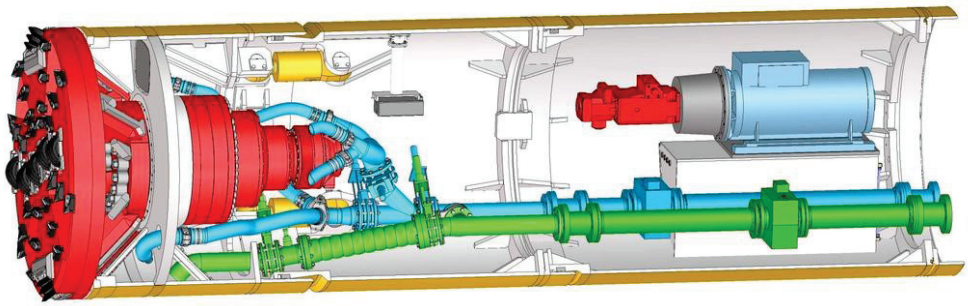

Figure A.16: Pipe jacking machine © *Herrenknecht* [107]

Another variation of pipe jacking is the direct pipe method which provided new possibilities of excavation in every geology. Indeed, the method combines the advantages of microtunnelling and horizontal directional drilling (HDD) technology. To have a clearer understanding, HDD is first introduced. A HDD rig is a special

steerable pipe installation method and can include fluid boring (excavation), ground displacement and reaming (enlargement of a pilot hole). Current powerful HDD technology (Figure A.17) enables long drives of up to 3 km. The operation consists of pilot boring followed by reaming to a larger diameter in the second step and the installation of pipes. It is especially suited for shallow depth pipe installations. An approximate 2 degrees of steering in the drill bits enables these machines to reach to a specific depth underground. The main advantage compared to pipe jacking is the capability of operating from surface without shaft excavation.

However, the diameter range is 0.2-2 m and it can only be applied in soft grounds and rocks which are relatively stable. Unlike HDD, the direct pipe method covers a wider range of geology. [24, 102]

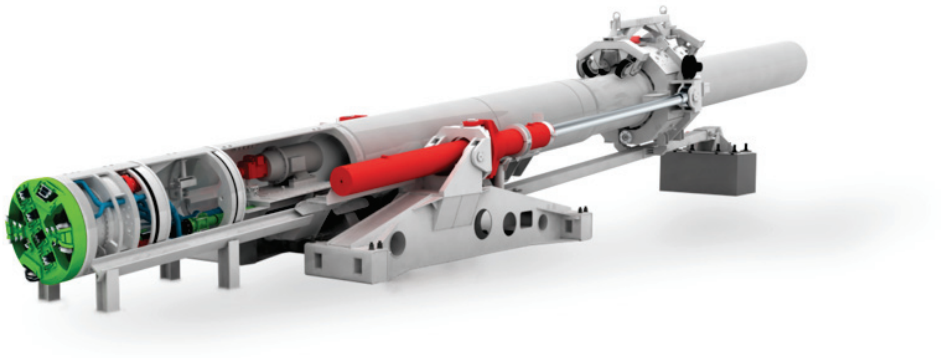

Figure A.17: Direct pipe technology © *Herrenknecht* [107]

Roller tools

Rock fracturing in full-face cutting operations is typically done with roller tools. Common types of roller tools applied in TBMs are single-disc, multi-disc or strawberry cutting tools (Figure A.18).

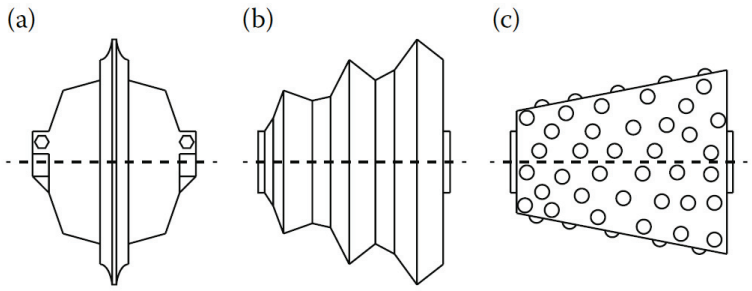

Figure A.18: Common types of roller tools: (a) Single-disc cutter, (b) Multi-disc cutter and (c) Strawberry cutter. [24]

Disc tools excavate rock through chipping by applying a normal and rolling force onto the rock, whereas strawberry cutters crush the rock [24].

Pipe jacking method

Pipe jacking is a trenchless technique for installation of underground pipelines (Figure A.19), ducts and culverts. Parallel to excavation taking place on the front of the machine, powerful hydraulic cylinders push especially designed pipes towards the tunnel face. The hydraulic jacks are situated at a drive shaft where pipes of different type (concrete, clay and steel) are continuously added to the whole pipe chain. Standard pipe diameters generally range from 150 to 2400 mm, or greater when required. [182]

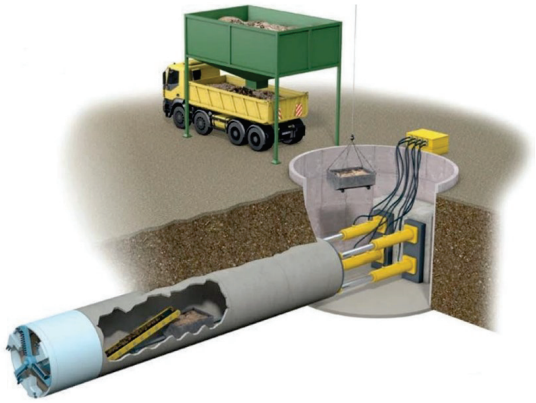

Figure A.19: Pipe jacking arrangement © *PipeJackingAssociation* [182]

The length of driving is not theoretically limited, practical considerations and economics impose restrictions on the maximum driving length. Up to several hundreds of meters of length can be provided from a single driving shaft depending on the ground condition and excavation method, but reaching greater lengths requires more jacking stations in between. Based on the ground condition, different mechanical excavation methods can be applied (Figure A.20). [182]

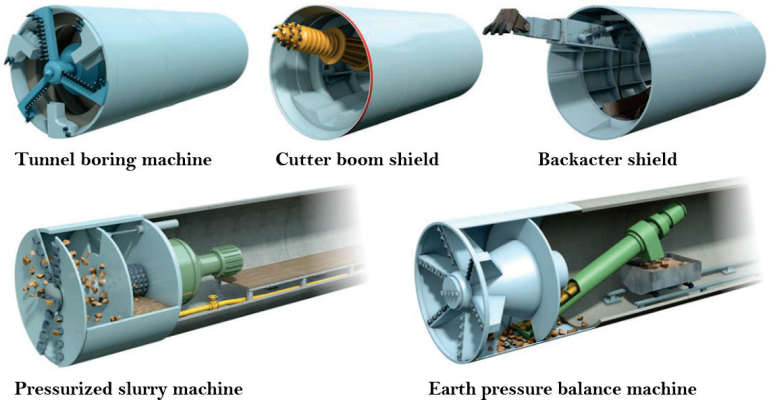

Figure A.20: Pipe jacking methods © *PipeJackingAssociation* [182]

The operation of a pipe jacking project requires thrust and reception pits at the beginning and ending of the project. The dimensions and construction of the pit depends on the specific requirements of a drive such as the excavation method and the economics as a key factor. Reaction forces of excavation and pushing the pipes forward is provided by a thrust wall. The thrust wall is almost always necessary, because the pipe jacking is done in shallow depth in cities, where weak grounds exists. A thrust ring is used to transfer the loads being applied by the thrust jacks around the circumference of a pipe. A reception pit is also required at the end of the driving path to remove the jacking shield. During the pipe jacking operation, a steerable shield maintains the accuracy of alignment. [24, 182]

Applicability to a small-scale mining robot
Full-face cutting machines, especially TBMs are profitable machines for tunnelling operations and exhibit good production rates. Applying this technology to a small robotic miner requires a very soft ground, in order to provide high enough thrust forces. A more detailed investigation on the applicability has been done and is described in Section 3.1.3.

A.2.4 Impact hammer

Impact hammers are mainly used for demolition tasks or scaling operations in the mining industry [24]. An impact hammer assembly can be seen in Figure A.21.

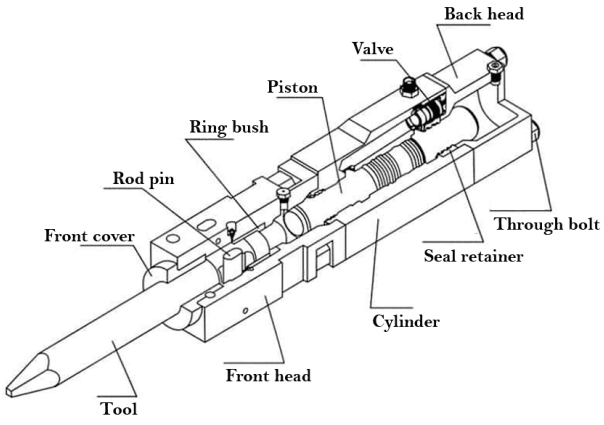

Figure A.21: Impact hammer © *JTExcavator* [183]

Hydraulic impact hammers are mostly mounted on excavators and smaller types are available in hand-held options. Their main applications in mining are breaking of boulders and scaling operations, but they have also been used for excavating metro tunnels [26]. Generally, two principles can be distinguished: Hydraulic splitting and hydraulic breaking.

Hydraulic splitting

Hydraulic rock splitting is a method to split softer materials by combining a high impulse stress wave with a wedge effect. A chisel is used to break the rock by working against the tensile strength of the material. A hydraulic rock splitter's operating principle can be seen in Figure A.22. [26, 184]

Figure A.22: Hydraulic rock splitter © *Yamamoto* [184]

Modern technologies are applying a counter wedge system in which a center wedge is pushed between those to extend them and break the rock [24].

Hydraulic breaking

Hydraulic breaking (Figure A.23) is a technique in secondary rock breaking and also called impact hammering due to its high frequency impacting work. This method requires higher impact energy and frequency compared to rock splitting. A proper down pressure and tool-rock contact are mandatory [24].

Figure A.23: Hydraulic rock breaker mounted on excavator © *Epiroc* [85]

In [114] and [115], the applicability of impact hammers has been evaluated and models for performance prediction have been developed. Hard rocks with uniaxial compressive strengths up to 150 MPa have been excavated in those tests.

Applicability to a small-scale mining robot
Generally, a small hydraulic rock breaker can be considered to be used as an excavation tool for soft rock material. The robot needs to be capable of handling the reaction forces and vibrations generated by the production tool. Excavation rates will be low and specific energy is estimated to be very high. Additionally, the fragmented rock will require a secondary breaking operation to crush to an even particle distribution. The applicability of an impact hammer has been assessed and is documented in Section 3.1.4.

A.2.5 Radial-axial splitting

Radial-axial splitting is a two-phase mechanical excavation method, which uses pre-drilled holes to break the rock and is working against the tensile strength of the rock to fracture it. A hand-held prototype is shown in Figure A.24 and such tool has been tested in the past for narrow vein mining. [33]

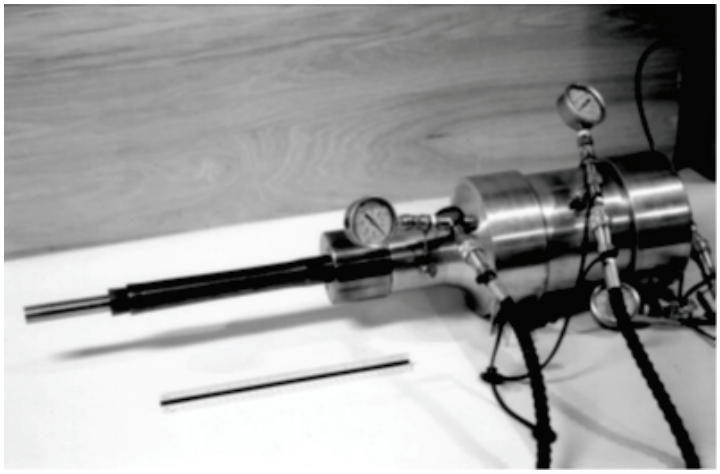

Figure A.24: Hand-held prototype of a radial-axial splitter [185]

A radial-axial splitter is inserted into a hole and breaks rock mainly by

1. Exerting a radial load F_r onto the side wall of a borehole.
2. Exerting a axial load F_a from the borehole bottom.

The combination of these loads are the main forces that fracture the rock. The design of the radial-axial splitter in the borehole that is being examined is shown in Figure A.25. [33, 185]

Working principle of a radial-axial splitter

1. The radial-axial splitter has two pistons. Piston B has a wedge attached and piston A is attached to a thrust rod. There is a conical part that begins to expand in diameter starting at the end of the feathers towards the borehole bottom. As the wedge part increases in diameter as it retracts into the casing, the feathers expand. This anchors the splitter within the borehole.
2. The feathers also exert a radial load F_r to the rock.
3. The thrust rod is attached to piston A. This rod supplies the thrust and the axial load F_a. The axial load is applied past the end of the feathers at the bottom of the borehole.
4. The splitter is prevented from being pushed out from the borehole due to the axial load. Additionally, the radial load also anchors it on the borehole walls.

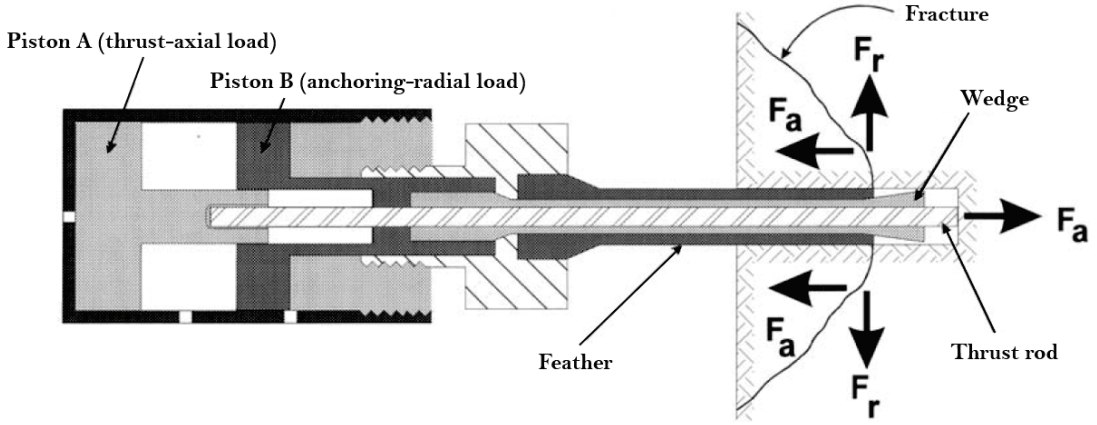

Figure A.25: Design and principle of a radial-axial splitter [33]

The combined action of radial and axial forces initiates a crack starting from the point of contact between the feathers and the surrounding rock. This crack propagates towards the nearest free surface. The rock is fractured between the end of the feathers and the free face. The depth of the breakage is therefore less than the depth of the borehole. [33, 185]

In [185], several tests with the tool presented in Figure A.24 have been conducted and successfully applied for splitting granodiorite with a uniaxial compressive strength of 190 MPa.

In Figure A.26, a concept of a radial-axial splitter, combining a rock drill and a rock splitter, is shown.

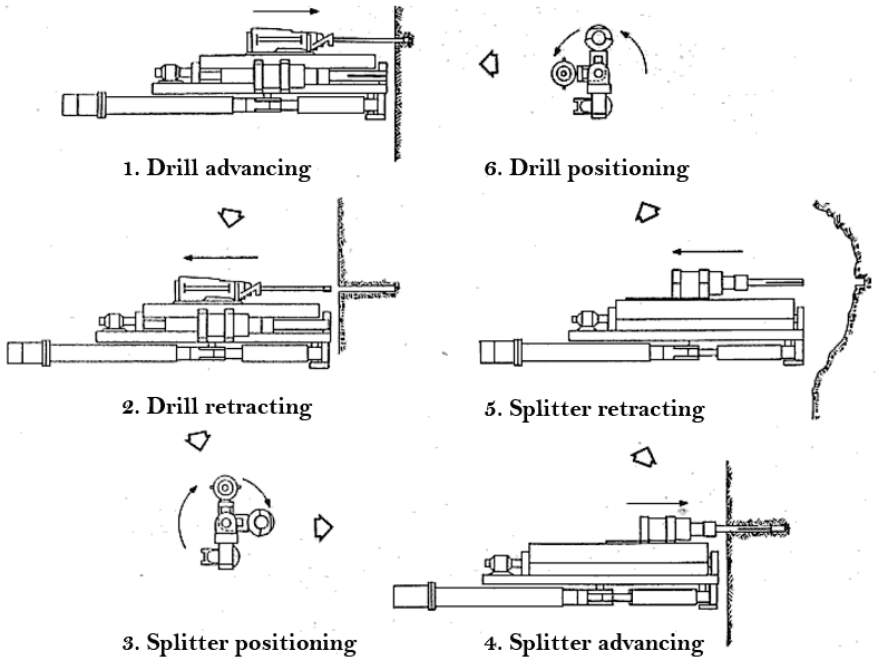

Figure A.26: Working cycle of a radial-axial splitter [186]

Applicability to a small-scale mining robot

Due to the capability to excavate hard rock, radial-axial splitting is an interesting method for a small-scale approach, but there are some points which need to be considered in a more detailed assessment:

- Reaction forces of the splitting process.
- Discontinuity and precision of excavation process.
- Power requirements.
- Need of additional rock crushing equipment.

The productivity and efficiency are again greatly influenced by the rock strength. As mentioned in the preface, a robotic miner is only capable of handling reaction forces with a certain magnitude and the prototype of [185] has a maximum axial load of 360 kN and a maximum radial load of 740 kN. Such high force magnitudes are doubtful, due to the fact that it was a hand-held tool, but based on this and the lack of detailed information, radial-axial splitting has not been considered further.

A.2.6 Dredging

Dredging is a mechanical excavation method mainly used in underwater land reclamation projects and dredging of harbours and fairways in soft rock, soil-type applications. The dredger is usually on the end of a long boom which is mounted on a vessel. Depending on the working method it can be distinguished between hydraulic and mechanical dredging, see Figure A.27. [187]

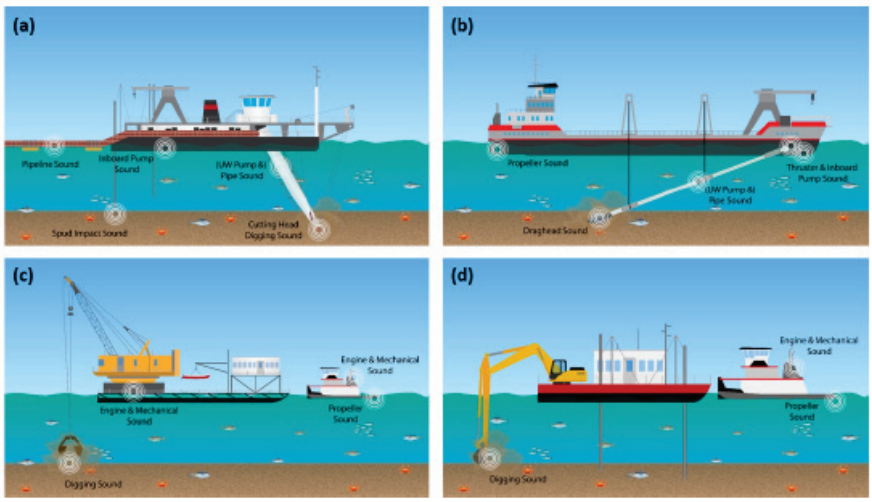

Figure A.27: Examples of hydraulic (top) and mechanical (bottom) dredger types: (a) Cutter suction dredge (CSD), (b) Trailing suction hopper dredge (TSHD), (c) Grab dredge (GD) and (d) Backhoe dredge (BHD). [187]

The cutter head of a hydraulic dredger is similar to a part-face cutter head of a longitudinal roadheader. Picks mounted on a base body which has openings to suck the material into the suction pipe (see Figure A.28). [187]

Figure A.28: Cutter head of a hydraulic suction dredger © *RoyalIHC* [188]

The strength of the material to be excavated is tendentially quite soft, because the long boom does not allow high cutting forces. [187]

Applicability to a small-scale mining robot
Dredging is only a viable excavation method when the main machine is a vessel floating on the sea surface. The cutting process of the cutter head is comparable to a part-face cutting method and is discussed throughout this thesis. This method is not declared as a feasible system for that exact case and has therefore not been considered as a potential excavation method for a robotic miner.

A.2.7 Bucket wheel excavation

Bucket wheel excavators (BWE) are surface mining machines in large-scale open pit mines extracting soft material. A bucket wheel excavator's excavation tool represents a rotating wheel with buckets mounted onto it. The buckets are continuously extracting overburden and ore. Depending on the material to be excavated, size, number and design of buckets change. Typically used in lignite mining, the bucket wheel has a large diameter to maximize the production rate of the machine and the maximum strength of the rock to be excavated is very low. Prototypes have been tested up to 50 MPa UCS. [25, 189]
For smaller operations, compact bucket wheel excavators also have been developed and used successfully (Figure A.29).

Figure A.29: Compact bucket wheel excavator © *Noen* [190]

A BWE in an open-pit mine requires a large infrastructure including a main conveyor belt which connects the BWE with the bulk material dump and different machinery to control the material flow. Also the flexibility and mobility are not very high compared to underground excavation systems and it is sensitive to ground conditions. [25]

Applicability to a small-scale mining robot
Several points rule out a bucket wheel as production tool for a robotic miner: Little flexibility and mobility due to a very detailed design and rigid structure,

underground mining and excavation of tunnels are not possible with this method and generally only in soft rock conditions applicable. Based on those shortcomings, a bucket wheel type excavation tool has not been taken into consideration for further evaluation.

A.2.8 Saw and diamond wire cutting

Rock cutting saws (Figure A.30) and diamond wire cutters are specialized tools to extract dimensional stones like marble and travertine from quarries. Application areas are underground and surface quarry operations with low to medium abrasive and soft to medium hard rocks. [24]

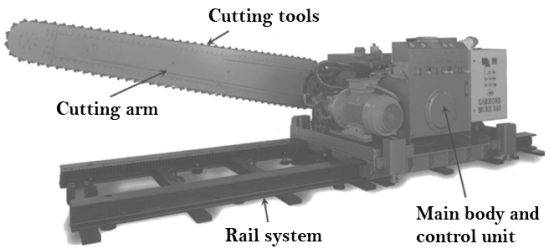

Figure A.30: Rock cutting saw [24]

A diamond wire saw machine is presented in Figure A.31, typically applied in dimensional stone cutting. The diamond wire spans a solid rock mass, is tensioned and pulled in a loop in order to create a cut.

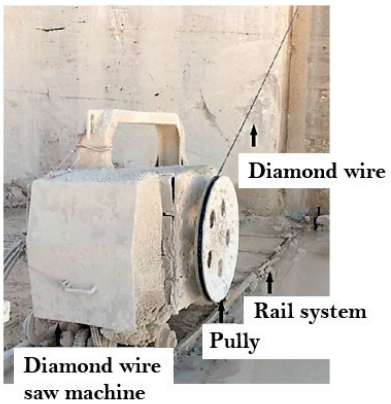

Figure A.31: Diamond wire saw [191]

Rock cutting saws and diamond wire cutters complete the mechanical excavation systems and have been disregarded due to the fact that they are used as extraction and not excavation tools.

A.3 Alternative excavation

A.3.1 High-pressure waterjet cutting

High-pressure waterjet cutting, originally used in industrial operations for precise material cutting, has also been investigated in mining scenarios but not applied in commercial solutions [33].
A waterjet is generated by a high-pressure pump, concentrated and released through a nozzle. The waterjet has a small stand-off distance to the rock and due to the high pressure (usually several hundred to thousand bar), the rock is eroded and cut.

In principle, two main technologies can be established: Pure or plain waterjet cutting (in a continuous or pulsed mode) and abrasive waterjet cutting. Both methods can be seen in Figure A.32.

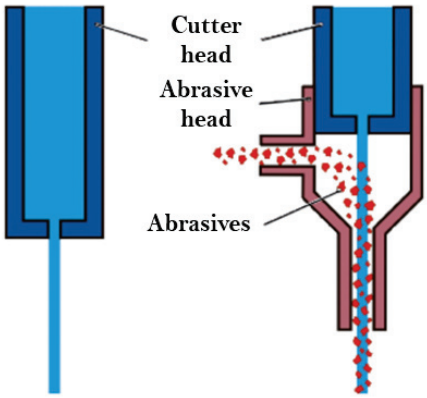

Figure A.32: Pure waterjet (left) and abrasive waterjet cutting (right) [192]

According to [193], the basic principles of abrasive waterjet cutting can be summarized:

- A high-pressure pump generates a high-pressure waterjet which is ejected from a small diameter orifice.
- The waterjet is ejected into a mixing chamber and due to its high velocity, it creates a partial vacuum.
- This vacuum pulls particles from an abrasive dispenser into the mixing chamber where the abrasives are entrained into the waterjet.
- The waterjet passes a focussing tube and exits from a nozzle.
- The cutting operation is controlled by the water pressure, flow rate, traverse speed, stand-off distance and the strength of the material to be cut.

Nowadays, abrasive waterjet cutting is much more popular than plain waterjet cutting, because higher cutting rates can be achieved, and harder materials can be cut. The abrasives allow higher magnitudes of erosion and shearing of the material, because the energy density is higher. Abrasives are typically sharp-edged mineral particles such as granite sand or olivine with a particle size of 0.1-0.3 mm. Although, the design of the plain waterjet is much simpler and much less parts are needed, the common choice for hard material cutting is the abrasive waterjet. [193, 194]

Jet diameters range from 0.1-0.5 mm, depending on the available pressure and flow rate, and pressure levels up to 6000 bar are feasible. Harder materials require higher pressure and cutting rock with any strength is possible, although a threshold pressure for cutting material with a certain strength has to be exceeded. [195]

Pure waterjet cutting

- Pure waterjet cutting uses pure water without any abrasive particles and a constant flow rate.
- The cutting rate is proportional to the waterjet power and significant erosion can only be achieved if a certain threshold pressure is reached.
- Higher cutting rate can be obtained easier by increasing the flow rate instead of the pressure, assuming power of the waterjet is constant.
- Cutting rate is depending on jet power, traverse velocity, water pressure and material to be cut. [194]

Abrasive waterjet cutting

- The diameter of the nozzle (Figure A.33) needs to be kept small enough to produce deeper cutting depths and large enough for abrasives to pass.

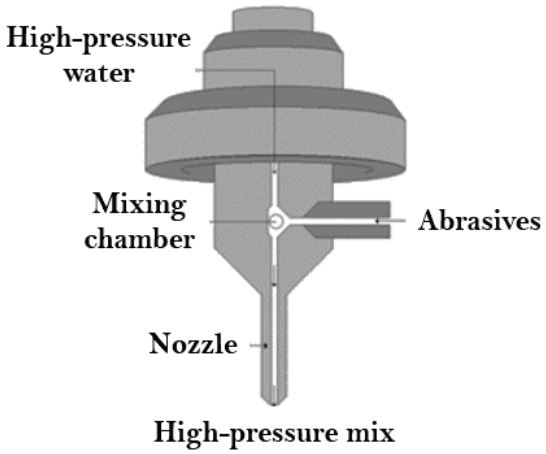

Figure A.33: Illustration of a nozzle with abrasive insertion [196]

- The cutting depth is linearly related to the waterjet pressure.
- Jet performance is highly dependent on the abrasive mass flow rate and the ratio of abrasive mass flow rate and water flow rate. [194]

Figure A.34 shows two high-pressure waterjet rock moving tools: A hand-held waterjet cutter, which is used to move broken rock in a stoping environment or sweeping in the stopes, and a hand-held water cannon, applied for moving broken rock down dip into a gully. [86]

Figure A.34: Hand-held waterjetting gun (top), hand-held water cannon (bottom) © *HPE* [86]

High-pressure waterjet excavation systems have already been used successfully in mining uranium in Saskatchewan [197]. High radiation of the orebody and unstable rock mass lead to the development of a novel jet boring system. The two main tools were a mobile drilling car and a jet boring tool (Figure A.35). [198]

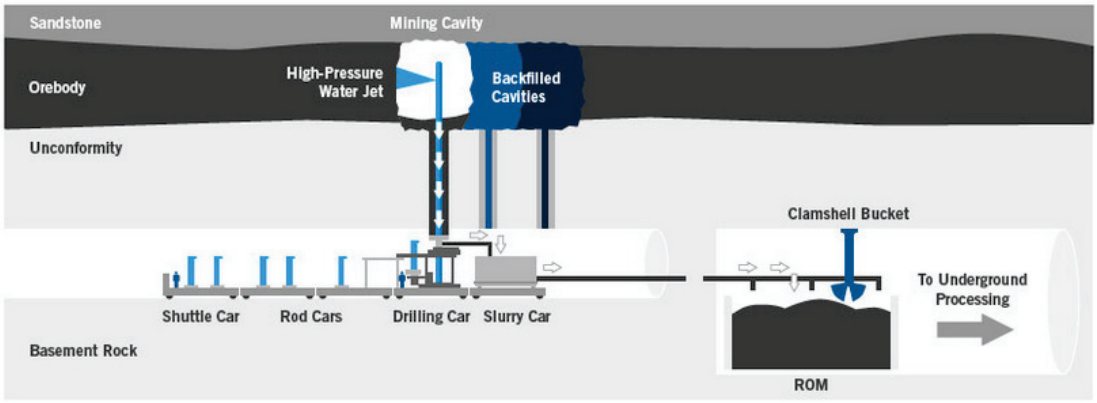

Figure A.35: Schematic of the jet boring system © *Cameco* [198]

A pilot hole is drilled vertically through host rock to the orebody and the jet boring nozzle is placed inside the pilot hole. High-pressure waterjets are excavating the ore and the loose material is flushed downwards. The mined ore is then slurrified and pumped to a processing station. [198]

Applicability to a small-scale mining robot
High-pressure waterjet cutting seems to have a potential for small mining operations. Multiple waterjets can be arranged to a full-fledged production tool for a robotic miner. Certain parameters need to be evaluated in order to estimate the performance of such an excavation tool in hard rock environments. Little to negligible reaction forces are very advantageous but on the other hand, the high specific energy would lead to a non-economical operation. Detailed investigations and studies have been made and are presented in Section 3.2.1.

A.3.2 Hydrofracturing

Hydraulic fracturing (hydrofracturing) is primarily known as a technique for enhancing the recovery from underground oil and gas reserves. In the recent years, other applications have been introduced for hydraulic fracturing in excavation projects. For instance, in deep excavations, hydraulic fracturing can alleviate the high in-situ stress conditions by inducing fractures and releasing the high existing energy in the rock mass. [199]
With some modifications it has also been suggested as an excavation method due to the advantages it can offer compared to drill and blast, aiming for a non-explosive, environmentally friendly excavation method of hard unfractured rocks [200].

An effective excavation similar to blasting boreholes requires imposing a fast-enough hydraulic pressure. The increasing rate of pressurization can lead to a transition from a typical pattern of fractures in the two principal stress planes to formation of multiple fractures in different directions (Figure A.36). [201]

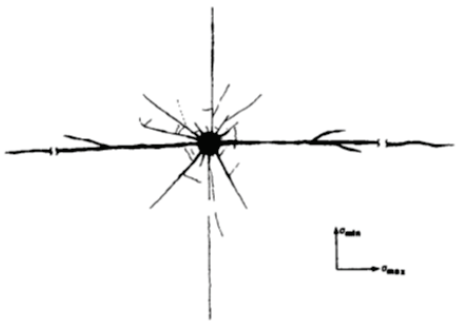

Figure A.36: Typical multiple fracture pattern [202]

Different techniques have been applied previously to provide this fast pressure exertion. Progressively burning propellants have been proven to be quite effective in tailoring pressure rates in a wellbore to generate multiple fractures and use the combustion gases to extend the cracks [202].

The most critical parameter affecting the fracturing process is the pressure loading rate [202]. In [203], *Schmidt* conducted several full-scale tailored-pulse shooting tests with progressively burning propellants. A correlation between the pressure rate and the resulting behaviour of fractures was established. Three levels of pressure rate (low, high and very high) were tested.

Other works in the past were dedicated to introducing fully hydraulic tools which omit any application of explosive or burning component. Different methods technically fall into two main divisions: Methods based on exertion of a mechanical impact in one stage and two-stage methods, where water is primarily pressurized inside a container and the energy is subsequently released into the borehole. In one-stage methods, a mechanical impact is transferred to a water-filled chamber.

For instance, *Swift* achieved controlled loading conditions by compressing fluid in a borehole by means of a piston [204]. The experimental apparatus is illustrated in Figure A.37.

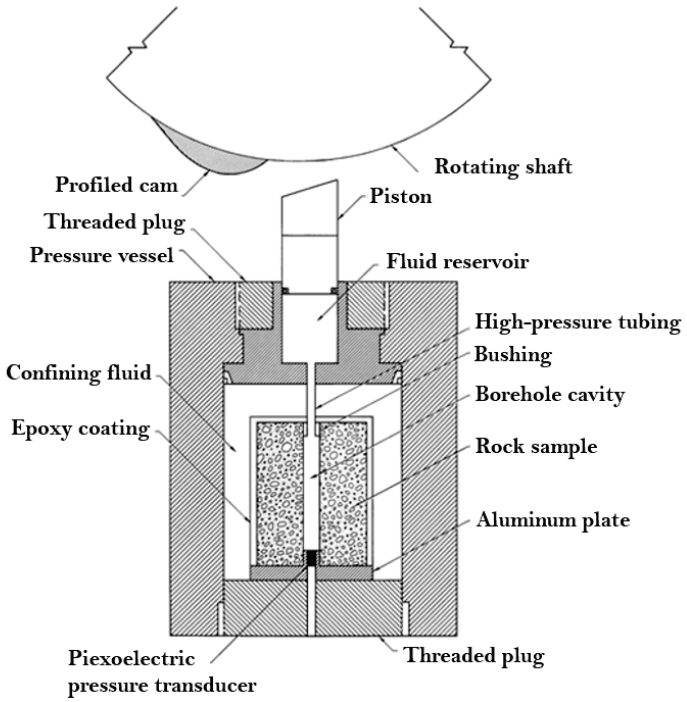

Figure A.37: Schematic of multiple-fracture experiment [204]

As can be seen, the piston is engaged by a profiled cam which is mounted on a

rotating shaft. Confined pressure conditions are also met in these experiments and intermediate loading rates are provided by this tool in a well-controlled manner.

As for the two-stage methods, works by *Kollé* led to the development of an experimental hydraulic tool capable of generating multiple fractures in hard rock (see Figure A.38) [205]. The tool consists of a pressure vessel capable of sustaining very high water pressures. A fast-opening valve discharges the water through an outlet tube towards the borehole. The conducted laboratory tests proved its capability in generating sufficiently high pressurization rates for fragmentation of an unconfined rock. In contrast, typical explosives or propellants would generate pressures that are sustained over a period of 10 to 100 ms. [205]

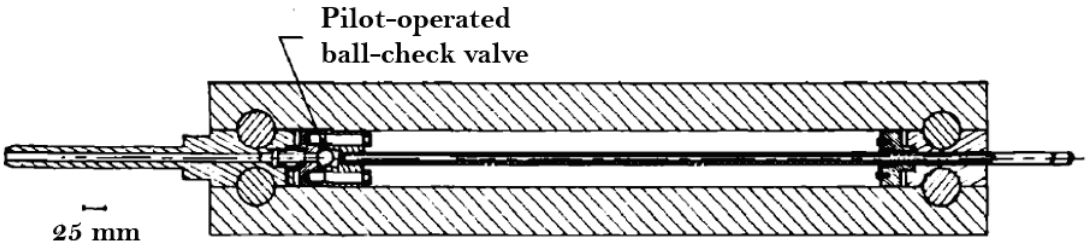

Figure A.38: Hydraulic explosive tool [205]

The low compressibility of water leads to a lower pressure pulse duration and consequently to incomplete fractures. This was one of the main uncertainties regarding the applicability of this method. Subsequent attempts in application of this concept in practice showed that sometimes blasting the same boreholes was necessary to move the fragmented rock out of the tunnel face. This should mean a higher number of boreholes to be drilled compared to a typical blasting pattern. It was tested in a South African underground mine and deemed as capable of fragmenting a confined quartzite rock with burdens of up to 350 mm. [206]

Applicability to a small-scale mining robot

Within this research, the focus is placed on environmentally friendly methods, where no explosive or burning propellants are applied. Compared to drill and blast, hydrofracturing doesn't require secondary tasks as cleaning the borehole after drilling or wiring explosives. The comparable trivial design of hydrofracturing tools is beneficiary for integrating it in a small robotic miner. High-pressure generation and storage are challenging topics and are assessed in Section 3.2.2. The goal was to evaluate the technical requirements needed to employ hydraulic multiple fracturing as excavation tool of a small-scale mining robot.

A.3.3 Plasma blasting

In 1990, *Nantel* has reviewed plasma blasting techniques for rock excavation applications [207]. If electrical energy is induced into a liquid medium, this energy can convert that fluid to high-temperature and high-pressure plasma. This plasma expands and the energy released can be used to initiate high pressure on a surrounding rock mass. [33, 207]
An illustration of a plasma blasting system is presented in Figure A.39.

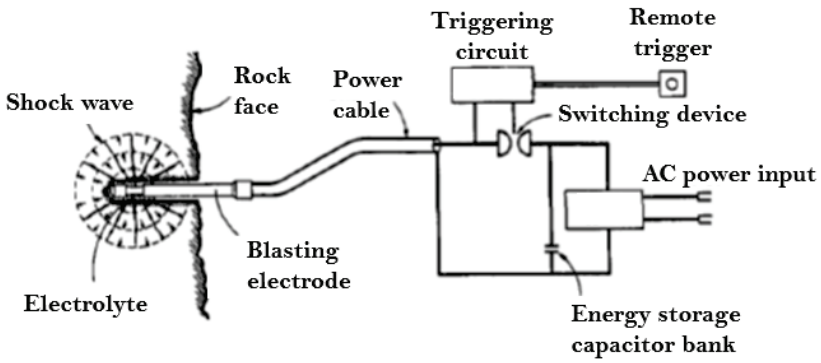

Figure A.39: Illustration of plasma blasting [207]

A drillhole is filled with an electrolyte and in the center of this hole is a coaxial blasting electrode. A capacitor is connected to a power supply which stores energy in form of electrical current. When the operational voltage is reached in the capacitor, a remote trigger turns a switch which connects the capacitor with the blasting electrode. The capacitor discharges with an energy delivery rate of 300 MW/s at a peak power of 3.5 GW. [207]
A 300 kJ rock breaker has been built to test a mobile plasma blasting machine for surface operations (Figure A.40) [208].

Figure A.40: Plasma blasting rock breaker unit [208]

Although, successful field tests have shown the high potential of plasma blasting, the technology had not been investigated any further [33, 208].

In general, this technology is very expensive and impractical. Mechanical and electrical components exhibit a very short lifespan and require constant maintenance.

A.4 Combined excavation

A.4.1 High-pressure waterjets assisted to drilling

The idea of superposing high-pressure waterjets with a mechanical excavation tool is the degradation of required excavation forces by pre-weakening the rock and reducing the tool wear. The principle of waterjet assisted drilling is shown in Figure A.41. A percussive drill is used as a rock drill and in the inner center a coaxial waterjet is passing the drill bit until it exits the tool and interacts with the rock. [209, 210]

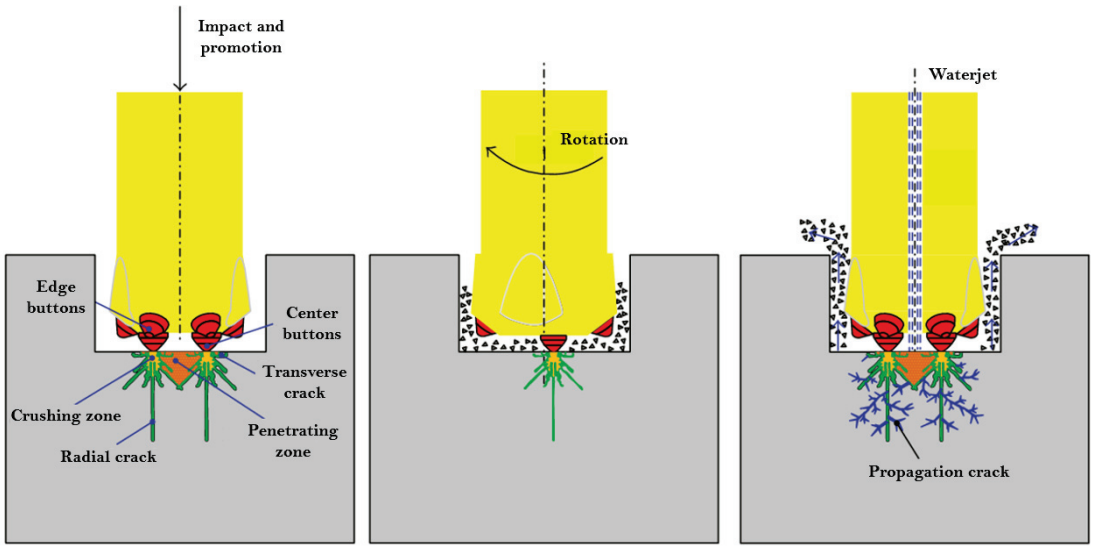

Figure A.41: Fragmentation mechanism of waterjet assisted drilling [209]

The waterjet forms cracks in the crushing zone both in radial and axial directions, which weaken the rock. In [209], *Liu et al.* developed and tested a concept of a high-pressure waterjet assisted drill (Figure A.42).

A sealing device has been built which connects a high-pressure water circuit with a hydraulic rock drill. The drill bit has a diameter of 45 mm and the pressure of the water inside the rock drill has been tested at levels from 100 to 400 bar.

Within this work, the drilling performance has been investigated with different rotational speeds, water pressures and different drill bits (Figure A.43).

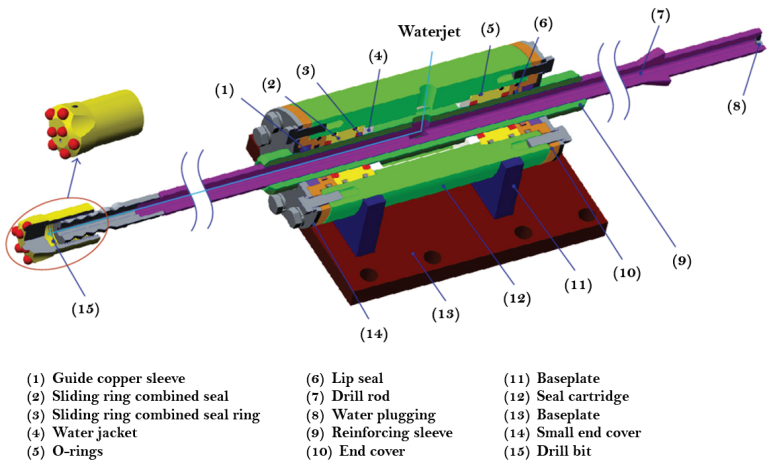

Figure A.42: Concept of high-pressure waterjet assisted drill [209]

In [209], following conclusions are stated:

- The performance of this system is highly depending on the drilling parameters and the water pressure and their synergy. Generally, the higher the water pressure is, the lower the rotational speed of the drill has to be.
- Theoretical work indicates a decrease of drilling force by superposing a waterjet, although the waterjet has to exceed a certain threshold pressure to erode the rock.

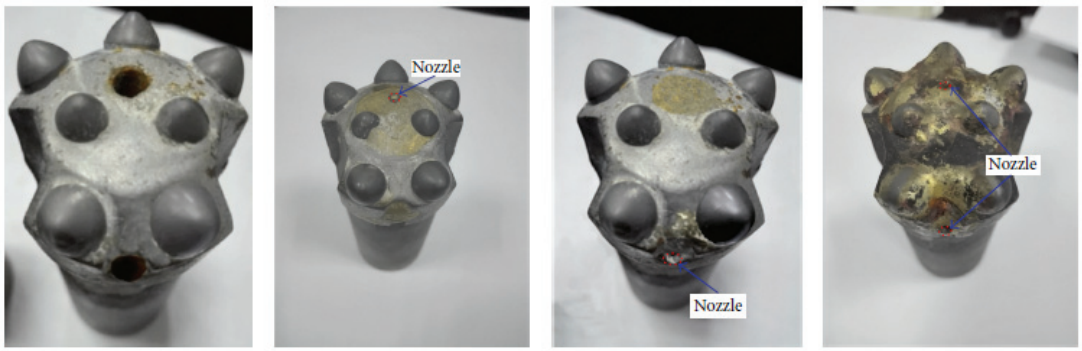

Figure A.43: Different bit configurations [209]

Applicability to a small-scale mining robot

The application of this combined excavation tool to a robotic miner is not seen as a practical solution. Rock drilling as a standalone production tool is only useful for exploration tasks or material sampling. It is not applicable for excavation or tunnelling. Further on, drilling is used as an auxiliary tool for a secondary

rock fragmentation system (blasting, radial-axial splitting, hydrofracturing). The drilling forces of small diameter drill systems are manageable even in hard rock scenarios and assisting high-pressure waterjet would be an additional power consumer. A trade-off between complexity and economical efficiency has to be made. An application might can be reconsidered in future scenarios in which a large number of drillholes needs to be created.

A.4.2 High-pressure waterjets assisted to cutting

Similar to high-pressure waterjets assisted to drilling, the idea of weakening the rock by reducing the rock mass rating and limiting cumulative wear with the assistance of a high-pressure waterjet to a mechanical cutting tool has been investigated in several studies, published in [211–214].

For single linear pick tool cutting tests, four configuration modes with different positions of the waterjet to the conical pick can be defined, presented in Figure A.44 from left to right [211]:

- Jet through the center of the pick (JCP).
- Jet at the front of the pick (JFP).
- Jet at the rear of the pick (JRP).
- Jet at the side of the pick (JSP).

The experimental work in [211] shows the following results: JCP performed the highest reduction of cutting force, followed by JFP, JRP and JSP.

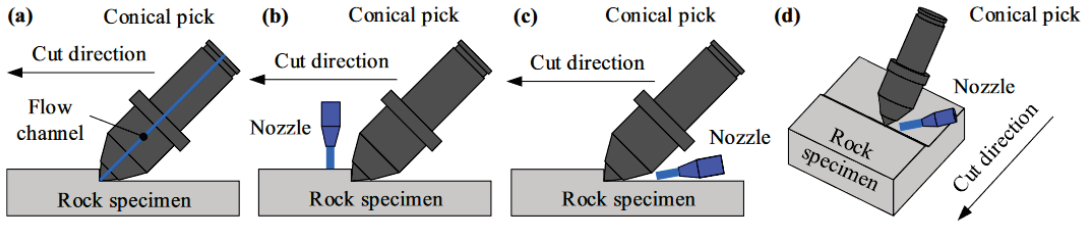

Figure A.44: Configurations of high-pressure waterjets assisted to a conical pick cutting tool [211]

The in [211] conducted tests with water pressure levels up to 460 bar and cutting depths up to 10 mm showed a maximum reduction of the cutting resistance of 41,78 %. Subsequent conclusions have been made:

- As waterjet pressure increases, the cutting resistance and specific energy are reduced, but the reduction ratio diminishes.

- Higher cutting depth increases the cutting resistance. Optimum cutting depth in the tests was 5 mm.
- Introducing a second cut cycle reduces the cutting resistance even more as the rock is already weakened and the excavated rock particles are finer and smaller.
- Wear of conical pick could be highly reduced and the cutting stability increased. [211, 212]

Kotwica summarized the combinations of high-pressure waterjets and disc cutting tools in various arrangements and the resulting increase of cutting speed by 50 % with high-pressure waterjets assisted to disc cutting tools [215].

In Figure A.45, a tunnel boring machine with high-pressure waterjets assisted to the disc cutting tools is presented. The TBM has been developed by *Wirth* in order to evaluate the influence of the high-pressure waterjets on the reduction of the thrust forces. Up to 70 nozzles with maximum water pressure levels of 400 MPa have been implemented. The conducted tests showed a decrease of the thrust force by 57 % and an increase of the mining speed by almost 100 %. [215]

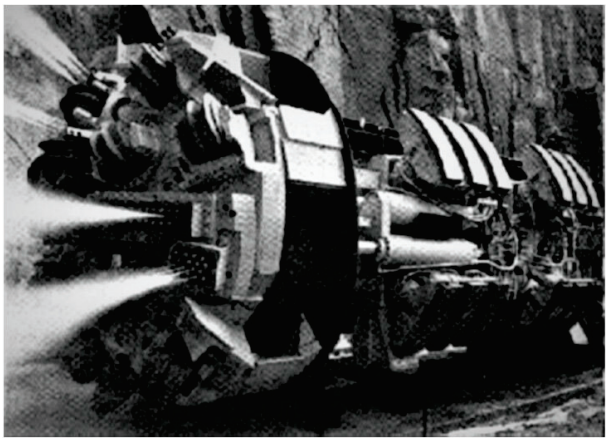

Figure A.45: *Wirth* tunnel boring machine with assisted high-pressure waterjets [216]

Applicability to a small-scale mining robot

Integrating this method in a robotic mining machine poses the similar problem as high-pressure waterjets assisted to drilling. The additional waterjet requires a supplementary water circuit with high-pressure pump which increases the overall power consumption. Pick and disc tools already lead to very high reaction forces and the maximum capabilities are the excavation of soft rock material (with a light machine). An additional waterjet is not profitable, as it won't lower the cutting resistance in a way that harder rock can be excavated.

A.4.3 Microwaves assisted to cutting

Microwave irradiation is affecting the rock strength by inducing micro-cracks, because of the different volume expansion between minerals in the rock. The electromagnetic energy is converted into heat and produces temperature gradients which subsequently generate stress. If this generated stress exceeds the material's strength, cracks can be initiated. [33, 217]

The wavelength has significant influence on heat production. Microwaves' wavelength varies between 1 mm and 1 m at a frequency of 0.3–30 GHz (Figure A.46). The transmitted energy is directly related to wavelength and frequency. Higher frequency and thus shorter wavelength lead to a higher energy. [33]

Although, the carried energy of microwaves is less than in other waves, the advantage of microwaves is the larger penetration depth into materials. The stress-strain curve of pyrite particles hosted in calcite and the effects of microwave irradiation to it can be seen in Figure A.46. [33, 218]

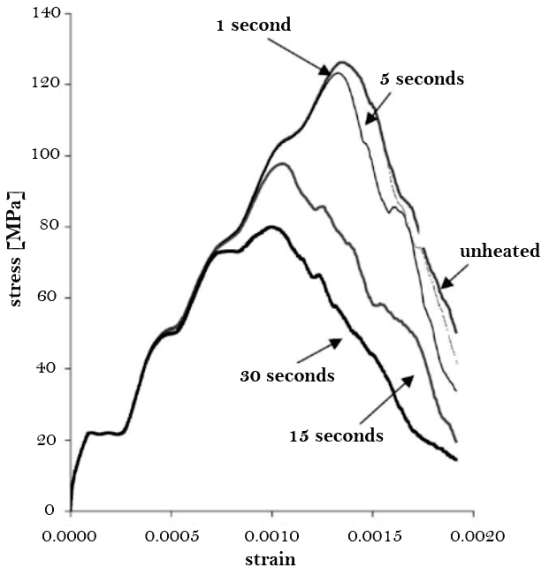

Figure A.46: Effect of varying heating times on the numerically modelled stress – strain curves for the theoretical calcite and pyrite sample (heated in a 2.6 kW, 2.45 GHz microwave cavity) [218]

A significant reduction of strength could be observed after 15 s of microwave treatment. [218]

Hartlieb made several studies and test on microwaves assisted to cutting. The microwave irradiation was done with 24 kW microwave source at a frequency of 2450 MHz and a granite block has been partly radiated (Figure A.47). [217]

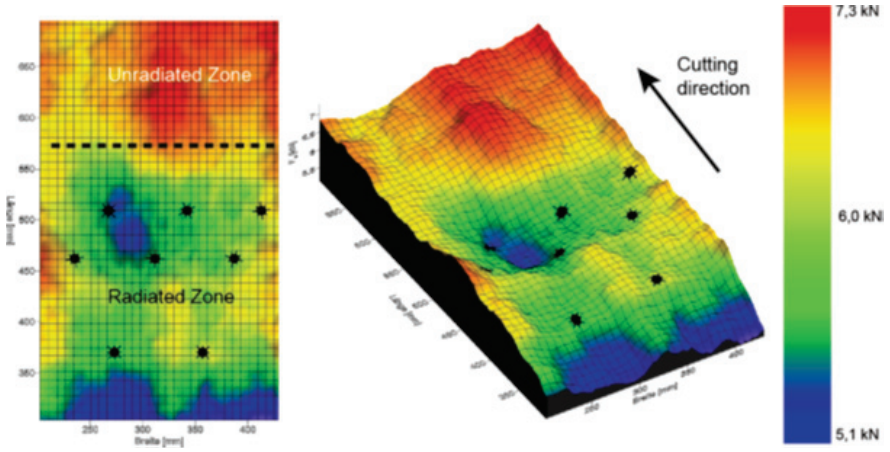

Figure A.47: Floating median calculation of cutting forces for partly radiated granite block [217]

Cutting tests conducted in [217] have shown, that the cutting force could be reduced by 10 % at microwave-treated rocks.

Applicability to a small-scale mining robot

The high-power requirements and the complexity of the excavation system make microwaves assisted to cutting unattractive in this scenario. Further on, many operating fields of the mining robot are either wet or completely submerged applications. Microwaves get absorbed by water and thus this idea will not be further investigated.

B Appendix - Applicability assessment

B.1 Rock drilling

Tophammer drilling

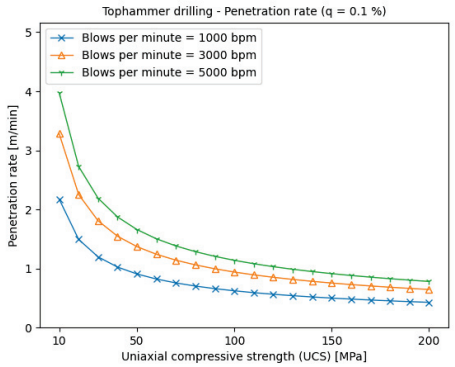

Figure B.1: Tophammer drilling - Penetration rates

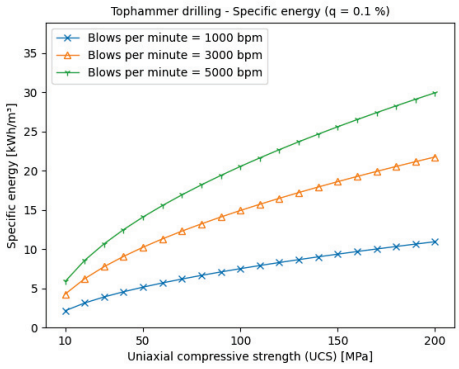

Figure B.2: Tophammer drilling - Specific energies

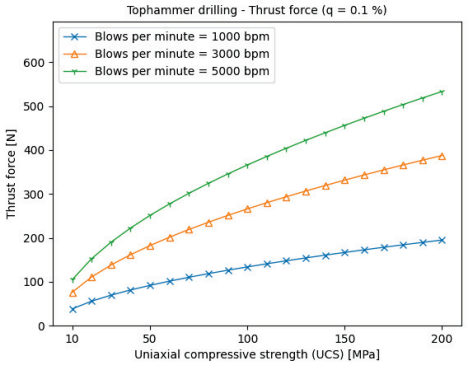

Figure B.3: Tophammer drilling - Thrust forces

Rotary-percussive drilling

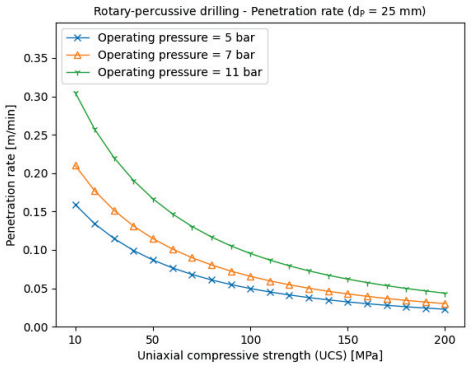

Figure B.4: Rotary-percussive drilling - Penetration rates

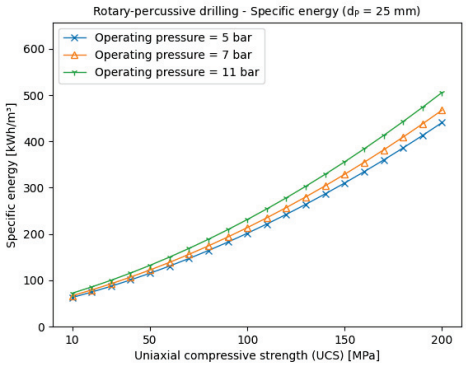

Figure B.5: Rotary-percussive drilling - Specific energies

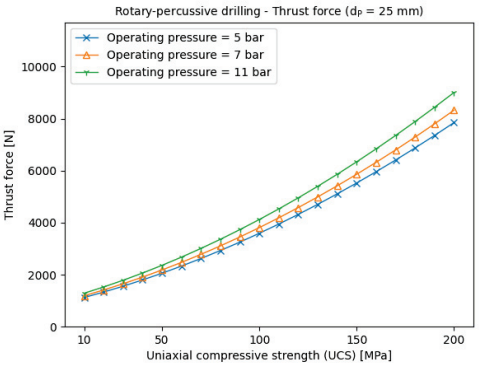

Figure B.6: Rotary-percussive drilling - Thrust forces

Rotary drilling

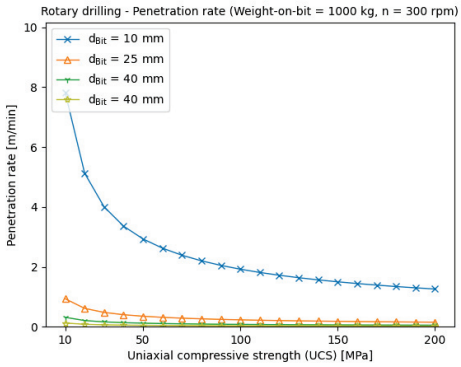

Figure B.7: Rotary drilling - Penetration rates 1

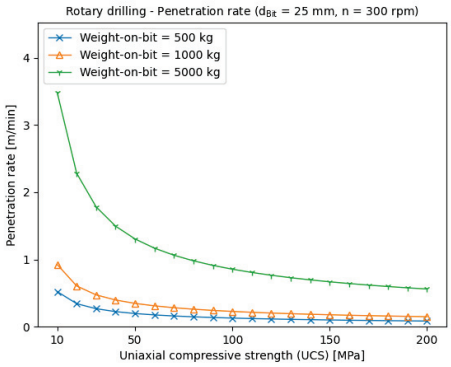

Figure B.8: Rotary drilling - Penetration rates 2

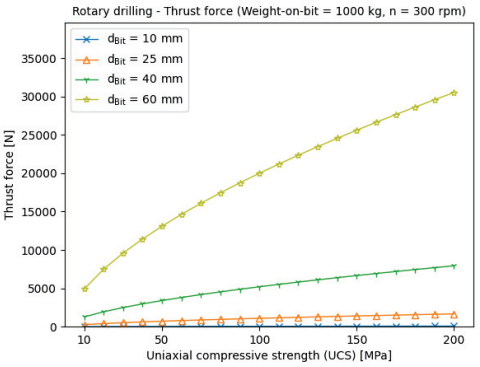

Figure B.9: Rotary drilling - Thrust forces 1

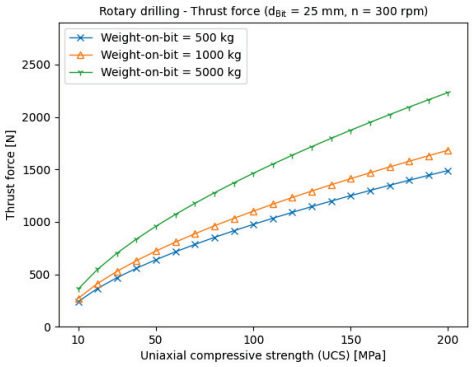

Figure B.10: Rotary drilling - Thrust forces 2

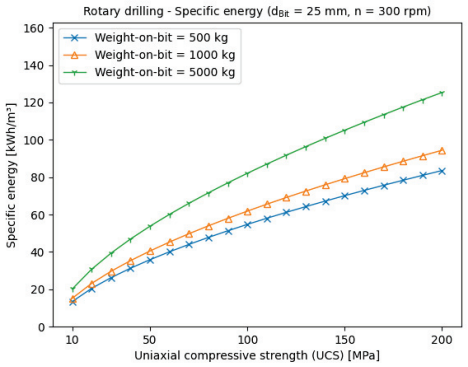

Figure B.11: Rotary drilling - Specific energies

B.2 Part-face cutting

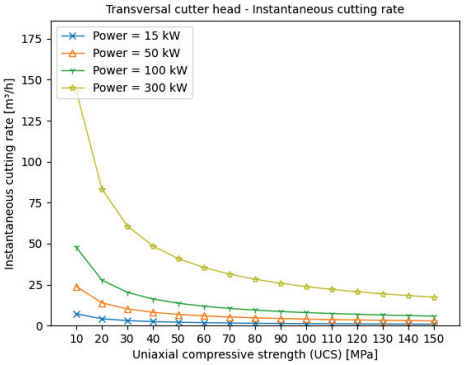

Figure B.12: Part-face cutting - Instantaneous cutting rates of transversal cutter heads

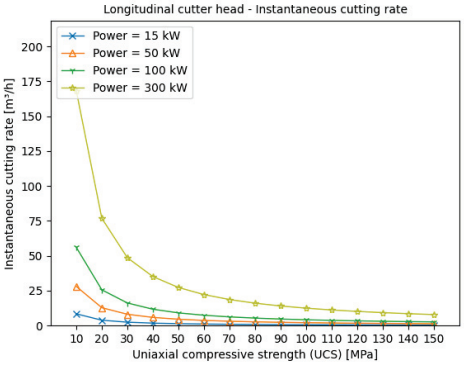

Figure B.13: Part-face cutting - Instantaneous cutting rates of longitudinal cutter heads

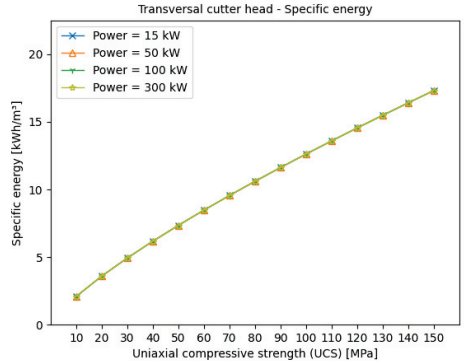

Figure B.14: Part-face cutting - Specific energies of transversal cutter heads

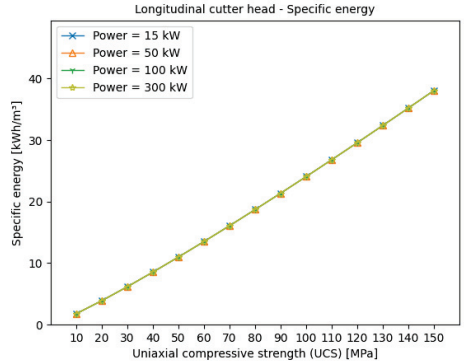

Figure B.15: Part-face cutting - Specific energies of longitudinal cutter heads

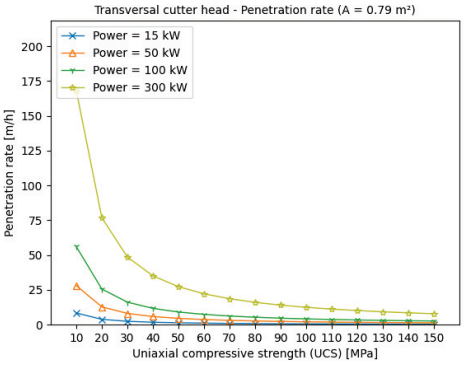

Figure B.16: Part-face cutting - Penetration rates of transversal cutter heads

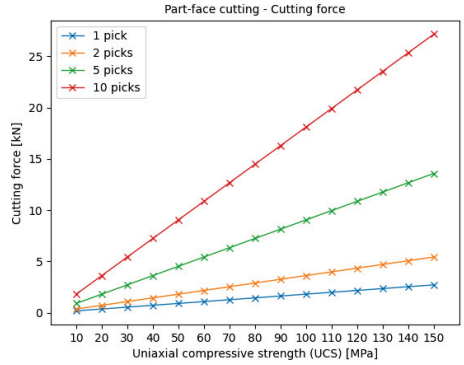

Figure B.17: Part-face cutting - Cutting forces depending of number of picks in contact

B.3 Full-face cutting

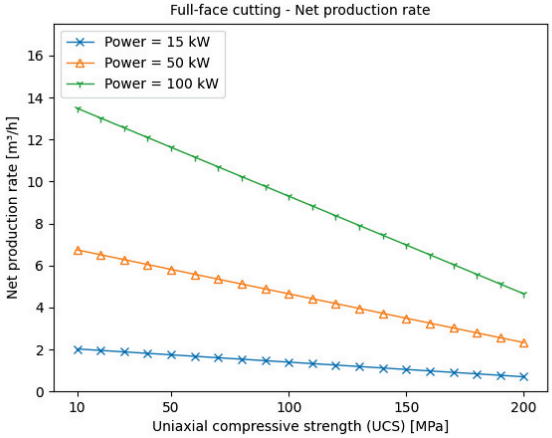

(a) Net production rate

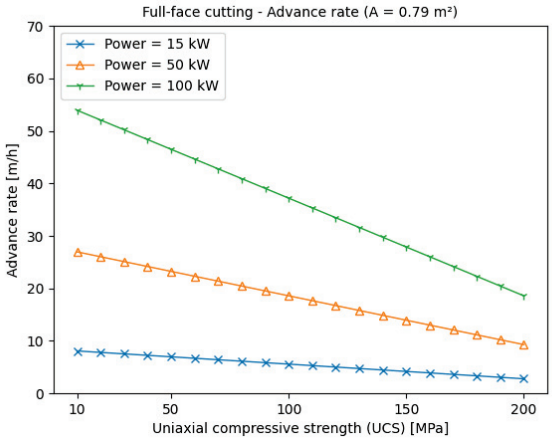

(b) Advance rate

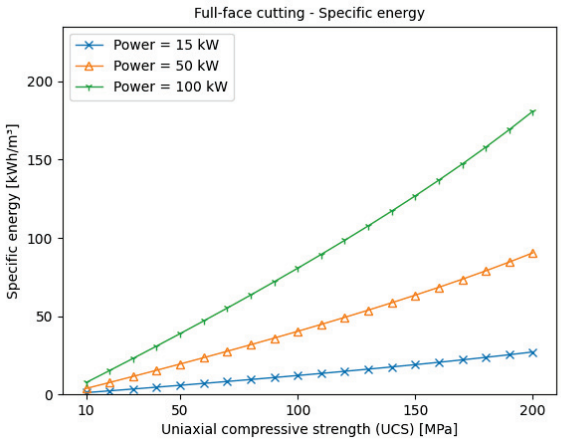

(c) Specific energy

Figure B.18: Full-face cutting - Performance parameters

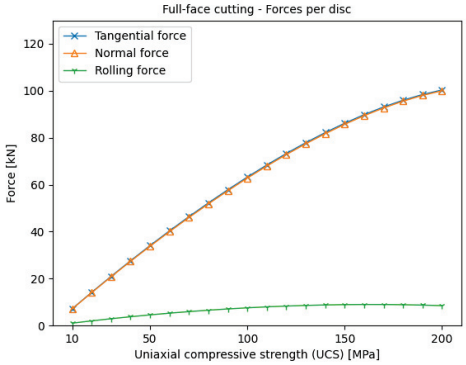

Figure B.19: Full-face cutting - Forces per disc

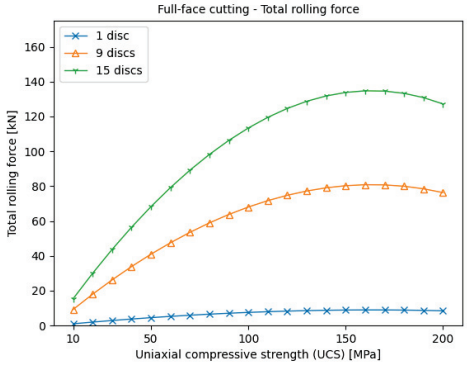

Figure B.20: Full-face cutting - Total rolling forces

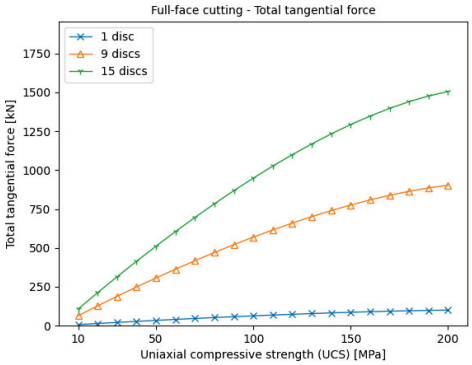

Figure B.21: Full-face cutting - Total tangential forces 1

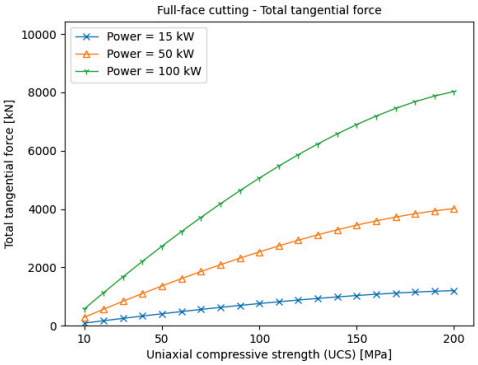

Figure B.22: Full-face cutting - Total tangential forces 2

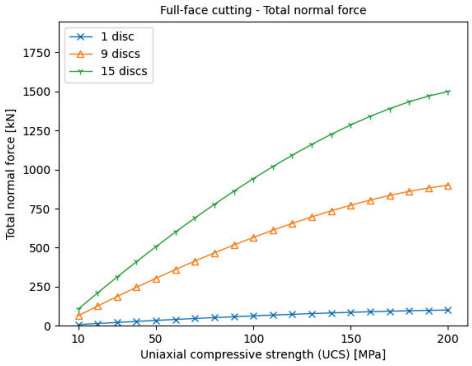

Figure B.23: Full-face cutting - Total normal forces

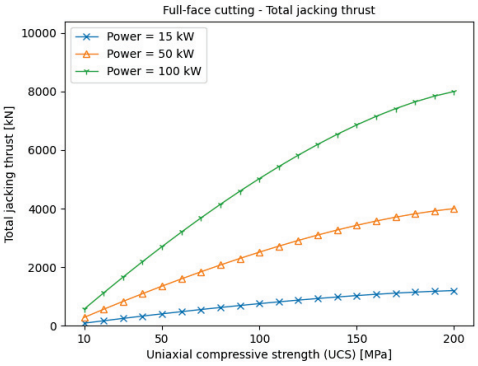

Figure B.24: Full-face cutting - Total jacking thrusts

B.4 Impact hammer

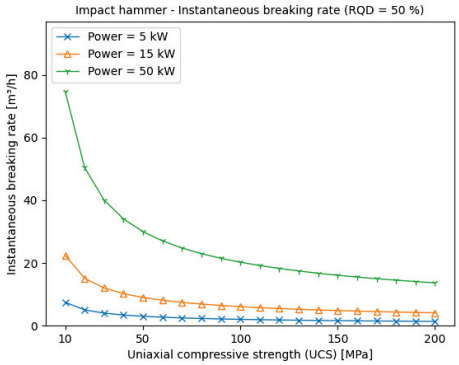

Figure B.25: Impact hammer - Instantaneous breaking rates 1

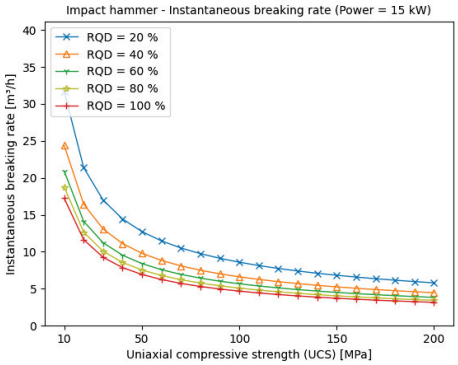

Figure B.26: Impact hammer - Instantaneous breaking rates 2

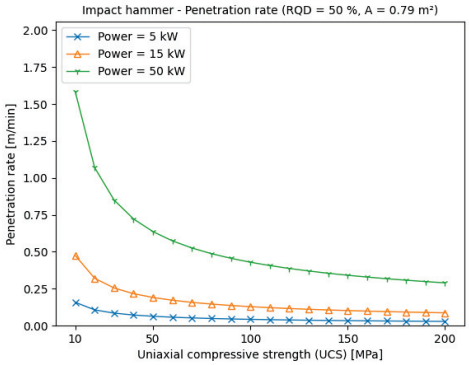

Figure B.27: Impact hammer - Penetration rates 1

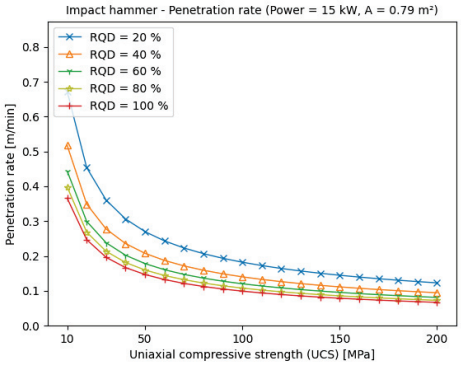

Figure B.28: Impact hammer - Penetration rates 2

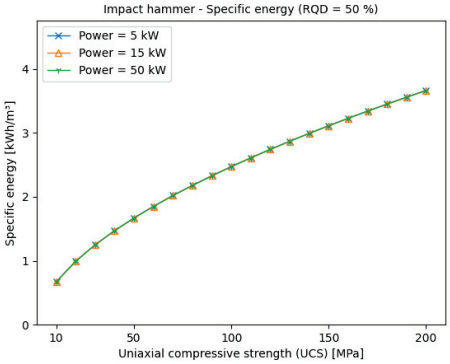

Figure B.29: Impact hammer - Specific energies 1

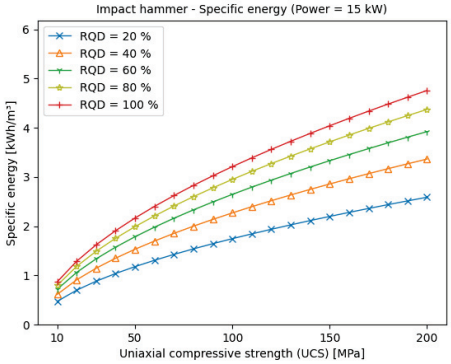

Figure B.30: Impact hammer - Specific energies 2

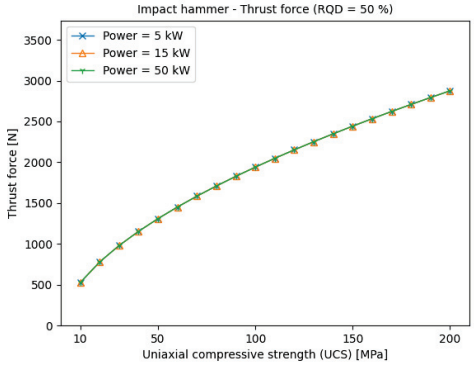

Figure B.31: Impact hammer - Thrust forces 1

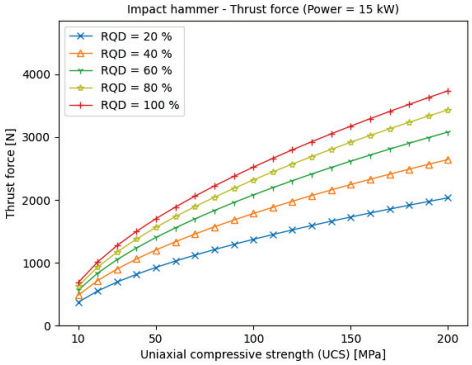

Figure B.32: Impact hammer - Thrust forces 2

B.5 High-pressure waterjet cutting

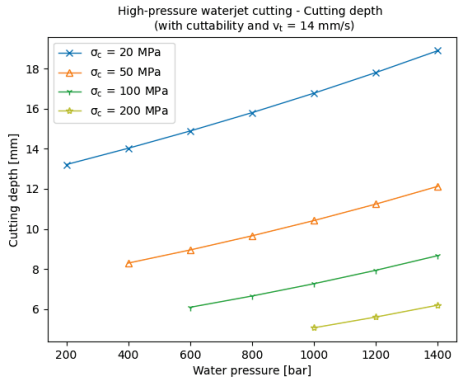

Figure B.33: High-pressure waterjet cutting - Cutting depths

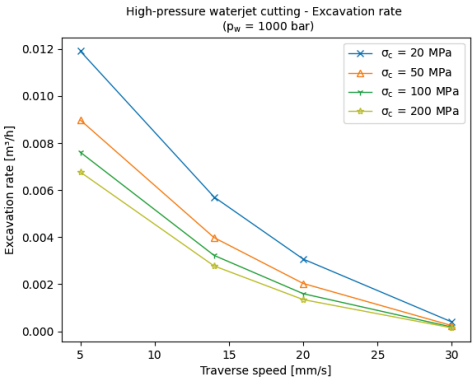

Figure B.34: High-pressure waterjet cutting - Excavation rates

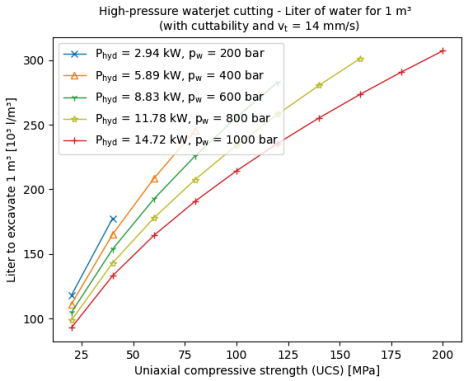

Figure B.35: High-pressure waterjet cutting - Liter to excavate 1 m^3

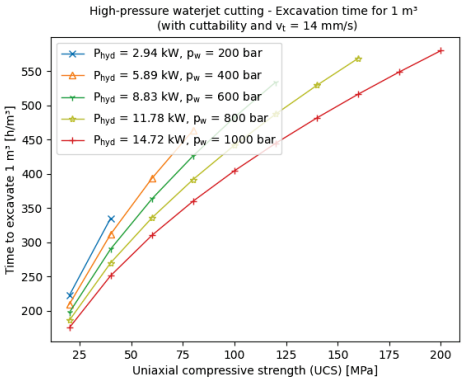

Figure B.36: High-pressure waterjet cutting - Time to excavate 1 m^3

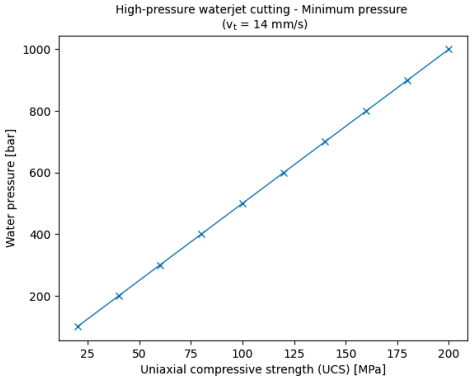

Figure B.37: High-pressure waterjet cutting - Minimum water pressure

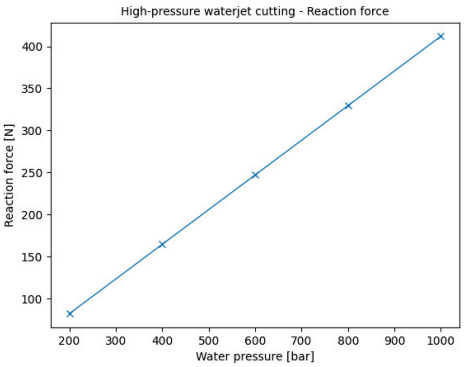

Figure B.38: High-pressure waterjet cutting - Reaction force

B.6 Minimum masses, traction forces

Minimum masses

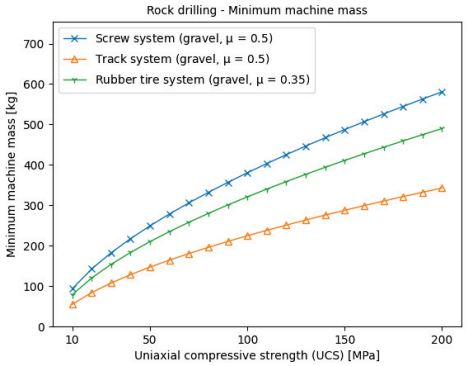

Figure B.39: Rock drilling - Minimum mass

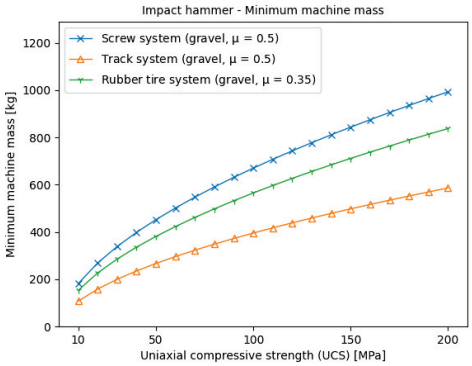

Figure B.40: Impact hammer - Minimum mass

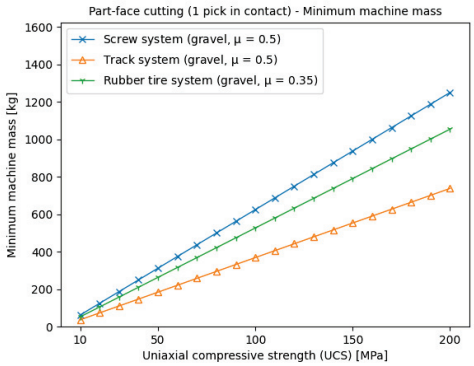

Figure B.41: Part-face cutting (1 pick) - Minimum mass

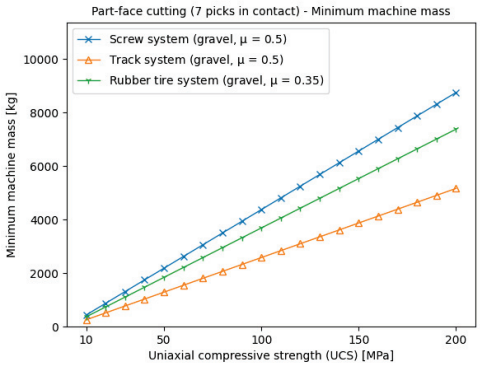

Figure B.42: Part-face cutting (7 picks) - Minimum mass

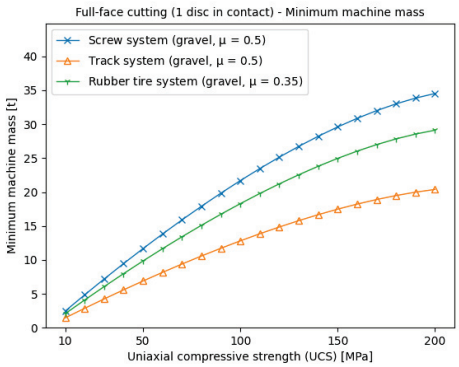

Figure B.43: Full-face cutting (1 disc) - Minimum mass

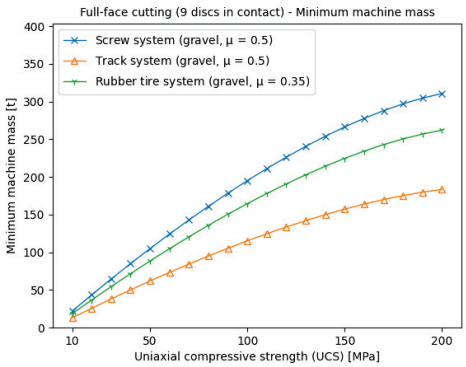

Figure B.44: Full-face cutting (9 discs) - Minimum mass

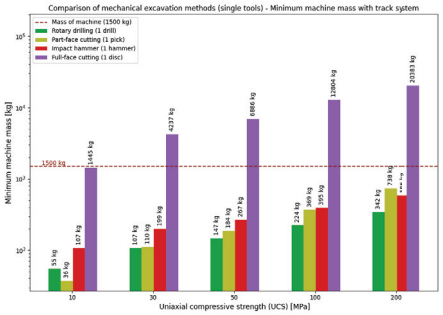

Figure B.45: Comparison of minimum machine masses (single tool use) for track system

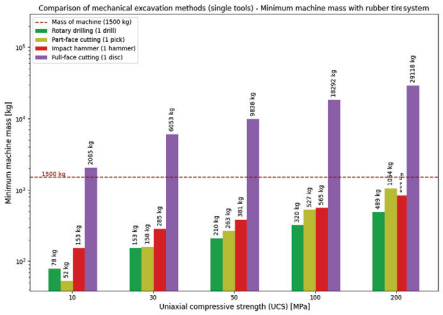

Figure B.46: Comparison of minimum machine masses (single tool use) for tire system

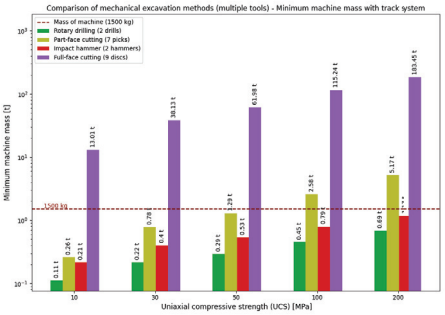

Figure B.47: Comparison of minimum machine masses (multiple tool use) for track system

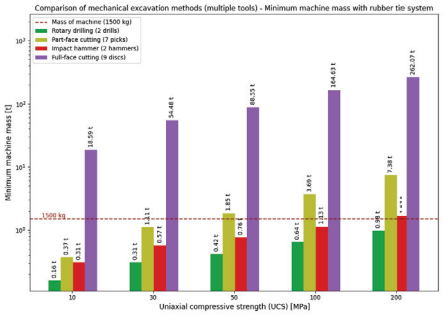

Figure B.48: Comparison of minimum machine masses (multiple tool use) for tire system

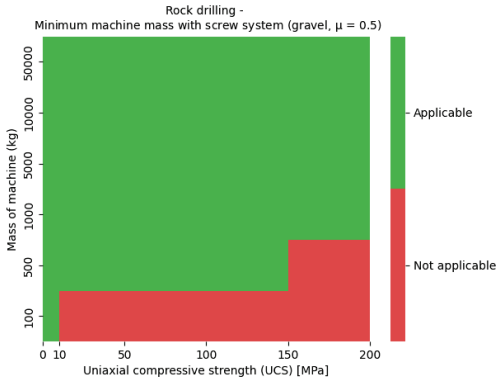

Figure B.49: Rock drilling - Minimum machine masses for screw system

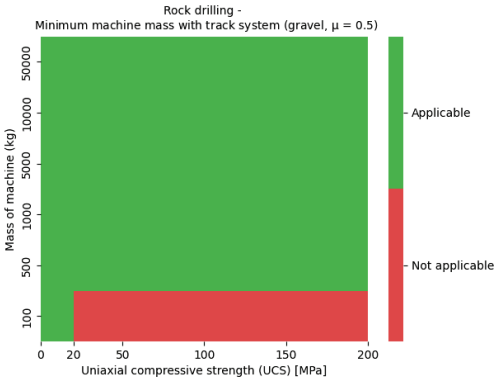

Figure B.50: Rock drilling - Minimum machine masses for track system

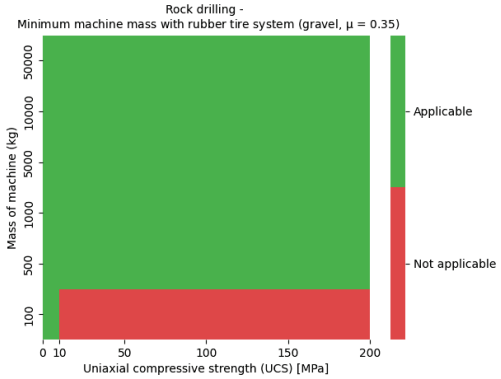

Figure B.51: Rock drilling - Minimum machine masses for tire system

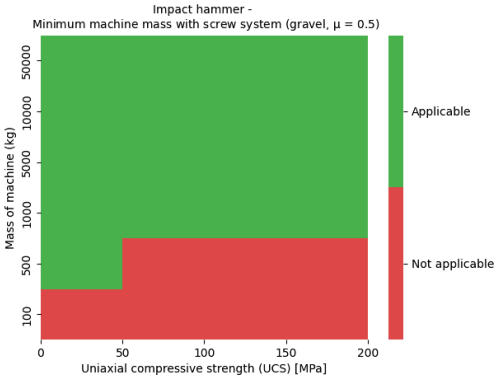

Figure B.52: Impact hammer - Minimum machine masses for screw system

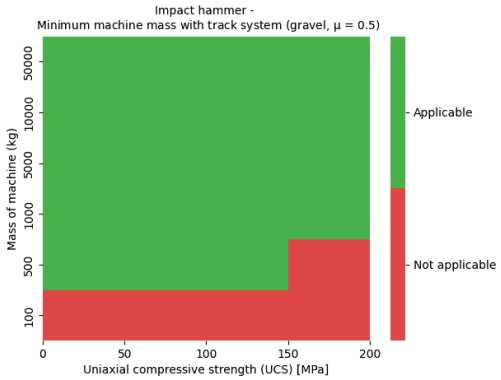

Figure B.53: Impact hammer - Minimum machine masses for track system

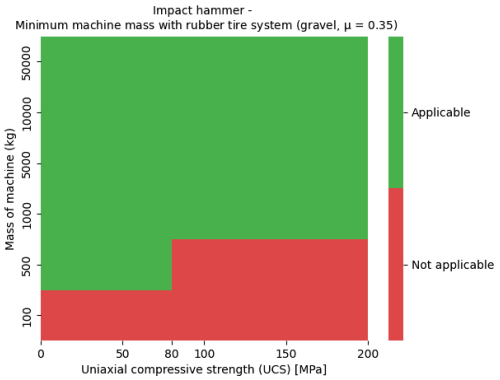

Figure B.54: Impact hammer - Minimum machine masses for tire system

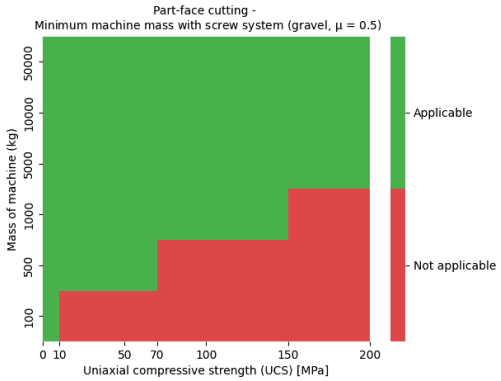

Figure B.55: Part-face cutting - Minimum machine masses for screw system

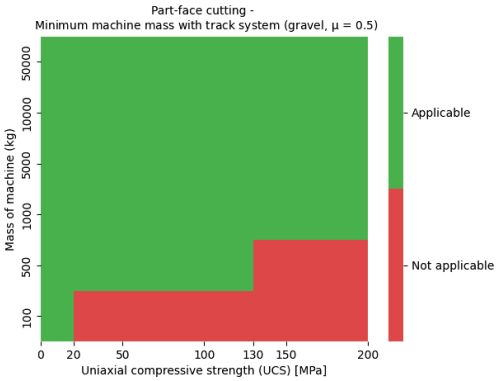

Figure B.56: Part-face cutting - Minimum machine masses for track system

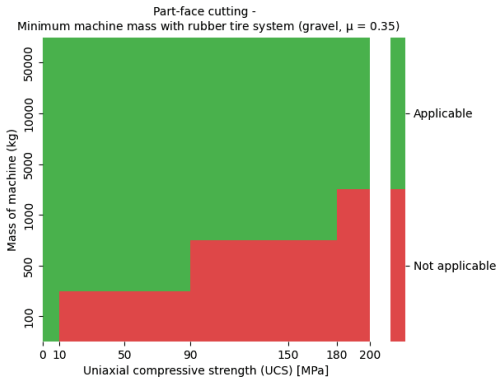

Figure B.57: Part-face cutting - Minimum machine masses for tire system

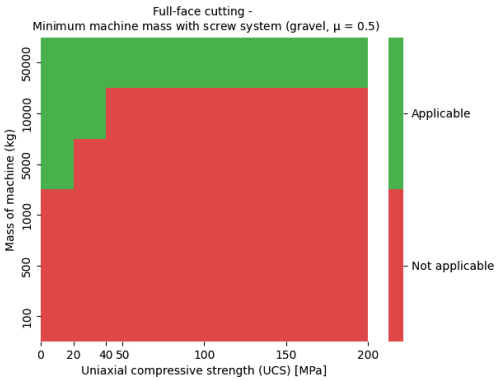

Figure B.58: Full-face cutting - Minimum machine masses for screw system

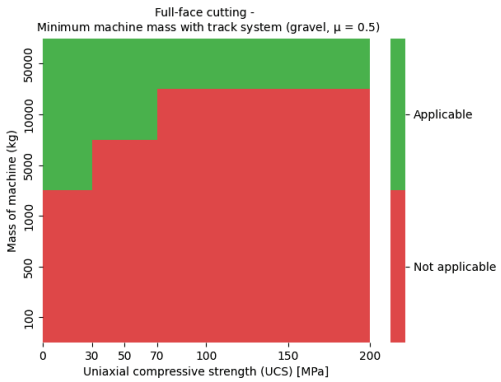

Figure B.59: Full-face cutting - Minimum machine masses for track system

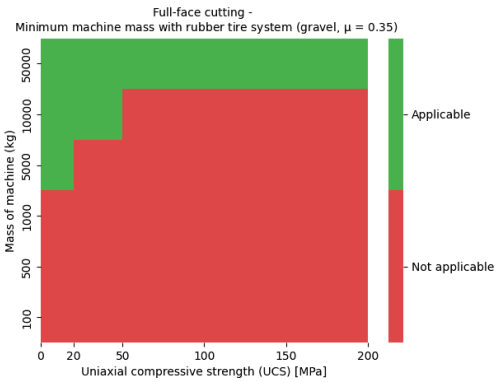

Figure B.60: Full-face cutting - Minimum machine masses for tire system

Reaction forces vs. traction forces

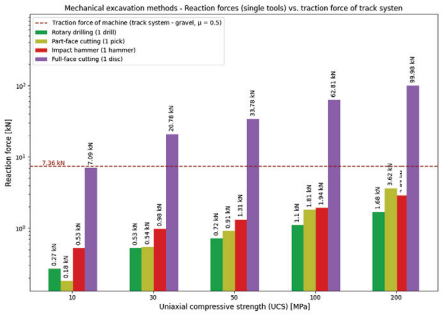

Figure B.61: Reaction forces (single tools) vs. traction forces with track system

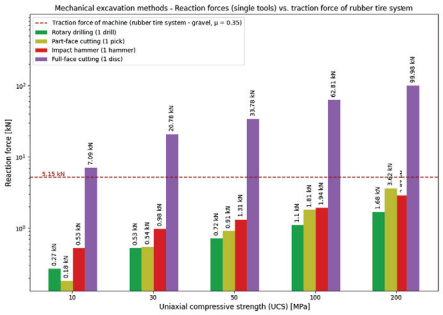

Figure B.62: Reaction forces (single tools) vs. traction forces with tire system

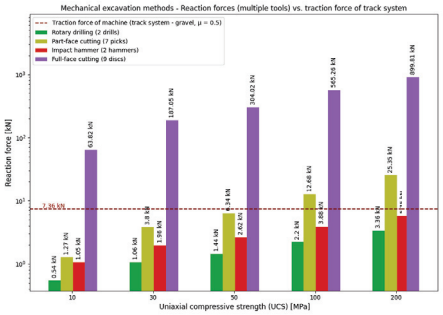

Figure B.63: Reaction forces (multiple tools) vs. traction forces with track system

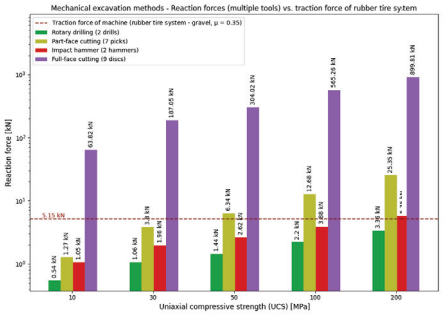

Figure B.64: Reaction forces (multiple tools) vs. traction forces with tire system

B.7 Hydrofracturing

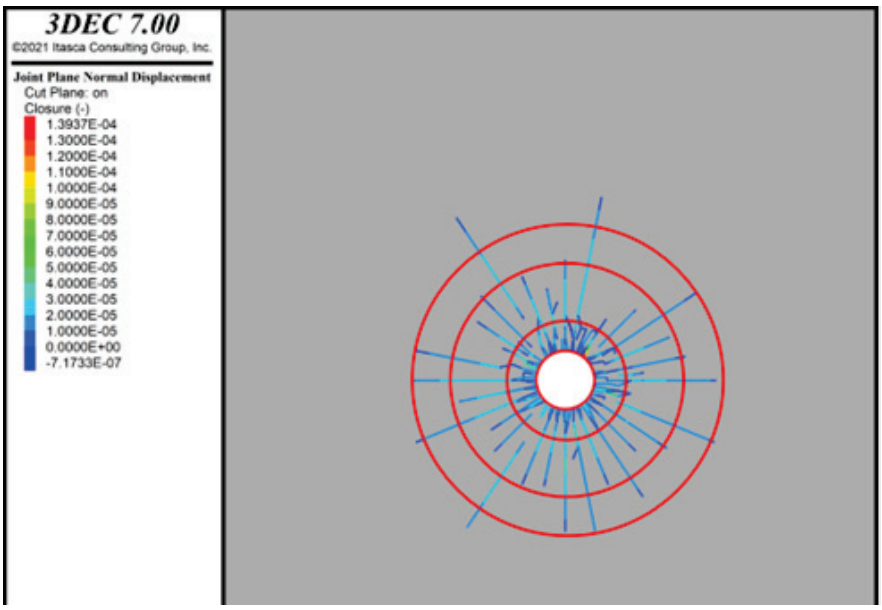

Figure B.65: Distinction of fractures exceeding 10 μm, hydraulic pressure of 50 MPa and flow rate of 2.43 l/s (Granodiorite 1) [137]

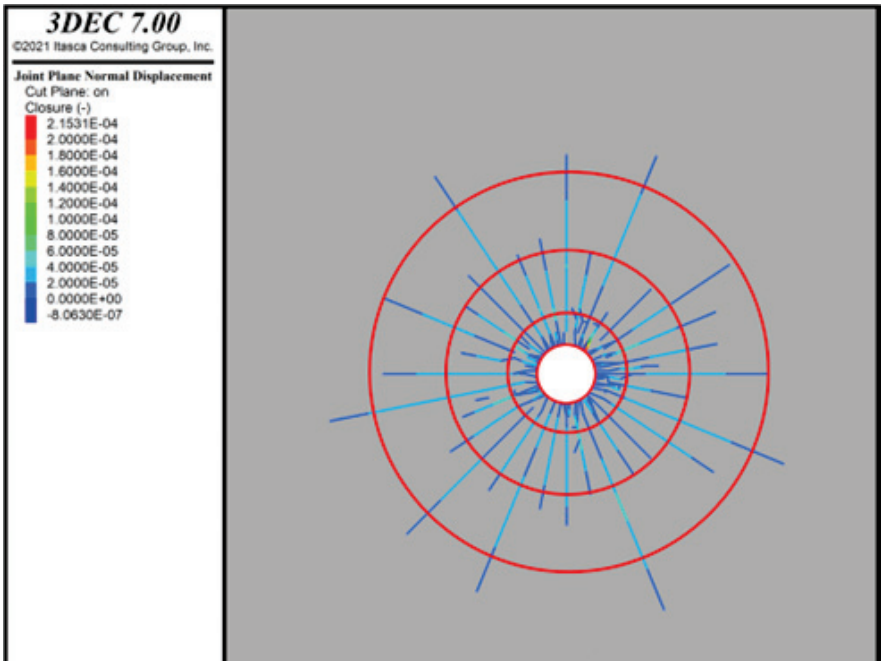

Figure B.66: Distinction of fractures exceeding 10 μm, hydraulic pressure of 60 MPa and flow rate of 2.79 l/s (Granodiorite 1) [137]

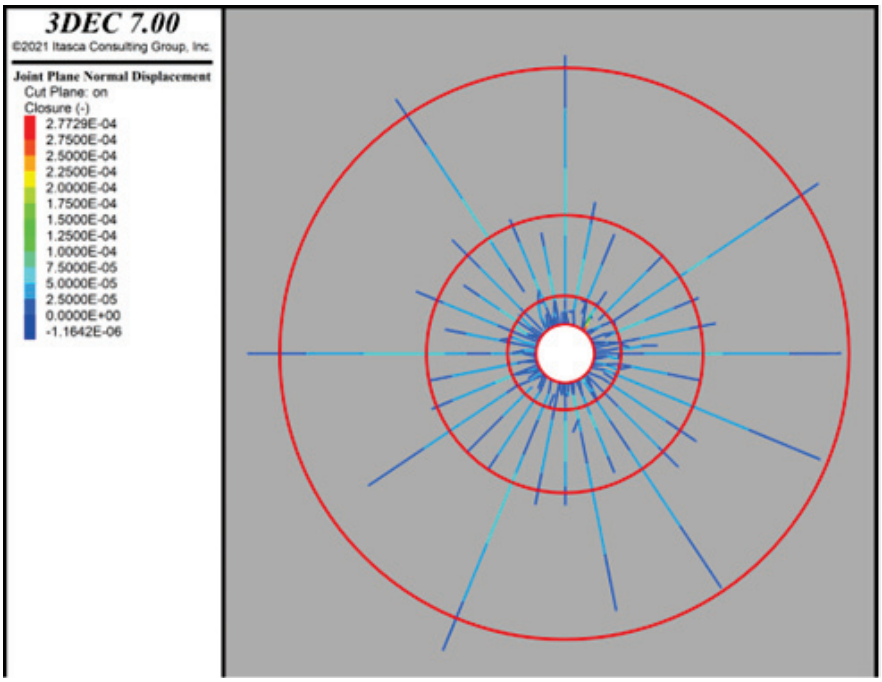

Figure B.67: Distinction of fractures exceeding 10 μm, hydraulic pressure of 70 MPa and flow rate of 4.3 l/s (Granodiorite 1) [137]

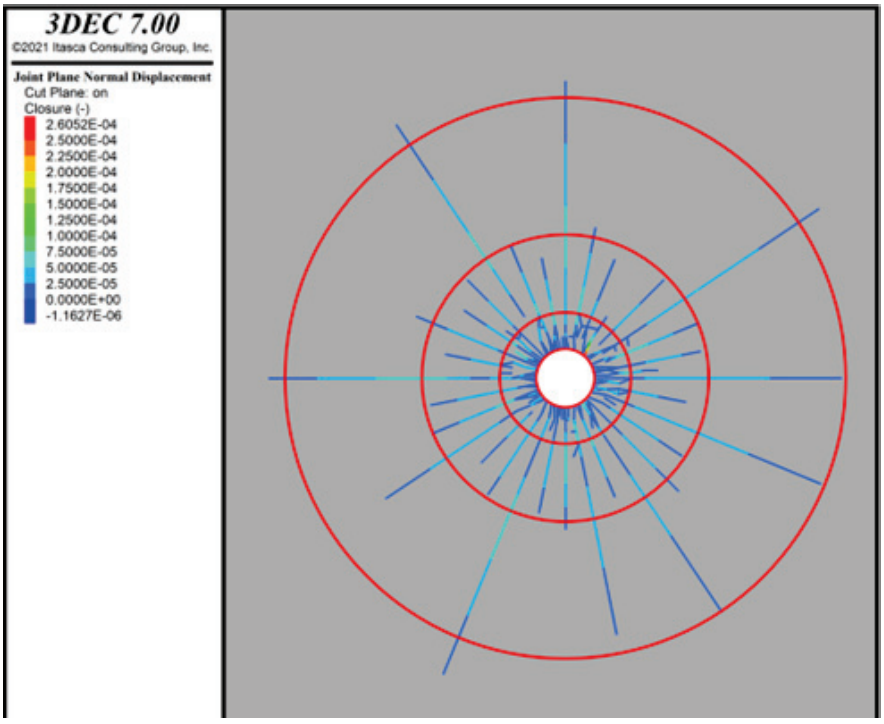

Figure B.68: Distinction of fractures exceeding 10 μm, hydraulic pressure of 70 MPa and flow rate of 4.94 l/s (Granodiorite 1) [137]

C Appendix - Experimental test results

C.1 Slow slew

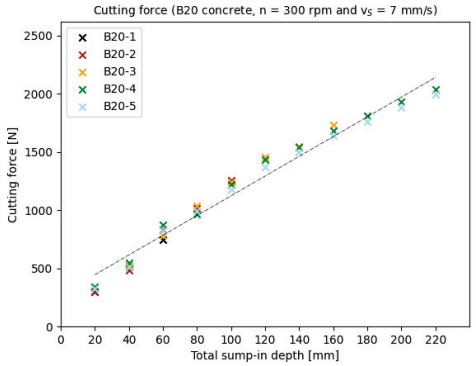

Figure C.1: Cutting forces - B20 concrete

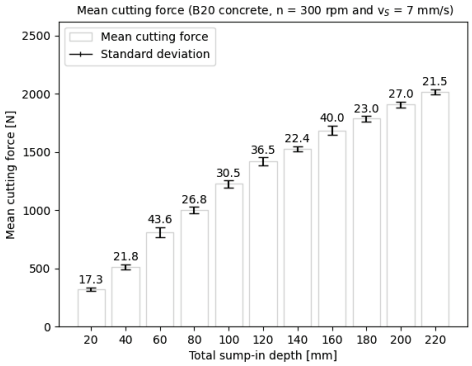

Figure C.2: Mean cutting forces - B20 concrete

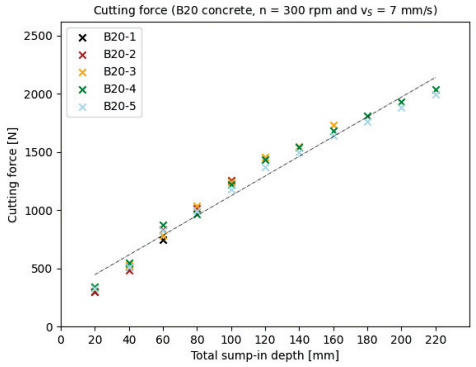

Figure C.3: Cutting forces - B30 concrete

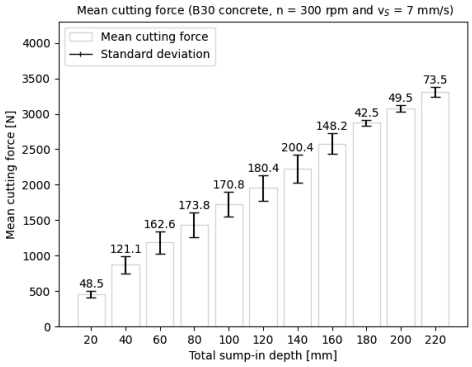

Figure C.4: Mean cutting forces - B30 concrete

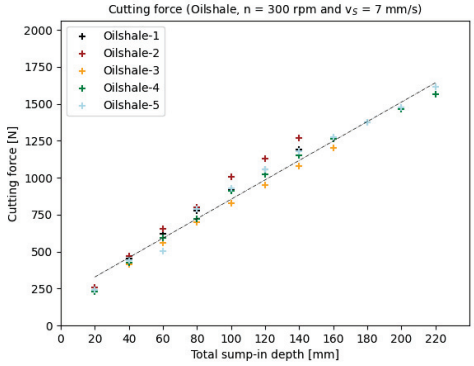

Figure C.5: Cutting forces - Oilshale

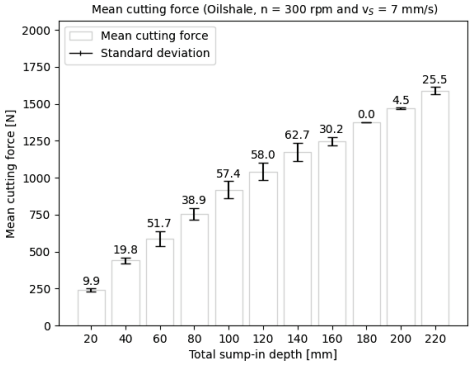

Figure C.6: Mean cutting forces - Oilshale

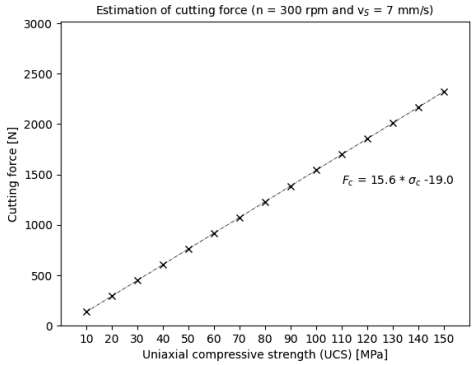

Figure C.7: Cutting forces - Linear regression

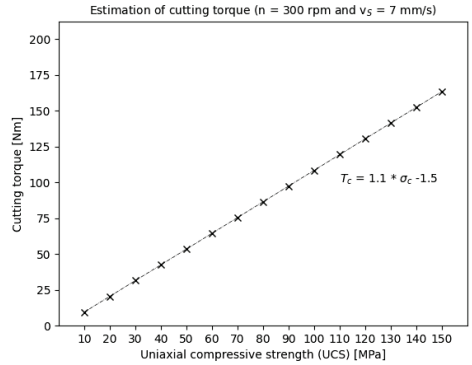

Figure C.8: Cutting torques - Linear regression

Table C.1: Slow slew - Cutting forces B20 concrete

Picks in contact	$F_{c,min}$ [N]	$F_{c,max}$ [N]	$\overline{F_c}$ [N]
1	300	343	320
2	483	550	515
3	745	872	811
4	967	1039	1003
5	1177	1257	1225
6	1367	1453	1417
7	1497	1549	1528
8	1636	1734	1685
9	1763	1809	1786
10	1879	1933	1906
11	1994	2037	2016

Table C.2: Slow slew - Cutting forces B30 concrete

Picks in contact	$F_{c,min}$ [N]	$F_{c,max}$ [N]	$\overline{F_c}$ [N]
1	400	538	459
2	684	1019	875
3	947	1402	1185
4	1194	1660	1436
5	1494	1947	1726
6	1700	2163	1956
7	1938	2451	2227
8	2380	2733	2581
9	2831	2916	2873
10	3029	3128	3079
11	3237	3384	3311

Table C.3: Slow slew - Cutting forces Oilshale

Picks in contact	$F_{c,min}$ [N]	$F_{c,max}$ [N]	$\overline{F_c}$ [N]
1	229	257	241
2	414	469	442
3	505	657	587
4	700	800	757
5	828	1009	919
6	951	1130	1042
7	1078	1272	1174
8	1205	1273	1247
9	1378	1378	1378
10	1465	1474	1470
11	1563	1614	1588

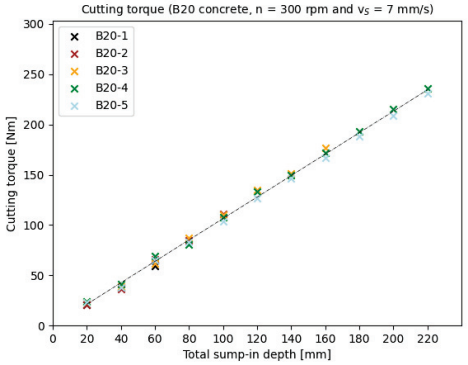

Figure C.9: Cutting torques - B20 concrete

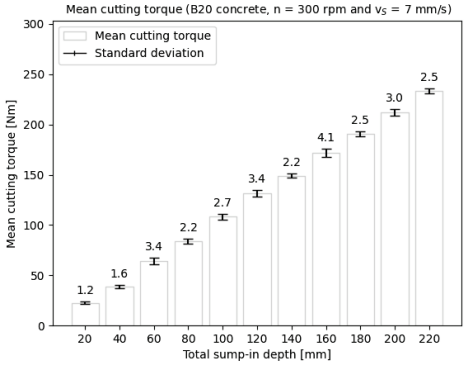

Figure C.10: Mean cutting torques - B20 concrete

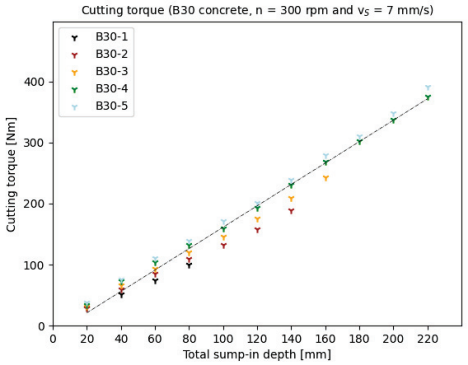

Figure C.11: Cutting torques - B30 concrete

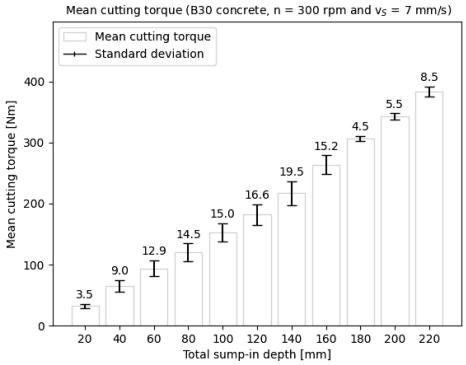

Figure C.12: Mean cutting torques - B30 concrete

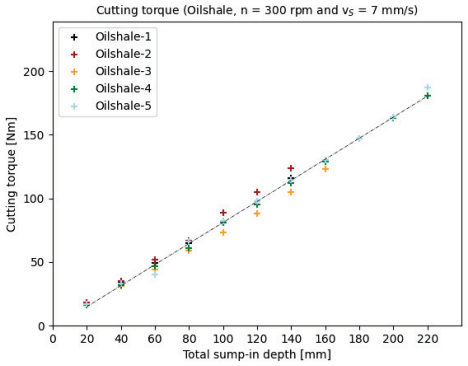

Figure C.13: Cutting torques - Oilshale

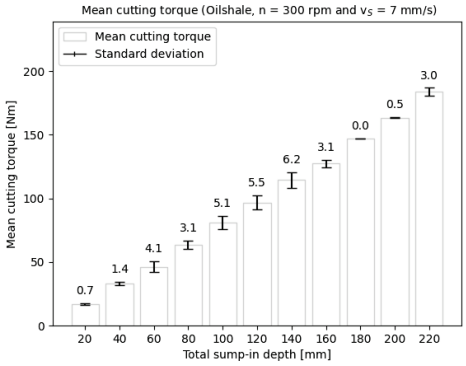

Figure C.14: Mean cutting torques - Oilshale

Table C.4: Slow slew - Cutting torques B20 concrete

Picks in contact	$T_{c,min}$ [Nm]	$T_{c,max}$ [Nm]	$\overline{T_c}$ [Nm]
1	21	24	22
2	36	41	38
3	59	69	64
4	81	87	84
5	104	111	108
6	127	135	132
7	146	151	149
8	167	177	172
9	188	193	191
10	209	215	212
11	231	236	234

Table C.5: Slow slew - Cutting torques B30 concrete

Picks in contact	$T_{c,min}$ [Nm]	$T_{c,max}$ [Nm]	$\overline{T_c}$ [Nm]
1	28	38	32
2	51	76	65
3	75	111	94
4	100	139	120
5	137	172	152
6	158	201	182
7	189	239	217
8	243	279	264
9	302	311	307
10	337	348	343
11	375	392	384

Table C.6: Slow slew - Cutting torques Oilshale

Picks in contact	$T_{c,min}$ [Nm]	$T_{c,max}$ [Nm]	$\overline{T_c}$ [Nm]
1	16	18	17
2	31	33	35
3	40	52	46
4	59	67	63
5	73	89	81
6	88	105	97
7	105	124	114
8	123	130	127
9	147	147	147
10	163	164	164
11	181	187	184

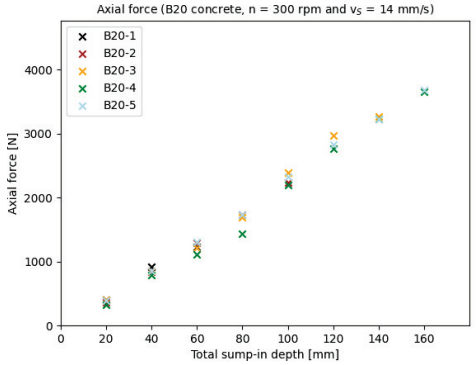

Figure C.15: Axial forces - B20 concrete

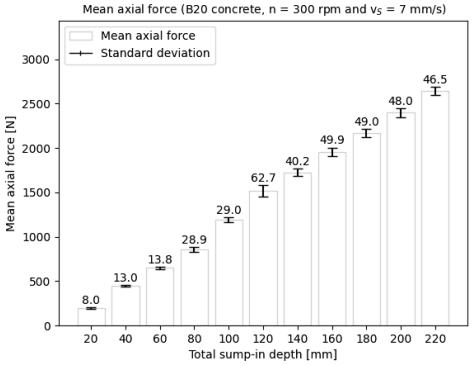

Figure C.16: Mean axial forces - B20 concrete

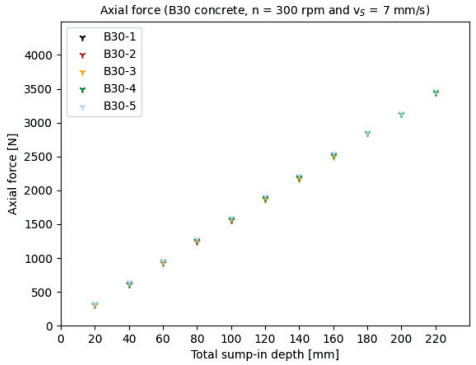

Figure C.17: Axial forces - B30 concrete

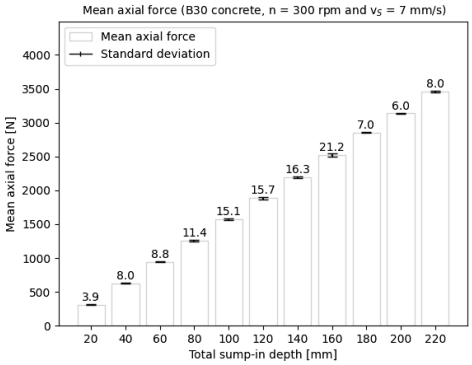

Figure C.18: Mean axial forces - B30 concrete

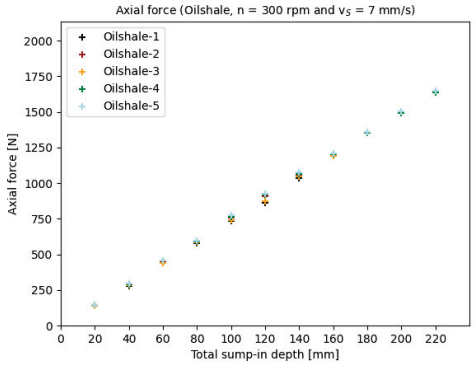

Figure C.19: Axial forces - Oilshale

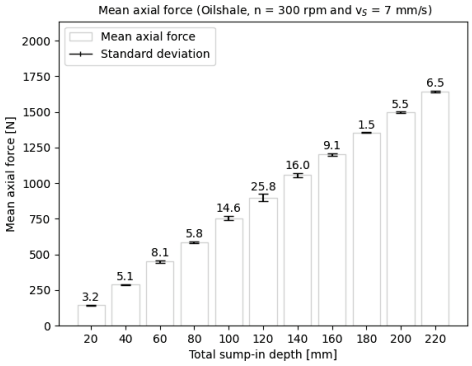

Figure C.20: Mean axial forces - Oilshale

Table C.7: Slow slew - Axial forces B20 concrete

Picks in contact	$F_{a,min}$ [N]	$F_{a,max}$ [N]	$\overline{F_a}$ [N]
1	186	210	199
2	434	471	447
3	637	670	652
4	810	884	859
5	1155	1230	1194
6	1430	1566	1519
7	1669	1758	1726
8	1886	2000	1956
9	2120	2218	2169
10	2349	2445	2397
11	2597	2690	2644

Table C.8: Slow slew - Axial forces B30 concrete

Picks in contact	$F_{a,min}$ [N]	$F_{a,max}$ [N]	$\overline{F_a}$ [N]
1	306	317	312
2	614	635	627
3	932	957	944
4	1244	1277	1258
5	1556	1594	1572
6	1867	1908	1884
7	2172	2216	2191
8	2492	2544	2518
9	2845	2859	2852
10	3132	3144	3138
11	3451	3467	3459

Table C.9: Slow slew - Axial forces Oilshale

Picks in contact	$F_{a,min}$ [N]	$F_{a,max}$ [N]	$\overline{F_a}$ [N]
1	139	147	143
2	280	294	287
3	438	460	450
4	577	594	585
5	734	773	754
6	862	927	897
7	1033	1078	1056
8	1189	1211	1201
9	1353	1356	1355
10	1490	1501	1496
11	1636	1649	1643

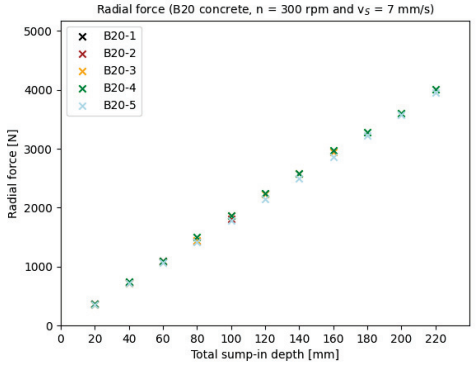

Figure C.21: Radial forces - B20 concrete

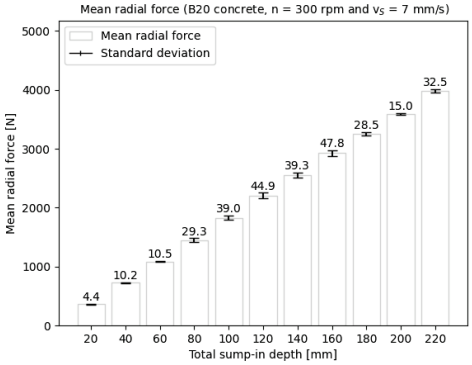

Figure C.22: Mean radial forces - B20 concrete

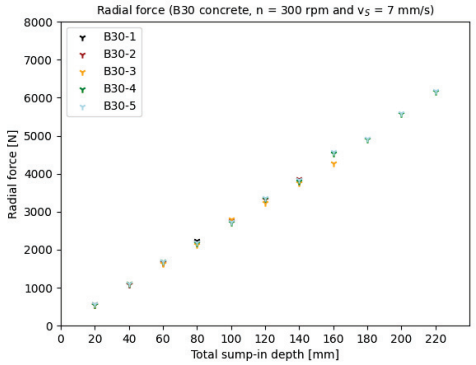

Figure C.23: Radial forces - B30 concrete

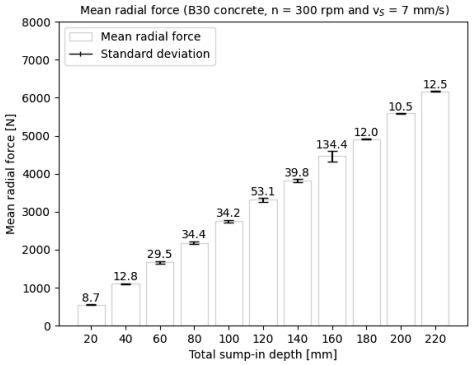

Figure C.24: Mean radial forces - B30 concrete

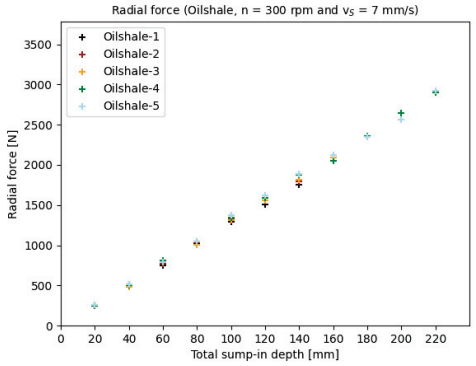

Figure C.25: Radial forces - Oilshale

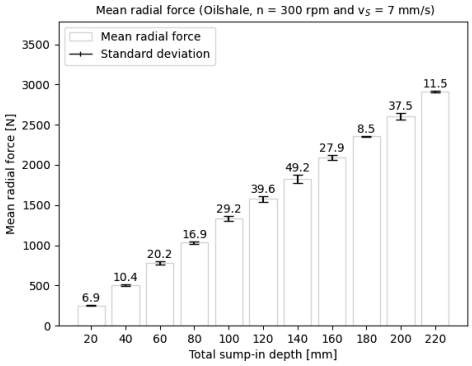

Figure C.26: Mean radial forces - Oilshale

Table C.10: Slow slew - Radial forces B20 concrete

Picks in contact	$F_{r,min}$ [N]	$F_{r,max}$ [N]	$\overline{F_r}$ [N]
1	357	370	363
2	715	744	727
3	1071	1102	1086
4	1422	1500	1452
5	1776	1870	1830
6	2147	2250	2210
7	2501	2588	2556
8	2863	2977	2928
9	3229	3286	3258
10	3577	3607	3592
11	3952	4017	3985

Table C.11: Slow slew - Radial forces B30 concrete

Picks in contact	$F_{r,min}$ [N]	$F_{r,max}$ [N]	$\overline{F_r}$ [N]
1	538	560	550
2	1088	1119	1102
3	1620	1704	1668
4	2126	2227	2183
5	2709	2803	2752
6	3226	3370	3313
7	3764	3868	3822
8	4274	4579	4462
9	4896	4920	4908
10	5578	5599	5589
11	6152	6177	6165

Table C.12: Slow slew - Radial forces Oilshale

Picks in contact	$F_{r,min}$ [N]	$F_{r,max}$ [N]	$\overline{F_r}$ [N]
1	243	263	251
2	486	516	503
3	750	809	783
4	1001	1047	1032
5	1292	1376	1332
6	1507	1625	1575
7	1758	1888	1827
8	2055	2123	2090
9	2345	2362	2353
10	2568	2643	2606
11	3952	4017	3985

C.2 Fast slew

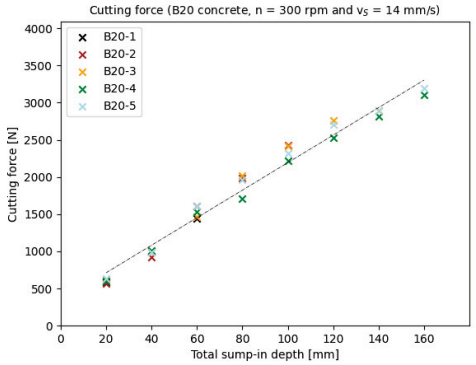

Figure C.27: Cutting forces - B20 concrete

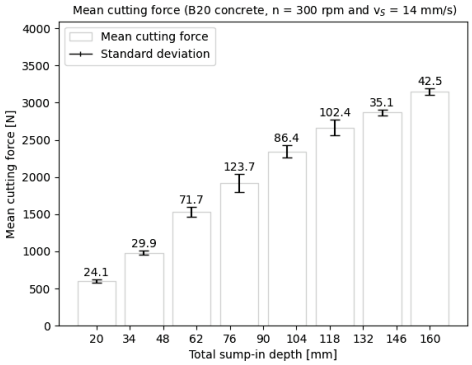

Figure C.28: Mean cutting forces - B20 concrete

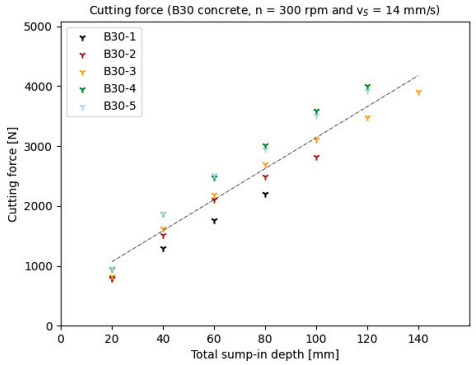

Figure C.29: Cutting forces - B30 concrete

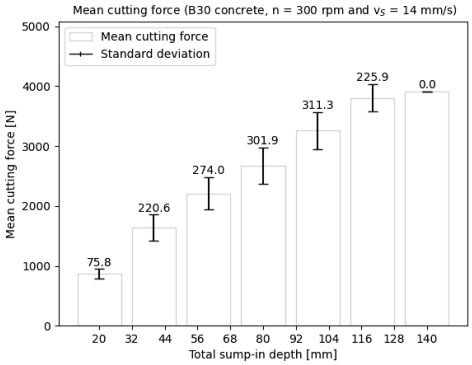

Figure C.30: Mean cutting forces - B30 concrete

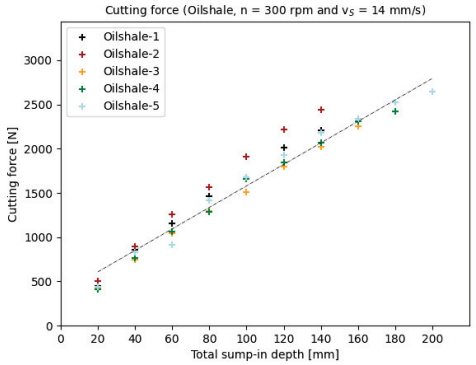

Figure C.31: Cutting forces - Oilshale

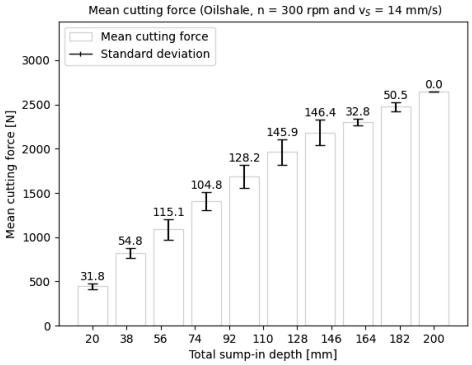

Figure C.32: Mean cutting forces - Oilshale

Table C.13: Fast slew - Cutting forces B20 concrete

Test sample	$F_{c,min}$ [N]	$F_{c,max}$ [N]	$\overline{F_c}$ [N]
1	563	629	601
2	924	1007	982
3	1438	1613	1531
4	1708	2020	1920
5	2215	2427	2344
6	2525	2766	2666
7	2818	2893	2868
8	3107	3192	3149
9	-	-	-
10	-	-	-
11	-	-	-

Table C.14: Fast slew - Cutting forces B30 concrete

Test sample	$F_{c,min}$ [N]	$F_{c,max}$ [N]	$\overline{F_c}$ [N]
1	788	966	869
2	1295	1877	1635
3	1759	2515	2210
4	2199	3019	2671
5	2821	3597	3259
6	3489	4004	3805
7	3911	3911	3911
8	-	-	-
9	-	-	-
10	-	-	-
11	-	-	-

Table C.15: Fast slew - Cutting forces Oilshale

Test sample	$F_{c,min}$ [N]	$F_{c,max}$ [N]	$\overline{F_c}$ [N]
1	412	504	446
2	751	891	819
3	912	1256	1086
4	1288	1566	1405
5	1513	1913	1689
6	1800	2215	1961
7	2020	2442	2182
8	2257	2336	2300
9	2424	2525	2474
10	2646	2646	2646
11	-	-	-

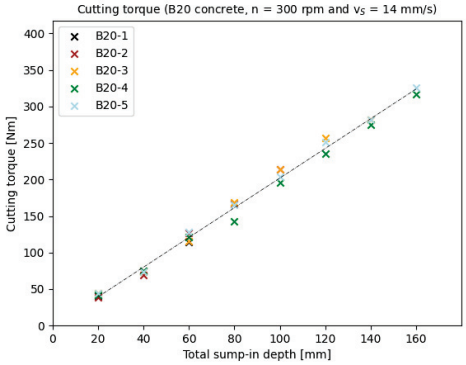

Figure C.33: Cutting torques - B20 concrete

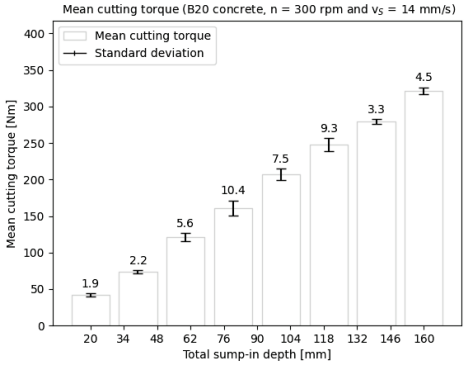

Figure C.34: Mean cutting torques - B20 concrete

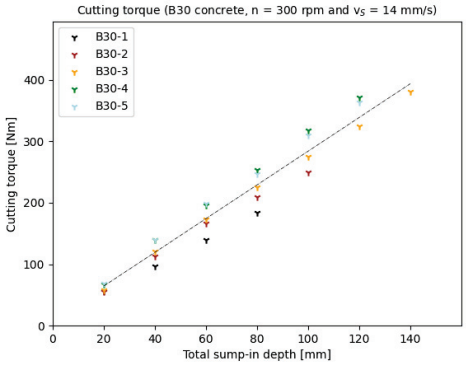

Figure C.35: Cutting torques - B30 concrete

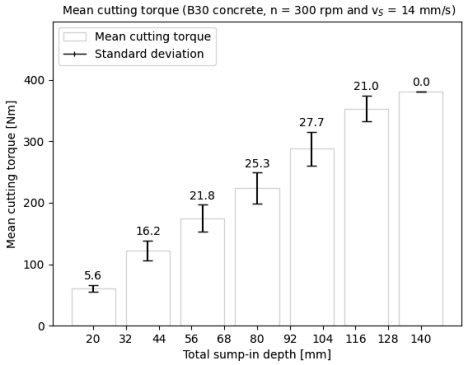

Figure C.36: Mean cutting torques - B30 concrete

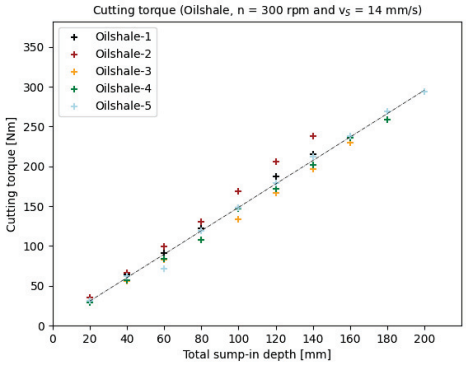

Figure C.37: Cutting torques - Oilshale

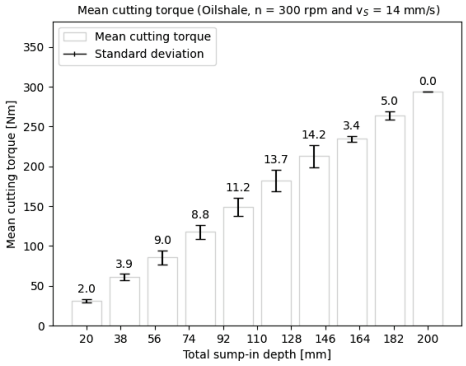

Figure C.38: Mean cutting torques - Oilshale

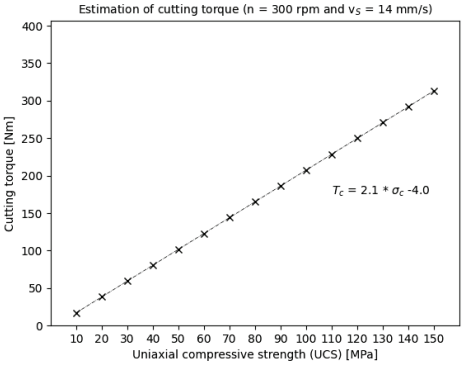

Figure C.39: Cutting torques - Linear regression

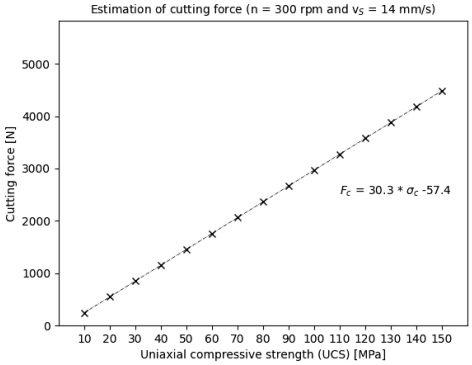

Figure C.40: Cutting forces - Linear regression

Table C.16: Fast slew - Cutting torques B20 concrete

Picks in contact	$T_{c,min}$ [Nm]	$T_{c,max}$ [Nm]	$\overline{T_c}$ [Nm]
1	39	44	42
2	69	75	73
3	114	128	121
4	143	169	161
5	196	214	207
6	235	257	248
7	275	282	280
8	317	326	321
9	-	-	-
10	-	-	-
11	-	-	-

Table C.17: Fast slew - Cutting torques B30 concrete

Picks in contact	$T_{c,min}$ [Nm]	$T_{c,max}$ [Nm]	$\overline{T_c}$ [Nm]
1	55	68	61
2	97	140	122
3	139	199	175
4	184	253	224
5	249	318	288
6	324	372	354
7	381	381	381
8	-	-	-
9	-	-	-
10	-	-	-
11	-	-	-

Table C.18: Fast slew - Cutting torques Oilshale

Picks in contact	$T_{c,min}$ [Nm]	$T_{c,max}$ [Nm]	$\overline{T_c}$ [Nm]
1	29	35	31
2	56	66	61
3	72	99	86
4	108	131	118
5	134	169	149
6	167	206	182
7	197	238	213
8	230	238	235
9	259	269	264
10	294	294	294
11	-	-	-

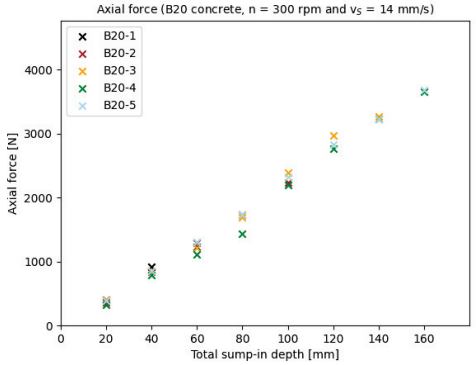

Figure C.41: Axial forces - B20 concrete

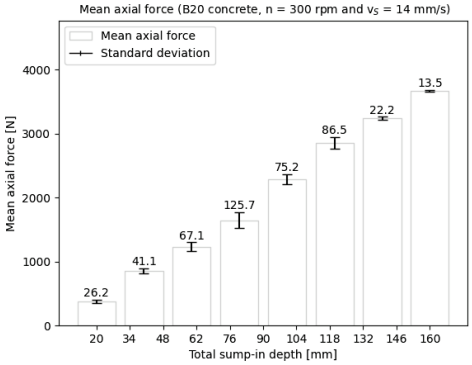

Figure C.42: Mean axial forces - B20 concrete

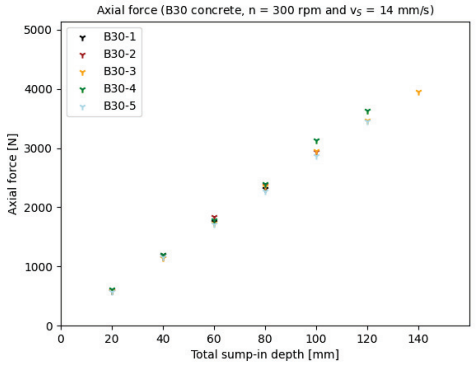

Figure C.43: Axial forces - B20 concrete

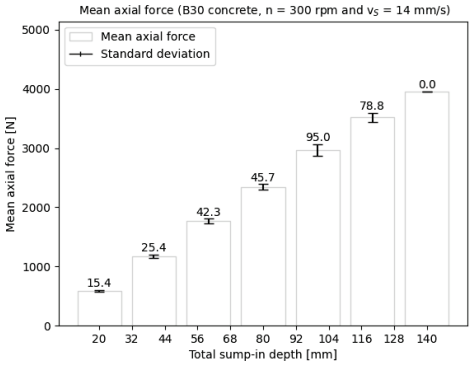

Figure C.44: Mean axial forces - B30 concrete

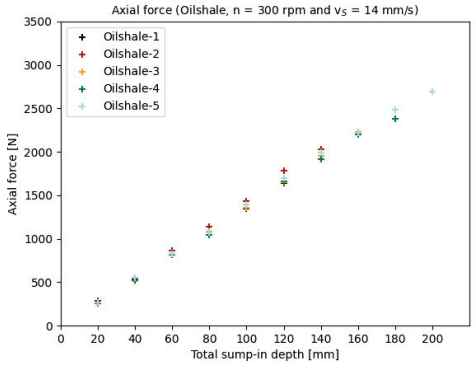

Figure C.45: Axial forces - Oilshale

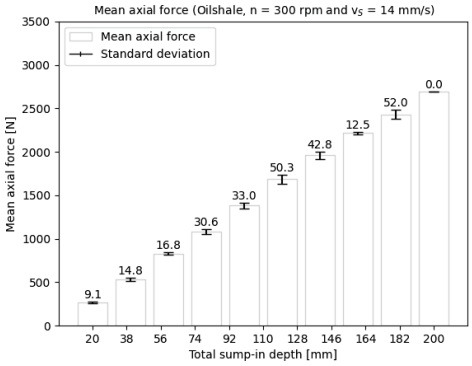

Figure C.46: Mean axial forces - Oilshale

Table C.19: Fast slew - Axial forces B20 concrete

Picks in contact	$F_{a,min}$ [N]	$F_{a,max}$ [N]	$\overline{F_a}$ [N]
1	328	398	375
2	795	924	854
3	1117	1306	1232
4	1430	1734	1646
5	2198	2389	2284
6	2762	2970	2855
7	3221	3269	3237
8	3653	3680	3666
9	-	-	-
10	-	-	-
11	-	-	-

Table C.20: Fast slew - Axial forces B30 concrete

Picks in contact	$F_{a,min}$ [N]	$F_{a,max}$ [N]	$\overline{F_a}$ [N]
1	568	613	592
2	1141	1203	1173
3	1716	1834	1765
4	2270	2398	2343
5	2869	3126	2970
6	3459	3630	3519
7	3955	3955	3955
8	-	-	-
9	-	-	-
10	-	-	-
11	-	-	-

Table C.21: Fast slew - Axial forces Oilshale

Picks in contact	$F_{a,min}$ [N]	$F_{a,max}$ [N]	$\overline{F_a}$ [N]
1	257	282	265
2	513	551	532
3	815	862	831
4	1047	1139	1084
5	1344	1436	1385
6	1644	1780	1644
7	1915	2028	1962
8	2198	2227	2215
9	2380	2484	2432
10	2694	2694	2694
11	-	-	-

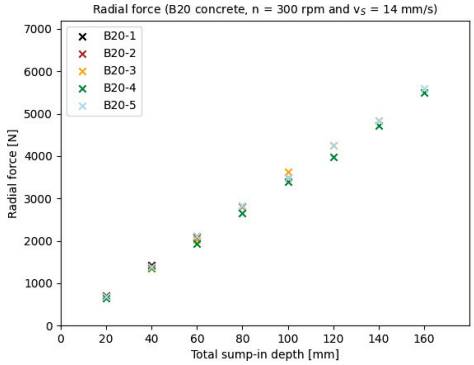

Figure C.47: Radial forces - B20 concrete

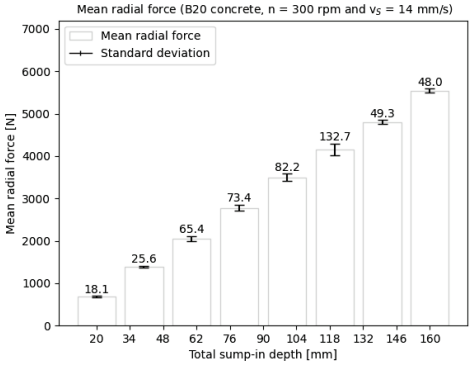

Figure C.48: Mean radial forces - B20 concrete

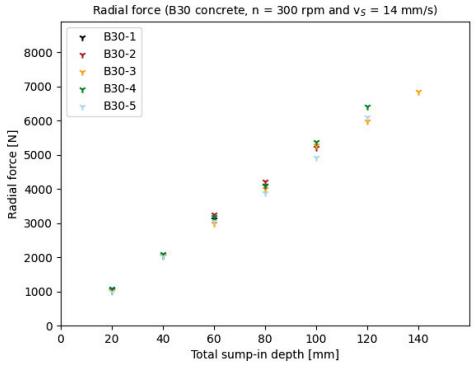

Figure C.49: Radial forces - B20 concrete

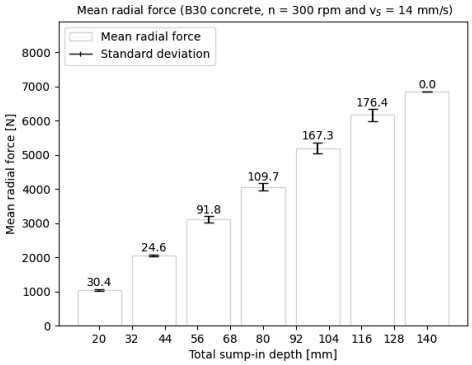

Figure C.50: Mean radial forces - B30 concrete

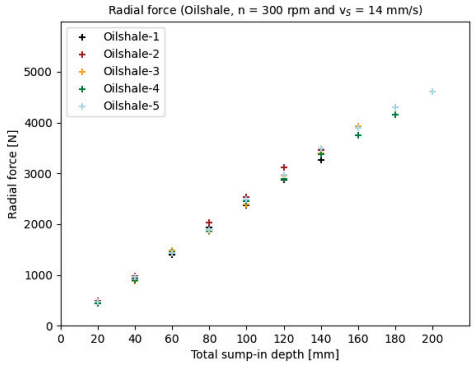

Figure C.51: Radial forces - Oilshale

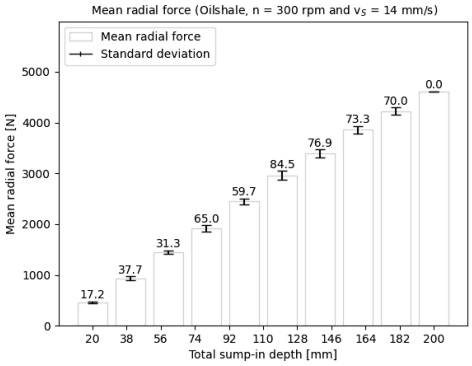

Figure C.52: Mean radial forces - Oilshale

Table C.22: Fast slew - Radial forces B20 concrete

Picks in contact	$F_{r,min}$ [N]	$F_{r,max}$ [N]	$\overline{F_r}$ [N]
1	653	710	683
2	1355	1425	1387
3	1933	2108	2052
4	2649	2824	2776
5	3388	3620	3499
6	3969	4251	4157
7	4727	4834	4797
8	5490	5586	5538
9	-	-	-
10	-	-	-
11	-	-	-

Table C.23: Fast slew - Radial forces B30 concrete

Picks in contact	$F_{r,min}$ [N]	$F_{r,max}$ [N]	$\overline{F_r}$ [N]
1	1002	1080	1043
2	2041	2109	2062
3	2987	3250	3118
4	3896	4217	4065
5	4928	5370	5200
6	5991	6410	6170
7	6854	6854	6854
8	-	-	-
9	-	-	-
10	-	-	-
11	-	-	-

Table C.24: Fast slew - Radial forces Oilshale

Picks in contact	$F_{r,min}$ [N]	$F_{r,max}$ [N]	$\overline{F_r}$ [N]
1	449	493	464
2	882	980	933
3	1401	1484	1447
4	1852	2029	1912
5	2365	2527	2446
6	2873	3111	2961
7	3260	3484	3394
8	3754	3922	3856
9	4155	4295	4225
10	4610	4610	4610
11	-	-	-

D Appendix - Modelling approach

D.1 Rock cutting theories - Parameter studies

General

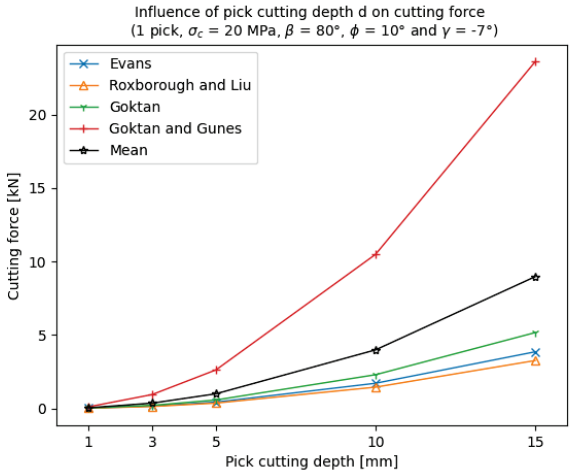

Figure D.1: Cutting forces depending on pick cutting depth

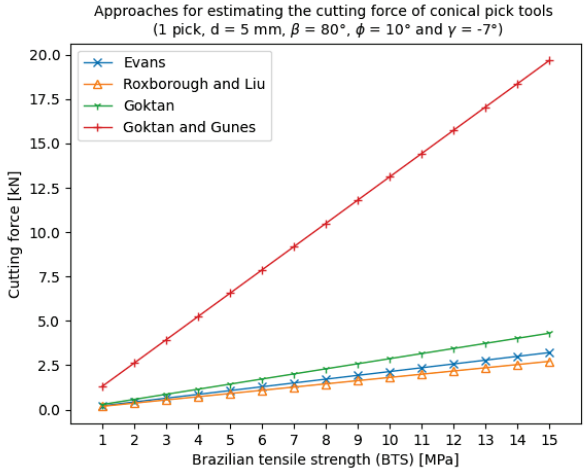

Figure D.2: Cutting forces depending on tensile strength of the rock

Theory of Evans [163]

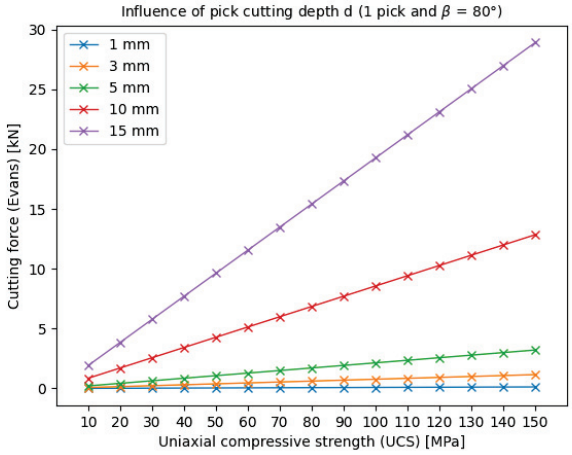

(a) Pick cutting depth

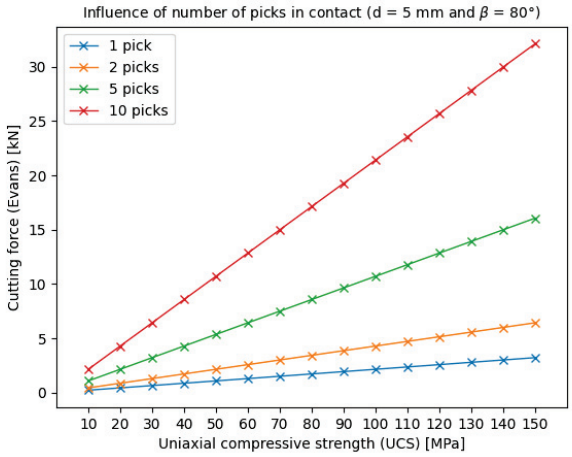

(b) Number of picks in contact

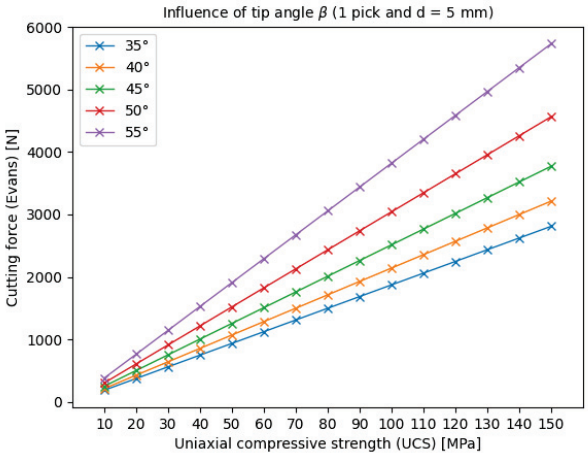

(c) Tip angle

Figure D.3: Influence of parameters on cutting force

Theory of Roxborough [92]

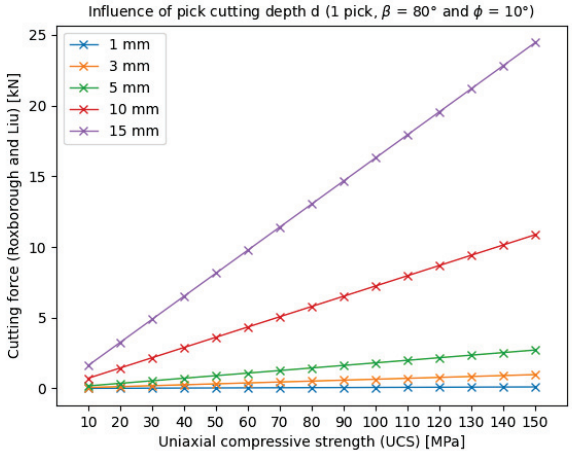

(a) Pick cutting depth

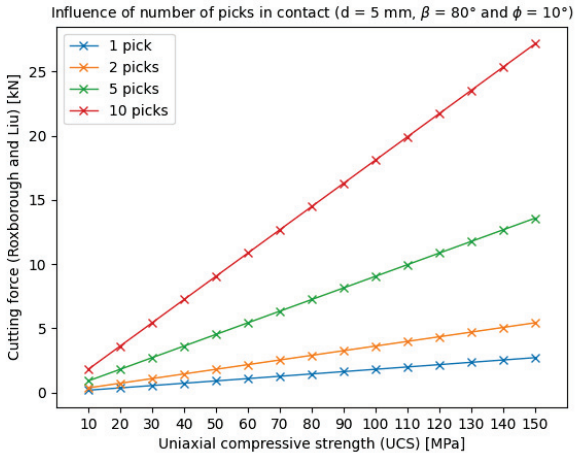

(b) Number of picks in contact

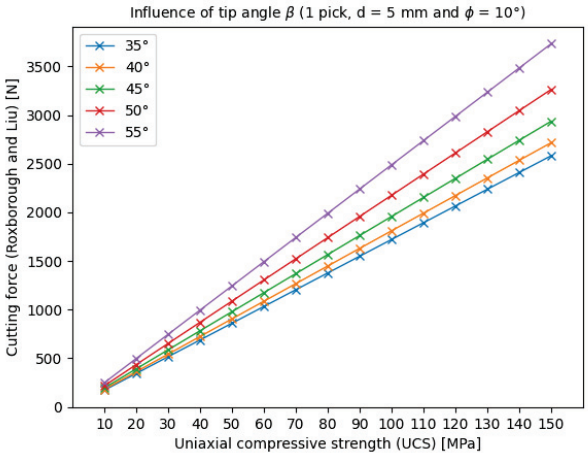

(c) Tip angle

Figure D.4: Influence of parameters on cutting force

Theory of Goktan [164]

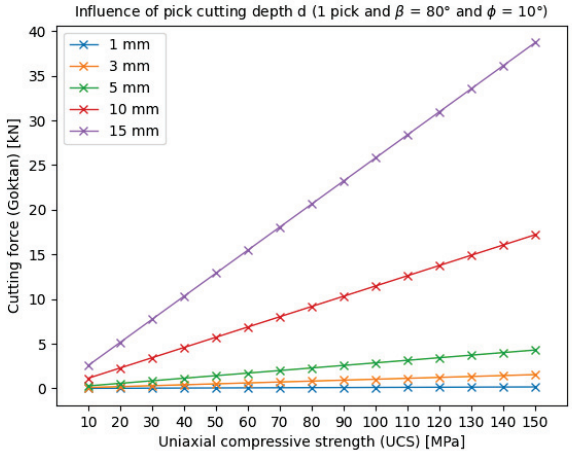

(a) Pick cutting depth

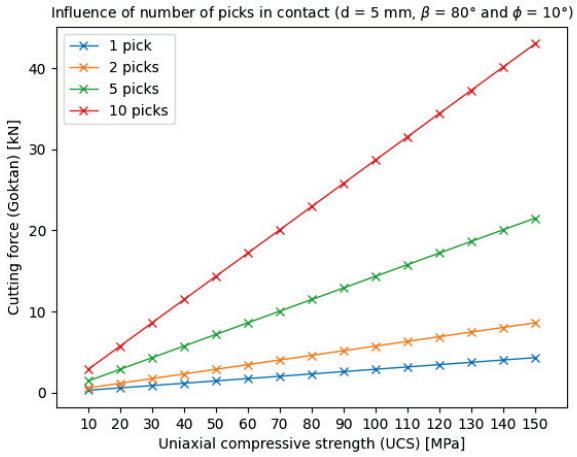

(b) Number of picks in contact

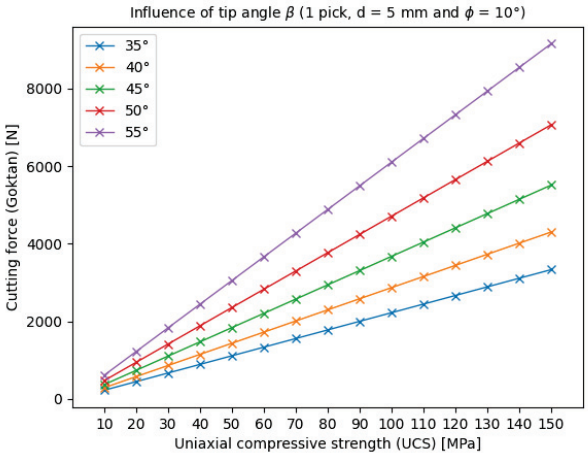

(c) Tip angle

Figure D.5: Influence of parameters on cutting force

Theory of Goktan and Gunes [165]

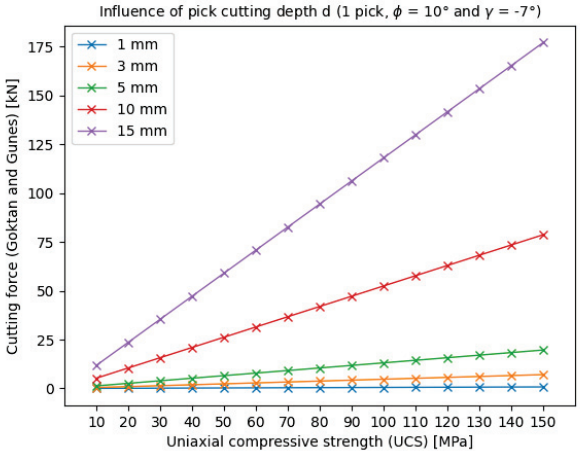

(a) Pick cutting depth

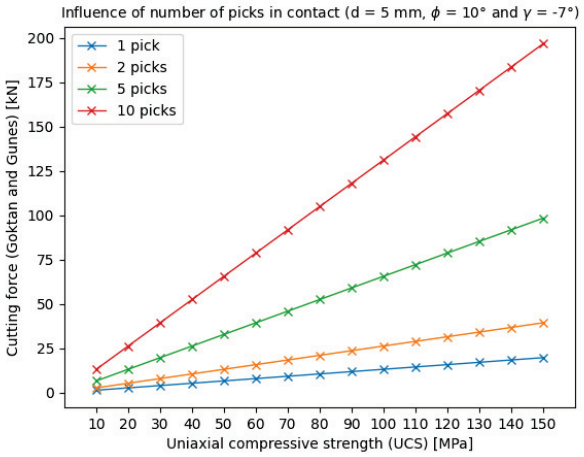

(b) Number of picks in contact

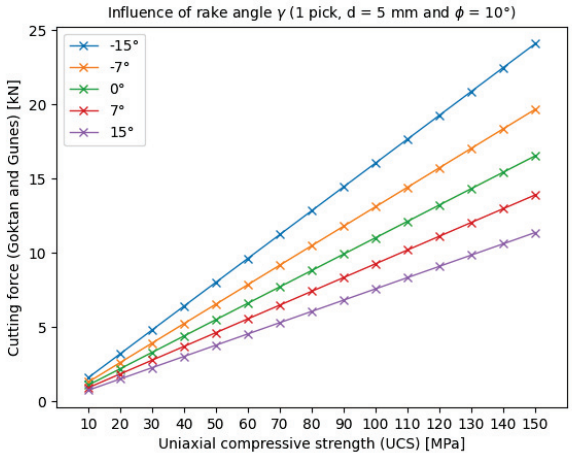

(c) Rake angle

Figure D.6: Influence of parameters on cutting force

D.2 Part-face cutter head simulation model

Full contact cutting

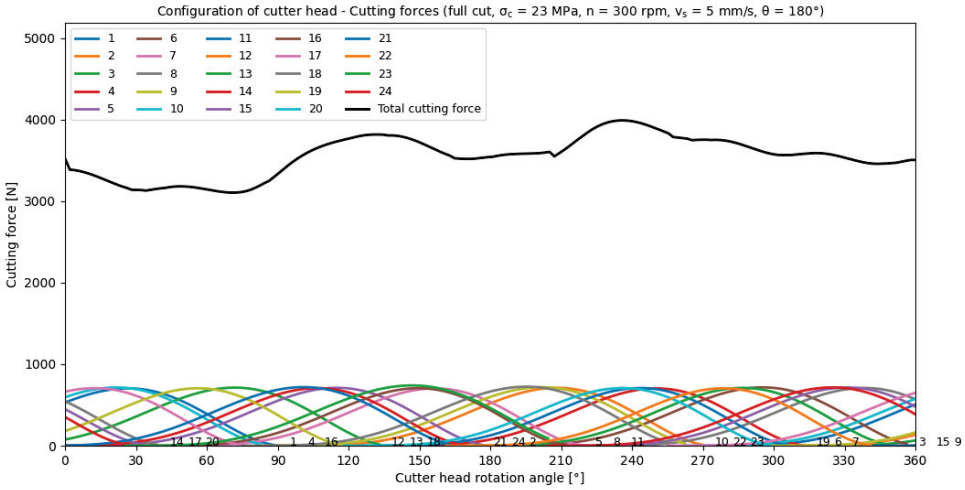

(a) Pick cutting forces

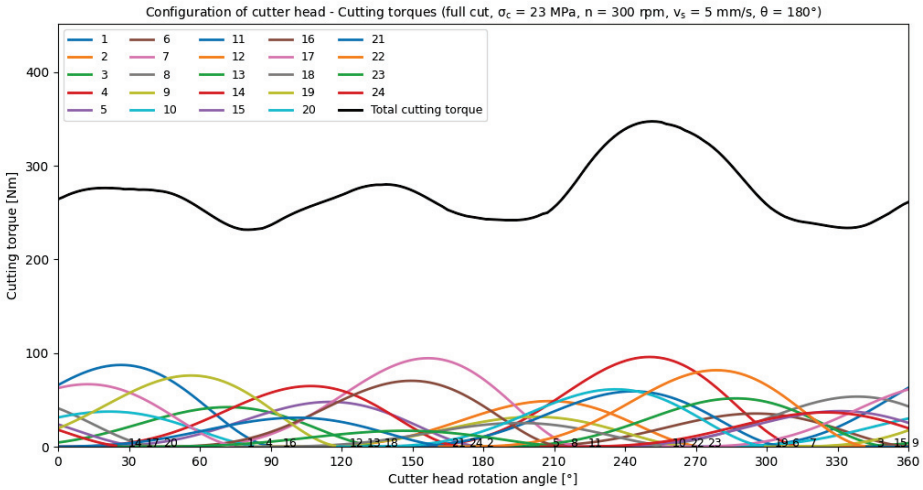

(b) Pick cutting torques

Figure D.7: Full contact cutting - Cutting parameters

Progressive cutting

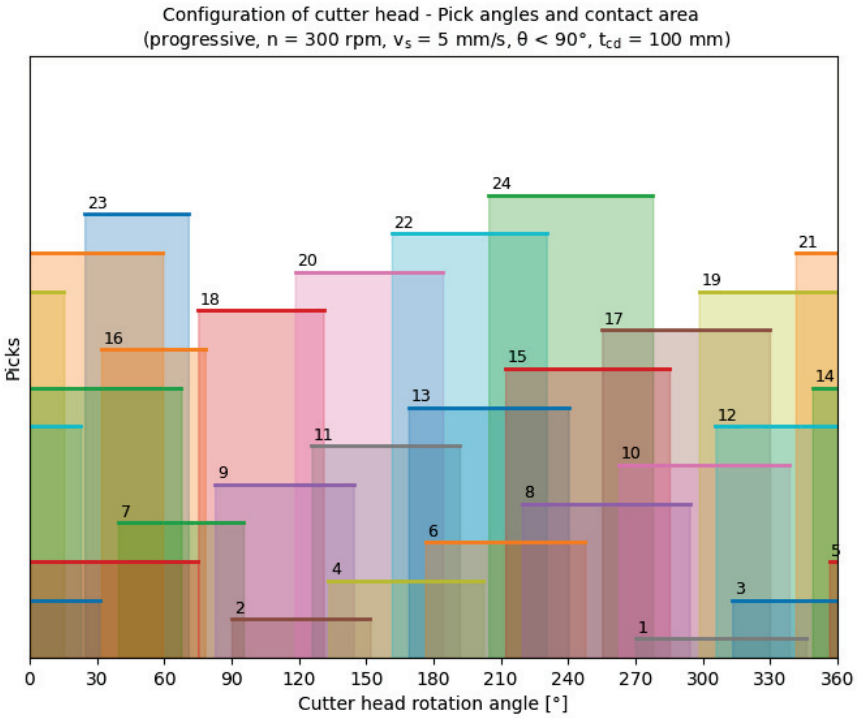

(a) Pick contact angles

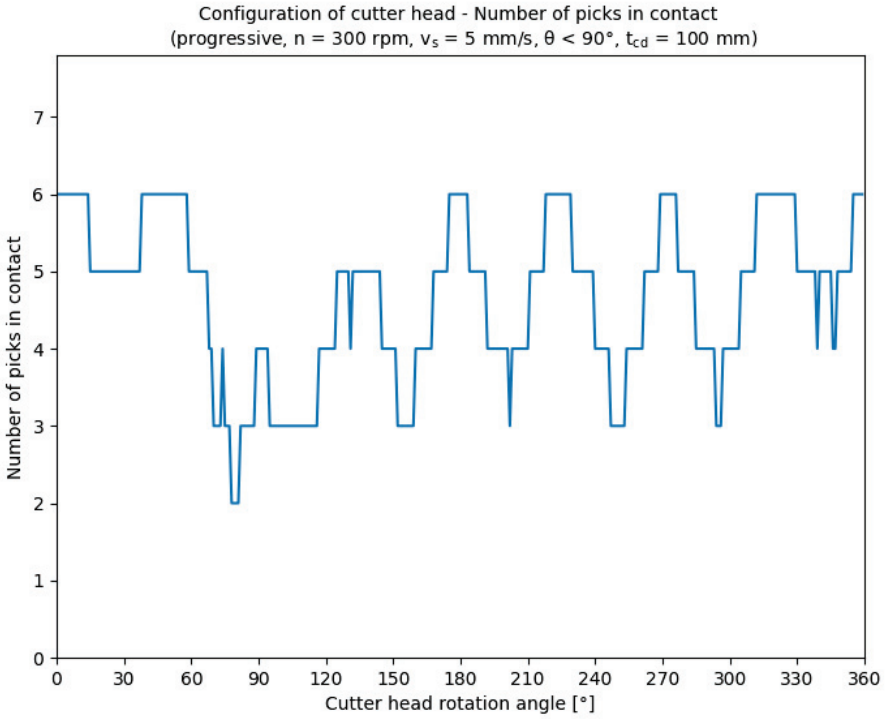

(b) Pick contact frequency

Figure D.8: Progressive cutting - Pick parameters

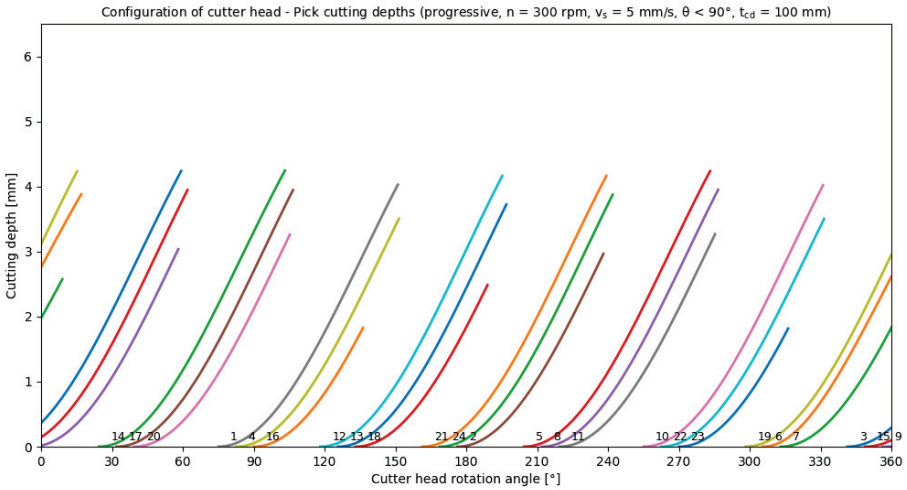

(a) Pick cutting depths

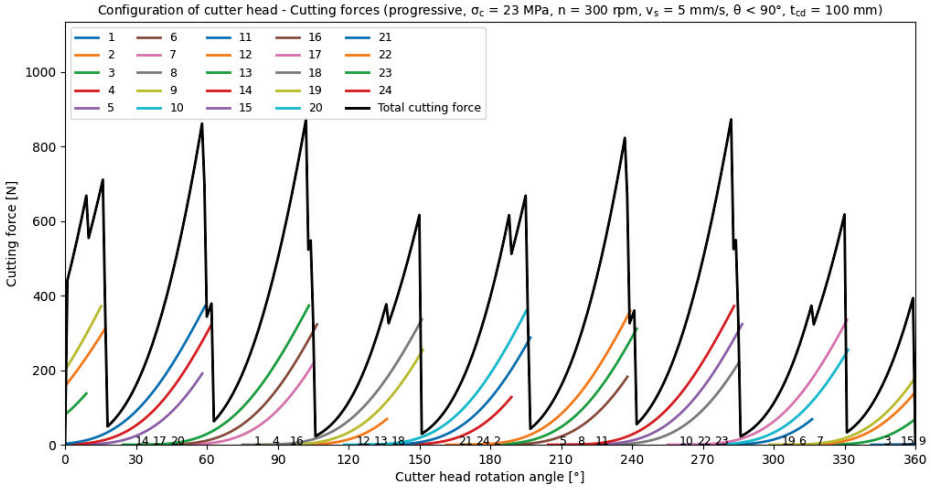

(b) Pick cutting forces

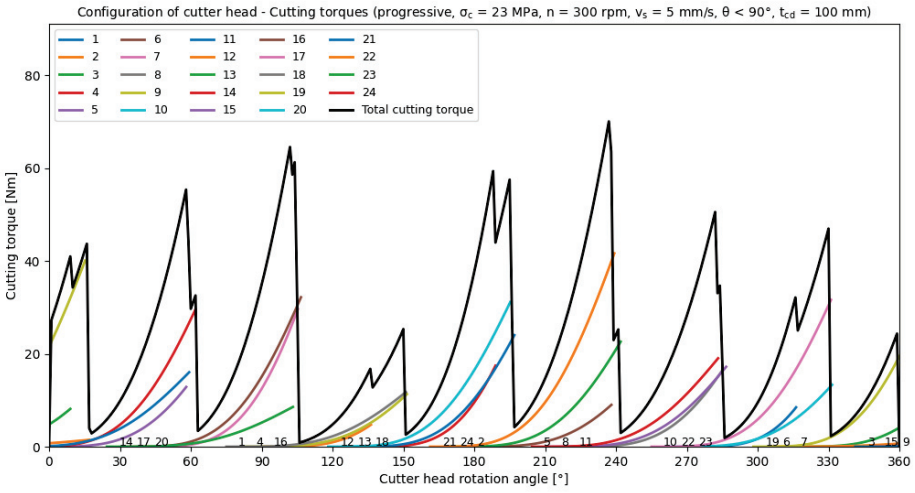

(c) Pick cutting torques

Figure D.9: Progressive cutting - Cutting parameters

D.3 Part-face cutter head kinematic model

Tranversal cutter head

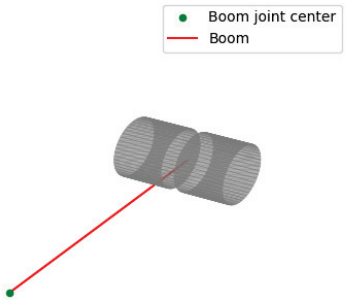

Figure D.10: Transversal cutter head model

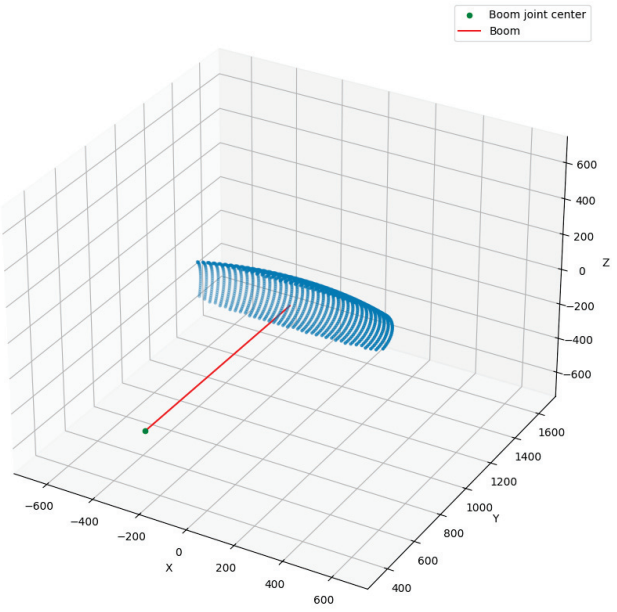

(a) Full contact cutting - Kinematic model

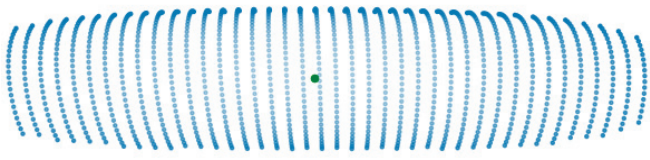

(b) Full contact cutting - Pick path

Figure D.11: Transversal cutter head model - Overview

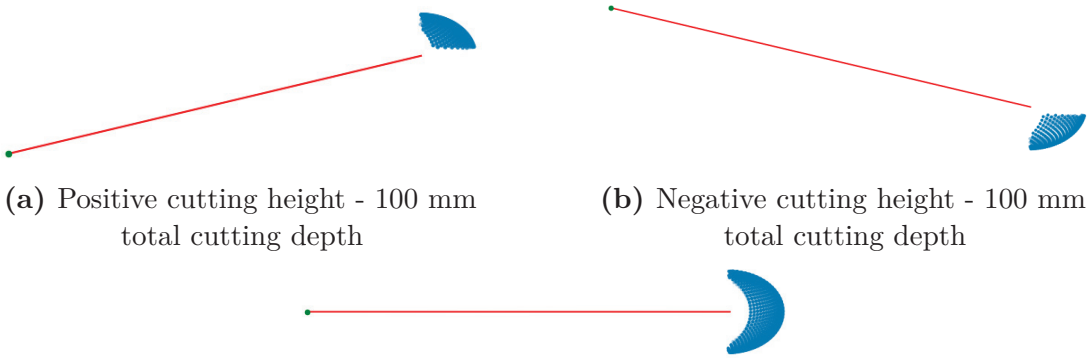

(a) Positive cutting height - 100 mm total cutting depth

(b) Negative cutting height - 100 mm total cutting depth

(c) Full contact cutting

Figure D.12: Transversal cutter head model - Pick cutting kinematics

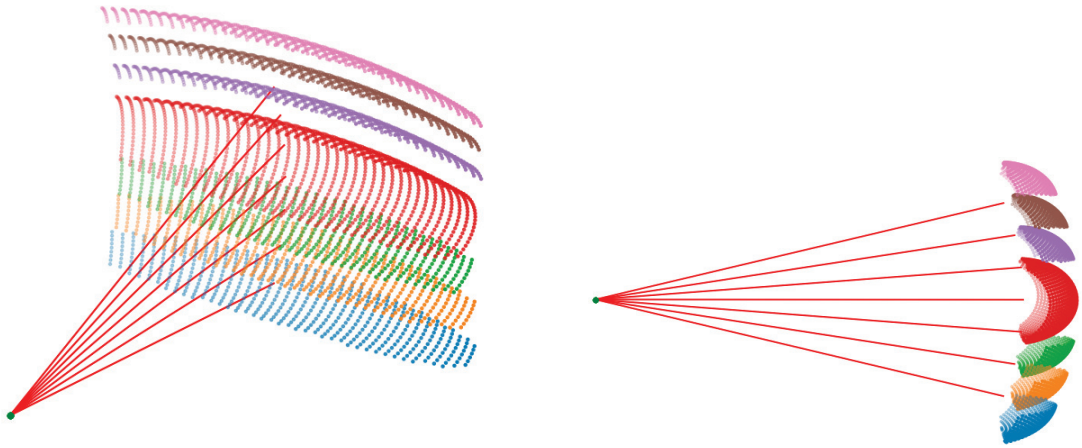

(a) Tunnel profile

(b) Tunnel profile - side view

Figure D.13: Transversal cutter head model - Combined 1 pick cutting kinematics

E Appendix - Verification and validation

E.1 Slow slew

B20 concrete

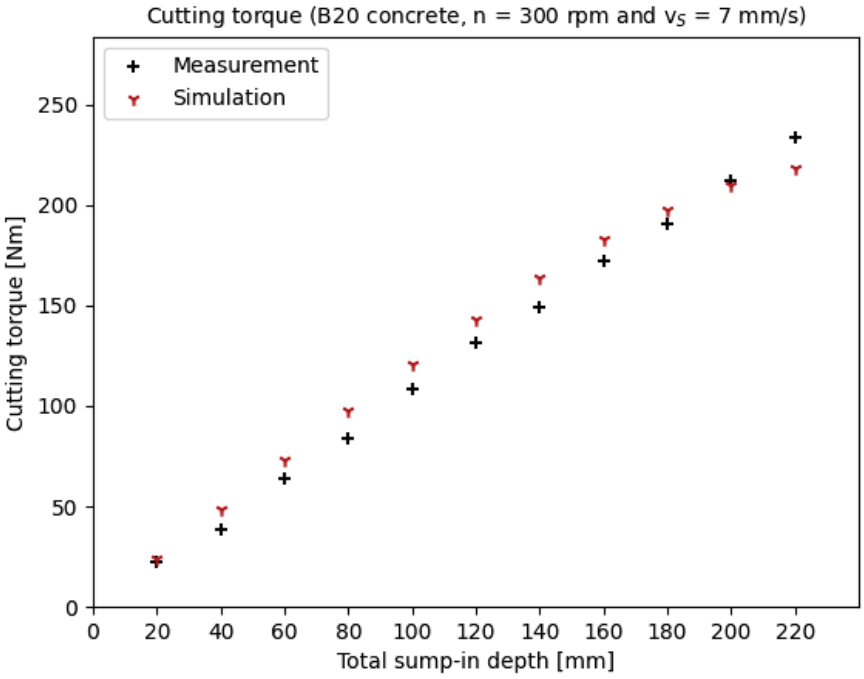

(a) Cutting torque depending on total sump-in depth of cutter head

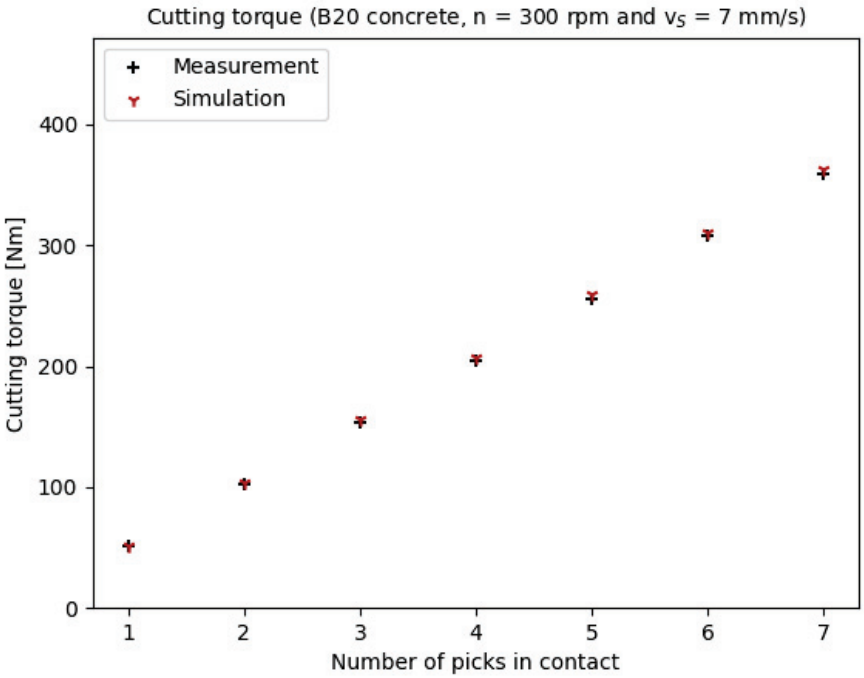

(b) Cutting torque depending on number of picks in contact

Figure E.1: Verification of simulated cutting torques - B20 concrete

B30 concrete

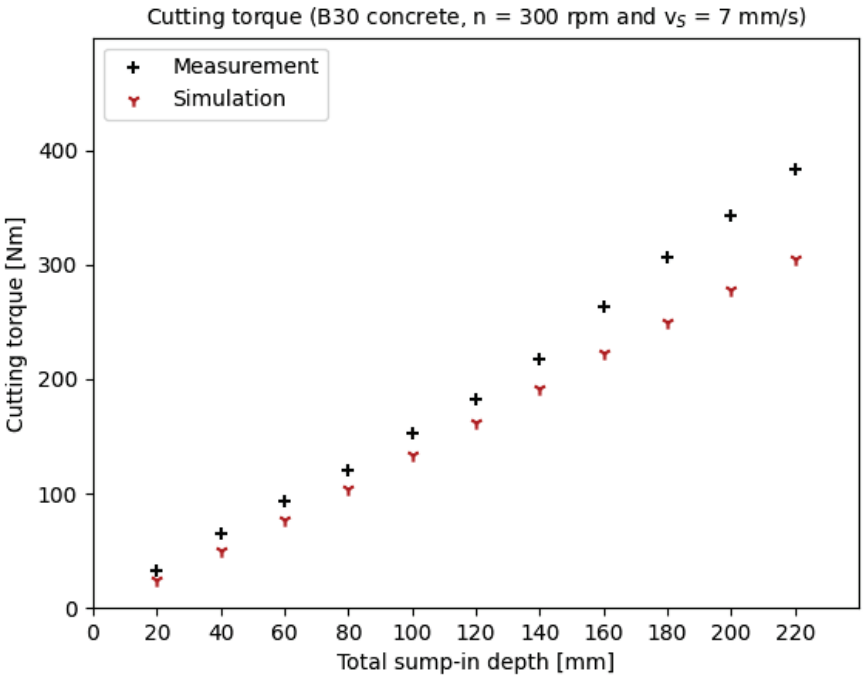

(a) Cutting torque depending on total sump-in depth of cutter head

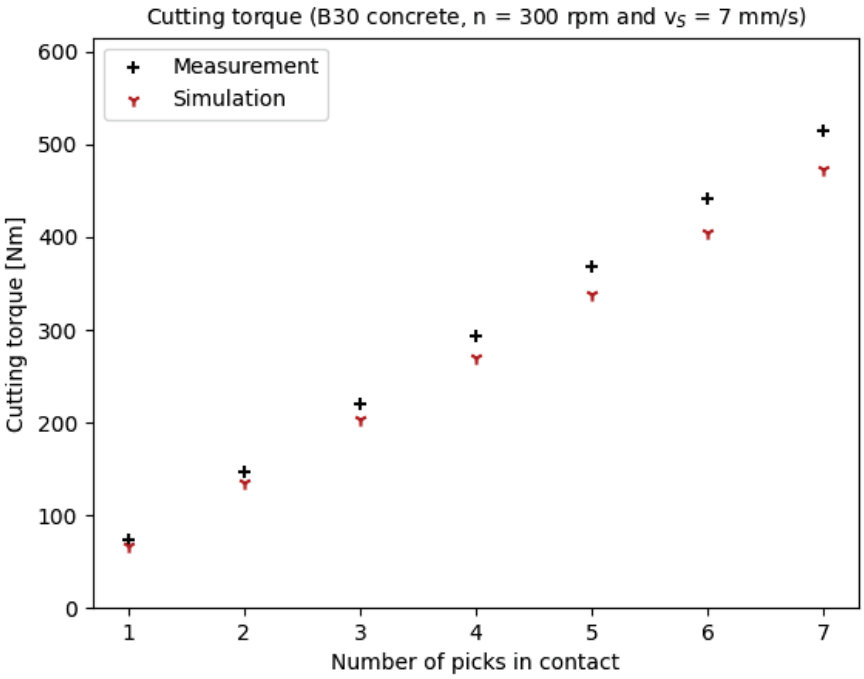

(b) Cutting torque depending on number of picks in contact

Figure E.2: Verification of simulated cutting torques - B30 concrete

Oilshale

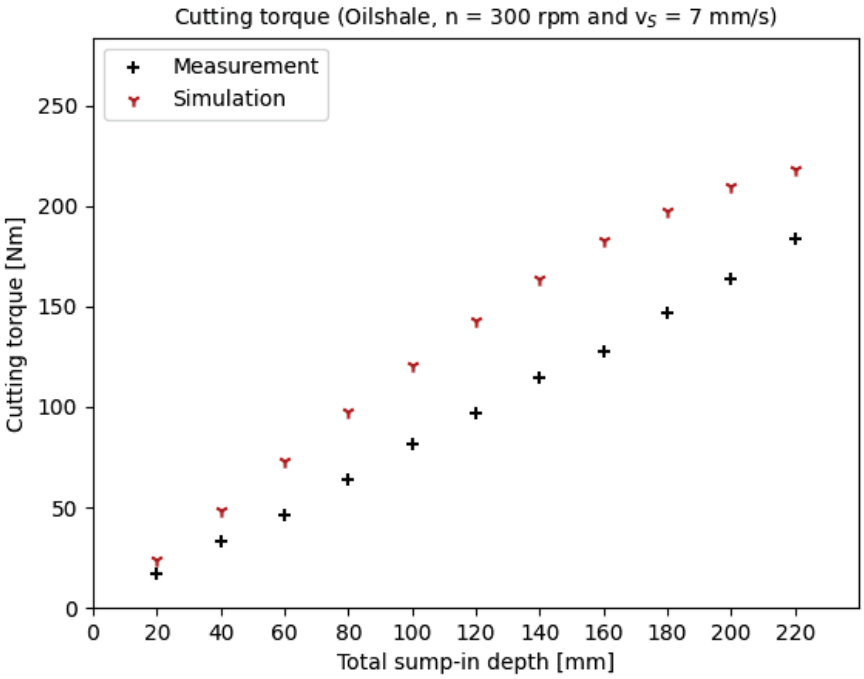

(a) Cutting torque depending on total sump-in depth of cutter head

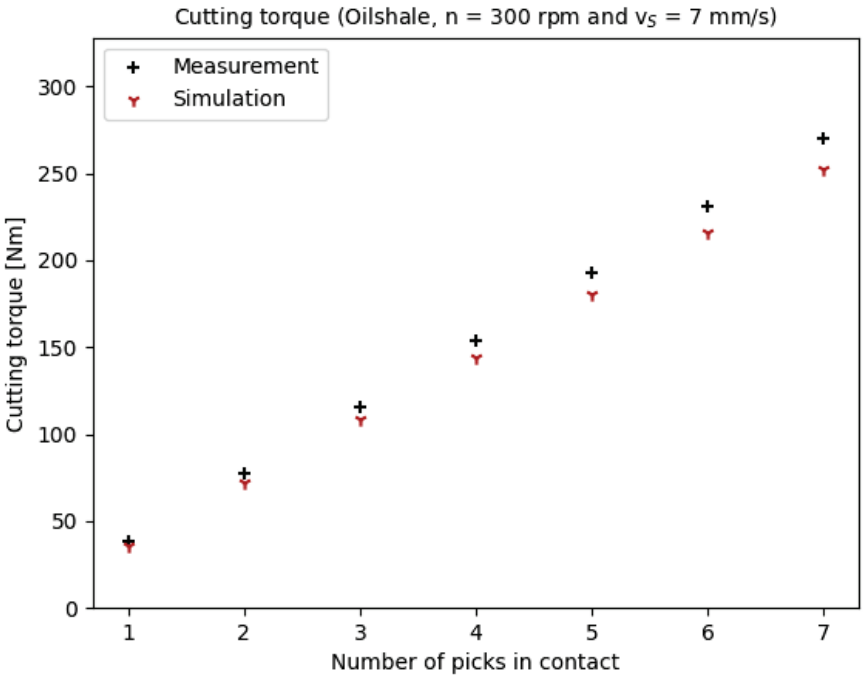

(b) Cutting torque depending on number of picks in contact

Figure E.3: Verification of simulated cutting torques - Oilshale

Deviation between experimental tests and simulation

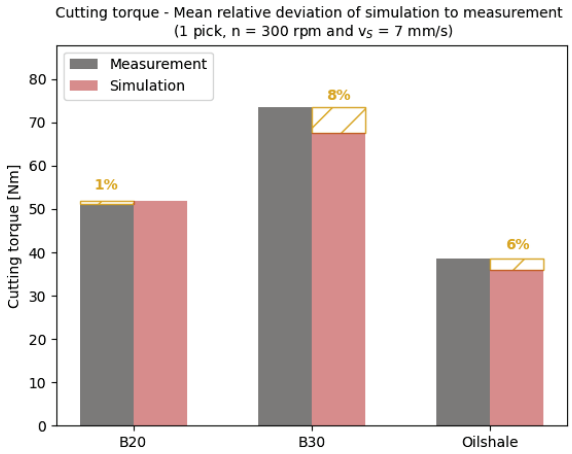

(a) Mean relative deviation the three test sample types

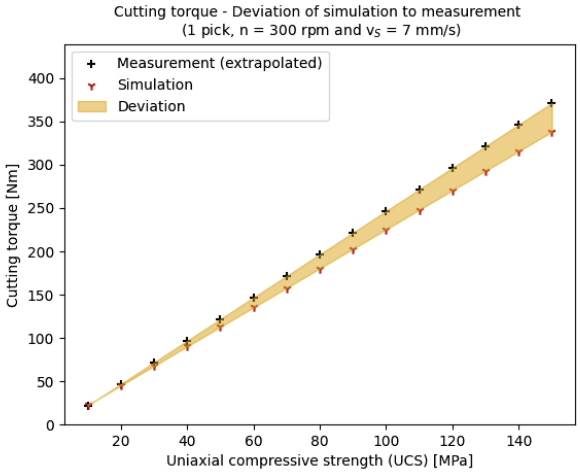

(b) Deviation depending on UCS

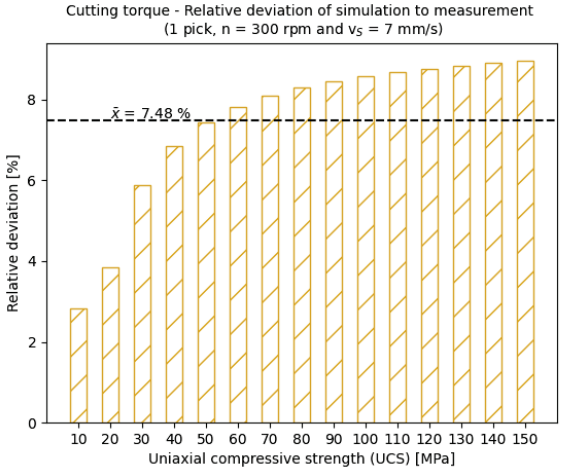

(c) Relative deviation depending on UCS

Figure E.4: Deviation between measurement and simulation - Cutting torque

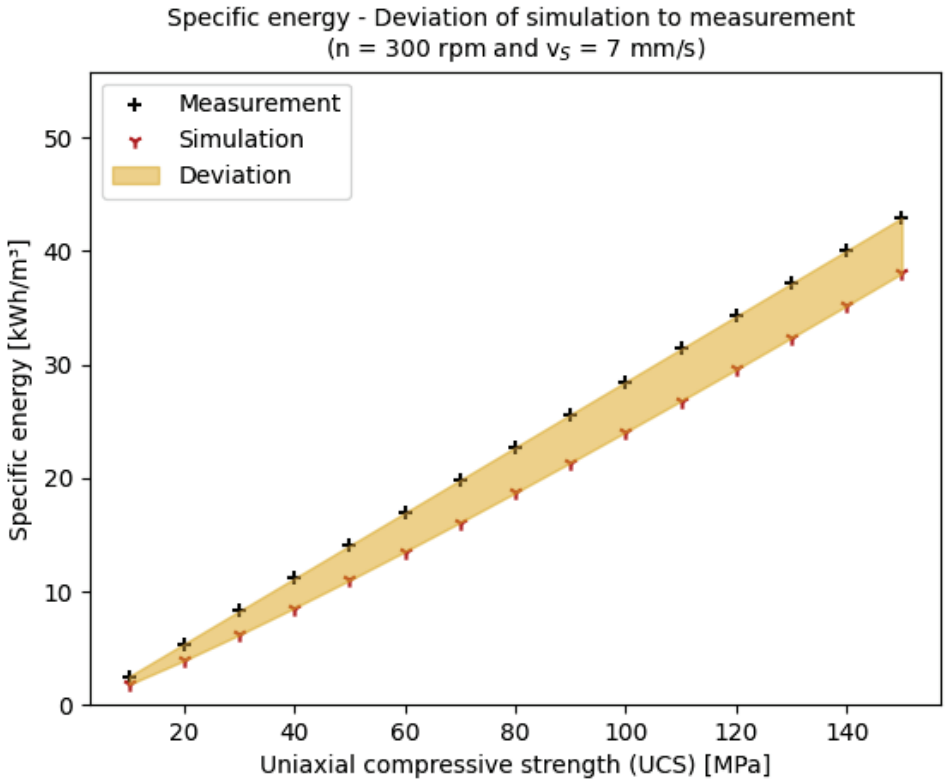

(a) Deviation depending on UCS

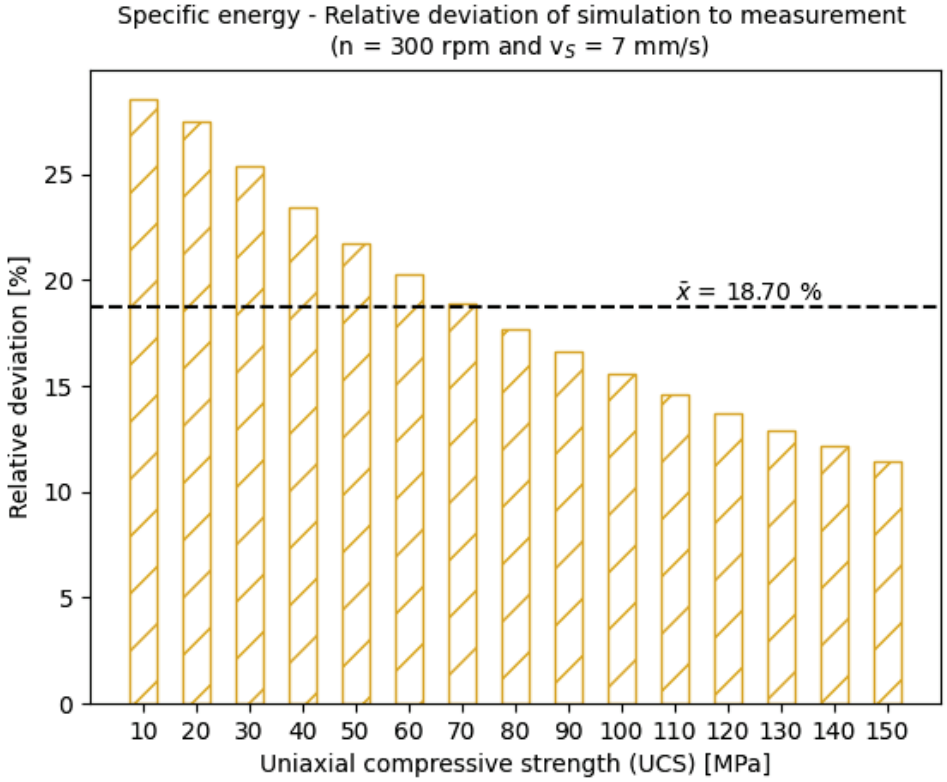

(b) Relative deviation depending on UCS

Figure E.5: Deviation between measurement and simulation - Specific energy

E.2 Fast slew

B20 concrete

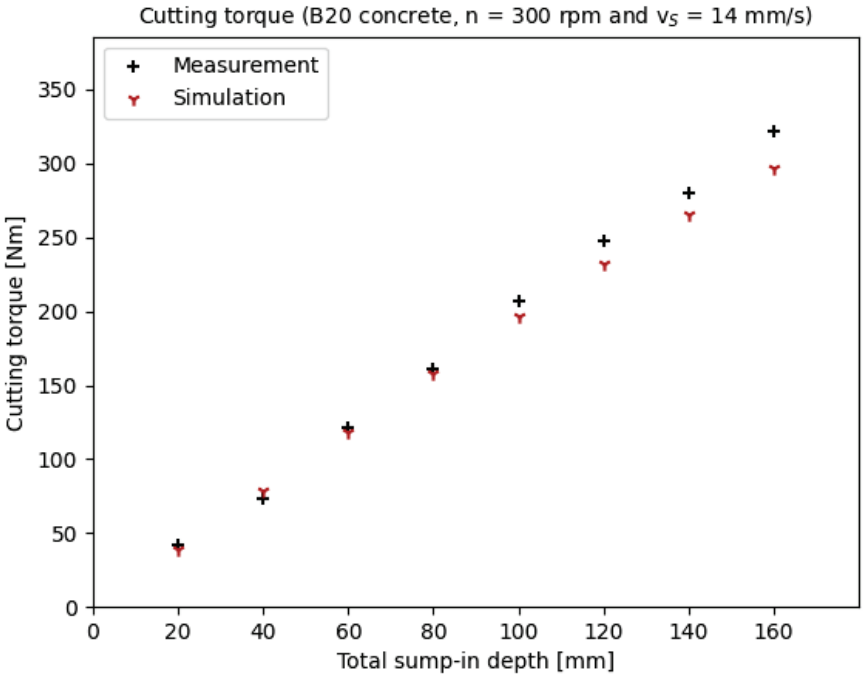

(a) Cutting torque depending on total sump-in depth of cutter head

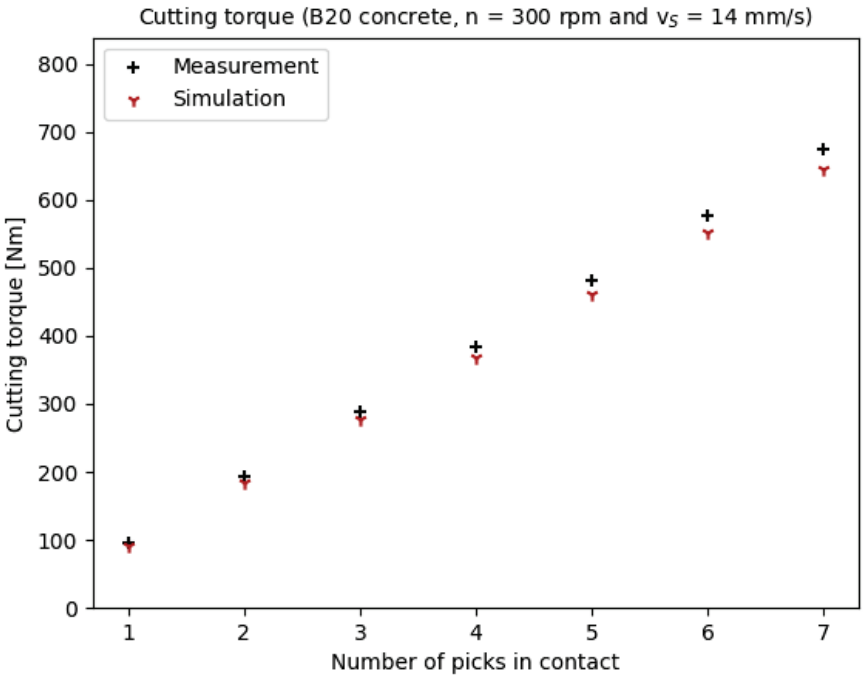

(b) Cutting torque depending on number of picks in contact

Figure E.6: Verification of simulated cutting torques - B20 concrete

B30 concrete

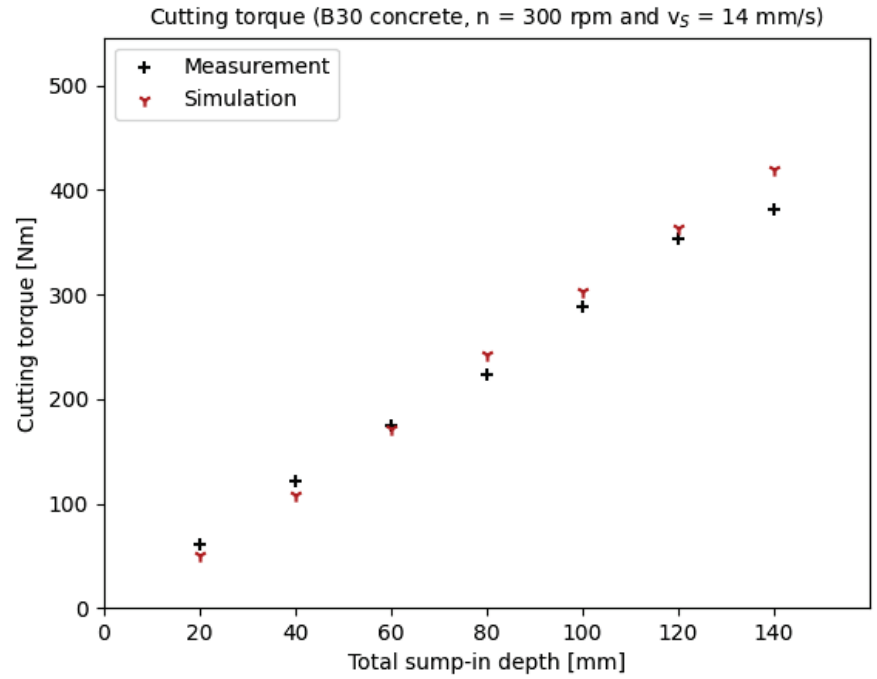

(a) Cutting torque depending on total sump-in depth of cutter head

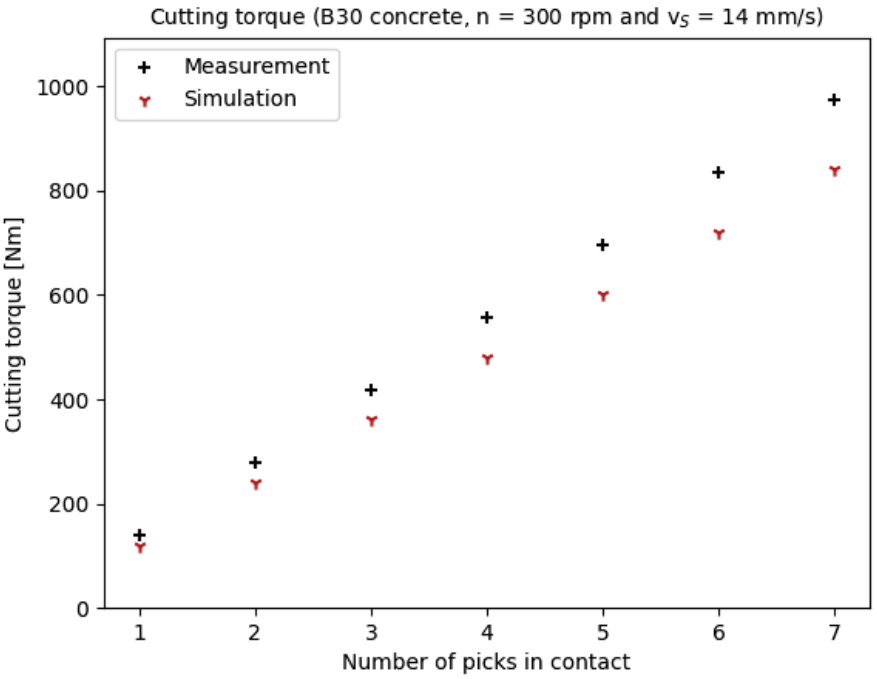

(b) Cutting torque depending on number of picks in contact

Figure E.7: Verification of simulated cutting torques - B30 concrete

Oilshale

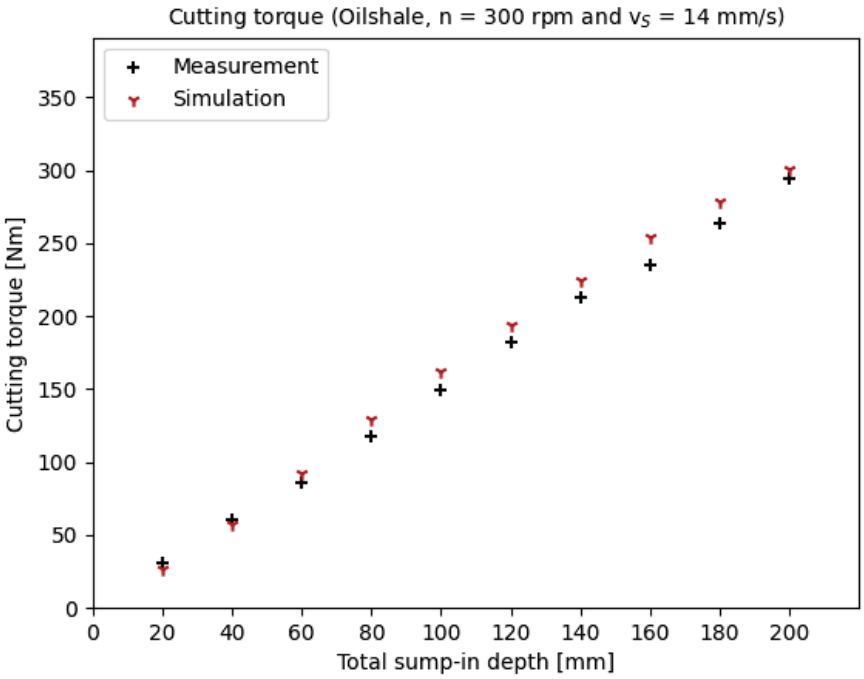

(a) Cutting torque depending on total sump-in depth of cutter head

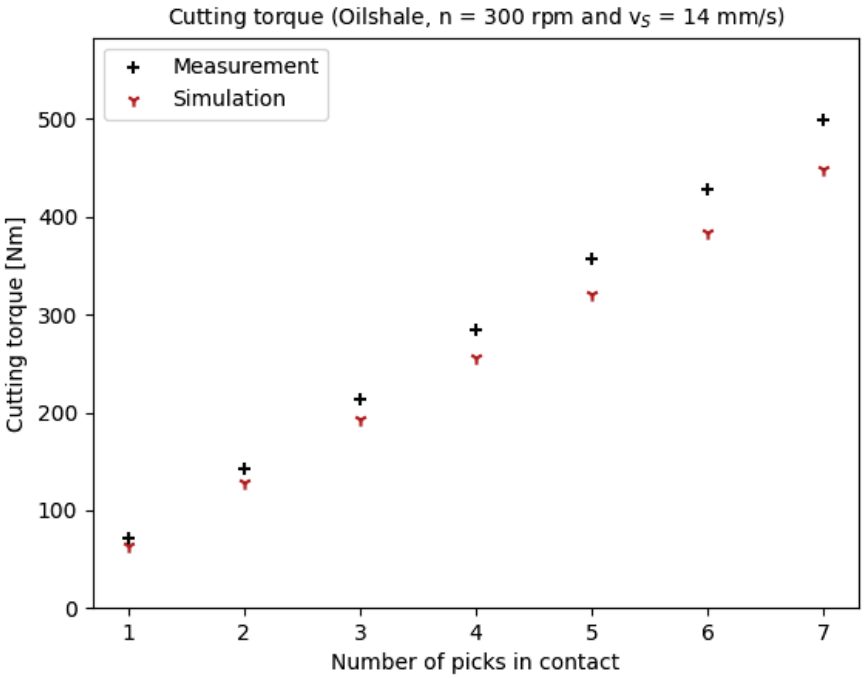

(b) Cutting torque depending on number of picks in contact

Figure E.8: Verification of simulated cutting torques - Oilshale

Deviation between experimental tests and simulation

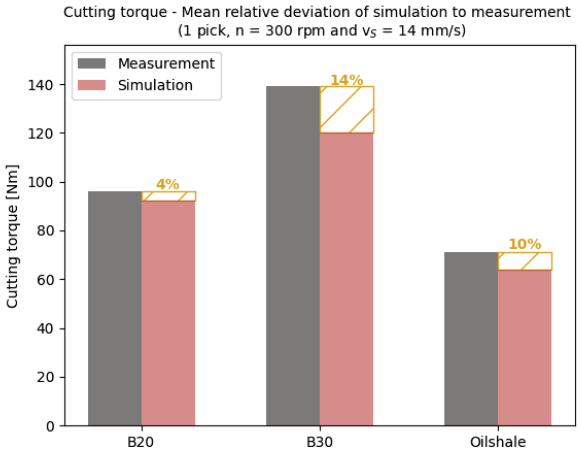

(a) Mean relative deviation for the three test sample types

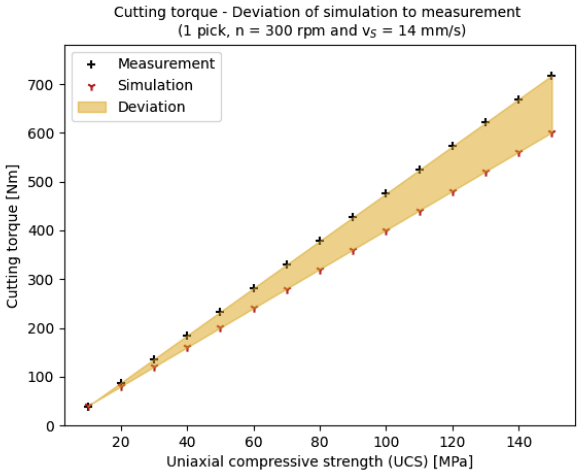

(b) Deviation depending on UCS

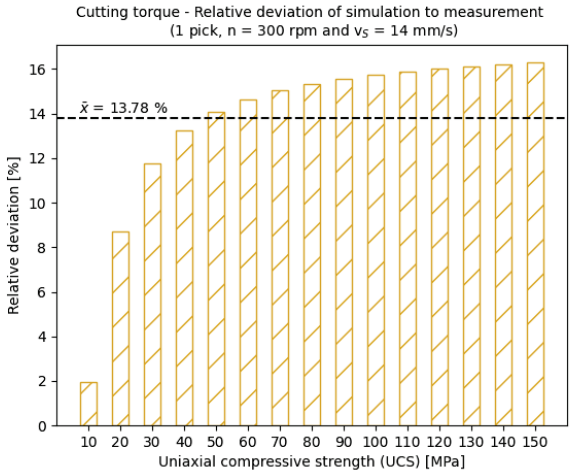

(c) Relative deviation depending on UCS

Figure E.9: Deviation between measurement and simulation - Cutting torque

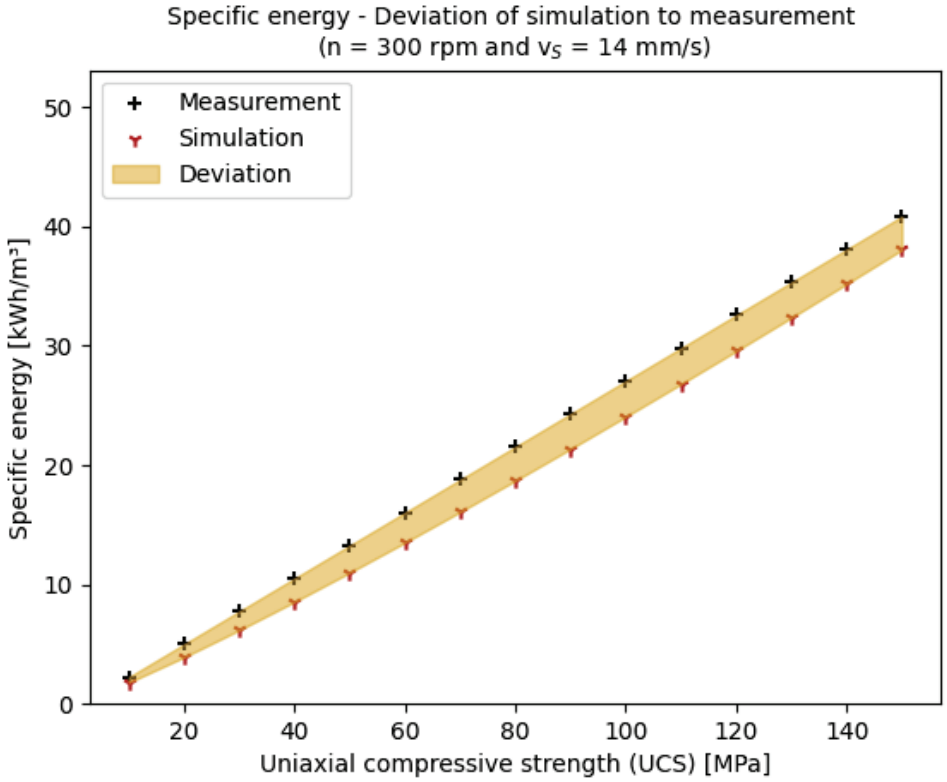

(a) Deviation depending on UCS

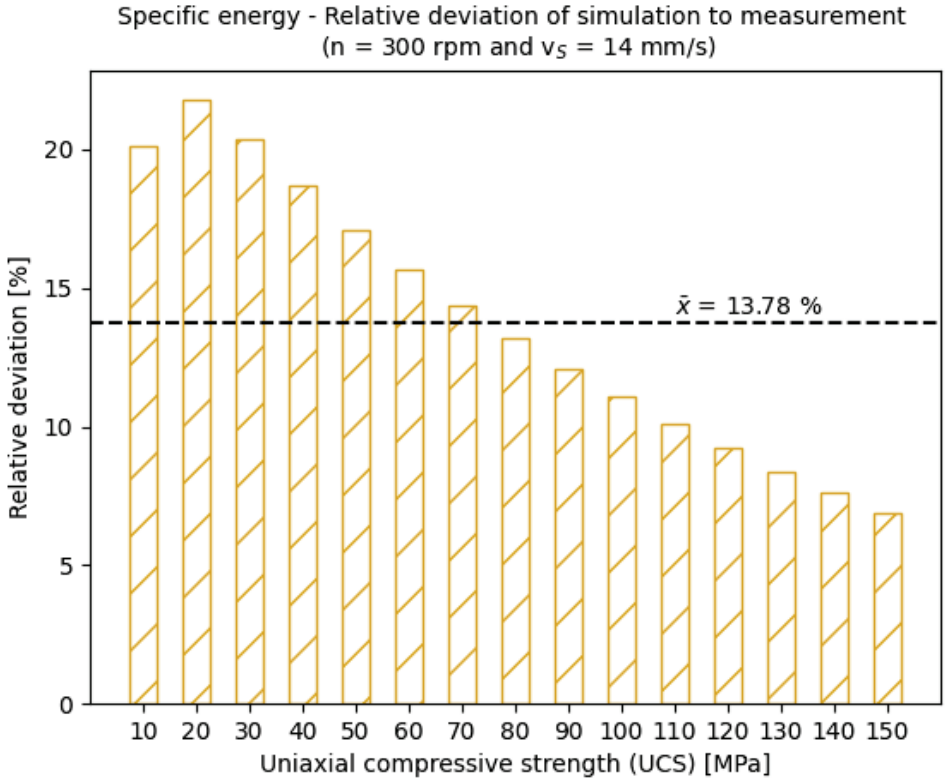

(b) Relative deviation depending on UCS

Figure E.10: Deviation between measurement and simulation - Specific energy